EG&G Idaho, Inc.

FORM EG&G 398
(Rev. 11-79)

INTERIM REPORT

Accession No. _____

Report No. EGG-CAAD-5432
CSNI 66

Contract Program or Project Title: Code Assessment and Applications Division

Subject of this Document: International Standard Problem 9 (LOFT Test L3-1) Preliminary Comparison Report

Type of Document: Preliminary Comparison Report

Author(s): A. C. Peterson
C. Polk
J. A. Sellars

NRC Research and Technical Assistance Report

Date of Document: April 1981

Responsible NRC Individual and NRC Office or Division: F. Odar, NRC-RSR

EG&G Idaho, Inc.
Idaho Falls, Idaho **83415**

Prepared for the
U.S. Nuclear Regulatory Commission
Washington, D.C.
Under DOE Contract No. **DE-AC07-76ID01570**
NRC FIN No. A6047

INTERIM REPORT

EGG-CAAD-5432
CSNI 66

NRC Research and Technical Assistance Report

INTERNATIONAL STANDARD PROBLEM 9 (LOFT TEST L3-1) PRELIMINARY COMPARISON REPORT

A. C. Peterson
C. Polk
J. A. Sellars

Published April 1981

EG&G Idaho, Inc.
Idaho Falls, Idaho 83415

Prepared for the
U.S. Nuclear Regulatory Commission
Washington, D.C. 20555
Under DOE Contract No. DE-AC07-76ID01570
FIN No. A6047

ABSTRACT

LOFT Test L3-1 was designated as International Standard Problem 9 by the Committee on the Safety of Nuclear Installations of the Organization for Economic Cooperation and Development. LOFT Test L3-1 was a single ended small cold leg break experiment initiated from typical pressurized water reactor operating conditions. Comparisons between measurements from Test L3-1 are made with calculations by eleven international participants using seven different computer codes.

SUMMARY

The Committee on the Safety of Nuclear Installations of the Organization for Economic Cooperation and Development designated LOFT Test L3-1 as International Standard Problem 9. LOFT Test L3-1 was conducted on November 20, 1979 at the Idaho National Engineering Laboratory. The LOFT test system was assembled to represent a small break in the cold leg of a commerical pressurized water reactor (PWR). The break size was 2.059 cm^2 which is equivalent to about a 2.5% break of the cold leg in a commercial PWR.

Test L3-1 was initiated from a primary coolant system initial conditions of: hot leg temperature, 574 $\pm$ 1 K; intact loop flow rate, 484 $\pm$ 6.3 kg/s; hot leg pressure, 14.85 $\pm$ 0.04 MPa; preblowdown power level, 48.9 $\pm$ 1 MW, with a maximum linear heat generation rate of 51.7 $\pm$ 1 kw/m.

Calculations were submitted by eleven participants using seven different computer codes and a comparison made between participants calculations and measurements from LOFT Test L3-1. Although relatively poor agreement occurred between the calculated and measured break mass flow rate, the agreement between the measured and calculated system pressure response was in general satisfactory. Most participants calculated the rod cladding temperature to remain near the system saturation temperature, however, a core heat up was obtained with four of the calculation.

CONTENTS

FIGURES

TABLES

1. INTRODUCTION

Test L3-1 conducted in the Loss-of-Fluid Test (LOFT) facility was identified by the Committee on the Safety of Nuclear Installations of the Organization for Economic Cooperation and Development (OECD) as International Standard Problem 9 (ISP-9). This report documents the comparisons between participant computer code calculations and measured results from LOFT Test L3-1. The experiment results from Test L3-1 were documented in Reference 1.

LOFT Test L3-1 simulated a single-ended break in the cold leg of a pressurized water reactor (PWR). The break size was 2.059 cm^2 which corresponds to about 2.5% of the area of the cold leg piping. This break size was large enough to cause a system depressurization. The system description and initial conditions are presented in Section 2. The effects of leakage of primary fluid through a warm up line and through the reflood assist blowdown valves (RABVs) on RELAP4/MOD7 calculated results are also discussed in Section 2.

The models used by the participants are summarized in Section 3 and the results of the comparisons between measurements and calculated results are summarized in Section 4. Section 5 presents the conclusions from the comparisons.

2. LOFT TEST L3-1 EXPERIMENTAL DESCRIPTION

Test L3-1 was conducted on November 20, 1979 in the LOFT facility. The LOFT facility is located at the Idaho National Engineering Laboratory (INEL) and is operated for the United States Nuclear Regulatory Commission by the Department of Energy. This section describes the LOFT facility, the initial test conditions, and the effects on RELAP4/MOD7 calculated results of leakage in the primary system.

2.1 System Description

The LOFT system configuration for Test L3-1 is shown in Figure 1. The major components of the LOFT system are: a reactor vessel including a core with 1300 unpressurized nuclear fuel rods; an intact loop with a pressurizer, steam generator, and two pumps arranged in parallel; a broken loop with a simulated steam generator and simulated pump, two break plane orifices and two quick opening blowdown valves (Q03V); an emergency core coolant system (ECCS) consisting of an accumulator, high pressure injection system and low pressure injection system, and a blowdown suppression system consisting of a header and suppression tank. The details of the LOFT system and instrumentation were presented in Reference 2.

For Test L3-1 the broken loop hot leg Q0BV remained closed and the break plane orifice in the broken loop cold leg simulated a 2.5% break in a commercial plant. The configuration of the orifice in the cold leg is shown in Figure 2.

2.2 Initial Conditions

A summary of the measured system conditions immediately prior to Test L3-1 initiation are shown in Table 1. The hot leg pressure was 14.85 $\pm$ 0.04 MPa. The mass flow rate in the intact loop was 484.0 $\pm$ 6.3 kg/s. The intact loop hot leg temperature was 574 $\pm$ 1 K. The initial core power was 48.9 $\pm$ 1 MW with a maximum linear heat generation rate of 51.7 $\pm$ 1 kw/m.

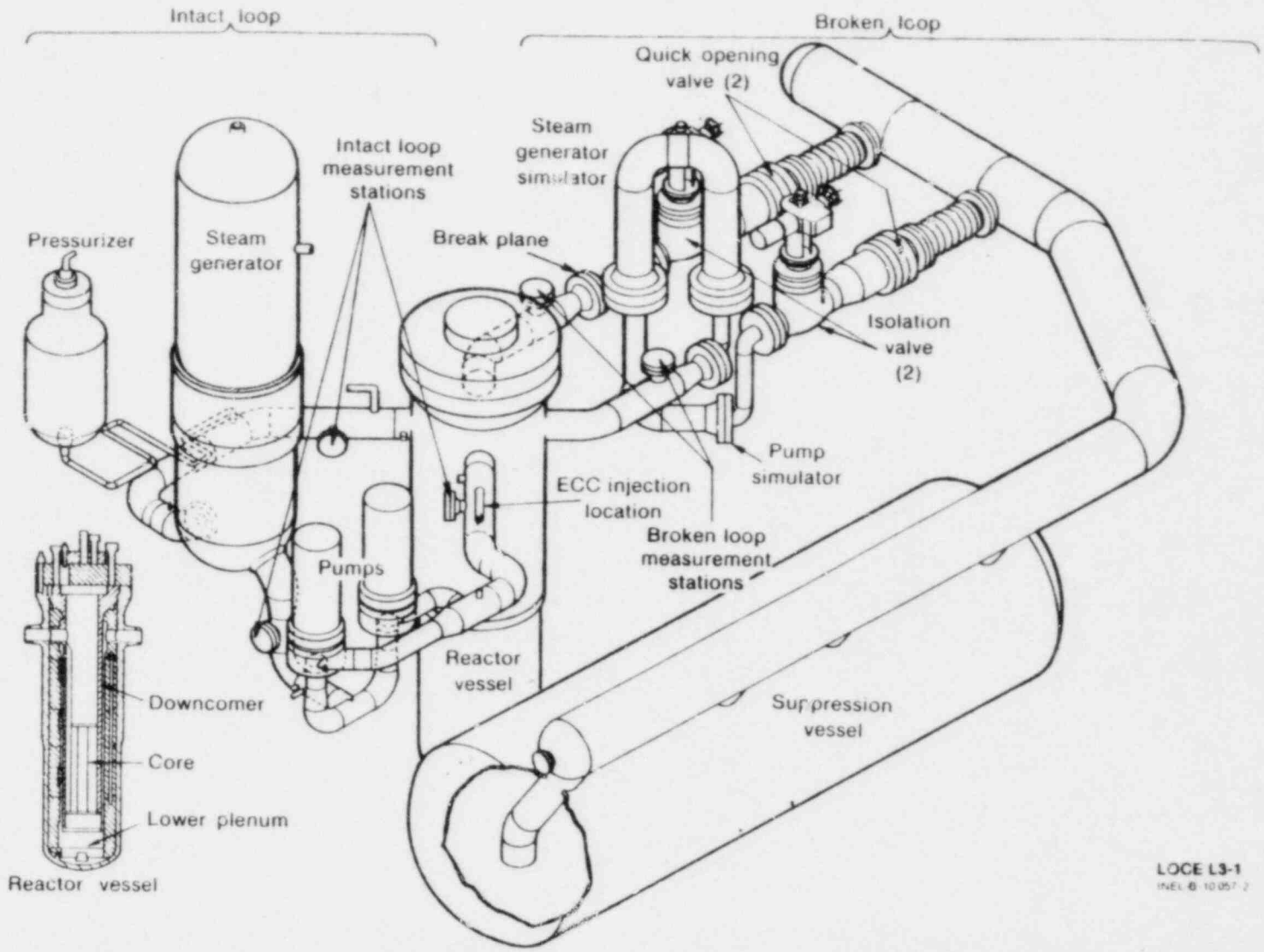

Figure 1: LOFT system configuration for Test L3-1

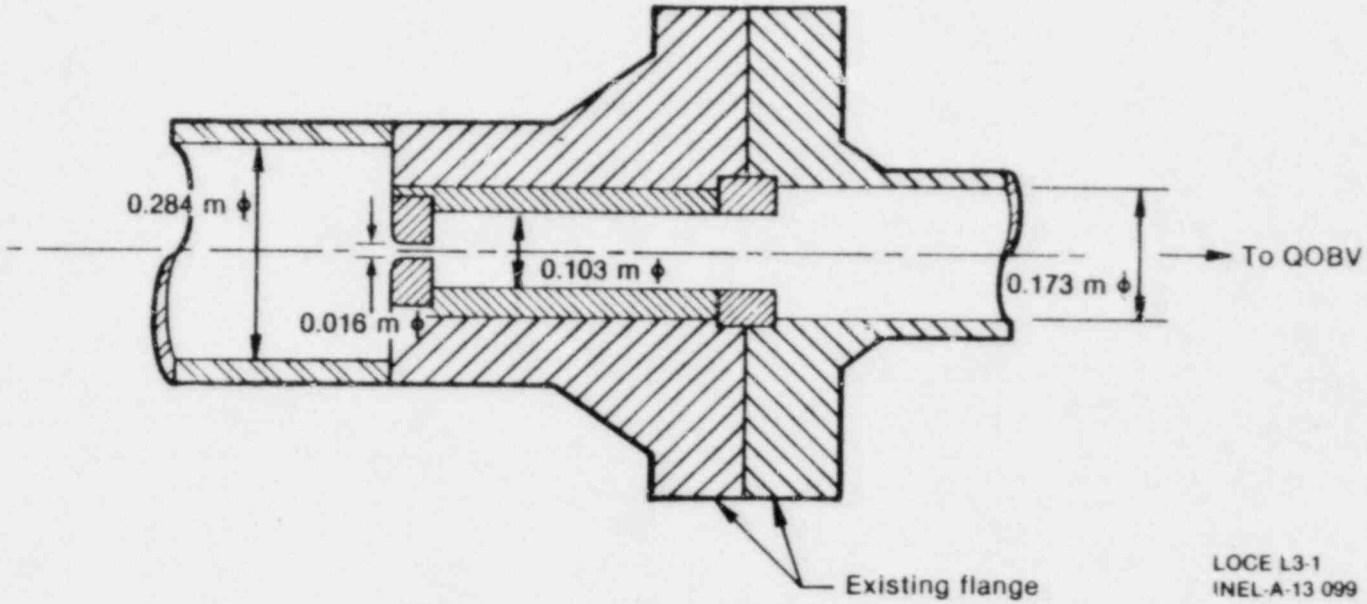

Figure 2: LOFT small break orifice configuration for Test L3-1

TABLE 1. INITIAL CONDITONS FOR LOFT TEST L3-1

Parameter	Measured Value
Primary Coolant System	
Mass flow rate (kg/s)	484.0 ± 6.3
Hot leg pressure (MPa)	14.85 ± 0.04
Cold leg temperature (K)	554.0 ± 3
Hot leg temperature (K)	574.0 ± 1
Boron concentration (ppm)	773 ± 15
Reactor Vessel	
Power level (MW)	48.9 ± 1
Maximum linear heat generation generation rate (kW/m)	51.7 ± 1
Control rod position (above full-in position (m)	1.371 ± 0.01
Pressurizer	
Steam volume (m^3)	0.343 ± 0.008
Liquid volume (m^3)	0.620 ± 0.008
Water temperature (K)	617.0 ± 3
Pressure (MPa)	14.81 ± 0.04
Level (m)	1.10 ± 0.01
Broken Loop	
Cold leg temperature (K)	557.3 ± 5.0
Hot leg temperature (K)	562.0 ± 5.0
Steam Generator Secondary Side	
Water level (m)[a]	0.20 ± 0.03
Water temperature (K)	536.0 ± 3.9
Pressure (MPa)	5.43 ± 0.11
Mass flow rate (kg/s)	25.0 ± 0.4
ECC Accumulator A	
Liquid level (m)	1.71 ± 0.01
Standpipe position (m)	0.48 ± 0.01
Gas volume (m^3)	1.39 ± 0.03
Pressure (MPa)	4.37 ± 0.06
Temperature (K)	304.7 ± 3
Boron concentration (ppm)	3314 ± 15

TABLE 1. (continued)

Parameter	Measured Value
HPIS	
Initial flow rate (l/s)	0.33 ± 0.02
LPIS	
Initiation pressure (MPa)	1.02 ± 0.03

a. The water level is defined as 0.0 at 2.95 m above the top of the tube sheet.

The reactor was scrammed 2 s before the blowdown. The experiment was initiated by opening the broken loop cold leg QOBV.

2.3 Effects of Primary System Leakage

Subsequent to the completion of Test L3-1, two leakage paths for primary system coolant were identified. These paths were through the cold leg warmup lines and core bypass flow which goes through the Reflood Assist Bypass Valves (RABVs). The effects of these flow paths on RELAP4/MOD7 calculations are discussed in this section.

2.3.1 Effect of Warmup Line Leakage

The cold leg warmup line provides a flow path for flow from the intact loop hot leg to the broken loop cold leg as indicated in Figure 3. Note that to facilitate the display of the leakage paths in Figure 3, the LOFT vessel was represented as split through the middle. The valve in this line is usually closed during a test, however, for Test L3-1 this valve failed to fully close prior to experiment initiation. Calculations were performed with a developmental version of RELAP4/MOD7 to investigate the effects of this flow path on calculated results.

An estimate of the cold leg warmup line leakage during Test L3-1 was obtained from data from Test L3-2. The leakage rate was estimated to be 0.6 kg/s at intact loop hot leg pressure above 6.7 MPa and linearly decreased to zero at pressures from 6.7 to 6.5 MPa. Below 6.5 MPa the flow was estimated to be zero since the pressure differential across the isolation valve was below the threshold required to seat the valve. The effect of the flow through the cold leg warmup line on the system pressure is shown in Figure 4. There was essentially no effect for the initial 200 s of the transient. At 500 s the effect of the warmup line leakage was to increase the system depressurization by about 0.4 MPa. This effect on system pressure is indicative of the effect on other calculated parameters and was considered small.

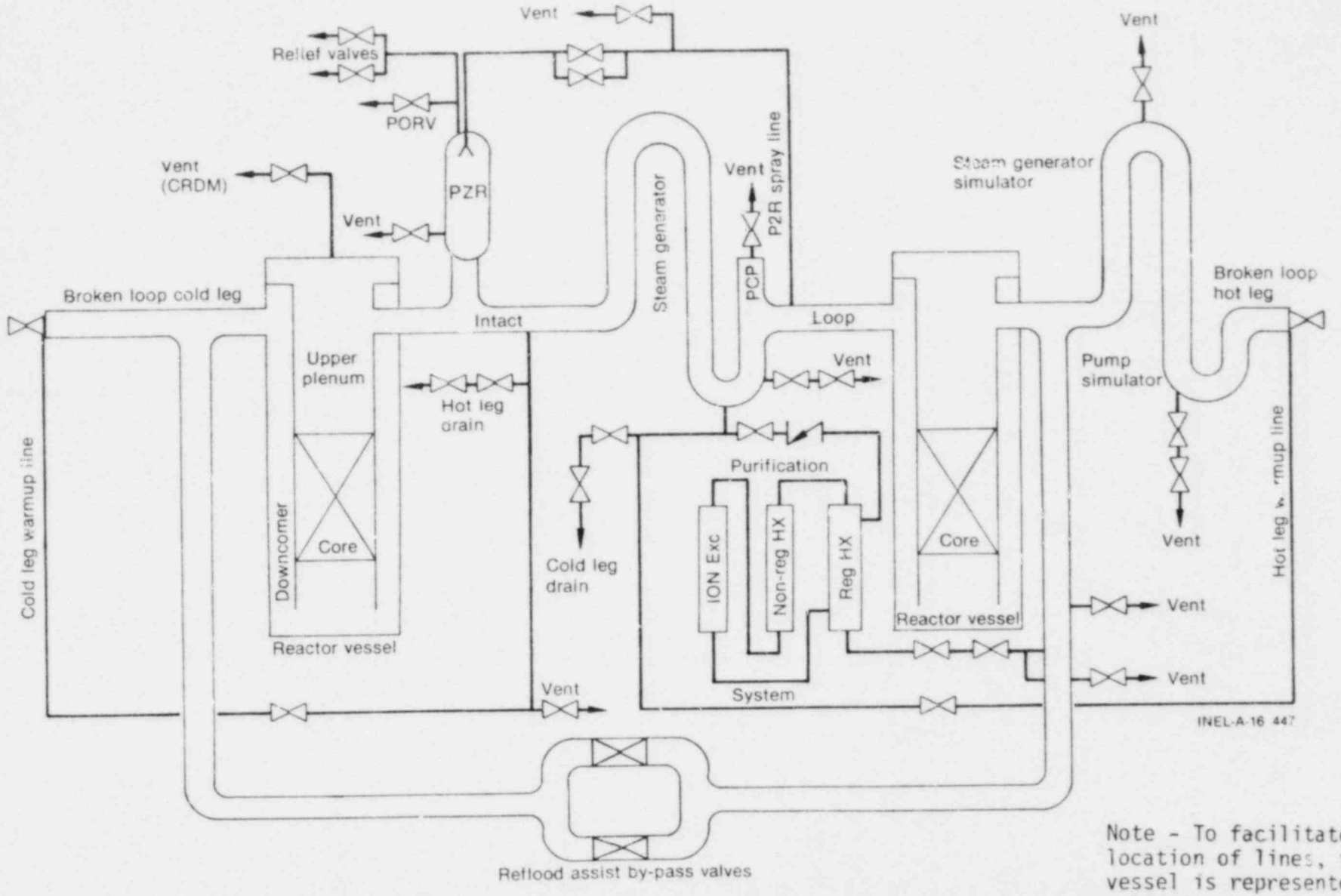

Figure 3: LOFT Leak and Bypass Paths

Note - To facilitate the location of lines, the vessel is represented as split in the middel

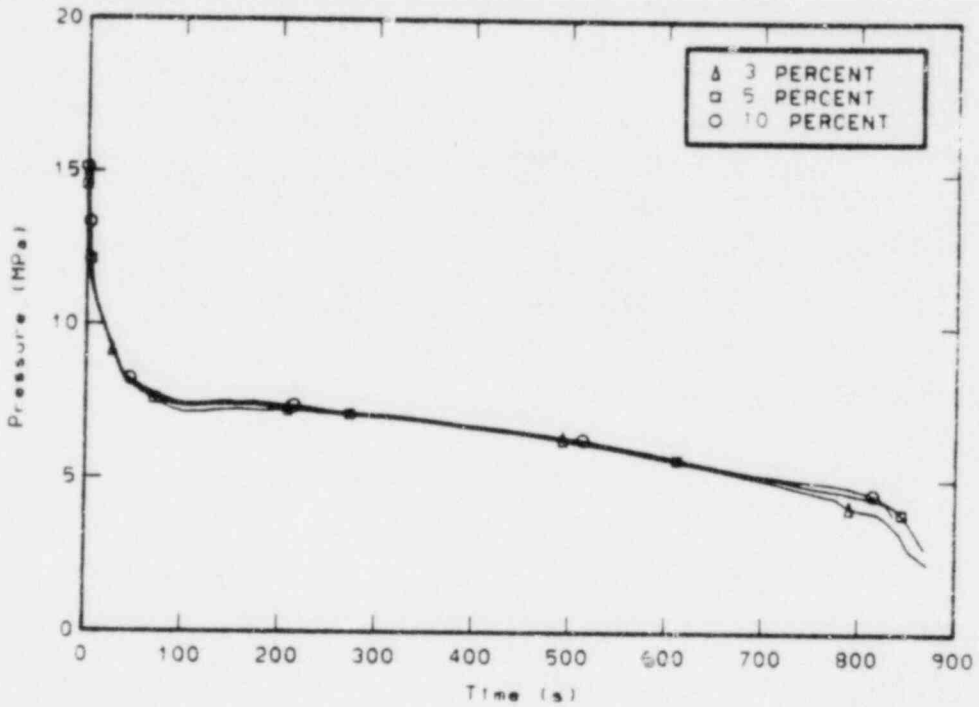

Figure 4. Effect of leakage through the RABVs on calculated upper plenum pressure.

2.3.2 Effect of Reflood Assist Bypass Valve Flow

LOFT utilizes the RABVs in a licensing procedure to protect against a large break LOCA in the LOFT intact loop. As shown in Figure 3 the RABVs connect the broken loop hot and cold legs. A pressure drop of about 1.0 MPa is required to seal this valve and during Test L3-1 lower pressure drops than that required to seal the valves occurred. The effects of this flow on calculated results were investigated with RELAP4/MOD7.

The total core bypass flow at steady state was estimated from measurements to be about 10% of the total steady state flow. Flow through the RABV's was estimated to be 3% of the core bypass flow. To assess the effect of bypass flow through the RABVs, calculations were performed assuming 3, 5 and 10% of the total steady state flow through the RABVs. The effects of this flow path on the upper plenum pressure are shown in Figure 5. This flow did not have a significant effect on the system pressure response. Analysis of the mass distribution in the system indicates that the distribution of mass in the system was effected by the flow through the RABVs, however, the long term differences were relatively small.

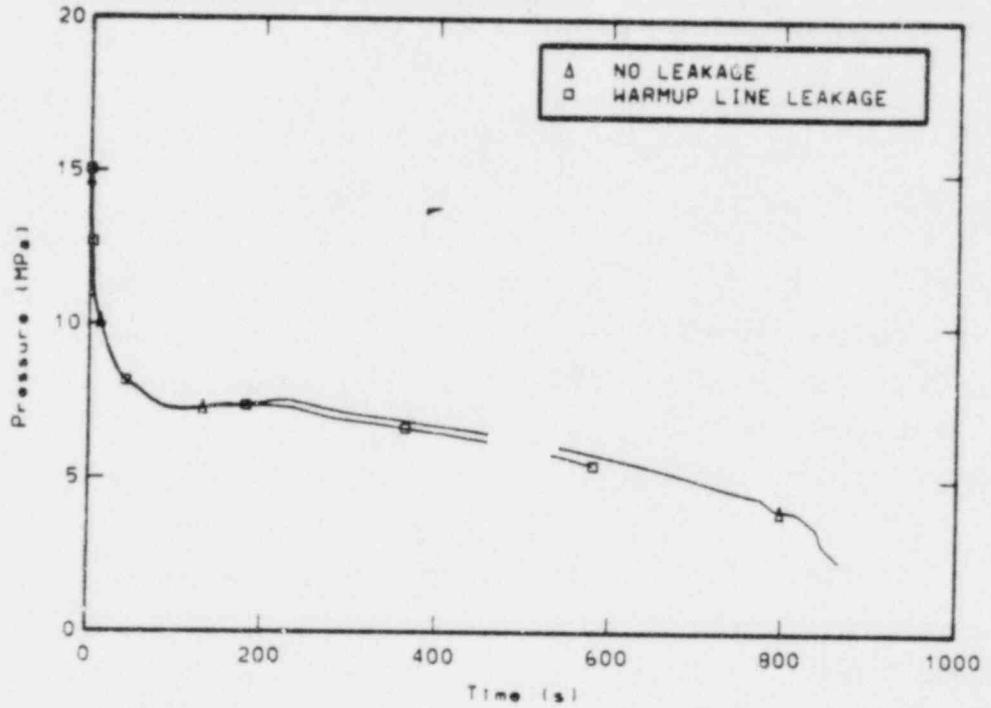

Figure 5. Effect of warmup line leakage on calculated upper plenum pressure.

3. SUMMARY OF PARTICIPANT MODELS

Submittals were received from 11 participants. Table 2 lists the participants and the identifier used for each participant in this report. Two participants submitted two calculations. Calculations were performed with seven different computer codes. The RELAP4/MOD6 computer was used for six of the calculations submitted. Table 3 summarizes the computer codes and models used by each participant. The relative run time of each calculation is also summarized in Table 3. A nodalization diagram for each participant is contained in Appendix A. The following discussion briefly summarizes the model of each participant.

3.1 Centre D'Etudes Nucleaires de Cadarache (CEA) Model

The calculation was performed by CEA using the RELAP4/MOD6 computer code. Slip was calculated at all junctions except the intact loop steam generator inlet, steam generator hot leg inlet to the tubes, pressurizer surge line and at the top of the broken loop steam generator simulator. Critical flow was calculated using the Henry-Fauske and homogeneous equilibrium model (HEM) with a multiplier of 1.0.

3.2 Energieonderzoek Centrum Nederland (ECN) Model

ECN used an updated version of the RELAP5/MOD"0" computer code to perform the calculation. The updates included a steam separator model, steam control valve model and the addition of the Thom correlation for the steam generator secondary heat transfer and a condensation heat transfer correlation for heat transfer to the wall.

3.3 EIDG. Institut für Reaktorforschung (EIR) Models

Two calculations were performed by EIR using the RELAP4/MOD6 computer code. The differences in the models were that for one calculation the volume in the broken loop cold leg was connected to the vessel with two

TABLE 2. PARTICIPANTS AND REPORT IDENTIFIERS

Participant	Report Identifier
Centre d'Etudes Nucleaires de Cadarache Commissariat a L'Energie Atomique Boite Postale No. 1 13-Saint-Paul-Lex-Durance France	CEA
Energieonderzoek Centrum Mederland Netherlands	ECN
EIDG. Institut für Reaktorforschung Institut Federal de Recherches en Matiere de Reacteurs 5303 Wurenlingen Switzerland	EIR1[a] EIR2[b]
Framatome Tour Fiat/Cedex 16/92084 Paris La Defense France	FRA
Gesellschaft für Reaktorsicherheit m.b.H. Forschungsgelände 8046 Garching Germany	GRS
Facolta di Ingegneria Istituto di Impianti Nucleari Via Diotisalvi, 2 56100 Pisa Italy	IDIN
Japan Atomic Energy Research Institute Division of Reactor Safety Evaluation Tokai Research Establishment Japan	JAERI
Los Alamos Scientific Laboratory Department Q-9 P.O. Box 1663 Los Alamos, New Mexico USA	LASL

TABLE 2. (continued)

Participant	Report Identifier
Nuclear Power Company Limited Cambridge Road, Whetstone, Leicester LE83LH United Kingdom	NPCDA[c] NPCBR[d]
United Kingdom Atomic Energy Authority Safety and Reliability Directorate Wigsnaw Lane Culcheth Warrington WA34NE United Kingdom	UKEA
United Kingdom Atomic Energy Establishment AEE Winfrith Dorchester Dorset DT2 8DH United Kingdom	UKEE

a. Four cold leg junctions.

b. Two cold leg junctions.

c. 0.9 HEM.

d. 1.0 HEM

TABLE 3. SUMMARY OF PARTICIPANT MODELS

Participant	Computer Code	Volume	Junctions	Heat Slabs	Transient Time (s)	CPU Time (s)	CPU/s	Computer
CEA	RELAP4/MOD6	23	28	24	1500	11500	7.7	CDC 7600
ECN	RELAP5/MOD"0"	110	120	46	740	N/A	N/A	CDC 176
EIR1	RELAP4/MOD6	31	38	17	307	N/A	N/A	N/A
EIR2	RELAP4/MOD6	31	36	17	700	N/A	N/A	N/A
FRA	FRARELAP	14	14	18	1500	N/A	N/A	N/A
GRS	RELAP4/GRS	52	61	26	2400	N/A	N/A	N/A
IDIN	RELAP4/MOD6	24	30	15	80	N/A	N/A	N/A
JAERI	THYDE-P	43	37	N/A	2000	18000	9.0	FACOM M-200
LASL	TRAC-PD2	120[a]	--	62	2112	14060	6.66	CDC 7600
NPCDA	RELAP4/MOD6	18	24	20	1130	10916	9.66	CDC 7600
NPCBR	RELAP4/MOD6	18	24	20	884	8539	9.66	CDC 7600
UKEA	RELAP4/MOD6	52	60	50	250	15732	62.9	IBM 3033
UKEE	RRELAP-UK MK IV	45	52	28	2130	N/A	N/A	IBM-370-168

a. mesh cells.

junctions and to the adjacent volume in the broken loop cold leg with two junctions (EIR1), whereas, the second model used one junction at these locations (EIR2). This resulted in one model having two more junctions than the second model. Vertical slip was not modeled in either calculation. Critical flow was calculated using the Henry-Fauske and HEM models. The saturated Henry-Fauske multiplier was 0.97 and the subcooled Henry-Fauske multiplier was 0.97. The multiplier on the HEM model was 0.86.

3.4 Framatome (FRA) Model

The FRARELAP computer code was used by FRA to perform the calculation. The FRARELAP was developed from RELAP4/MOD3. RELAP4/MOD3 was modified to include improved analytical models for small break transients. Critical flow was calculated using the Zaloudek model for subcooled conditions and the Moody model for saturated and superheated conditions. A multiplier of 1.0 was used with each model.

3.5 Gesellschaft für Reaktorichenheit (GRS) Model

GRS used the RELAP4/GRS computer code to perform the calculation. RELAP4/GRS is a modification of the RELAP4/MOD3 Update 54 computer code. The models for critical flow and heat transfer were modified. Phase separation was modeled in the pressurizer, steam generator secondary, upper plenum and the broken loop cold leg. Critical flow was calculated using modified Bernoulli and HEM models with a multiplier of 1.0 for each model.

3.6 Instituto di Impianti Nucleani (IDIN) Model

The RELAP4/MOD6 computer code was used by IDIN to perform the calculation. IDIN had acquired the computer code only a short time before submitting their calculation and, therefore, they did not have enough time to complete the entire transient. Phase separation was modeled in all volumes except for the two volumes containing the pumps. Vertical slip was

modeled in the core, the primary side of the steam generator and in the downcomer and lower plenum. Critical flow was calculated using the Henry-Fauske and HEM models with multipliers of 1.0 for each model.

3.7 Japan Atomic Energy Research Institute (JAERI) Model

The calculation was performed by JAERI using the THYDE-P computer code. A time delay model for density changes was used after accumulator injection was initiated. The time delay parameters were proportional to the volume of a node with a time delay of 1 s used for the core nodes. Critical flow was calculated using the Moody model with a multiplier of 0.8.

3.8 Los Alamos Scientific Laboratory (LASL) Model

The TRAC-PD2 computer code was used by LASL to perform the calculation. TRAC-PD2 is the most recent released version of the TRAC computer code. The code features a three-dimensional treatment of the pressure vessel and its internals, two-phase nonequilibrium hydrodynamics models, and flow regime-dependent constitutive equations.

3.9 Nuclear Power Company Limited (NPC) Models

Two calculations were performed by NPC using the RELAP4/MOD6 computer code. The differences in the models for the two calculations were that a multiplier of 0.9 was used for the HEM model for saturated blowdown and the broken loop cold leg was modeled as homogeneous for the first calculation (NPCDA) , whereas, a multiplier of 1.0 was used for the HEM model for saturated blowdown and a phase separation model was used for the broken loop cold leg for the second calculation (NPCBR). For each calculation, the Henry-Fauske model with a multiplier of 1.0 was used for subcooled flow conditions. Bubble rise was modeled in all vertical components.

3.10 United Kingdom Atomic Energy Authority (UKEA) Model

UKEA used the RELAP4/MOD6 computer code to perform the calculation. Phase separation was modeled for volumes with vertical flow, except for the top of the steam generator tubes and the top of the pump simulator. Vertical slip was modeled between stacked volumes and other volumes with vertical flow. Critical flow was calculated with the Henry-Fauske model for subcooled conditions and the HEM model for saturated conditions with a multiplier of 1.0.

3.11 United Kingdom Atomic Energy Establishment (UKEE) Model

The RELAP-UK MK IV computer code was used by UKEE to perform the calculation. RELAP-UK MK IV is an extreme modification of RELAP3. The principle code options used for the calculation were the Bryce two phase slip correlation and the "long-pipe, slip 1.0" option in conjunction with a contraction coefficient of unity for critical flow.

4. SUMMARY OF RESULTS

The comparisons of the participants calculated results with selected LOFT measurements are presented in this section. Results were not submitted from each participant for all the measurements selected, therefore, every participant may not have a result for comparison with measured data. All submitted calculated results were compared with LOFT measurements on the same figure to provide an overall indication of the range of calculated results. To provide additional insight into the comparison of the calculated and measured results, each participants calculated results are compared with LOFT measurements in Appendices B through N. The calculated results were digitized at the INEL to prepare the comparisons and this process may result in some loss of detail in the calculated results. As indicated in Table 3, the time period of the transient calculated by the participants varied from an 80 s calculation by IDIN to a 2400 s calculation by GRS. The effect of the difference in the time of the transient calculation is not included in the summary of results.

The calculated pressure in the upper plenum, broken loop cold leg, broken loop hot leg and the pressurizer are compared with measurements in Figures 6, 7, 8, and 9, respectively. The trends of the comparisons of the upper plenum pressure shown in Figure 6 are typical of all the primary system pressure comparisons. Most participant calculations followed the trend of the depressurization following initiation of the break for the initial 300 s of the transient. The UKEE calculation, however, had a higher pressure than was measured and was also higher than the pressure calculated by the other participants. The depressurization rate in the test increased at about 300 s when the system liquid level decreased below the break orifice and steam flowed out the break increasing the volumetric break flow. Several participants calculated this transition quite accurately, resulting in relatively good agreement between the measured and calculated primary pressure for most of the transient.

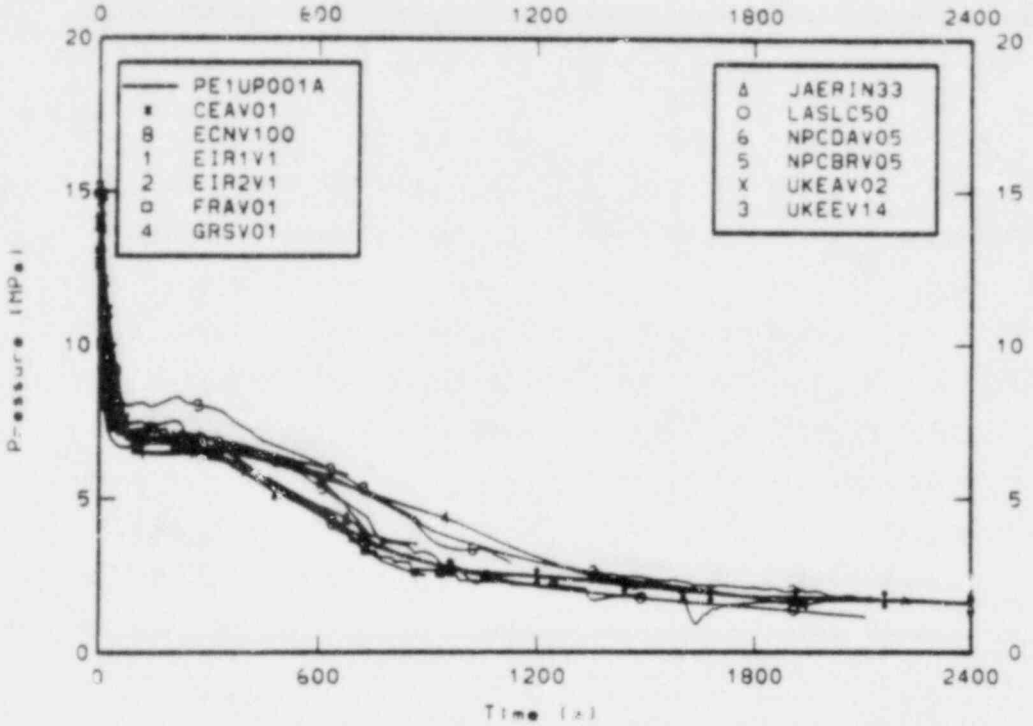

Figure 6. Comparison of measured and calculated upper plenum pressure.

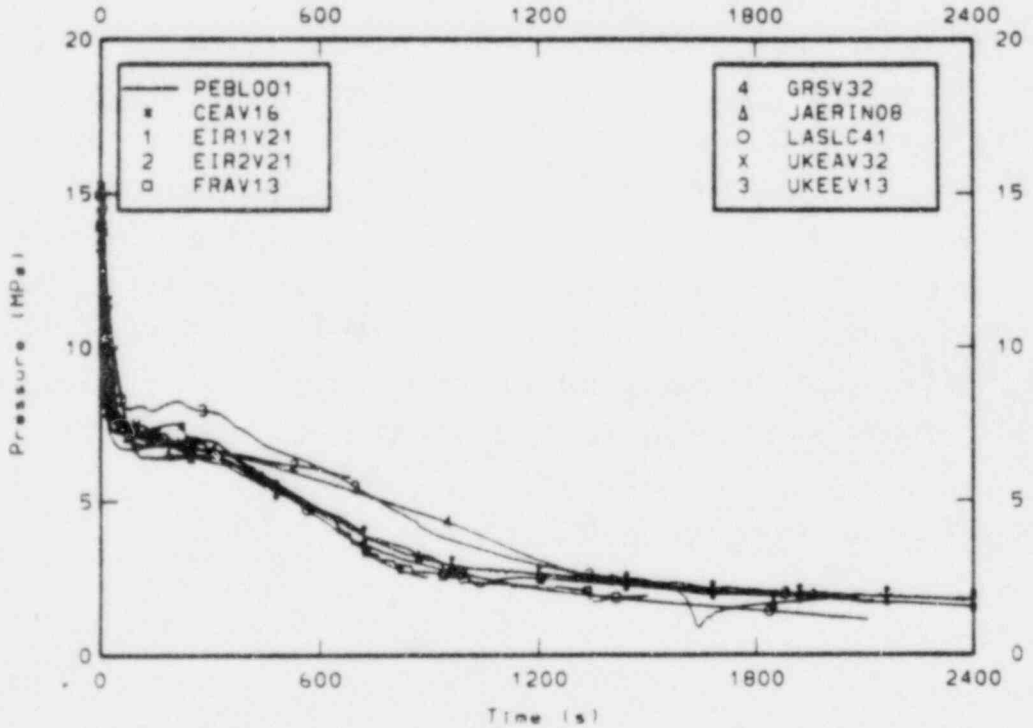

Figure 7. Comparison of measured and calculated broken loop cold leg pressure.

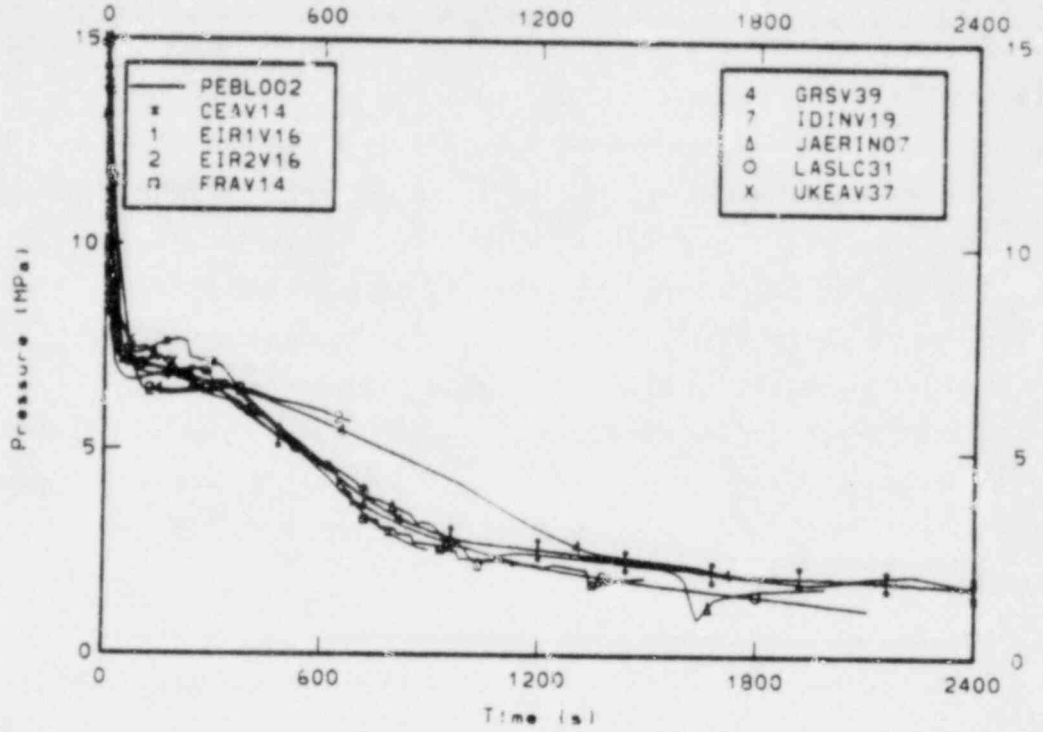

Figure 8. Comparison of measured and calculated broken loop hot leg pressure.

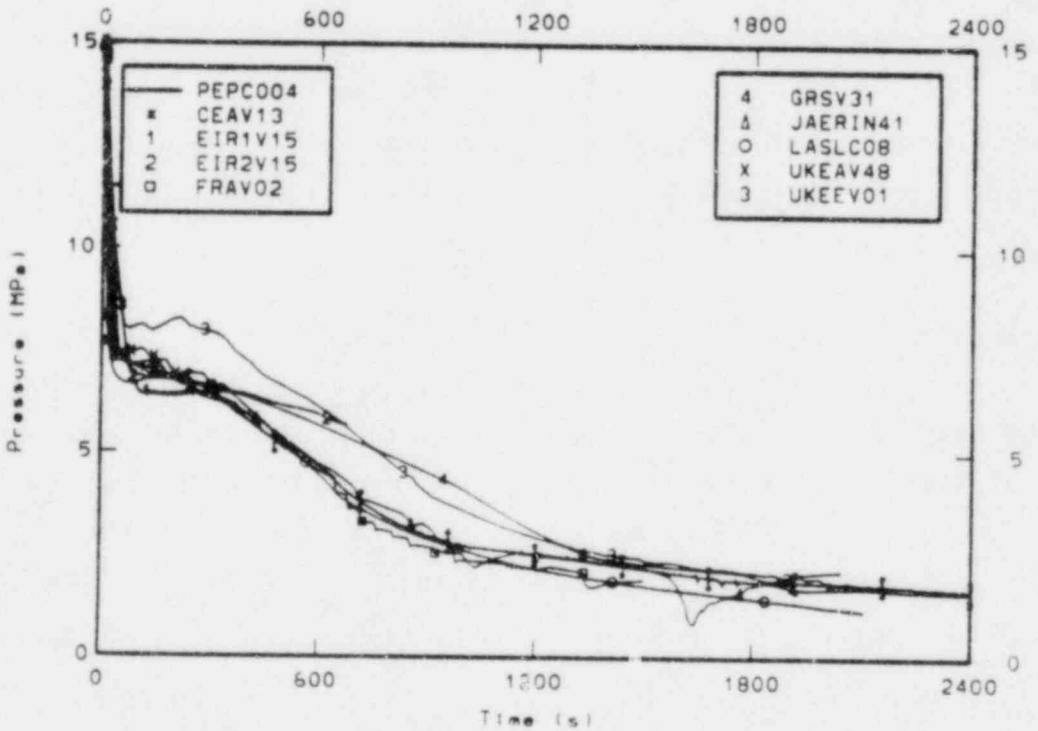

Figure 9. Comparison of measured and calculated pressurizer pressure.

The comparisons between the calculated and measured steam generator secondary pressures are shown in Figure 10. The steam generator secondary pressure increased after scram due to the closing of the main steam flow control valve in the test and in each participants calculation. Auxiliary feedwater flow was initiated at 75 s in the test. This flow cooled the secondary side of the steam generator and caused a decrease in the secondary pressure during the test. The calculated pressure of each participant also decreased at about 75 s as a result of auxiliary feed flow. The secondary pressure calculated by UKEE was as much as 1.8 MPa higher than the measured pressure, whereas, the secondary pressure calculated by GRS, NPC, and JAERI was lower than the measured pressure after about 800 s.

The comparison of the measured and calculated accumulator pressure is shown in Figure 11. Several participants did not calculate the initiation of accumulator injection. The accumulator pressure was initially 4.37 MPa and accumulator flow was initiated at 634 s in the test. The initiation of accumulator flow was calculated accurately by LASL. The calculation by UKEE and the NPC model that used a break flow multiplier of 0.9 with the HEM model resulted in the initiation of accumulator injection about 200 s later than was measured. The NPC model that used a multiplier of 1.0 with the HEM model resulted in accumulator injection about 100 s later than the data. The shape of the pressure curve with the JAERI calculation indicates the flow rate was intermittent, whereas, the experimental results indicate a continuous flow. An intermittent flow was also calculated by both of the NPC models.

The density in the intact loop cold leg, intact loop hot leg and broken loop cold leg are indicated by the measurements shown in Figures 12, 13, and 14 respectively. The measured results shown in Figure 12 are an average calculated from three chordal measurements. The measured results shown in Figures 13 and 14 are chordal measurements. Averages were not calculated at these latter two locations because of the failure of at least one beam of the gamma densitometer. The comparisons shown in Figure 13

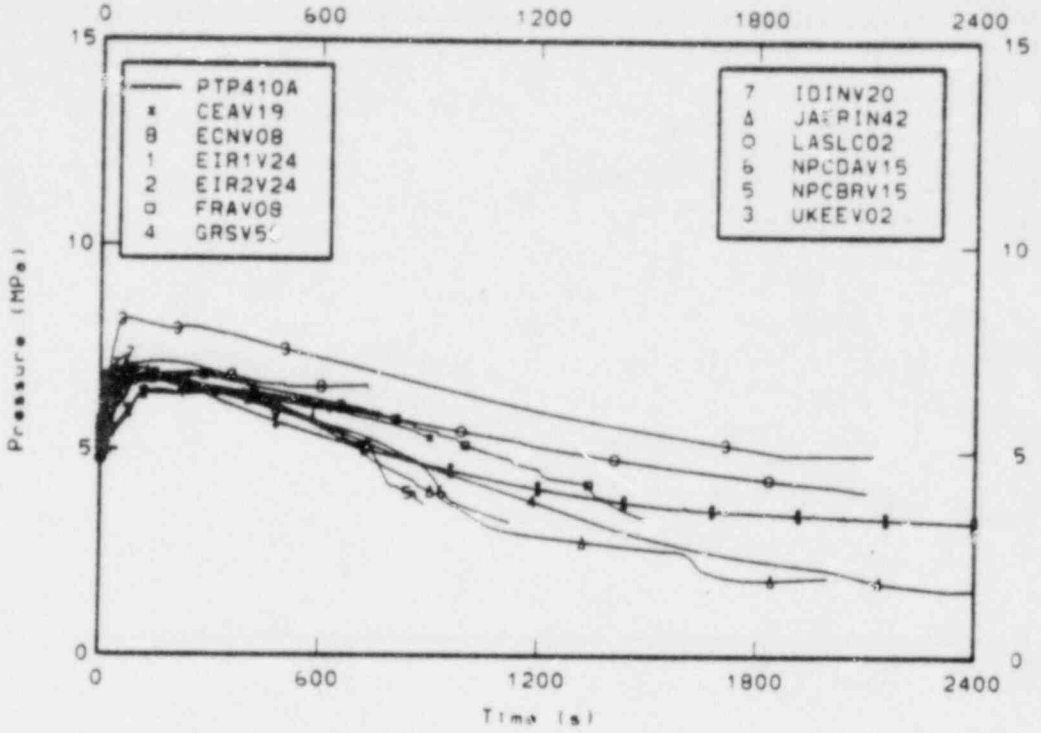

Figure 10. Comparison of measured and calculated steam generator secondary pressure.

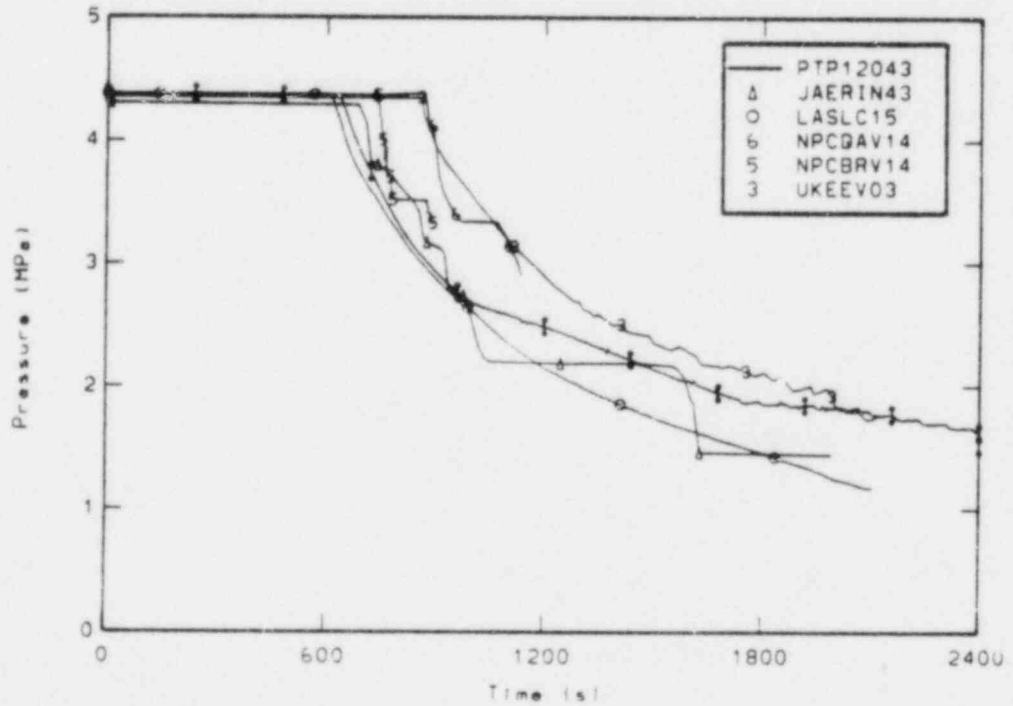

Figure 11. Comparison of measured and calculated accumulator pressure.

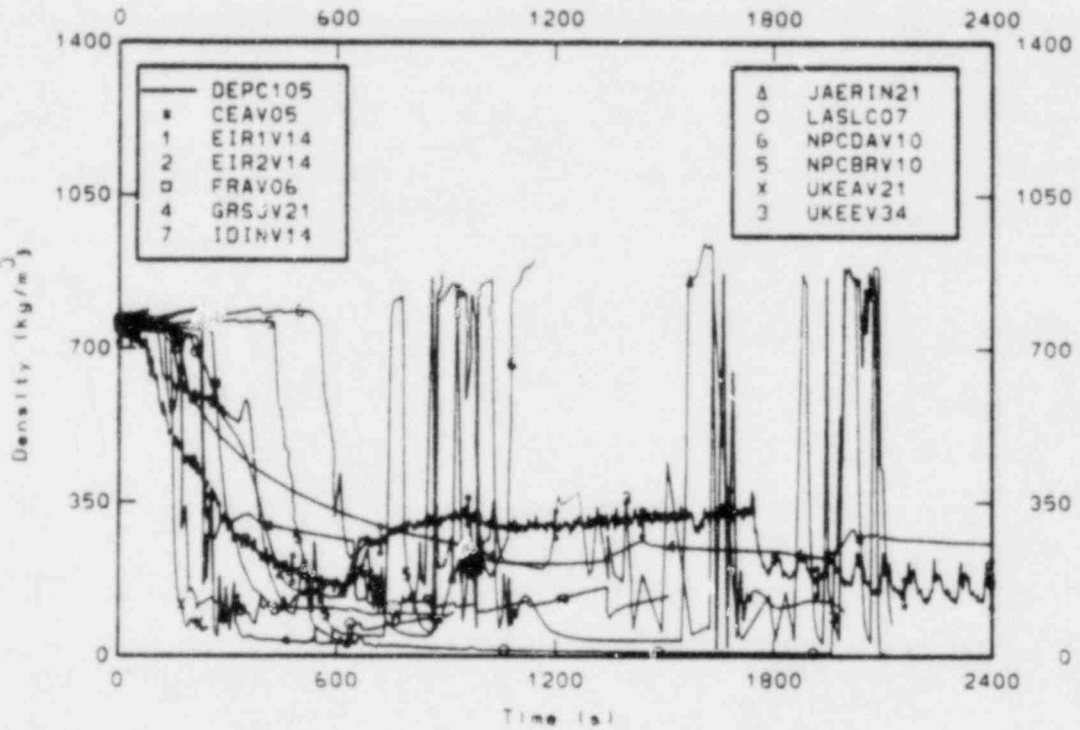

Figure 12. Comparison of measured and calculated average density in the intact loop cold leg.

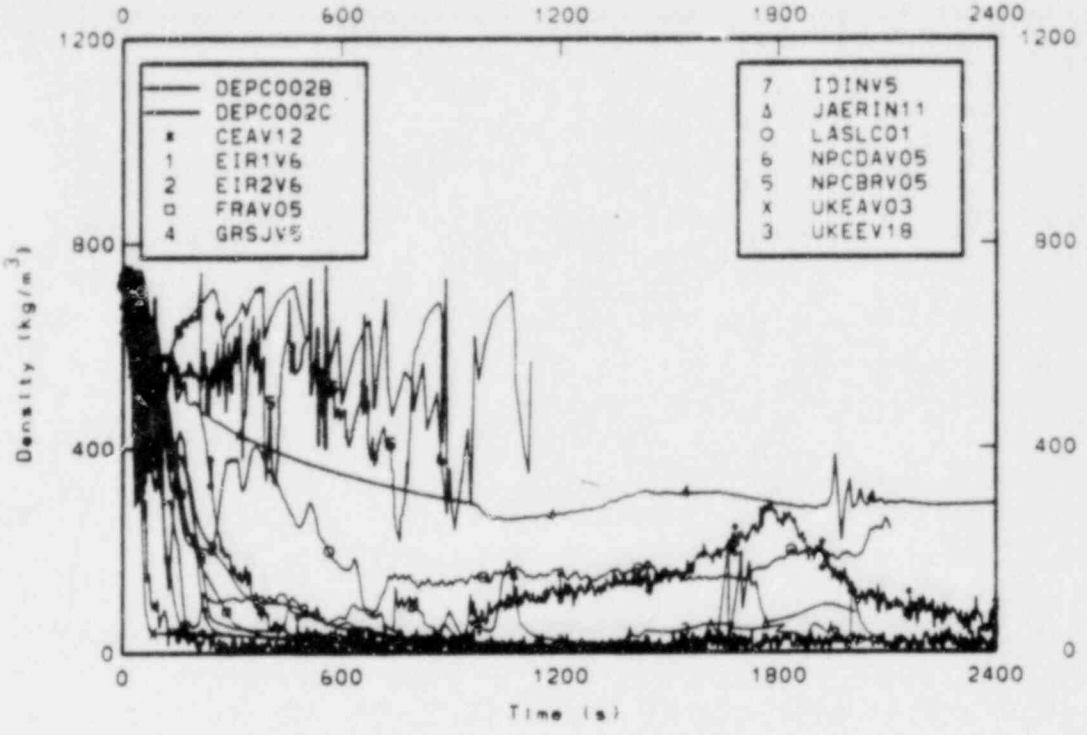

Figure 13. Comparison of measured chordal densities and calculated average density in the intact loop hot leg.

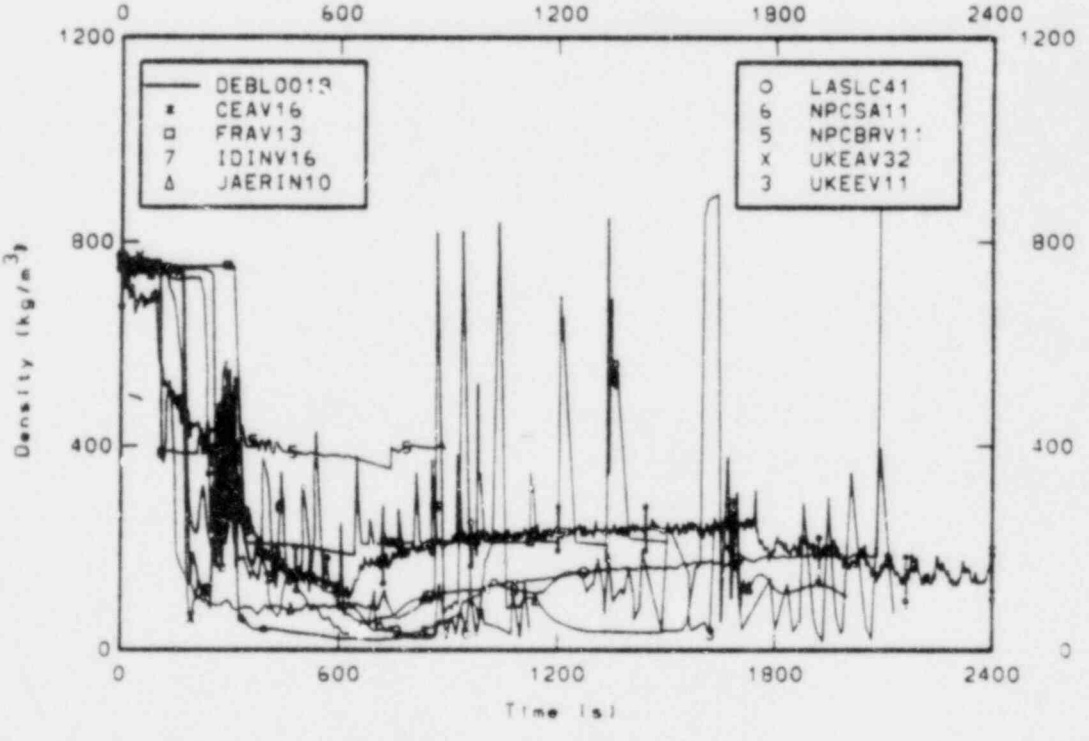

Figure 14. Comparison of measured chordal density and calculated average density in the broken loop cold leg.

indicate that the intact loop cold leg voided earlier in the test than was calculated by the participants. The voiding was calculated by some of the participants to occur over a shorter time period than was measured in the experiment. A slight increase in the average density was measured at accumulator injection. The calculations by NPC indicate the pipe was filled shortly following accumulator injection. The JAERI, UKEE, and LASL calculations indicate the pipe was filled later in the calculation, whereas, the measurements did not indicate the intact loop cold leg refilled.

Two chordal density measurements in the intact loop hot leg and participant calculated intact loop hot leg densities are shown in Figure 13. The chordal density measurements indicate significant voiding in the top section of the pipe at about 30 s in the transient. The chordal density measurement at a midpipe location, the lower data trace, also indicated significant voiding at about 70 s in the transient. The calculation by UKEE, CEA and FRA indicated somewhat more voiding than was measured, whereas, the calculations by NPC, GRS and LASL indicated less voiding than was measured.

The chordal density measurement in the broken loop cold leg and participant calculations are shown in Figure 14. The chordal density measurements corresponds to a midpipe location. The calculated results indicate that most participants calculated the initiation of significant voiding later than was measured. The voiding calculated by NPC was in reasonable agreement with the measurement.

The measured and calculated upper plenum fluid temperatures are compared in Figure 15. The test measurements and most participants calculated temperature decrease following the reactor scram and initiation of the test and remained near the system saturation temperature. The GRS calculation resulted in an initial increase in the upper plenum temperature from about 500 to 1200 s in the transient the fluid temperature calculated by GRS was above the measured temperature. Several 60 K spikes in the

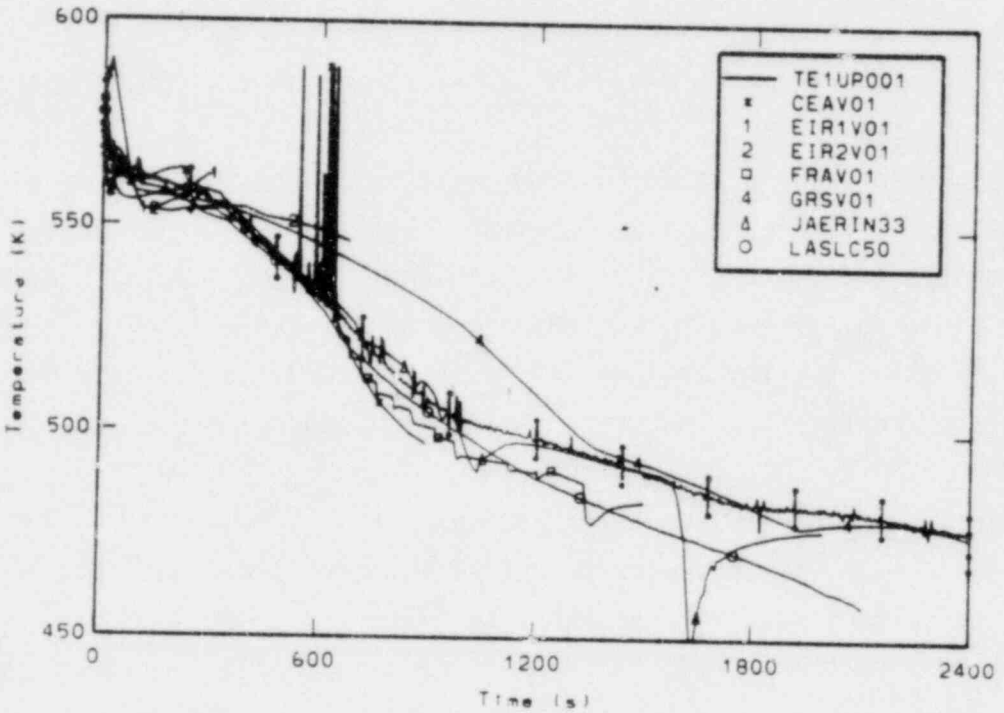

Figure 15. Comparison of measured and calculated upper plenum fluid temperature.

upper plenum fluid temperature were calculated by CEA between 550 s and 650 s. A 50 K subcooling of the upper plenum fluid at about 1600 s was calculated by JAERI. Neither of these phenomena occurred in the measurements.

The comparison of the measured and calculated lower plenum temperature are shown in Figure 16. The measured and calculated temperature in general were near the system saturation temperature. However, the LASL calculation indicated significant subcooling after accumulator injection initiation at about 630 s. The JAERI calculation indicated a large increase in subcooling at about 1600 s. This increase in subcooling in the JAERI calculation resulted from a large surge in the flow from the accumulator.

The measured and calculated fluid temperature in the broken loop cold leg are compared in Figure 17. The measured temperature remained at the initial value for the first 300 s of the transient and then decreasd as the system saturation temperature decreased. Some participants calculated a slight drop in the fluid temperature at the initiation of the test and then the temperature decreased as the system saturation temperature decreased.

A comparison of the measured and calculated mass flow out the break is shown in Figure 18. The calculated mass flow rates ranged from about 12 to 23 kg/s at the initiation of the break. The measured value was about 18 kg/s. There were significant differences in the trend and the magnitude of the calculated results. The trend of the data which indicated an initial drop from 18 kgs/ to about 13 k/s and then an increase to 15 kg/s is different than the trends of most of the calculations. The increase in the measured mass flow rate was attributed to the measurement technique and is not considered to be caused by a physical process. The mass flow rate could be expected to remain relatively constant during this period rather than increase. The overall agreement between the measured and calculated mass flow rate was poor.

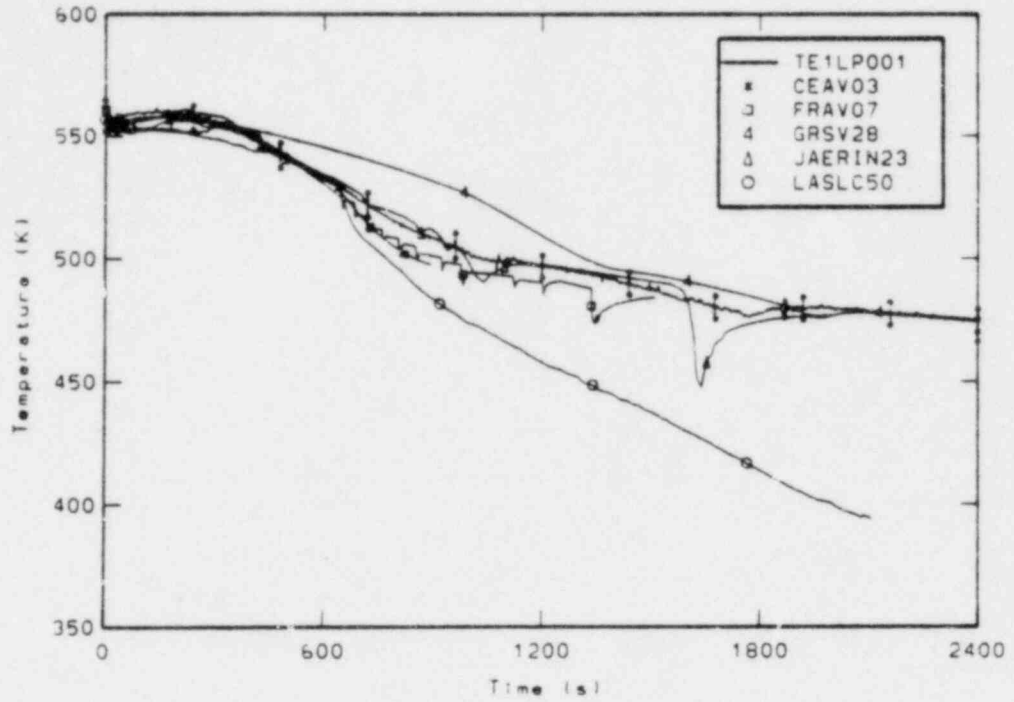

Figure 16. Comparison of measured and calculated lower plenum fluid temperature.

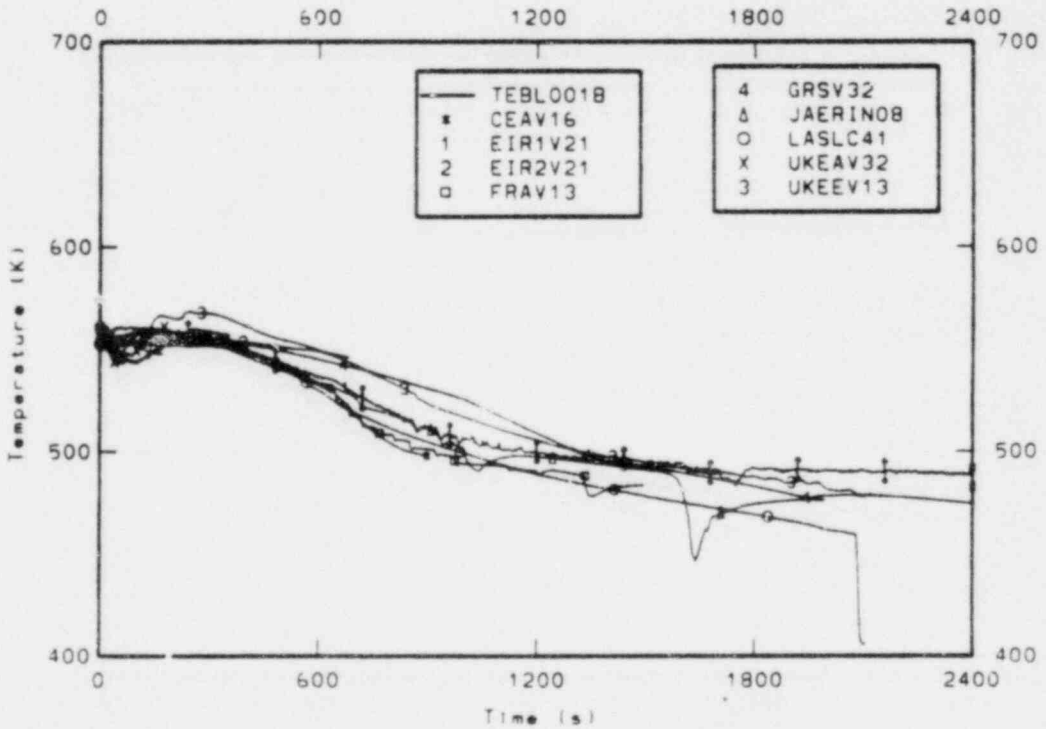

Figure 17. Comparison of measured and calculated broken loop cold leg fluid temperature.

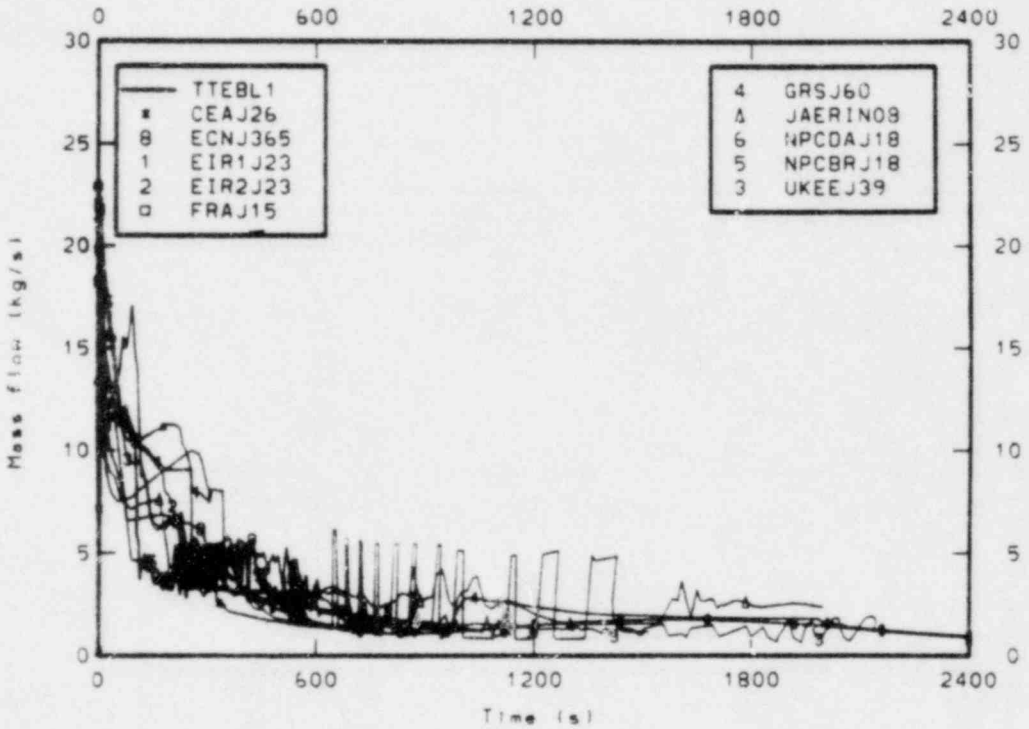

Figure 18. Comparison of measured and calculated mass flow rate at the break.

The measured and calculated rod cladding temperatures at the 20, 66, 104 and 147 cm elevations are compared in Figures 19, 20, 21 and 22, respectively. Except for calculations submitted by EIR, UKEA and UKEE, there were no calculated increases in the rod cladding temperature. The cladding temperatures essentially followed the system saturation temperature. For the EIR calculations the rod cladding temperatures at all elevations in the core were rapidly increasing when the calculations were terminated for each model. UKEA calculated rod cladding temperature increase at about 115 s and a subsequent quench at 210 s. A hot rod calculation performed by UKEA indicated a peak clad temperature of 692 K. The UKEE calculation resulted in a temperature increase in the upper core elevation (1.47 m) at about 575 s and a quench at about 880 s. A hot rod calculation performed by UKEE indicated a peak clad temperature of 1054 K at 880 s.

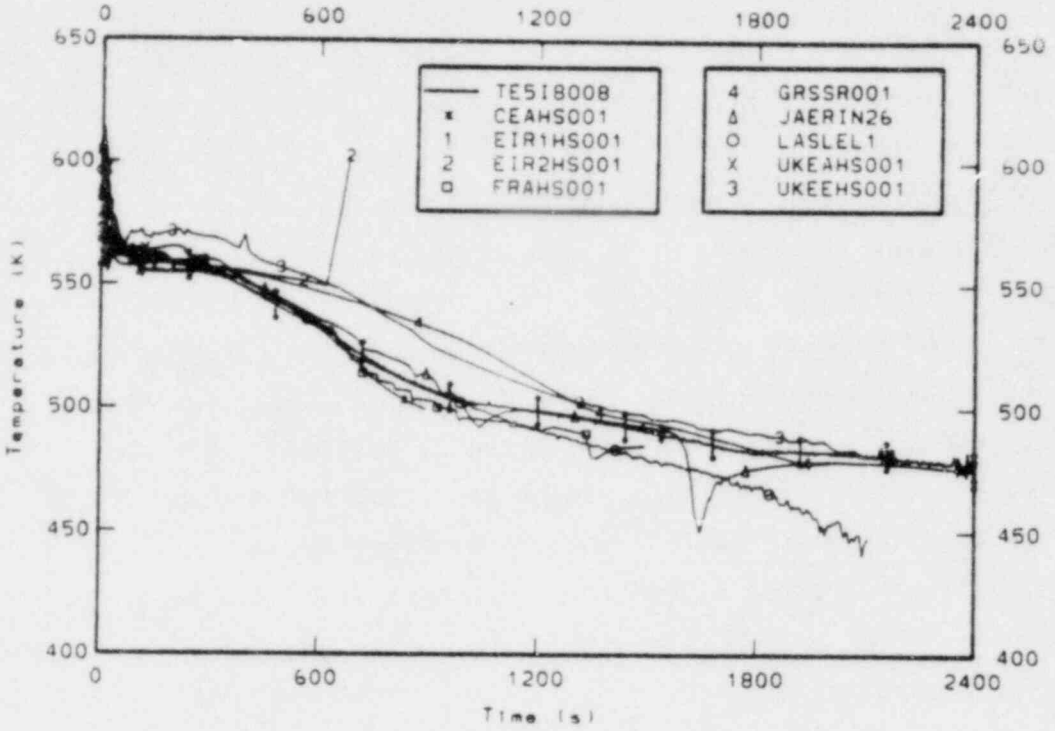

Figure 19. Comparison of measured rod cladding temperature at the 0.20m elevation and calculated rod cladding temperature.

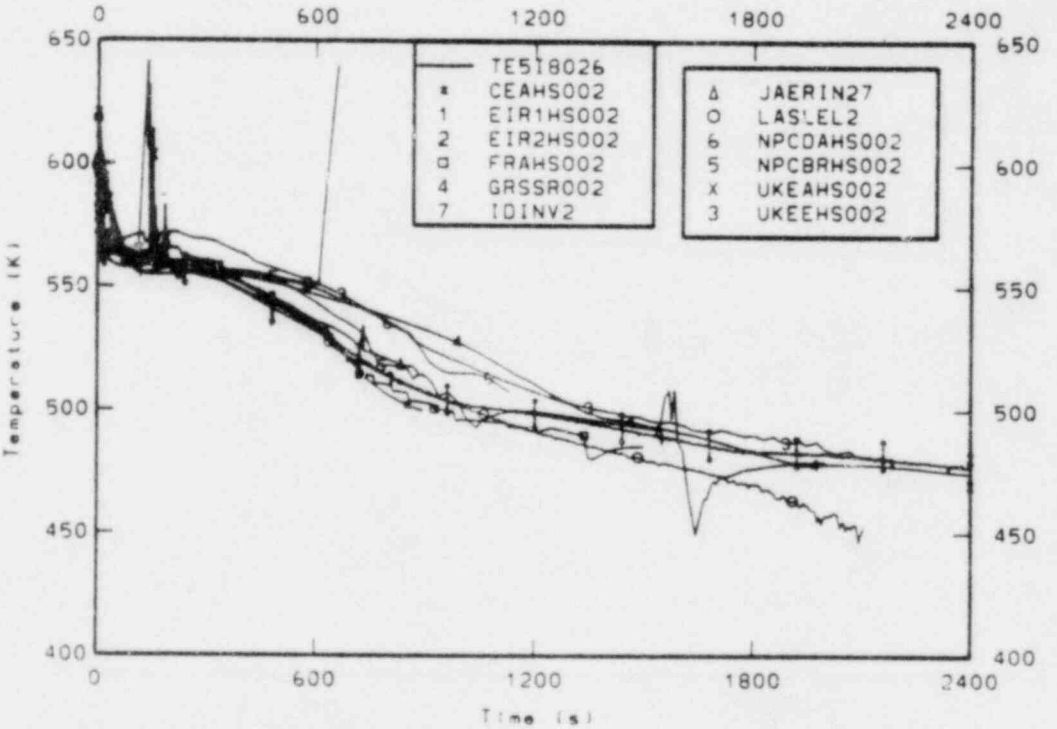

Figure 20. Comparison of measured rod cladding temperatures at the 0.66m elevation and calculated rod cladding temperatures.

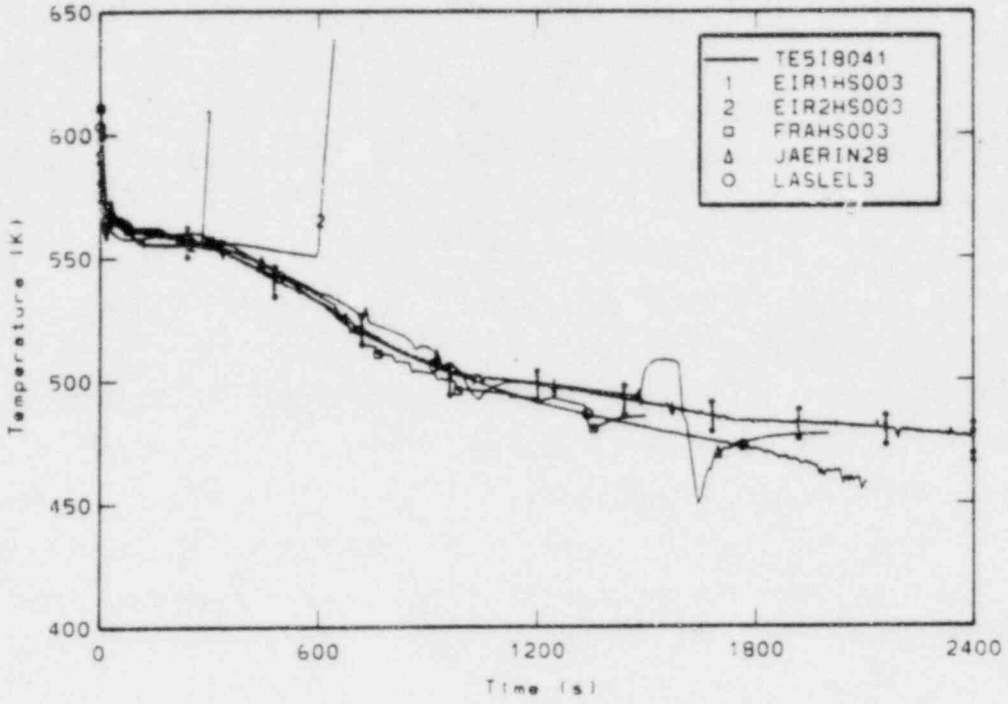

Figure 21. Comparison of measured rod cladding temperatures at the 1.04m elevation and calculated rod cladding temperatures.

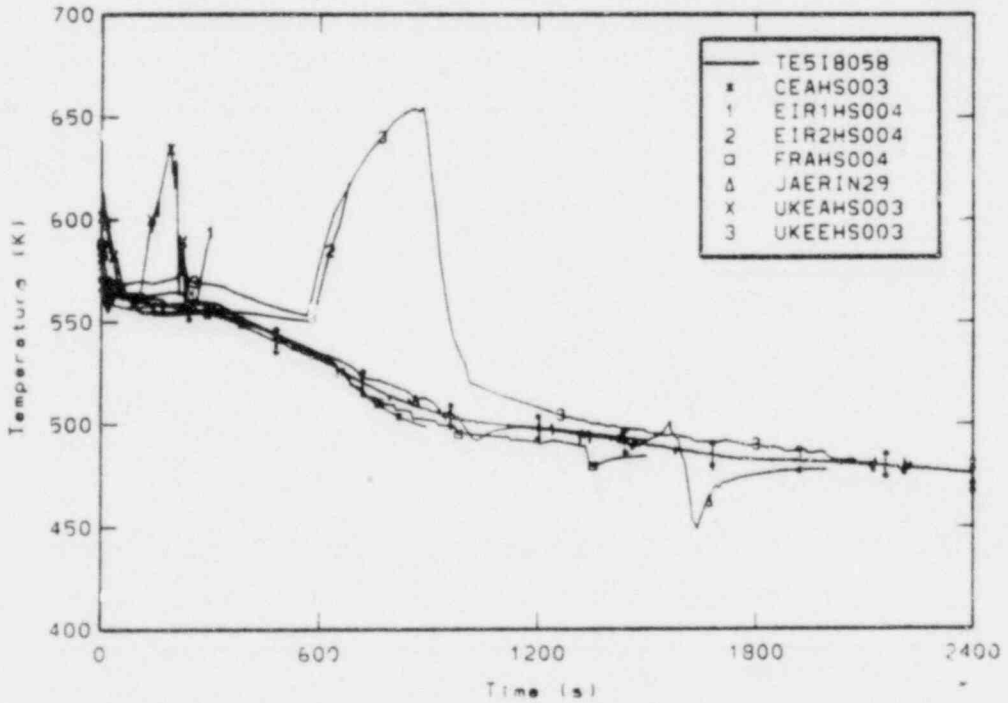

Figure 22. Comparison of measured rod cladding temperature at the 1.47m elevation and calculated rod cladding temperature.

5. CONCLUSIONS

Comparisons between measurements from LOFT Test L3-1 and calculations from eleven participants using seven different computer codes have lead to the following conclusions.

The system pressure during the initial 300 s of the transient was calculated satisfactorily by most participants, whereas, later in the transient the agreement was not good for some participants. The measured system depressurization increased at about 300 s when the volumetric flow out the break increased due to the system liquid level decreasing below the break orifice and steam flowing out the break. Several participants calculated this transition quite accurately and relatively good agreement with measurements was obtained. The participants that did not calculate this transition and the increased depressurization calculated a higher pressure than was measured.

The trends of the secondary pressure response were calculated by most participants. However, a higher pressure was generally calculated than was measured during the initial 700 s of the transient. After about 700 s, some participants calculated a lower pressure than was measured.

The initiation of voiding in the loops of the primary system was generally calculated by all participants to occur later than was measured. Several participants calculated signficantly less voiding of the intact loop hot leg than was indicated by measurements.

Significant differences between the measured and calculated mass flow rate at the break occurred. In general, the trend and magnitude of the mass flow rate were not calculated. Significant differences in the calculated break mass flow rate were obtained.

Most participants calculated the response of the rod cladding temperatures. The measured rod cladding temperatures were near the system

saturation temperature for most of the transient. This response was calculated by most participants, however, a core heatup was obtained with four of the calculations.

REFERENCES

1. P. D. Bayless et al., Experiment Data Report for LOFT Nuclear Small Break Experiment L3-1, NUREG/CR-1145, EGG-2007 (January 1980).

2. D. L. Reeder, LOFT System and Test Description (5.5 ft Nuclear Core 1 LOCEs), NUREG/CR-0247, TREE-1208 (July 1978).

APPENDIX A

PARTICIPANT NODALIZATION DIAGRAMS

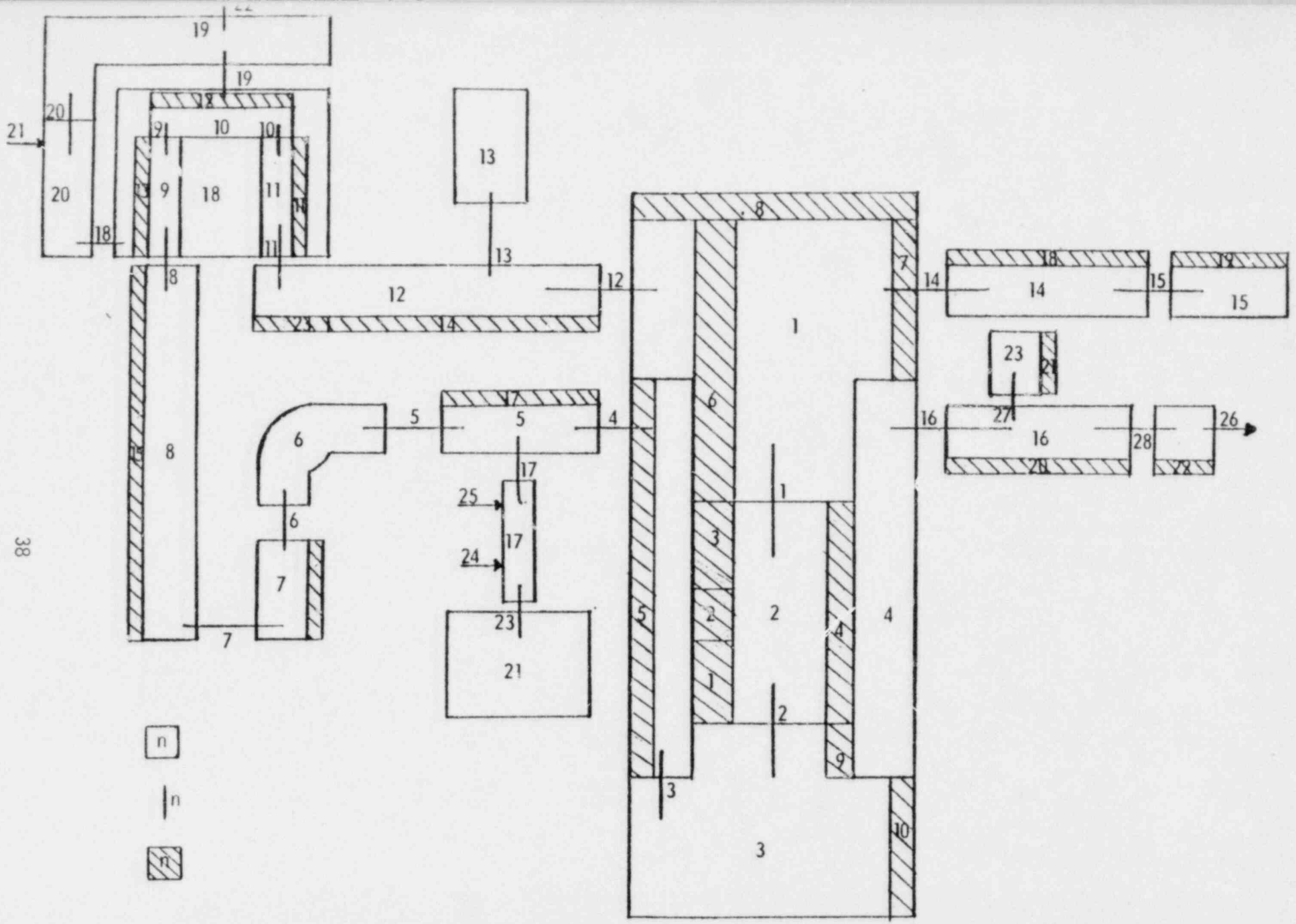

Figure A-1. CEA system nodalization.

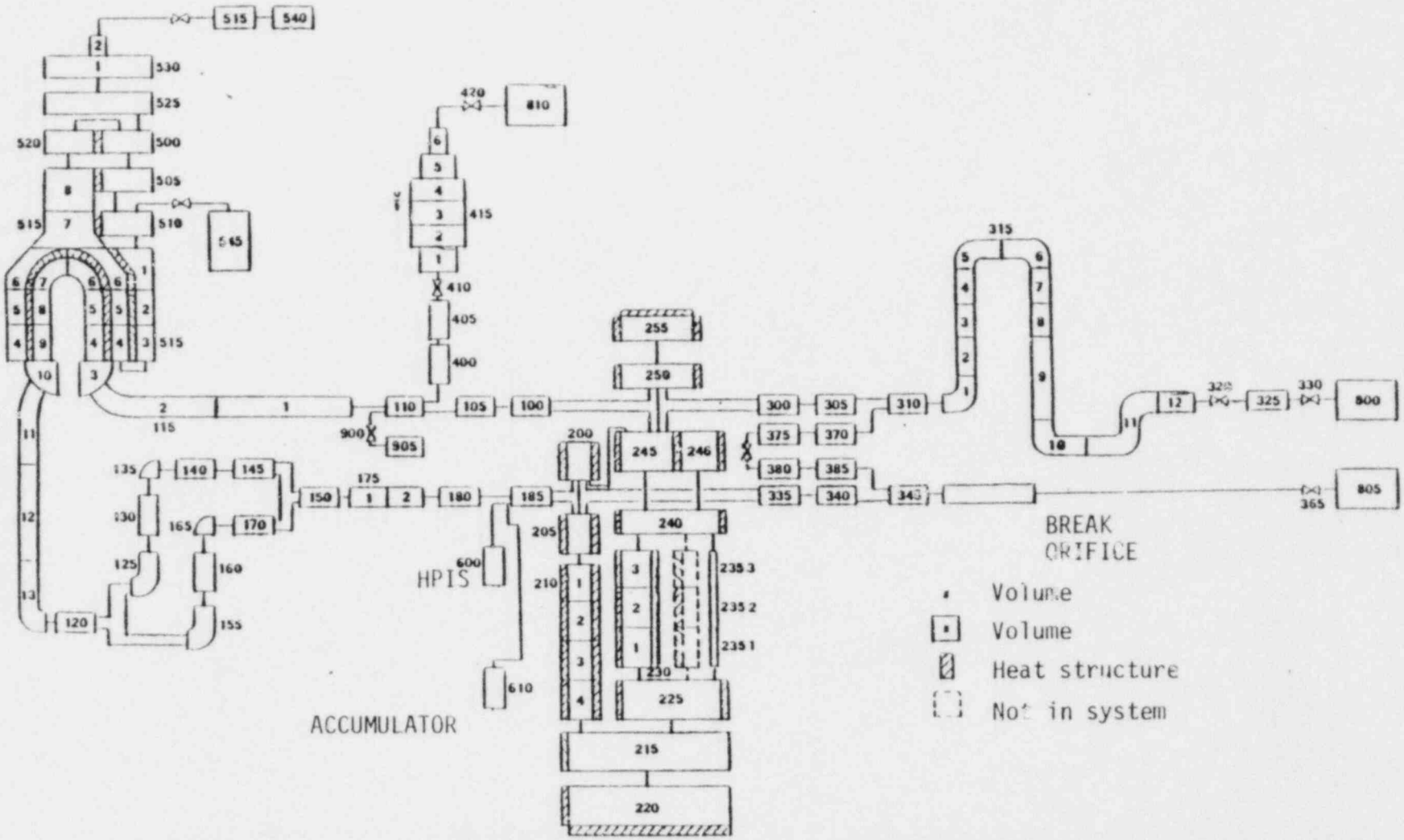

Figure A-2, ECN system nodalization.

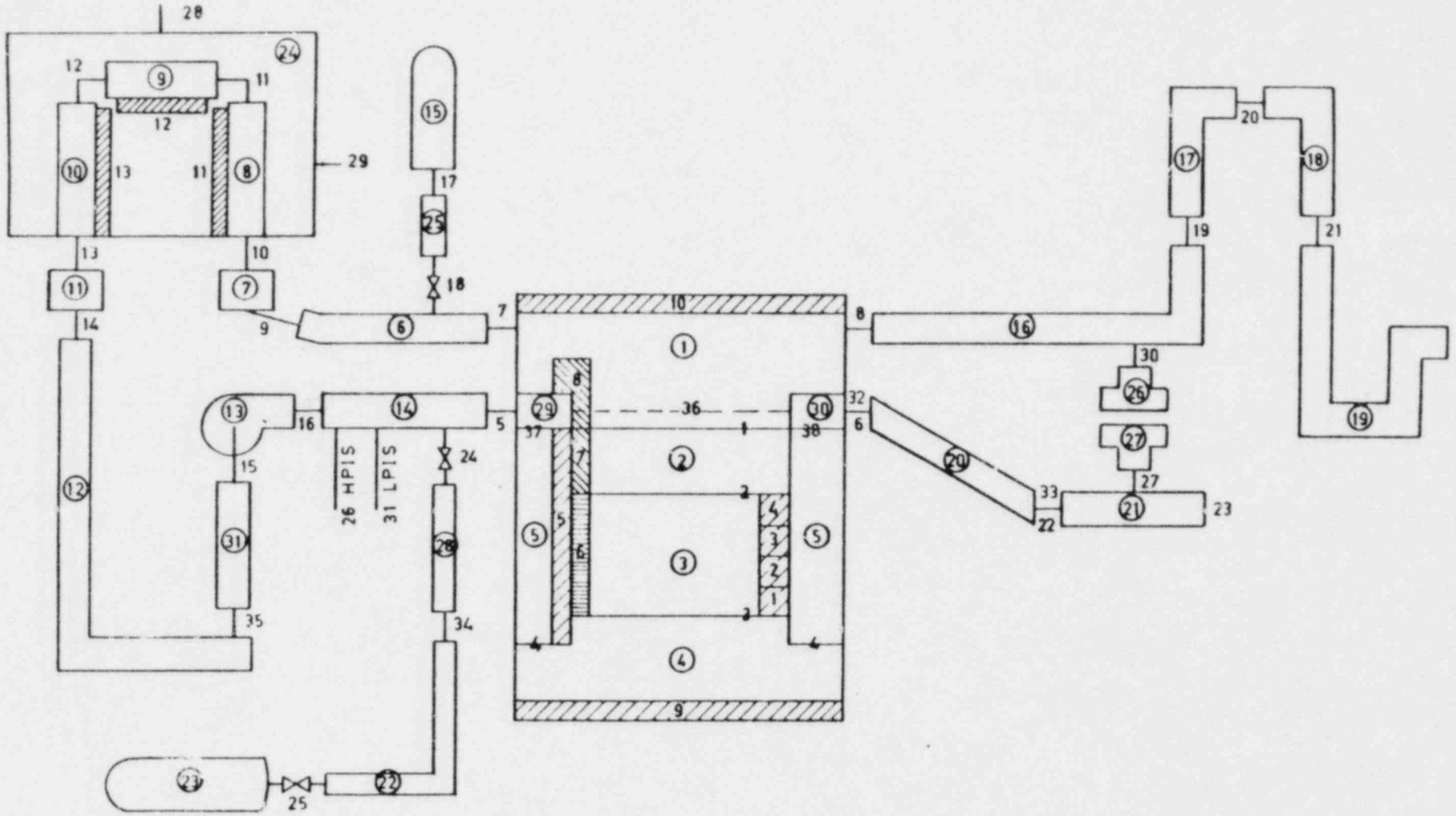

Figure A-3. EIR1 system nodalization.

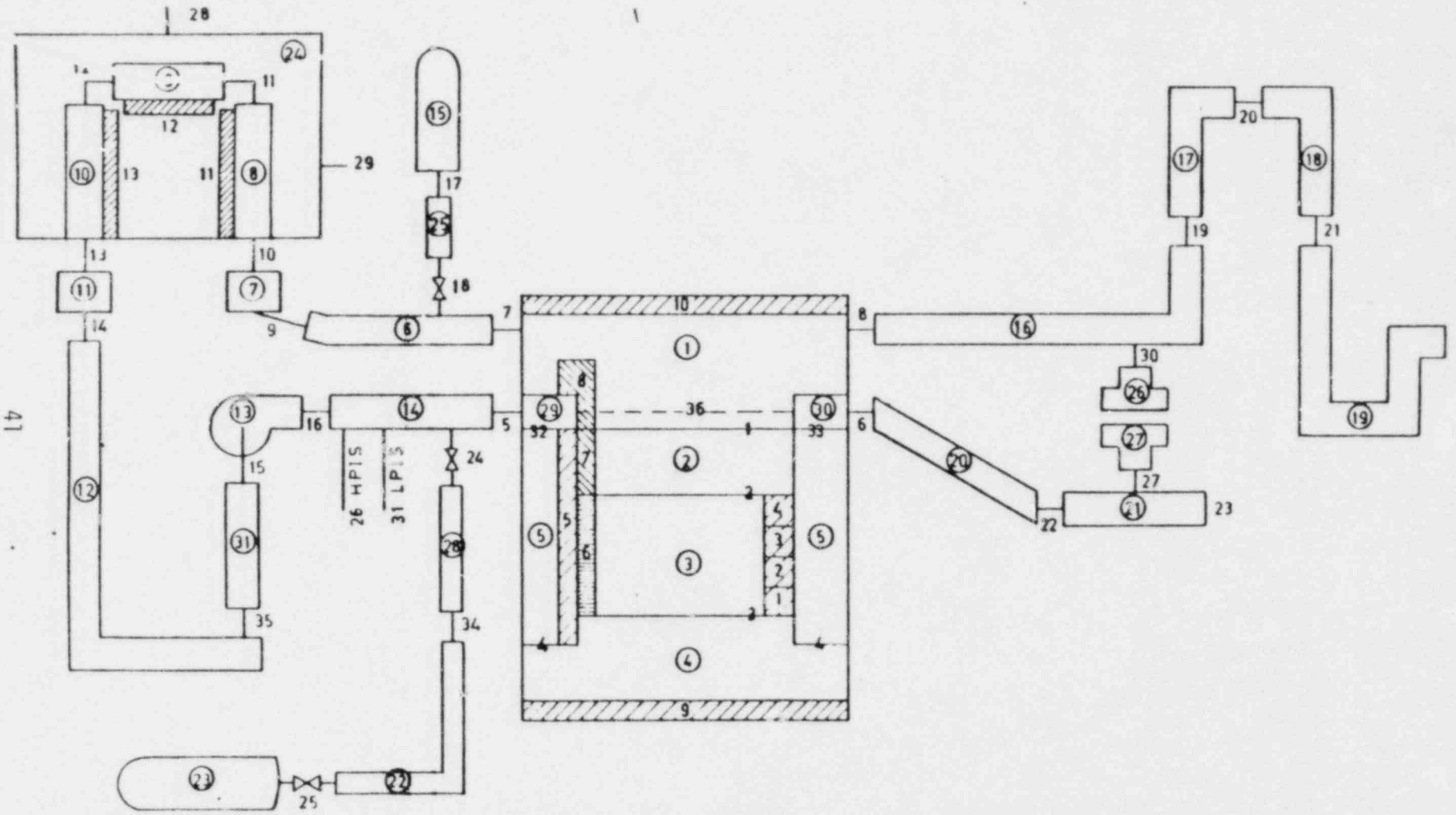

Figure A-4. EIR2 system nodalization.

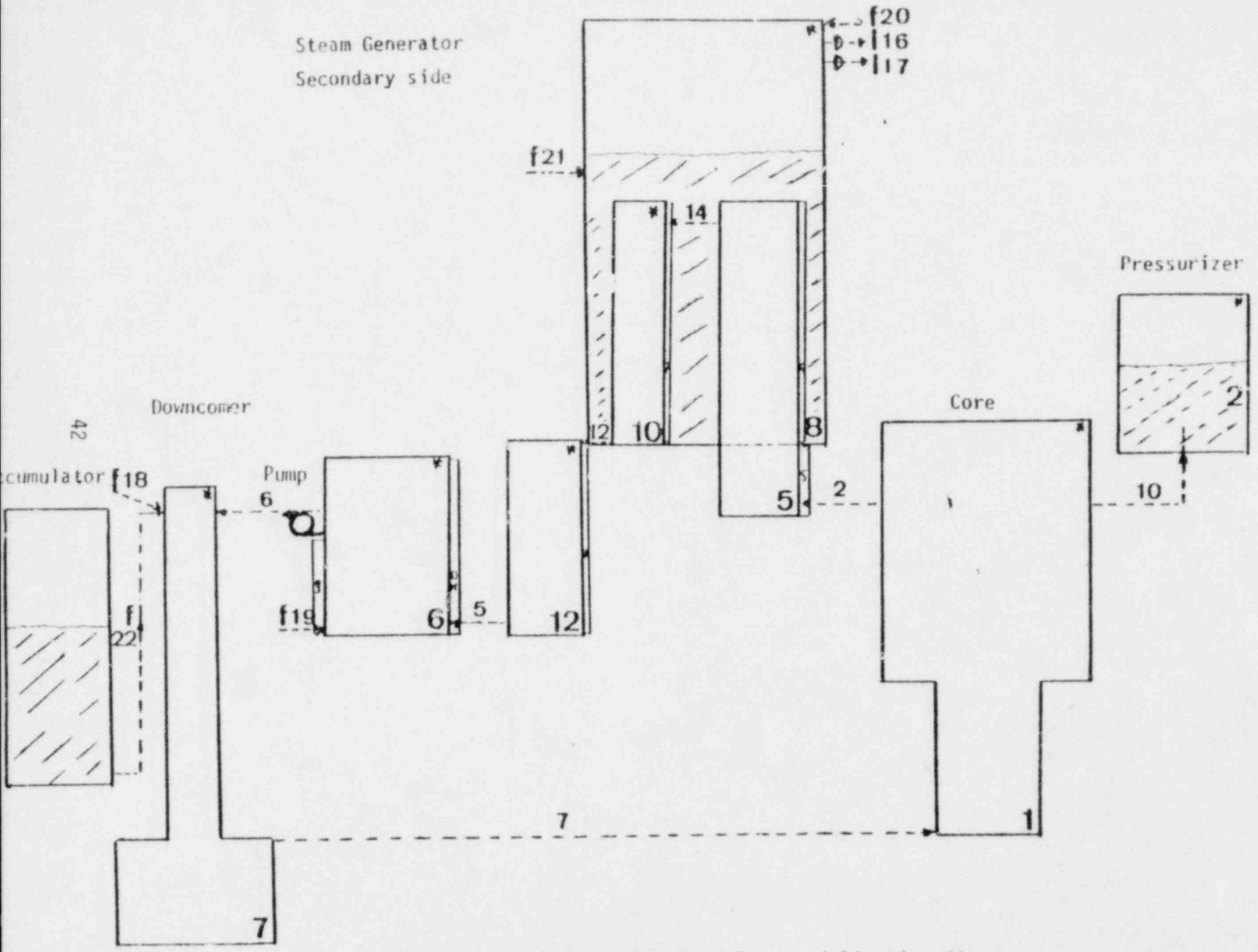

Figure A-5. FRA intact loop nodalization diagram.

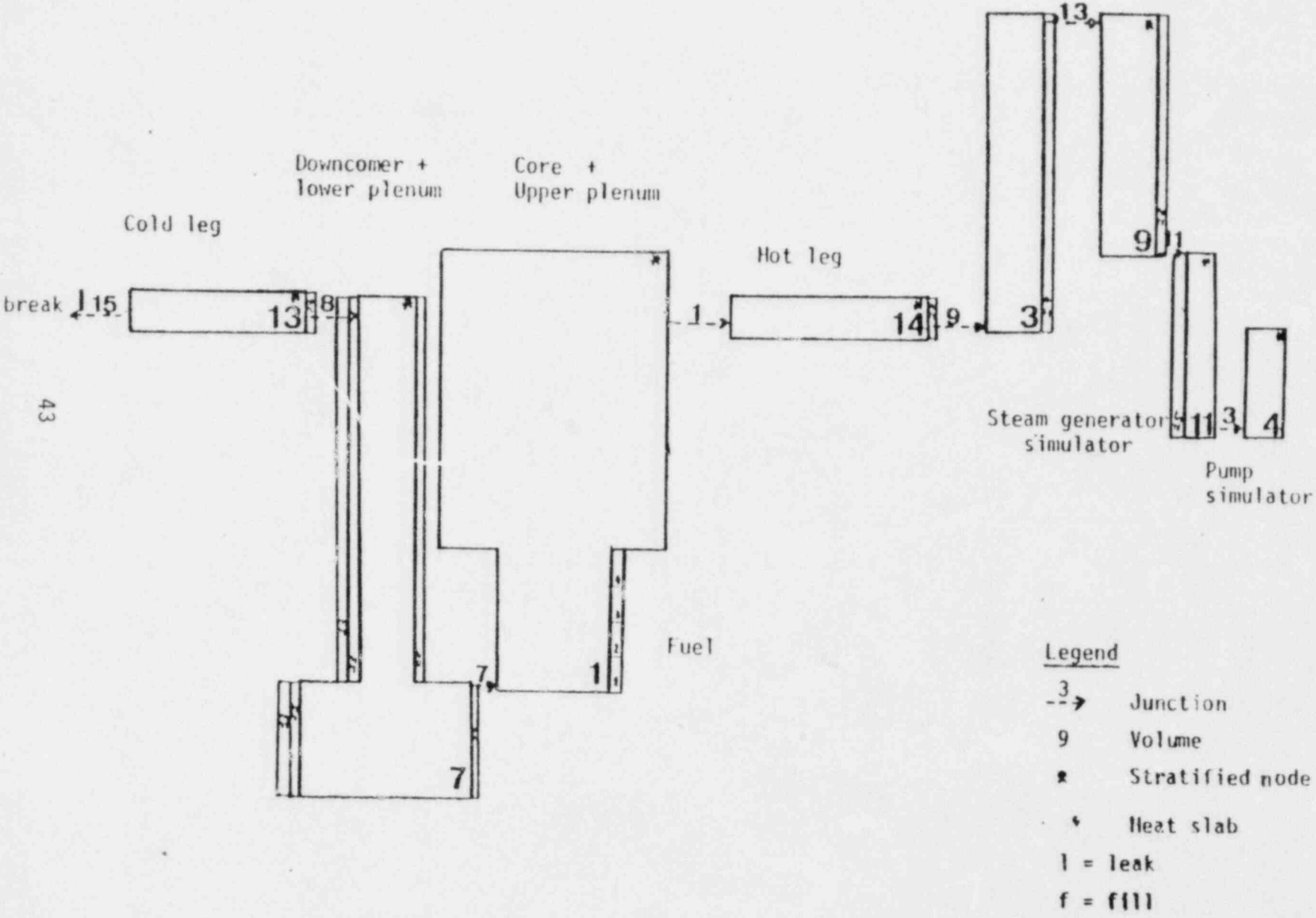

Figure A-6. FRA broken loop nodalization diagram.

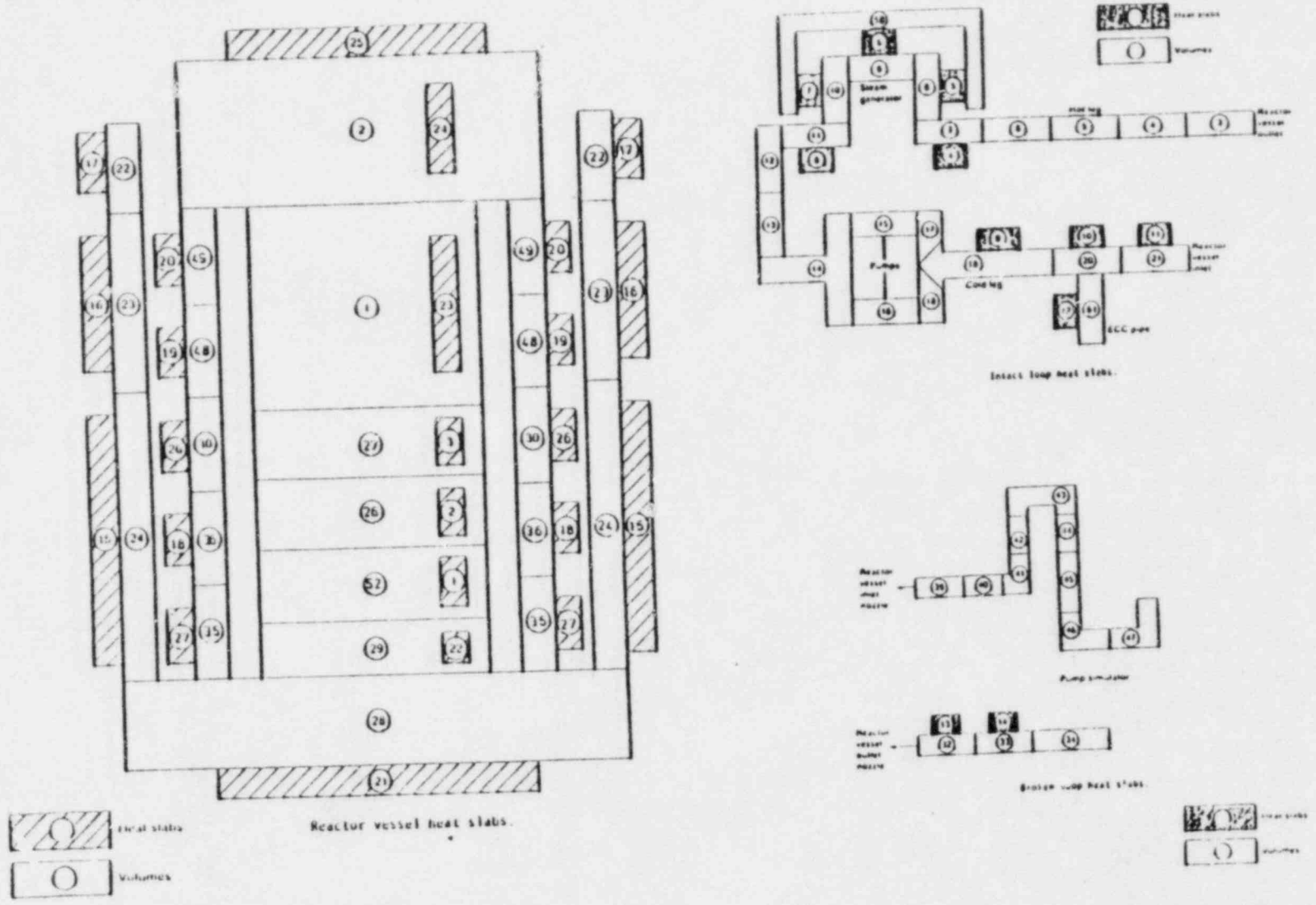

Figure A-7. GRS system nodalization diagram.

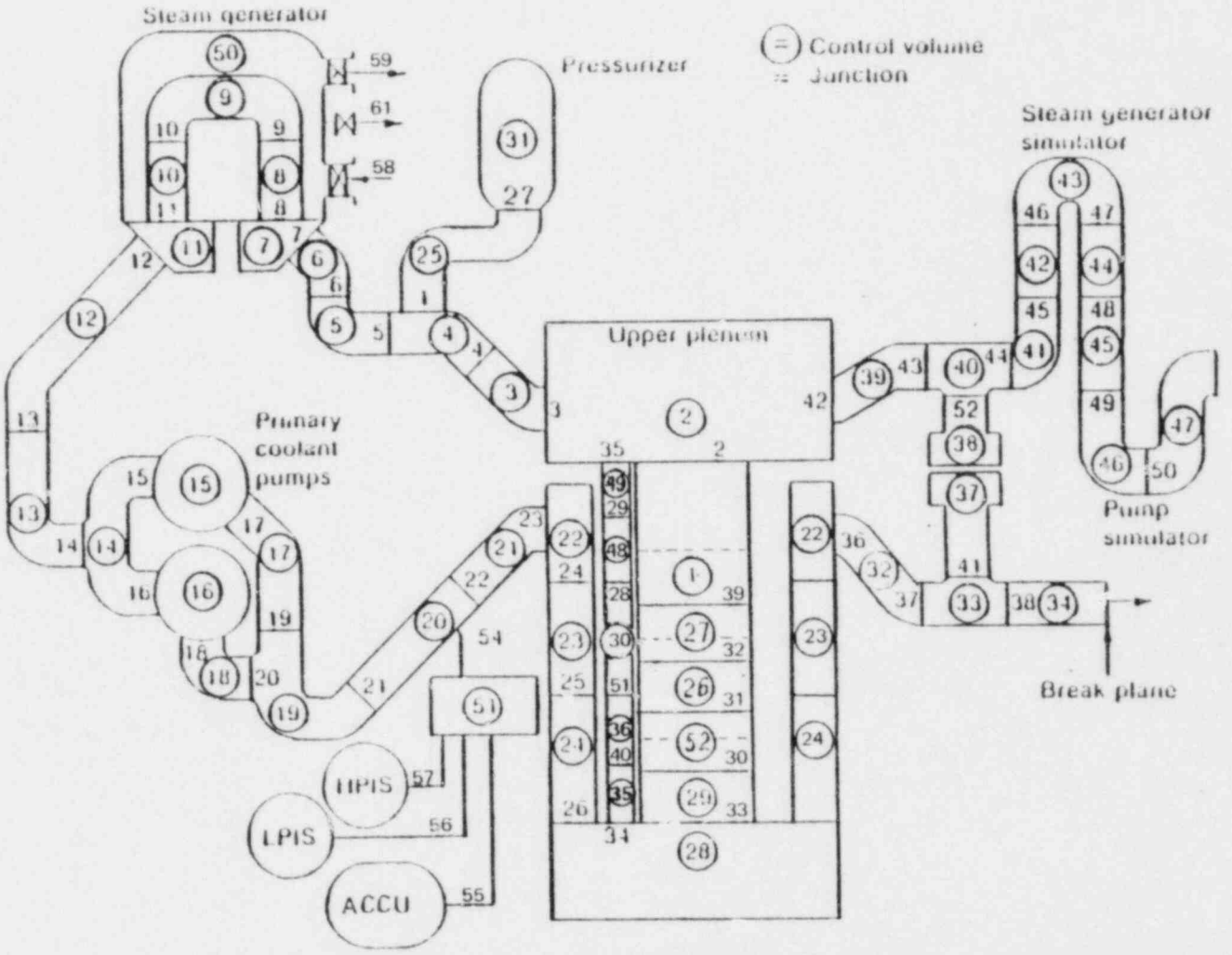

Figure A-8. GRS heat slab nodalization diagram.

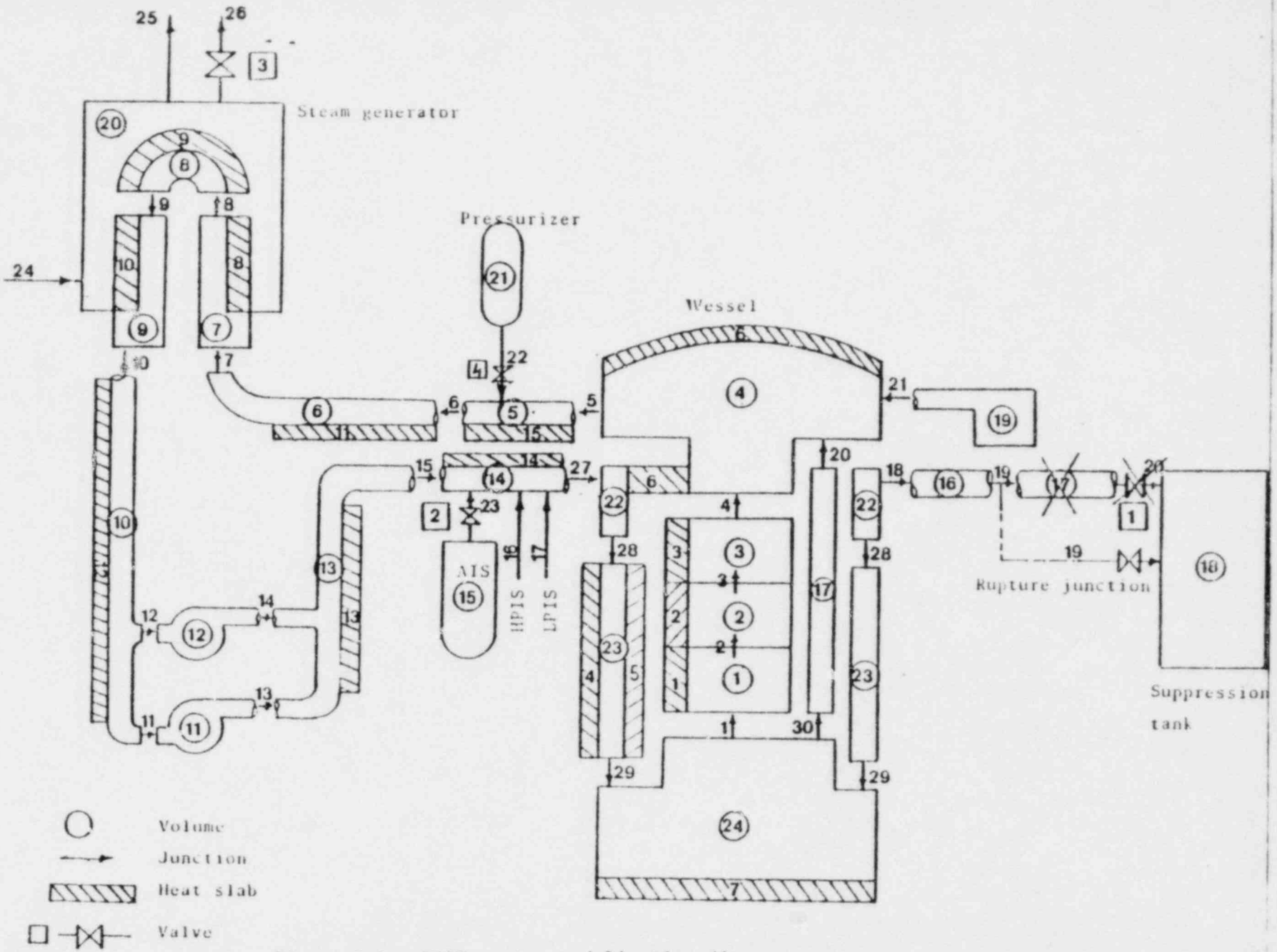

Figure A-9. IDIN system nodalization diagram.

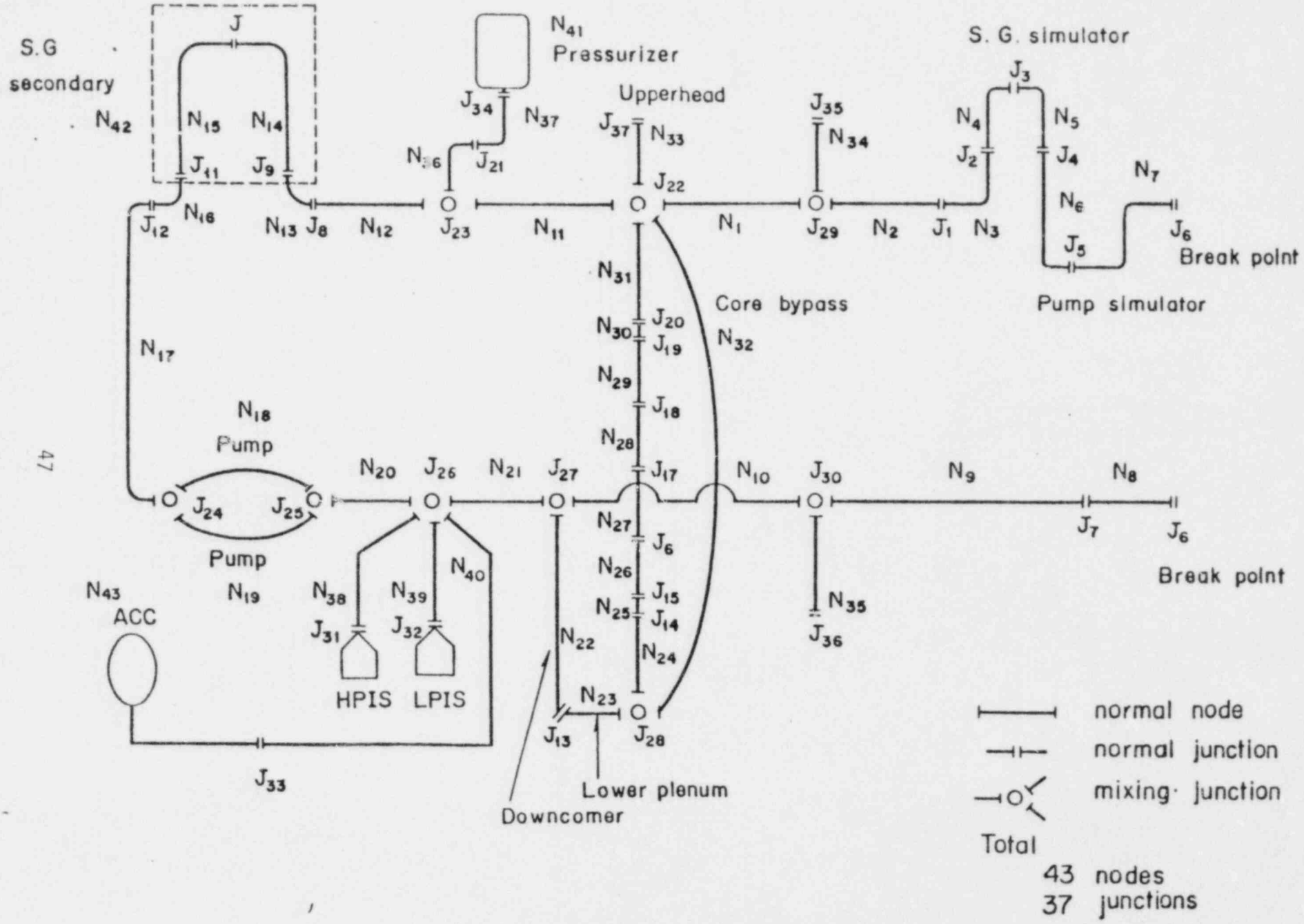

Figure A-10. JAERI system nodalization diagram.

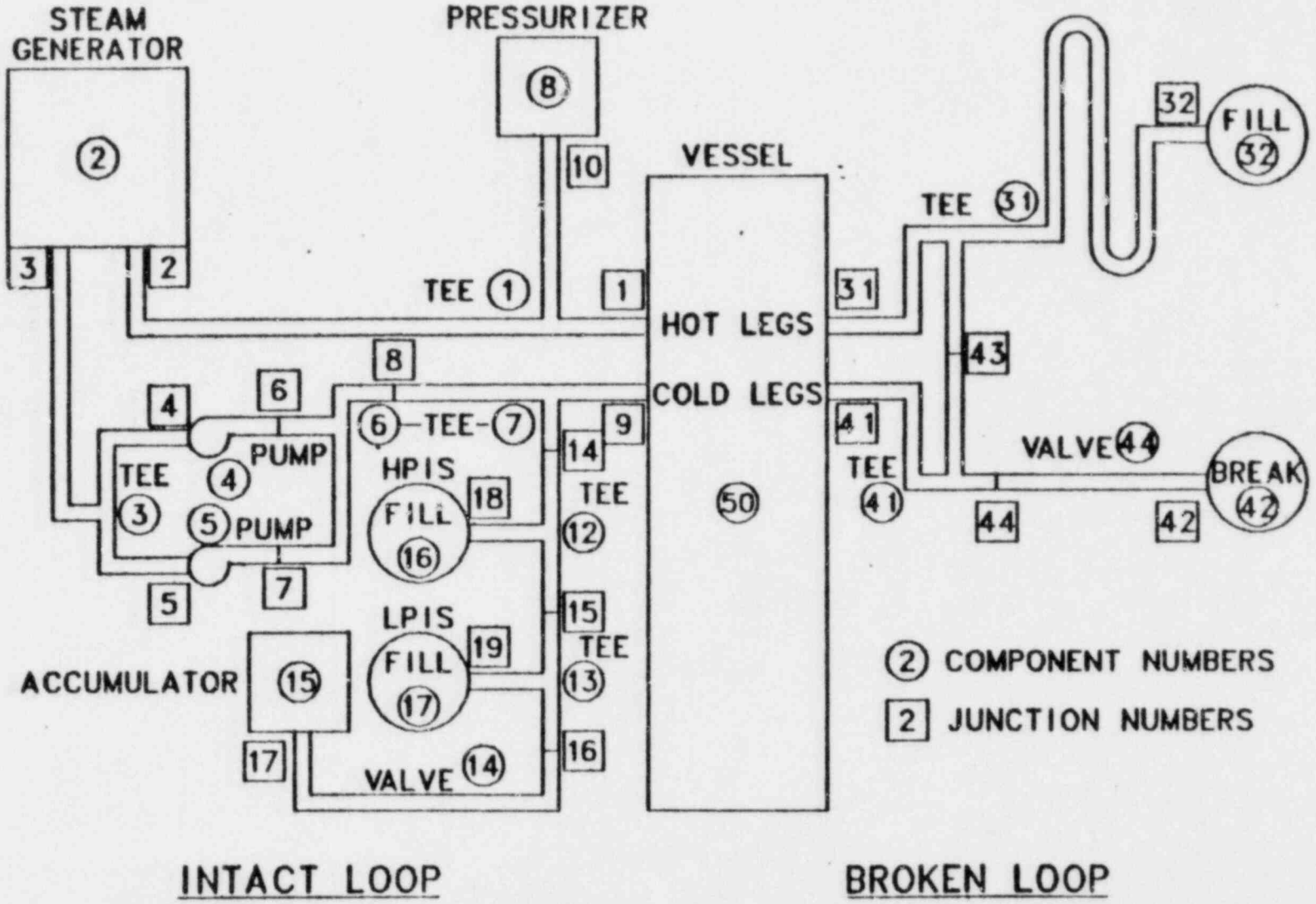

Figure A-11. LASL system nodalization diagram.

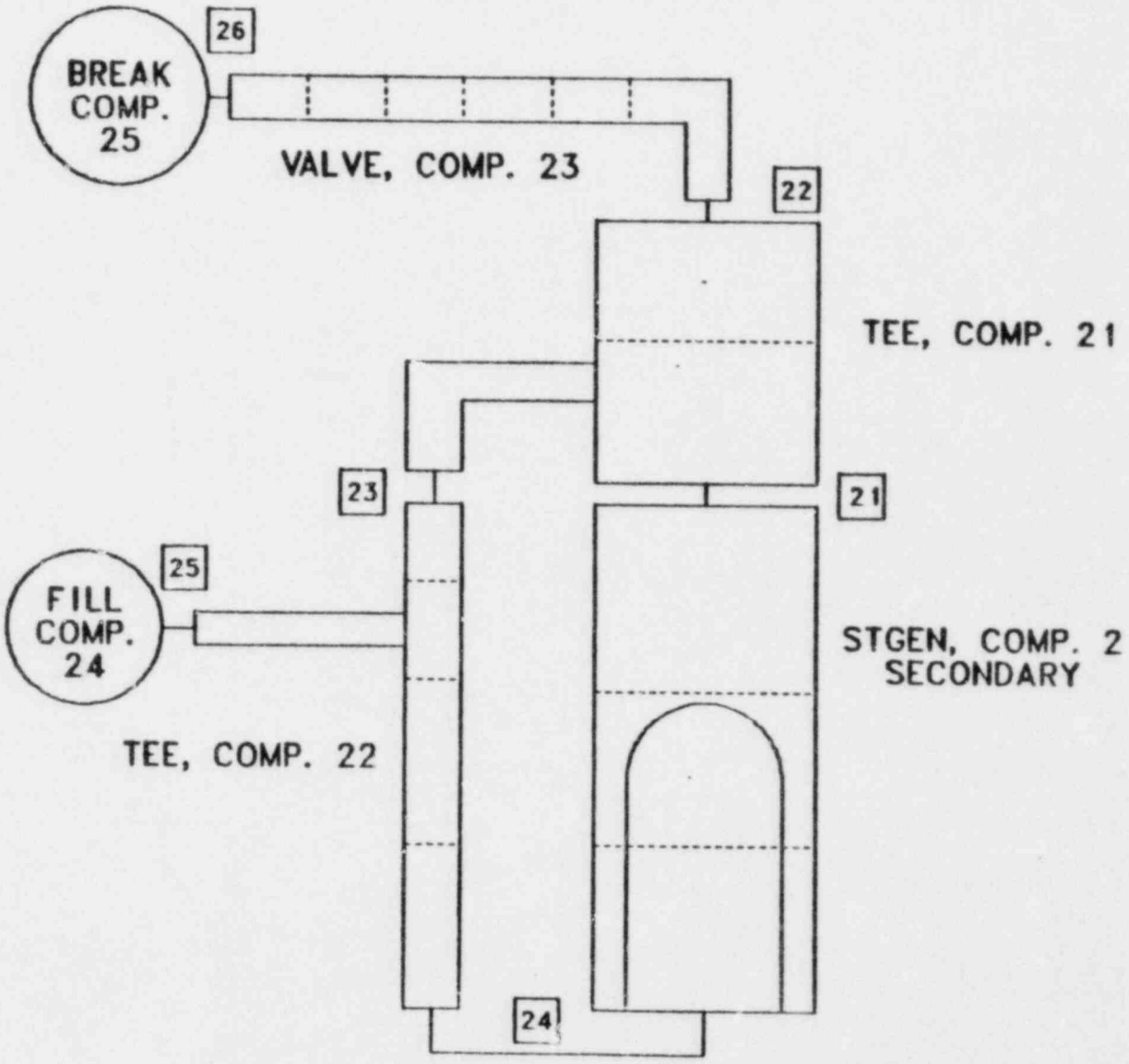

Figure A-12 LASL steam generator secondary nodalization diagram.

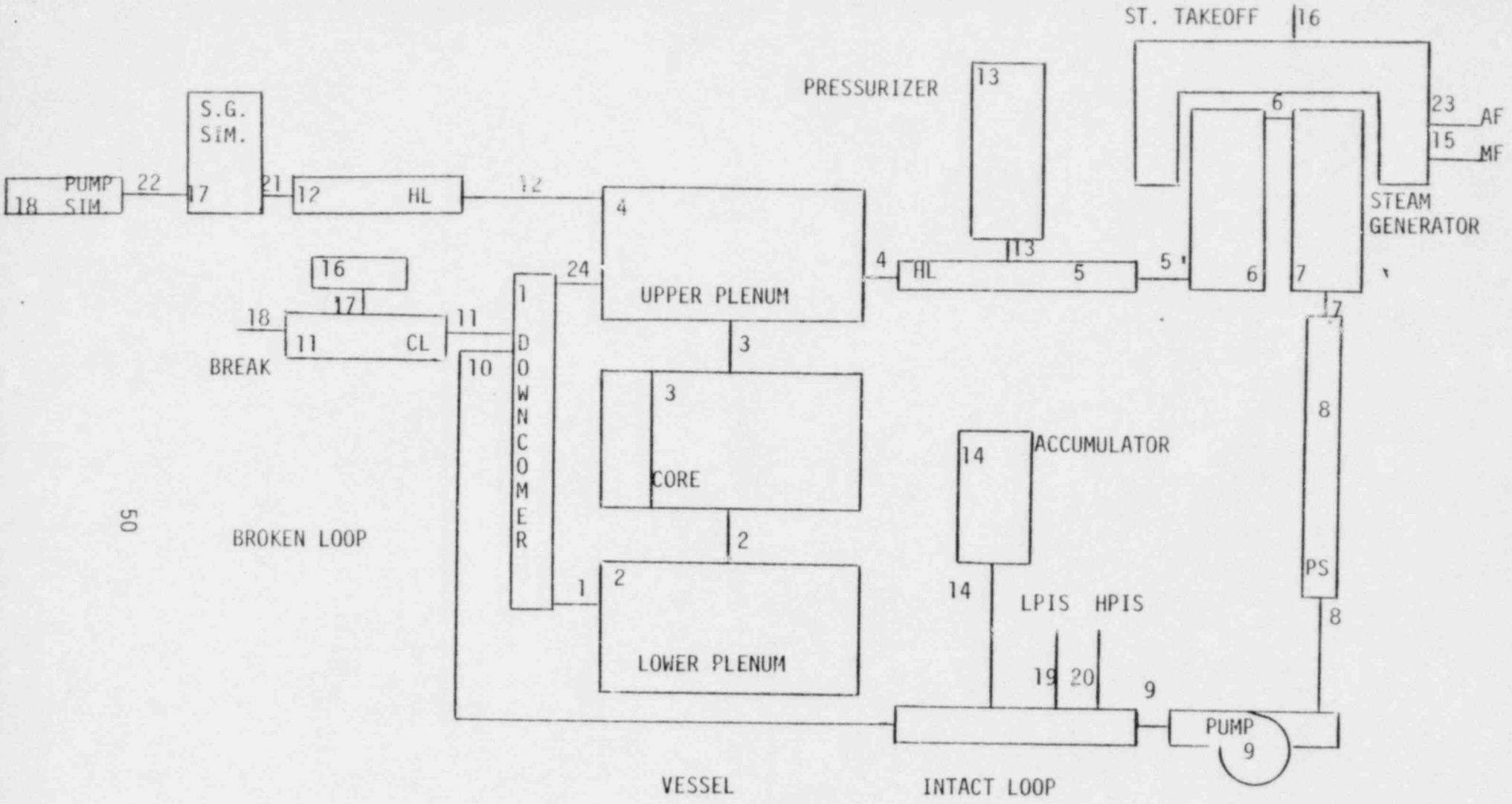

Figure A-13. NPCDA and NPCBR system nodalization diagram.

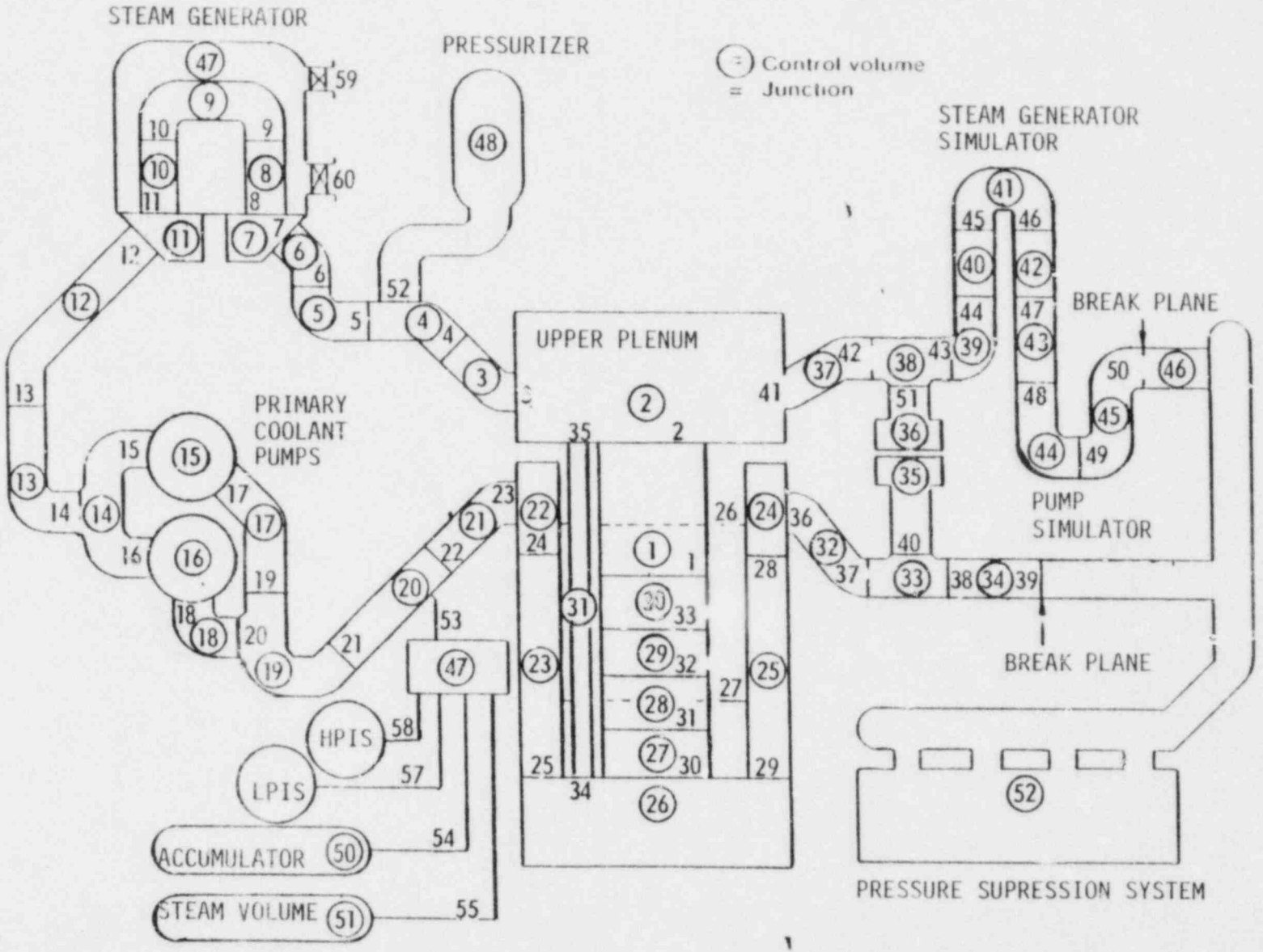

Figure A-14. UKEA system nodalization diagram.

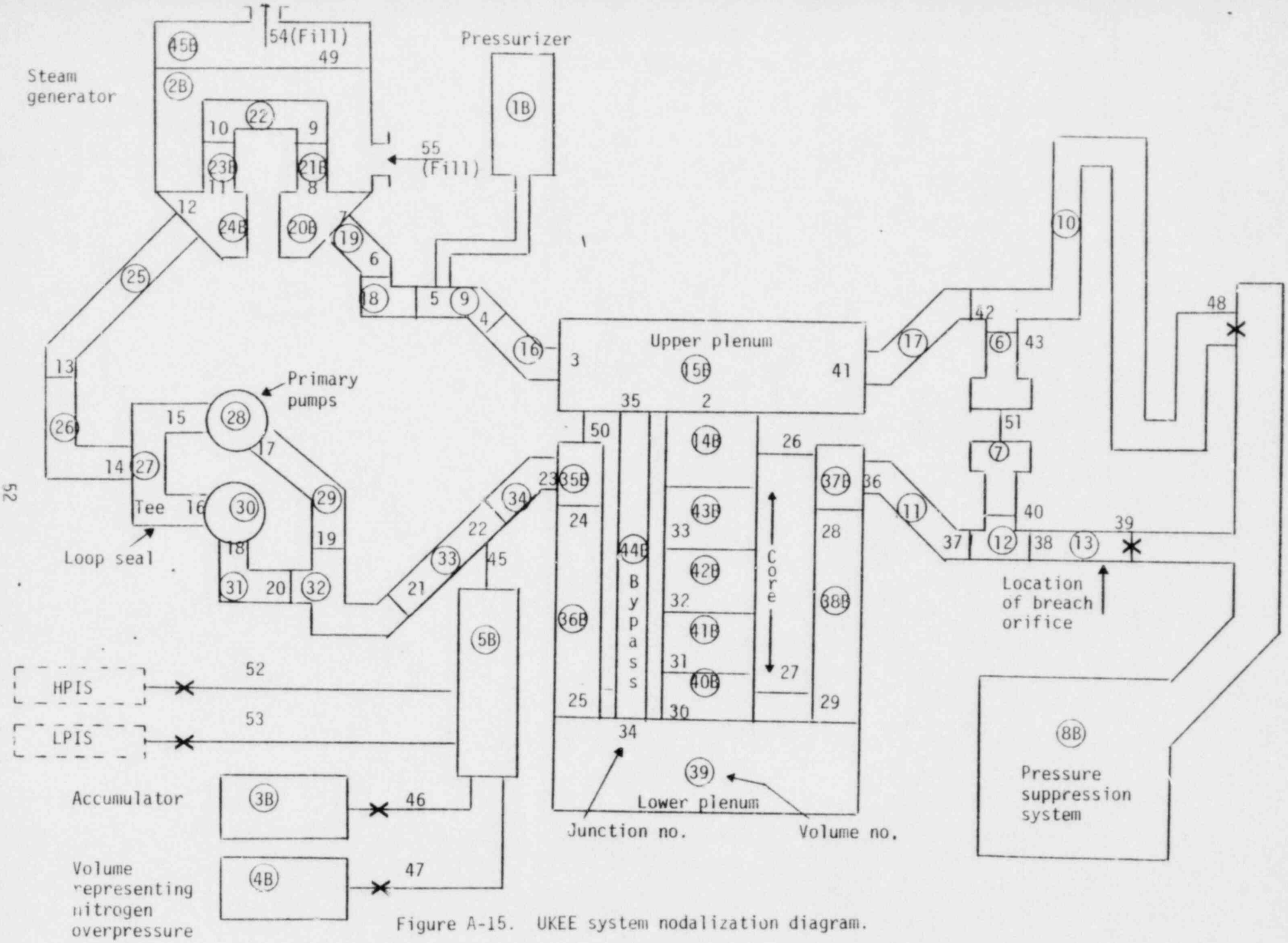

Figure A-15. UKEE system nodalization diagram.

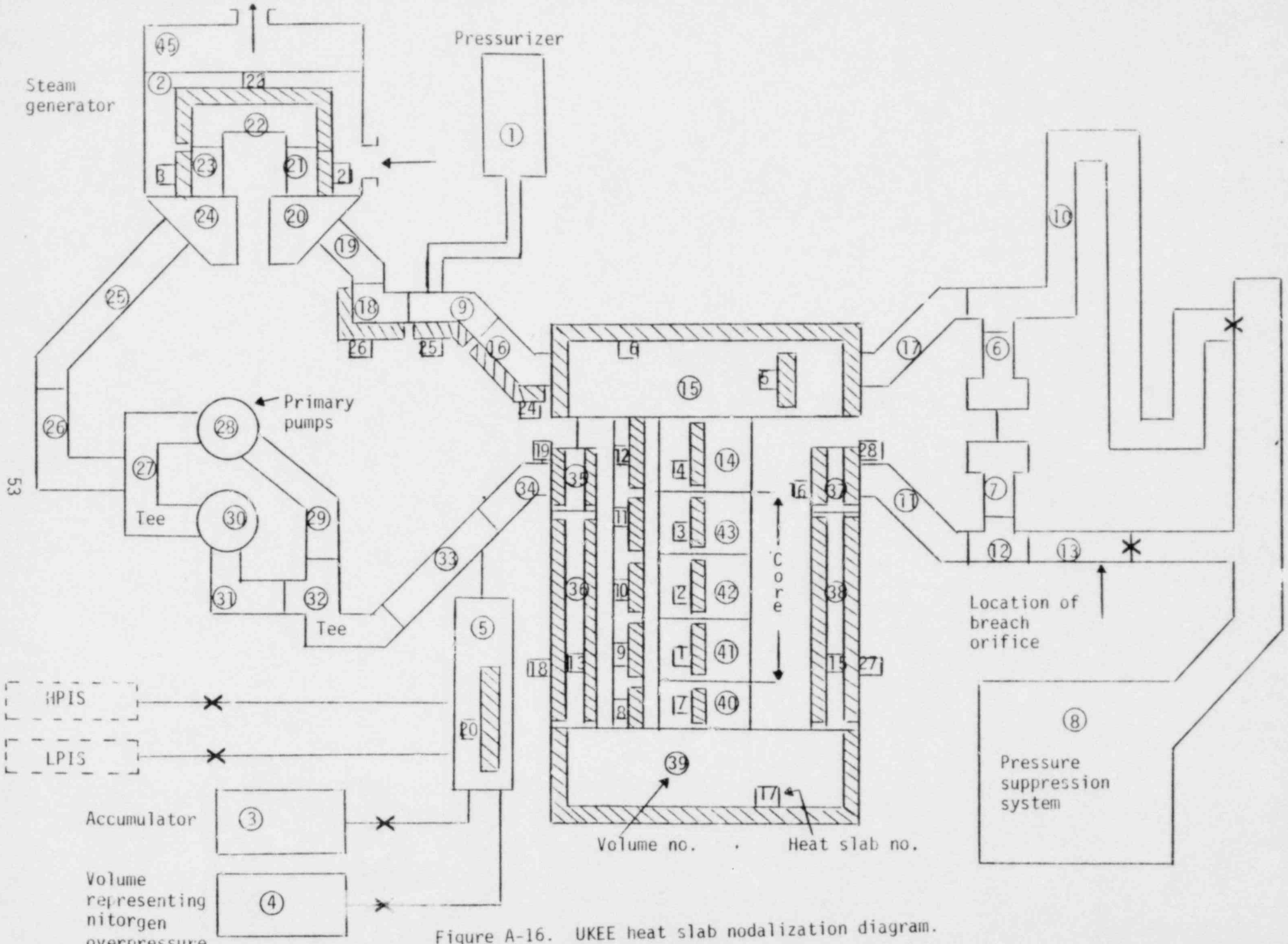

Figure A-16. UKEE heat slab nodalization diagram.

APPENDIX B

COMPARISON OF CENTRE D'ESTUDES NUCLEAIRES DE CADUVACHE CALCULATED RESULTS WITH LOFT EXPERIMENT MEASUREMENTS

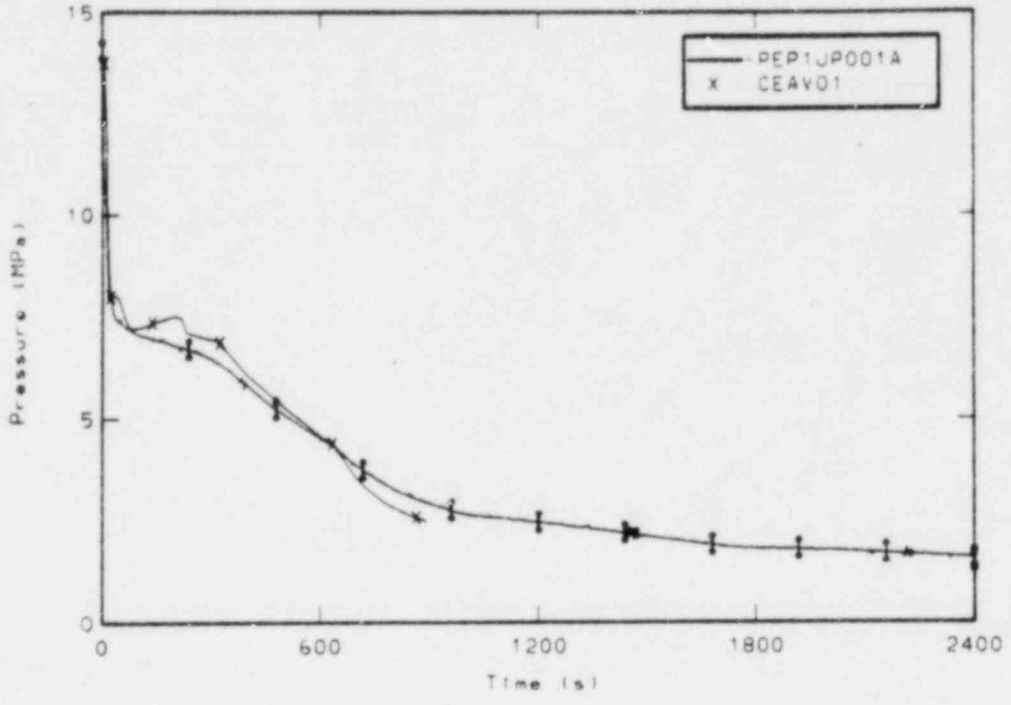

Figure B-1. Comparison of measured and CEA calculated upper plenum pressure.

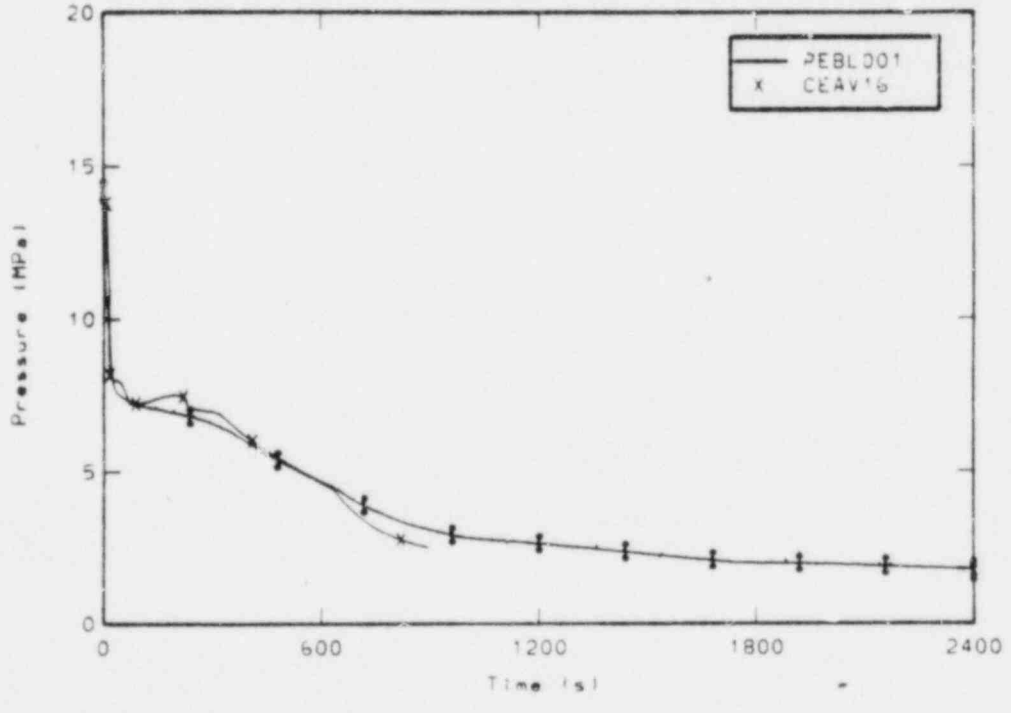

Figure B-2. Comparison of measured and CEA calculated broken loop cold leg pressure.

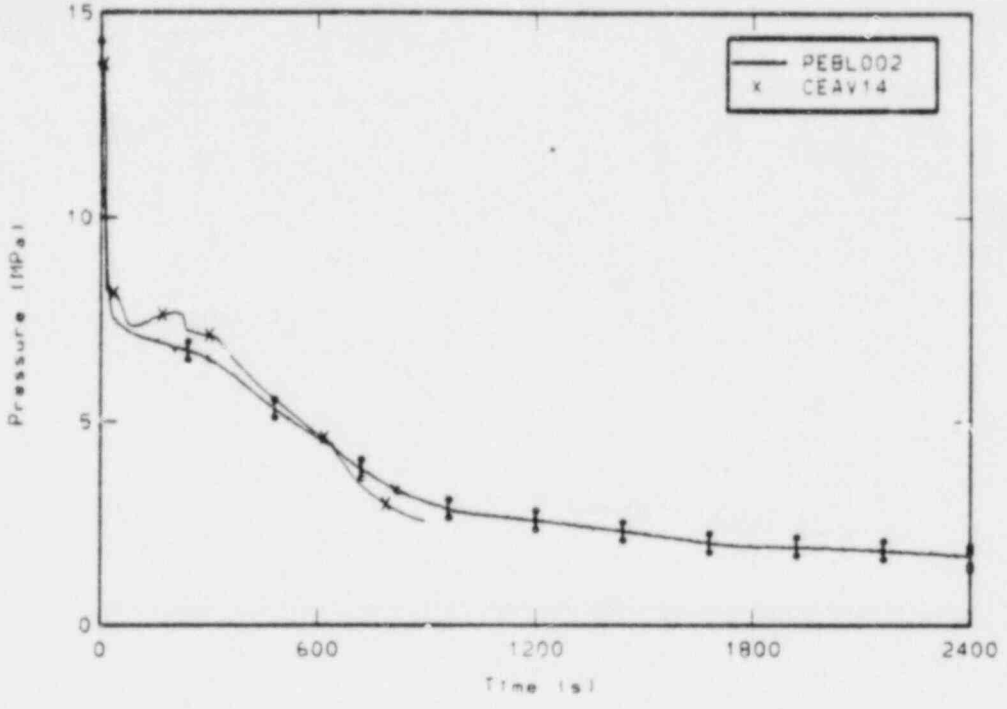

Figure B-3. Comparison of measured and CEA calculated broken loop hot leg pressure.

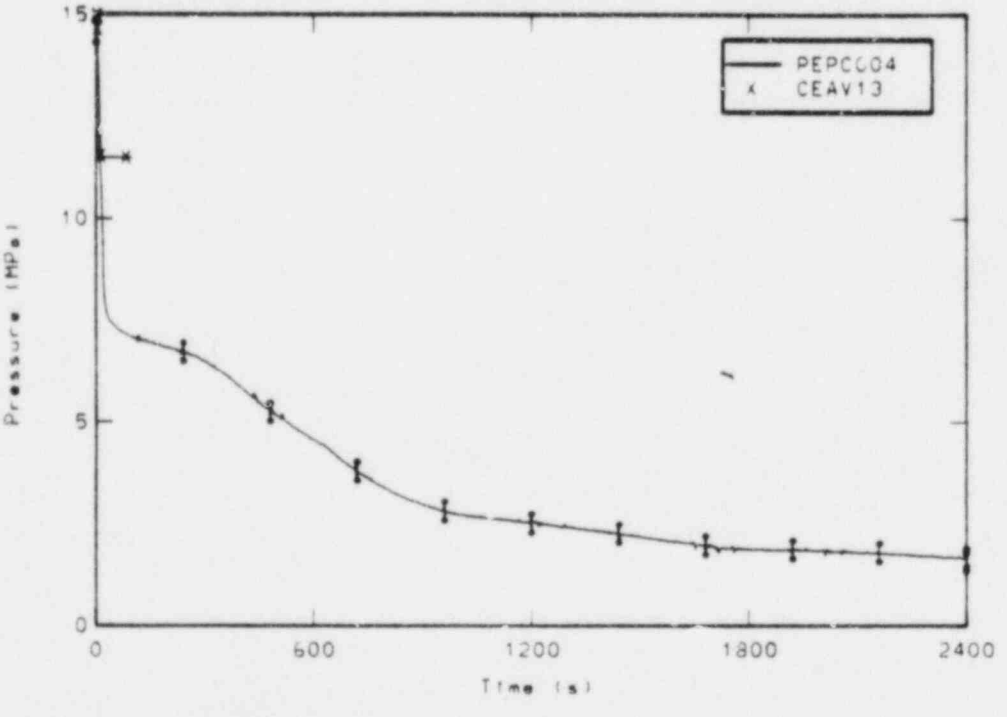

Figure B-4. Comparison of measured and CEA calculated pressurizer pressure.

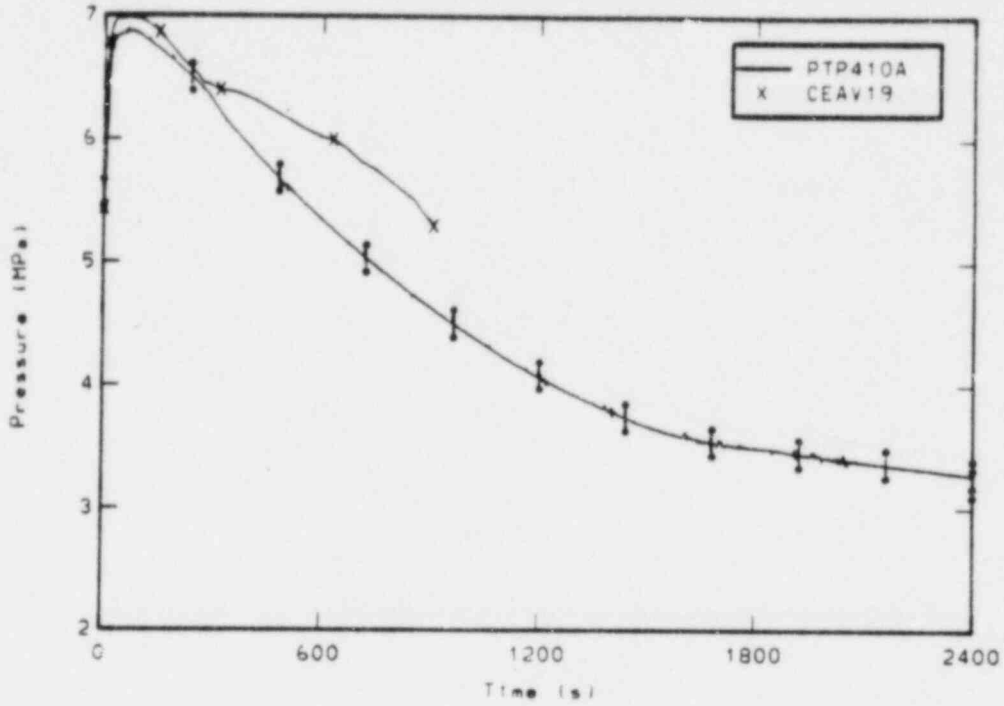

Figure B-5. Comparison of measured and CEA calculated steam generator secondary pressure.

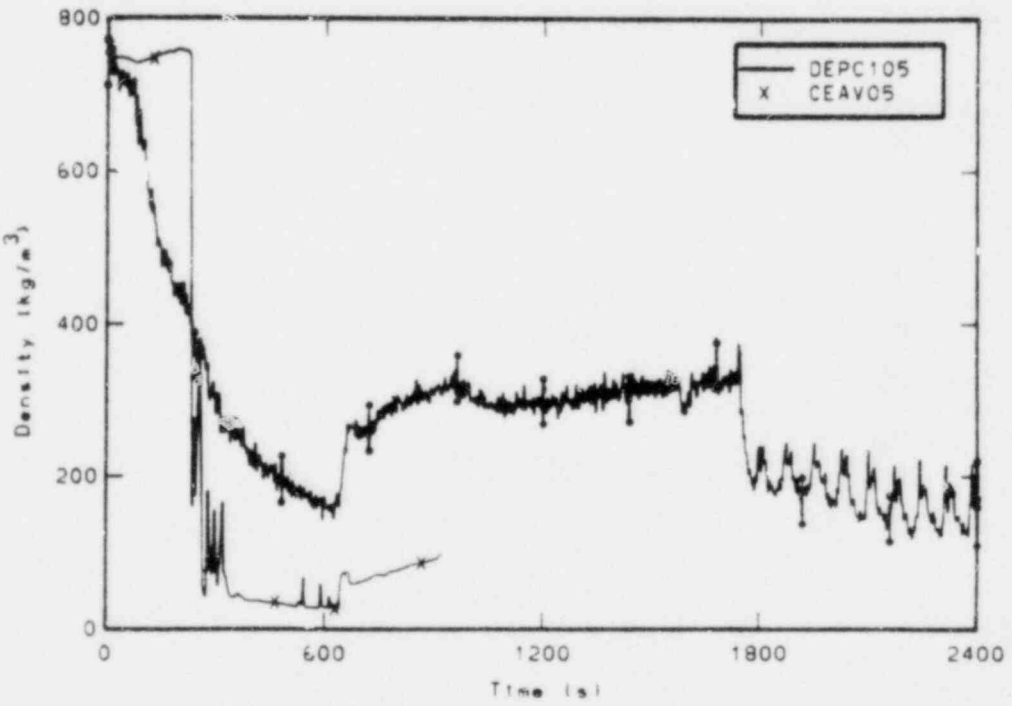

Figure B-6. Comparison of measured and CEA calculated average density in the intact loop cold leg.

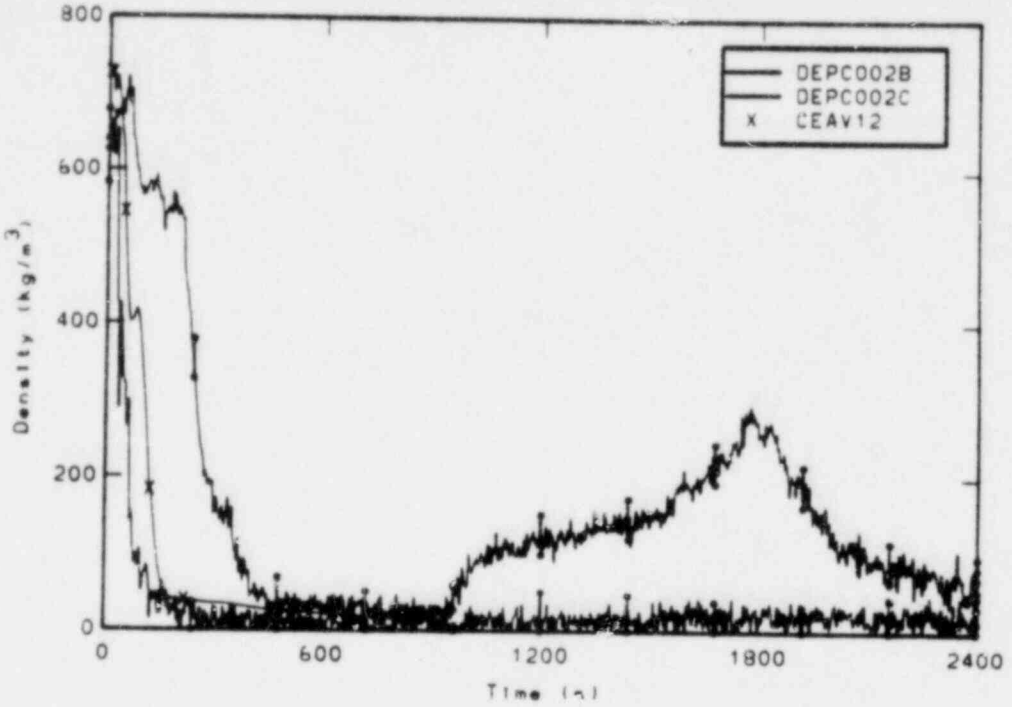

Figure B-7. Comparison of measured chordal densities and CEA calculated average density in the intact loop hot leg.

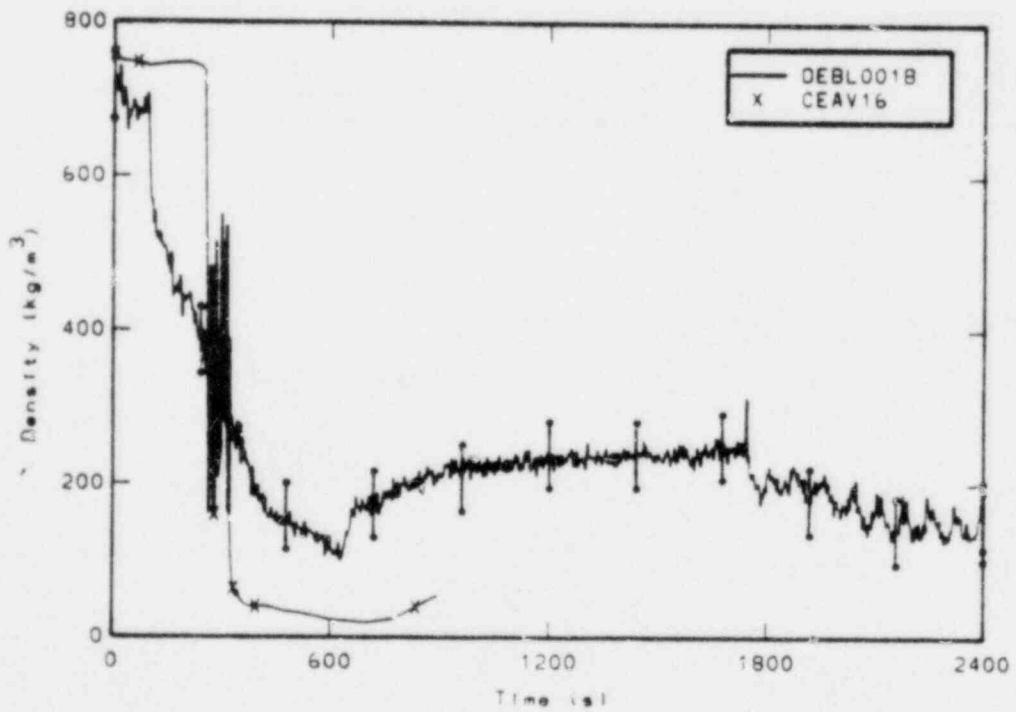

Figure B-8. Comparison of measured chordal density and CEA calculated average density in the broken loop cold leg.

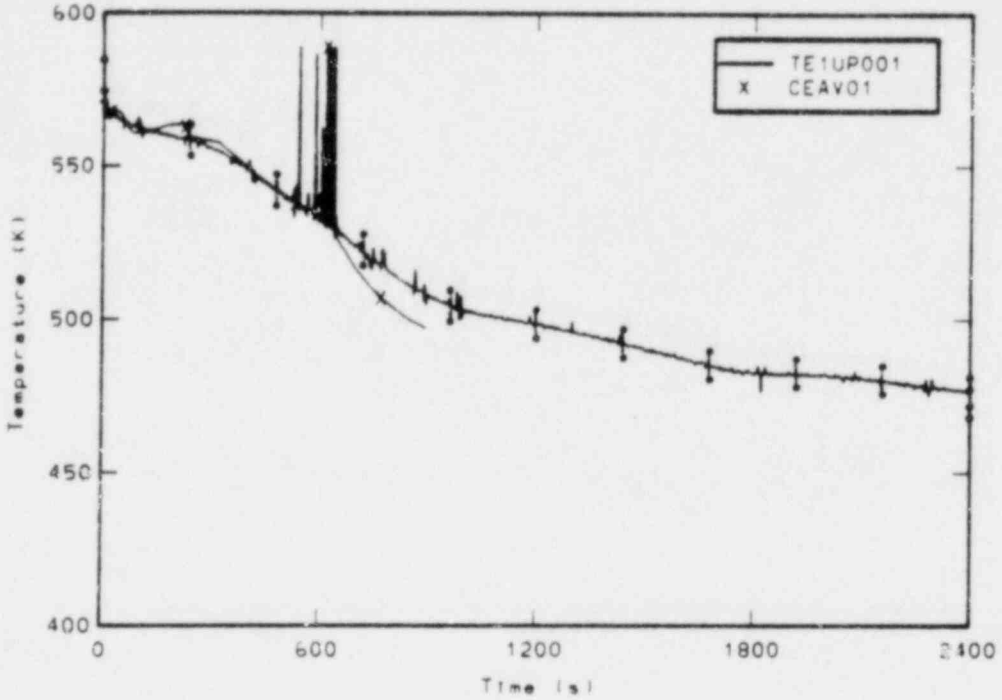

Figure B-9. Comparison of measured and CEA calculated upper plenum fluid temperature.

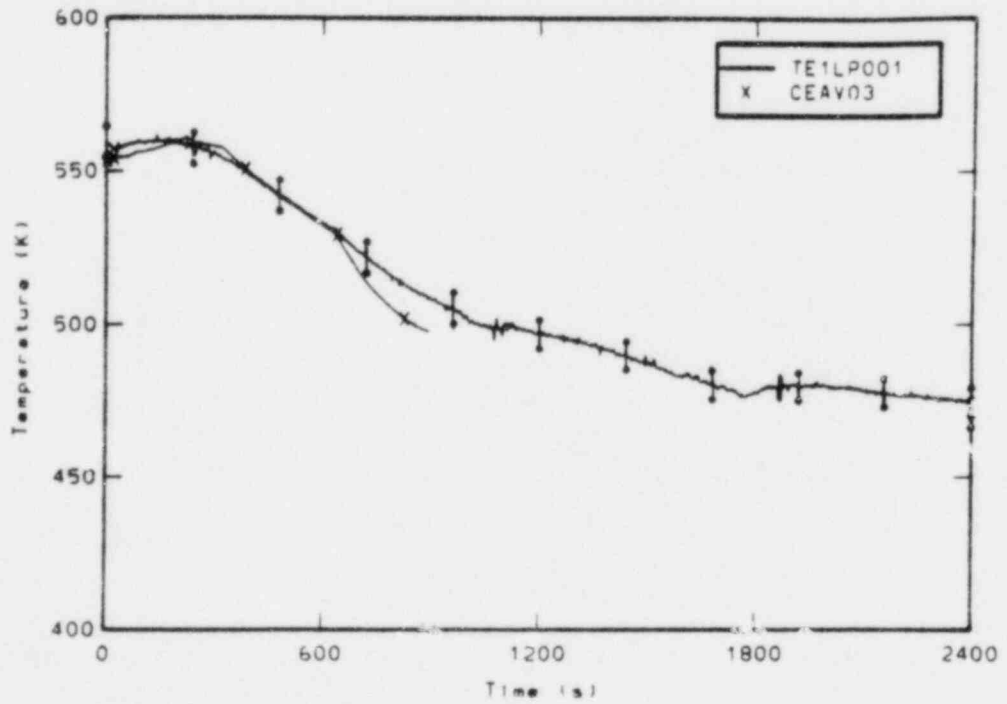

Figure B-10. Comparison of measured and CEA calculated lower plenum fluid temperature.

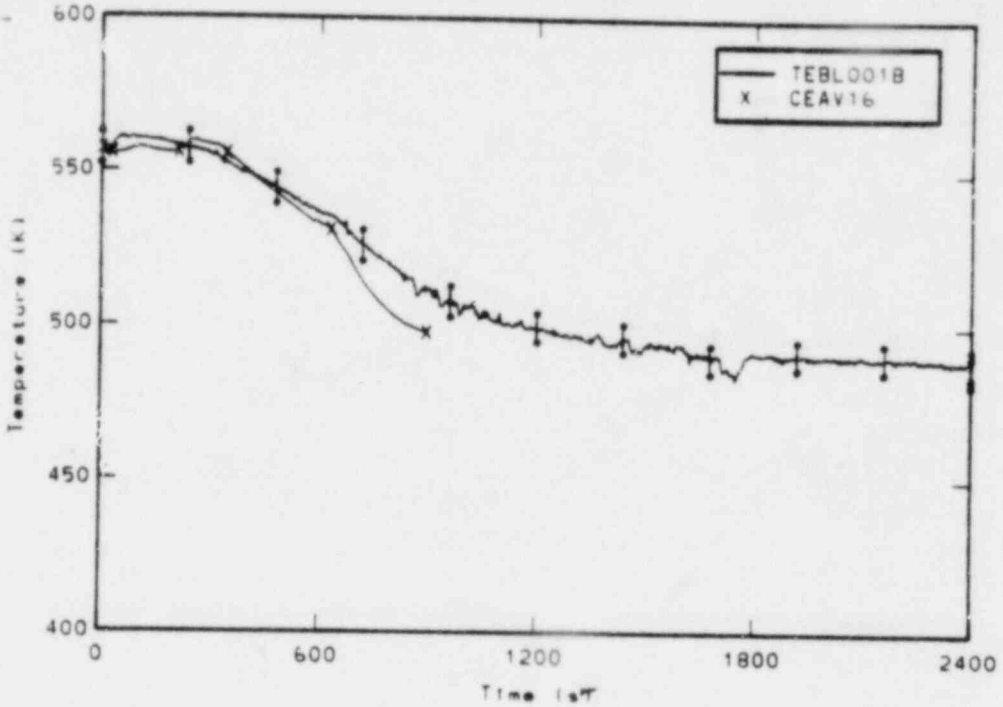

Figure B-11. Comparison of measured and CEA calculated broken loop cold leg fluid temperature.

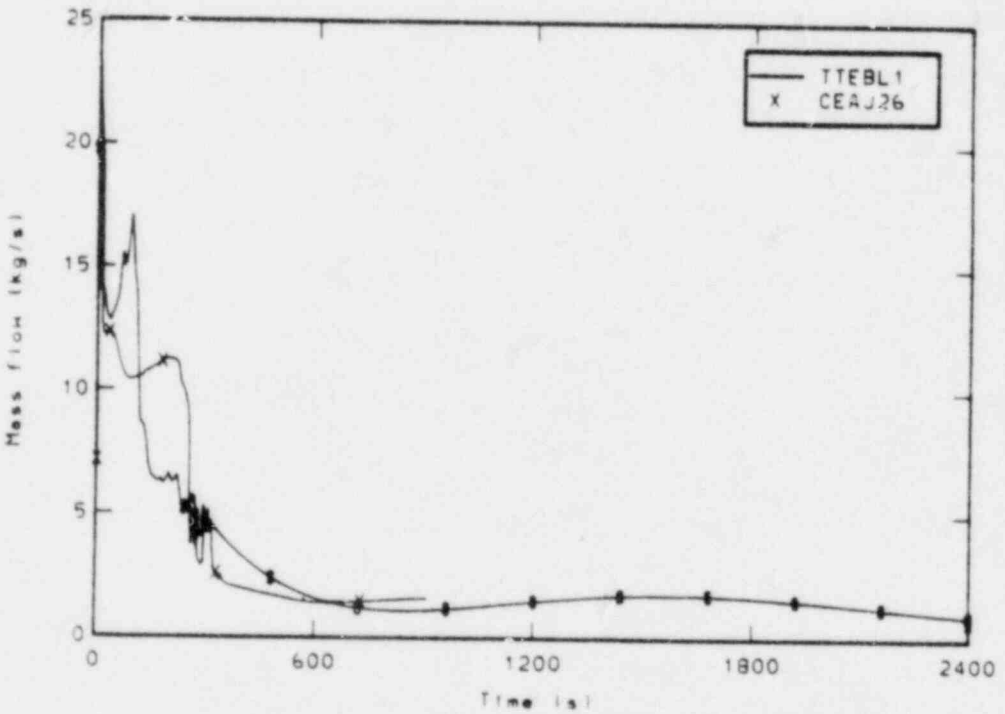

Figure B-12. Comparison of measured and CEA calculated mass flow rate at the break.

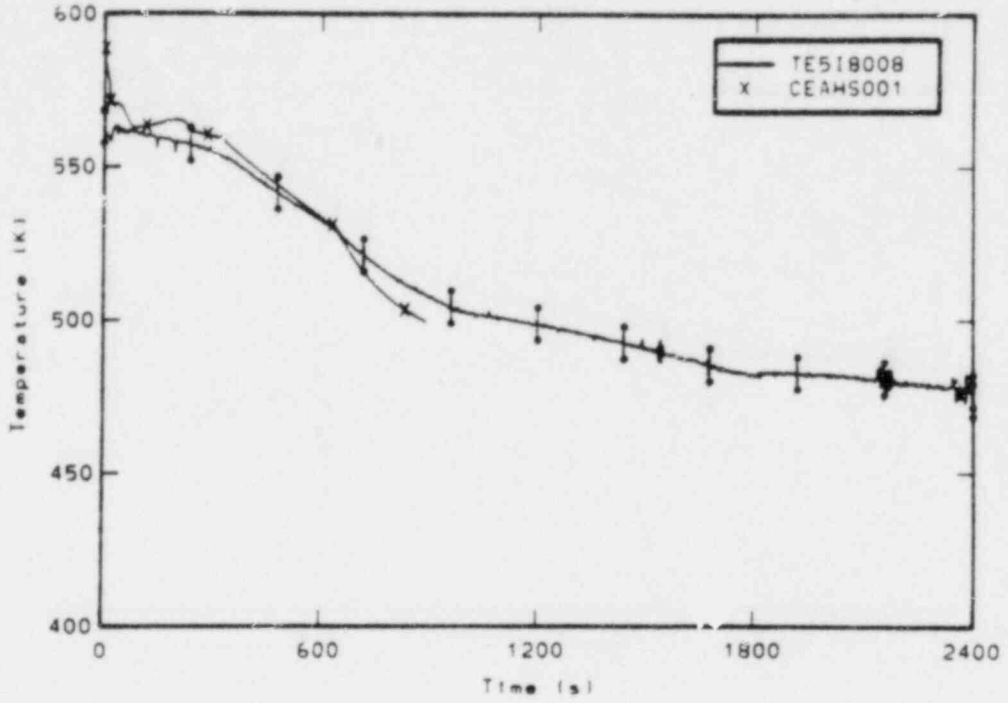

Figure B-13. Comparison of measured rod cladding temperature at the 0.20m elevation and CEA calculated rod cladding temperature.

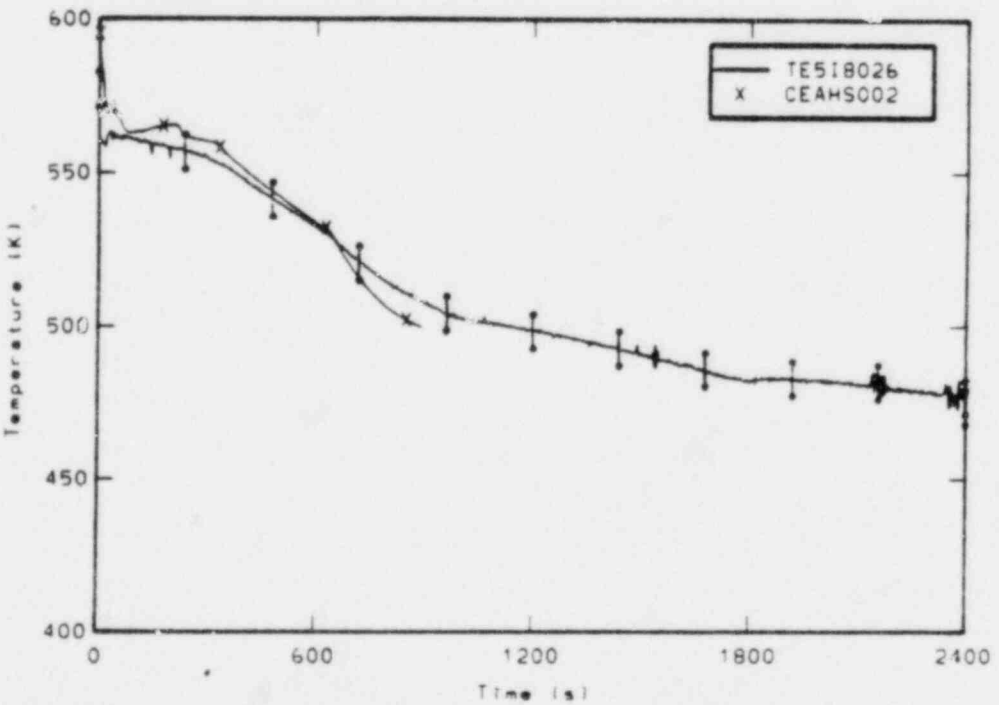

Figure B-14. Comparison of measured rod cladding temperature at the 0.66m elevation and CEA calculated rod cladding temperature.

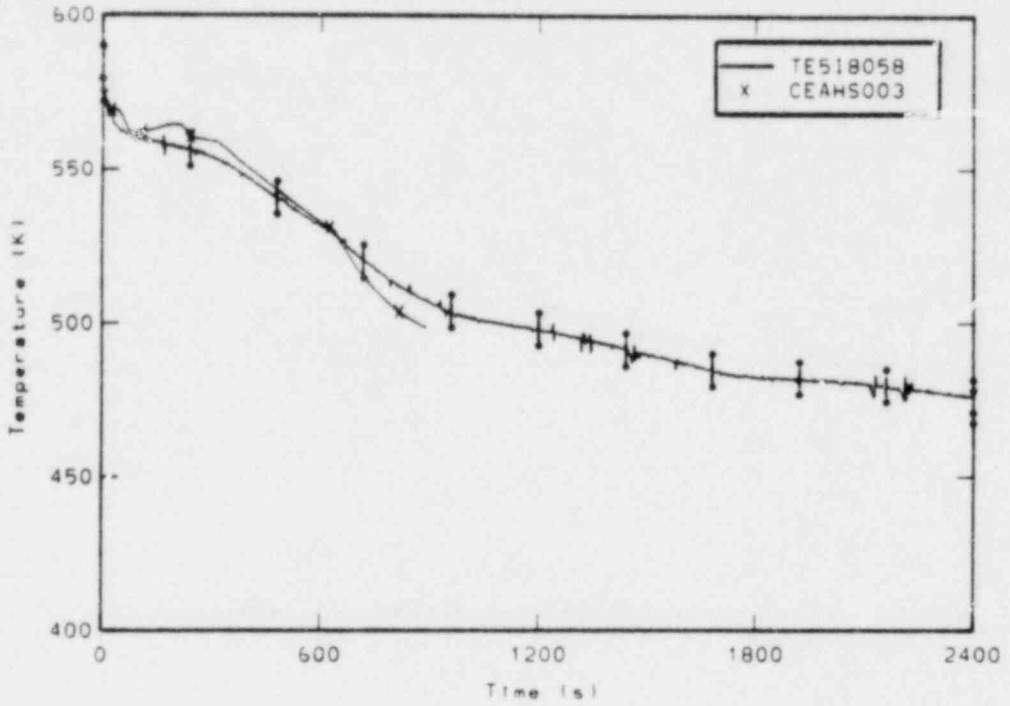

Figure B-15. Comparison of measured rod cladding temperature at the 1.47m elevation and CEA calculated rod cladding temperature.

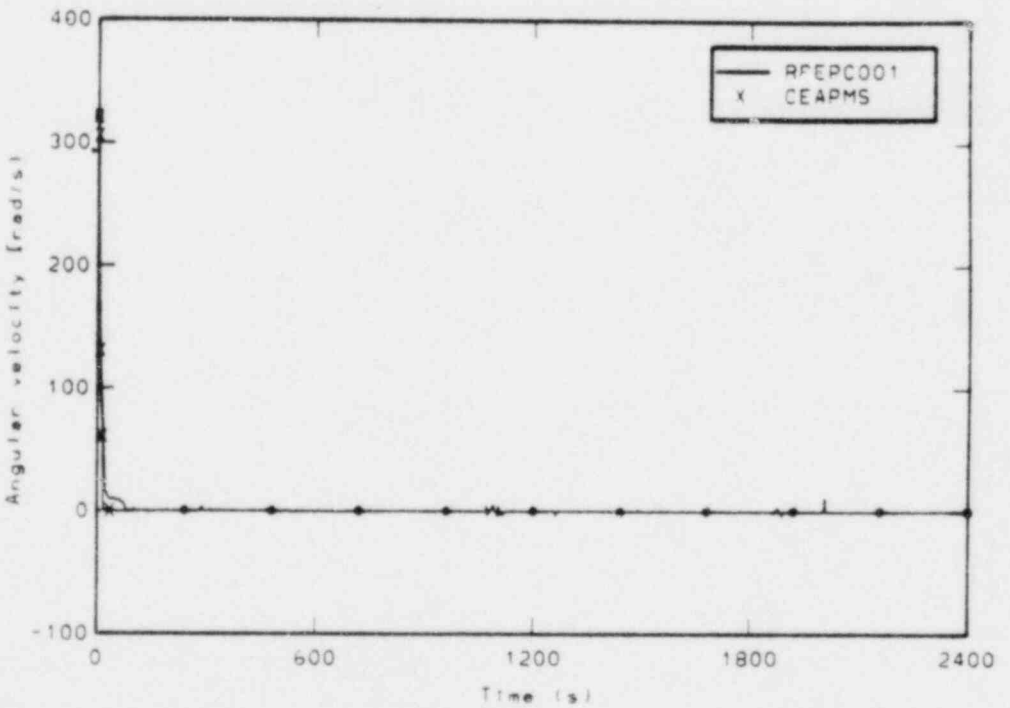

Figure B-16. Comparison of measured and CEA calculated pump speed.

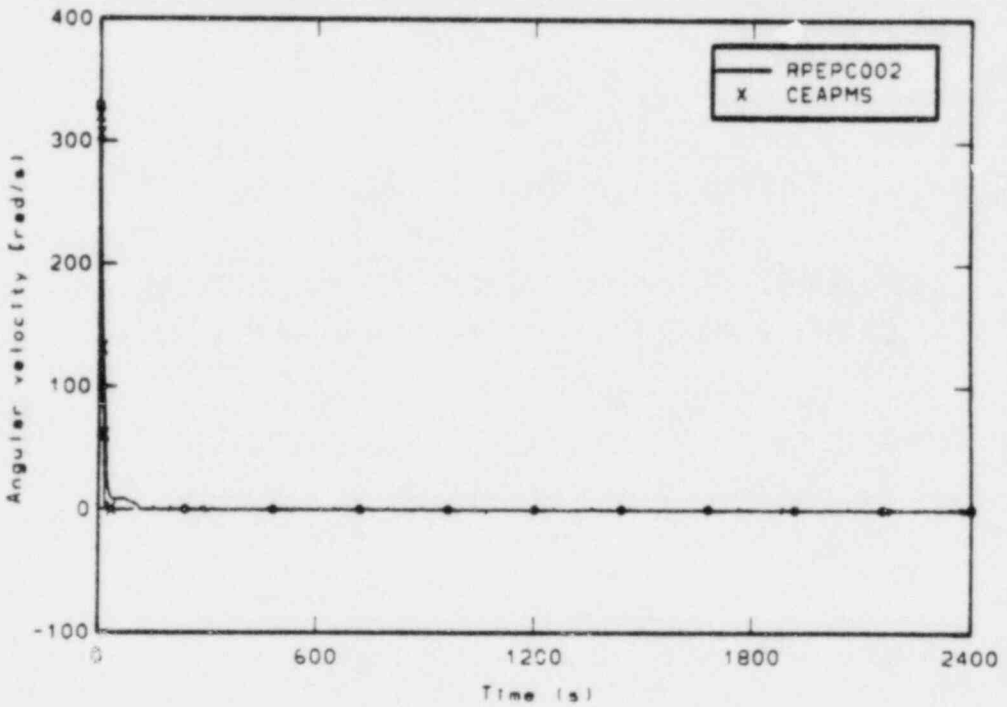

Figure B-17. Comparison of measured and CEA calculated pump speed.

APPENDIX C

COMPARISONS OF ENERGIEONDERZOEK CENTRUM NEDERLAND CALCULATED RESULTS WITH LOFT EXPERIMENT MEASUREMENTS

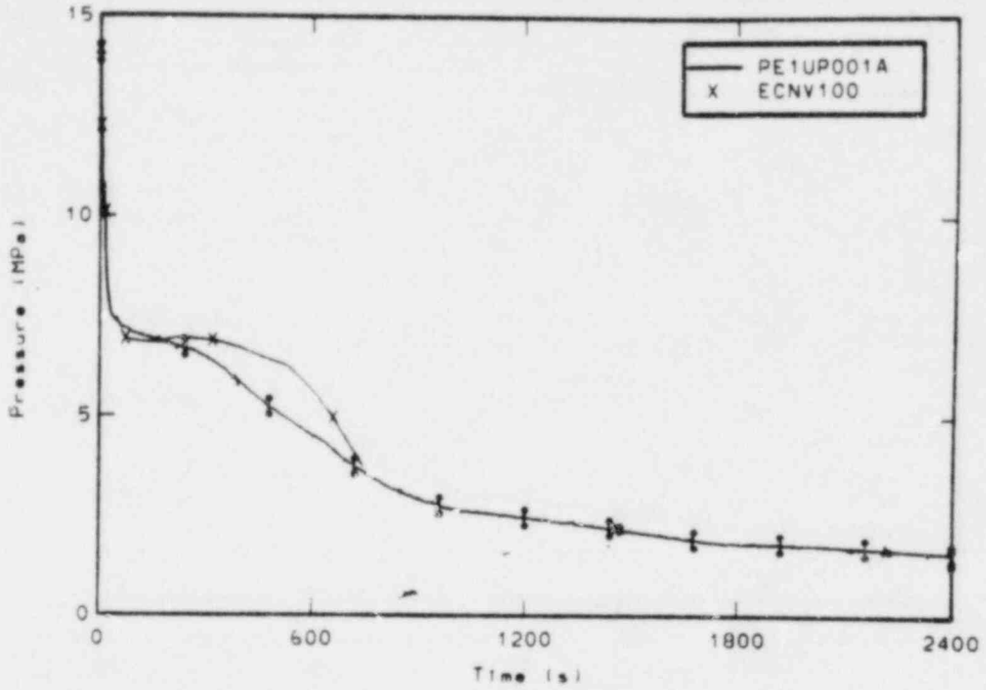

Figure C-1. Comparison of measured and ECN calculated upper plenum pressure.

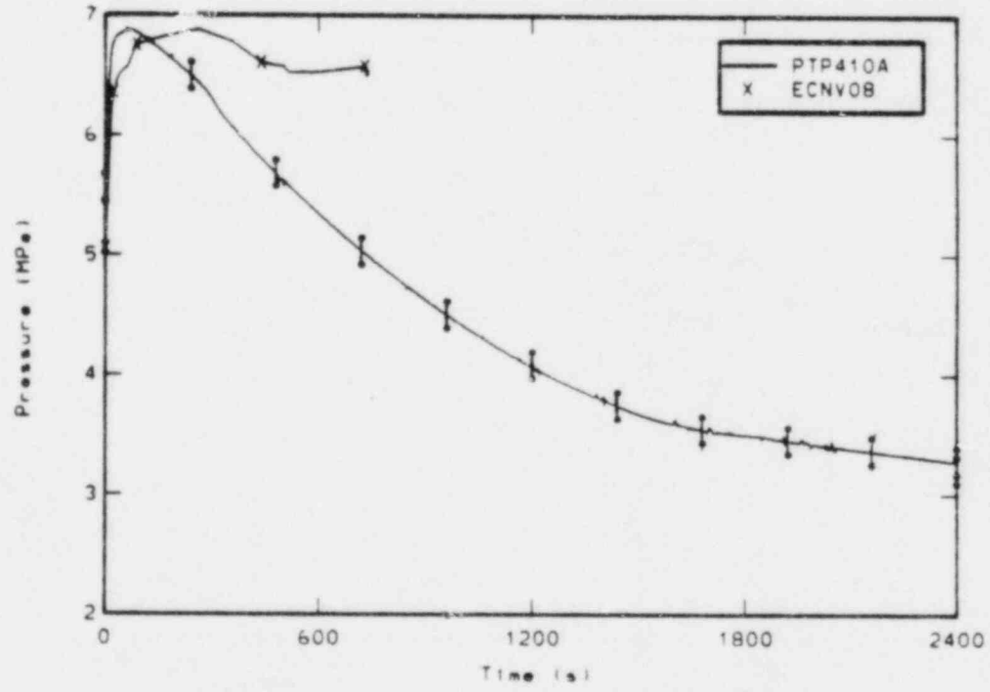

Figure C-2. Comparison of measured and ECN calculated steam generator secondary pressure.

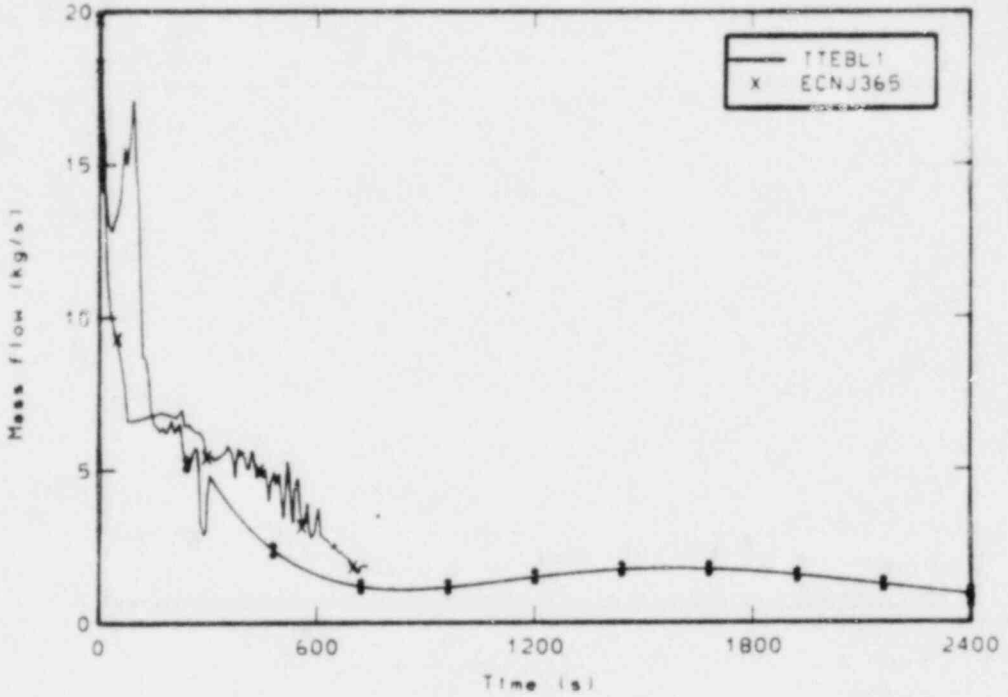

Figure C-3. Comparison of measured and ECN calculated mass flow rate at the break.

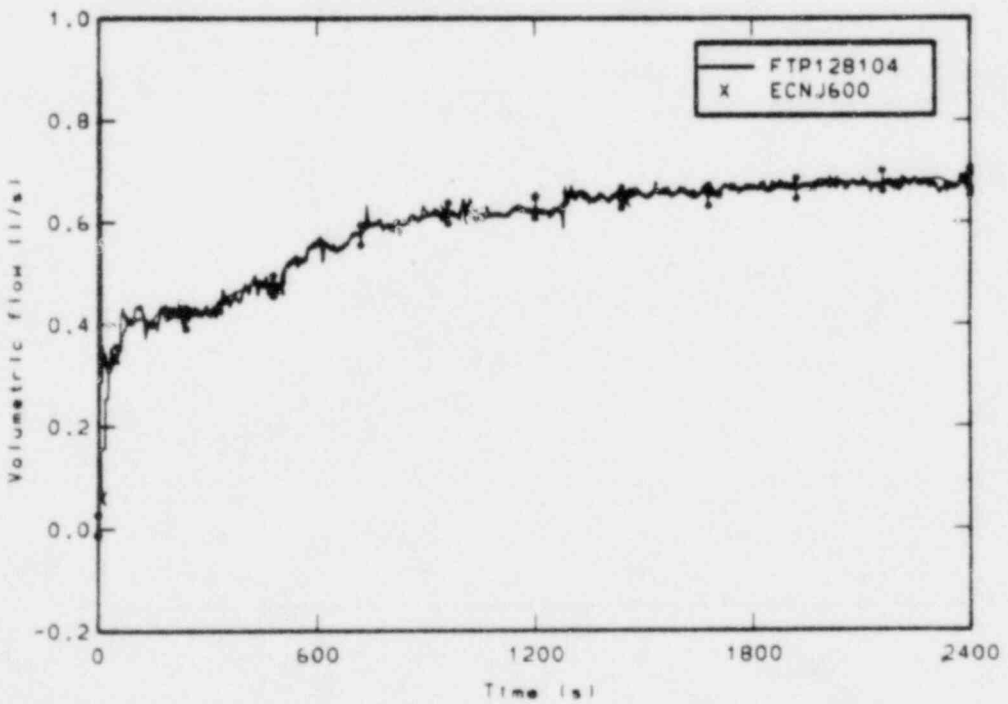

Figure C-4. Comparison of measured and ECN calculated high pressure injection system (HPIS) volumetric flow rate.

APPENDIX D

COMPARISONS OF EIDG. INSTITUT FÜR REAKTORFORSCHUNG MODEL 1 CALCULATED RESULTS WITH LOFT EXPERIMENT MEASUREMENTS

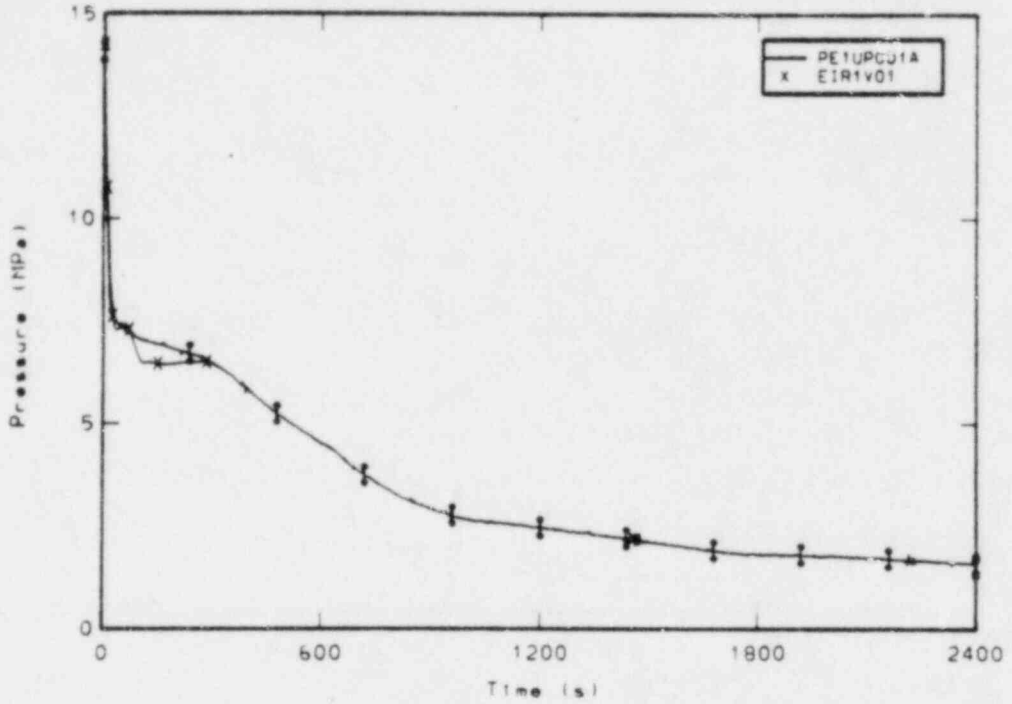

Figure D-1. Comparison of measured and EIR1 calculated upper plenum pressure.

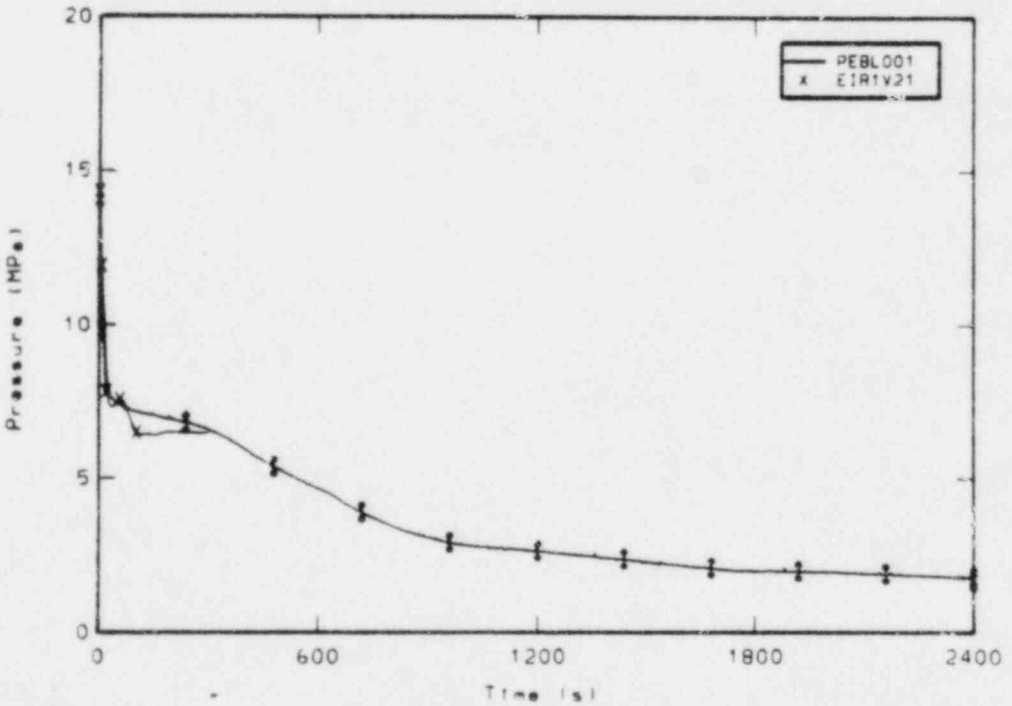

Figure D-2. Comparison of measured and EIR1 calculated broken loop cold leg pressure.

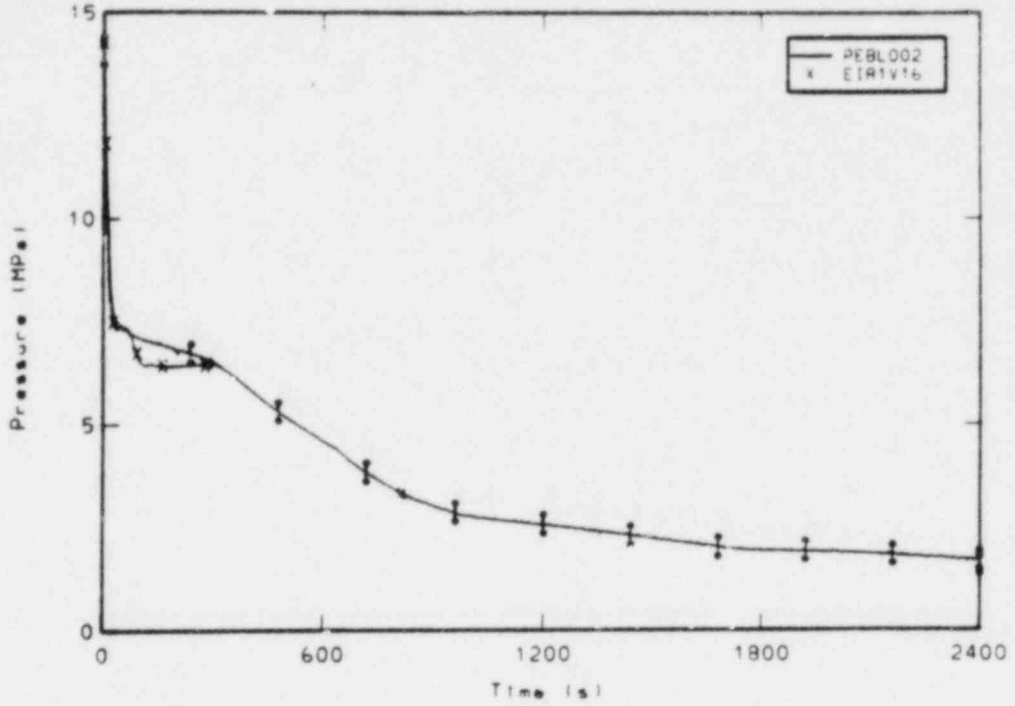

Figure D-3. Comparison of measured and EIR1 calculated broken loop hot leg pressure.

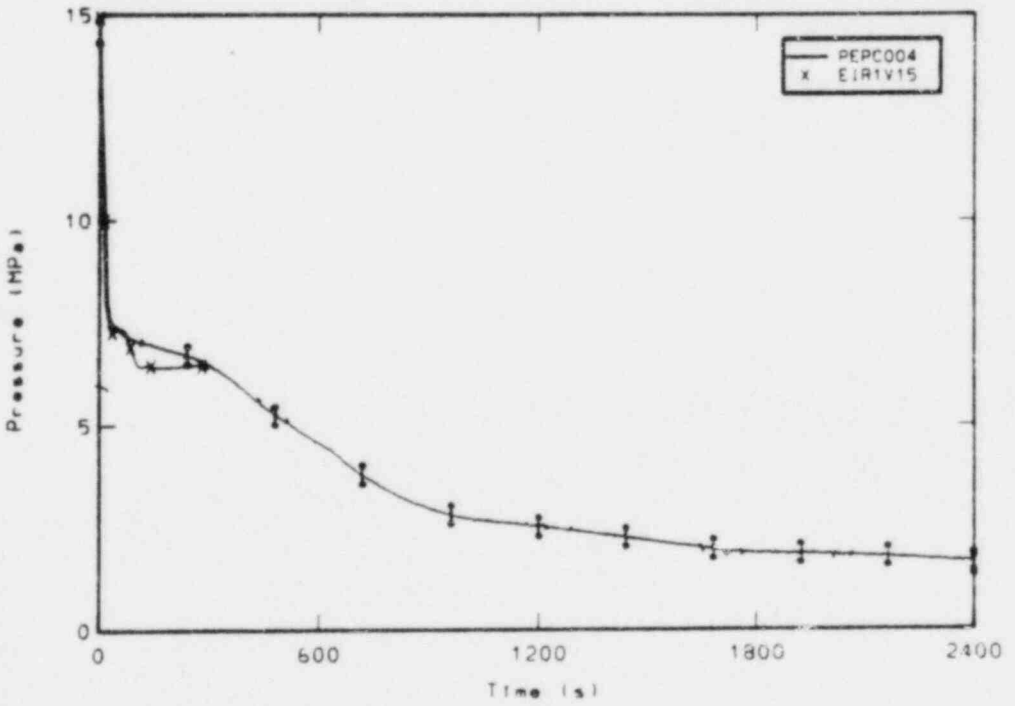

Figure D-4. Comparison of measured and EIR1 calculated pressurizer pressure.

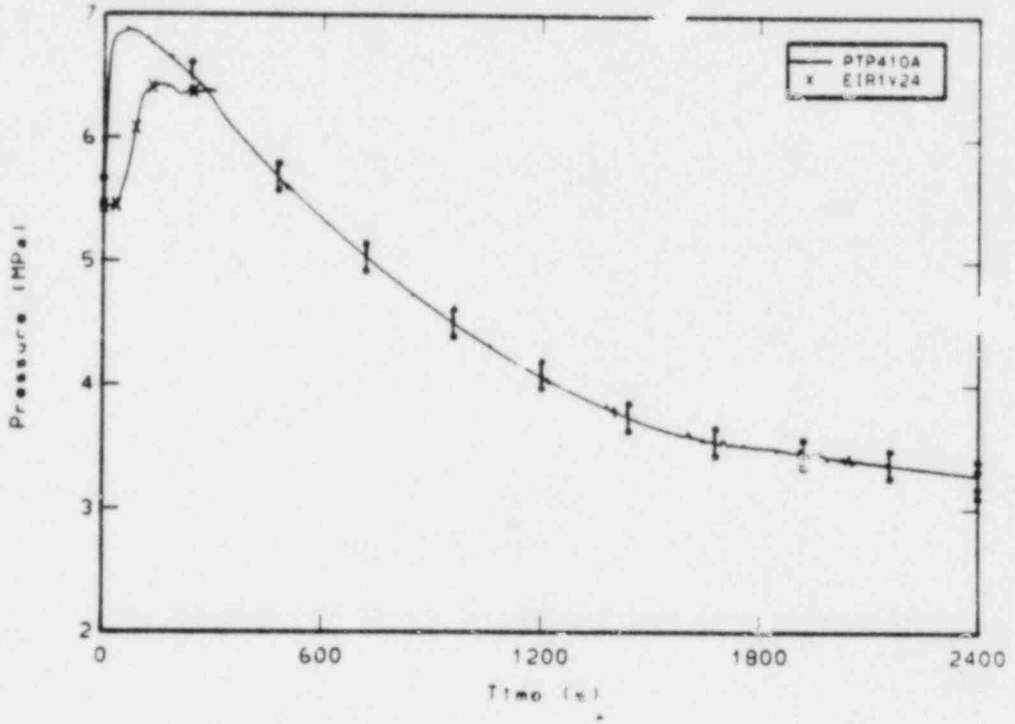

Figure D-5. Comparison of measured and EIR1 calculated steam generator secondary pressure.

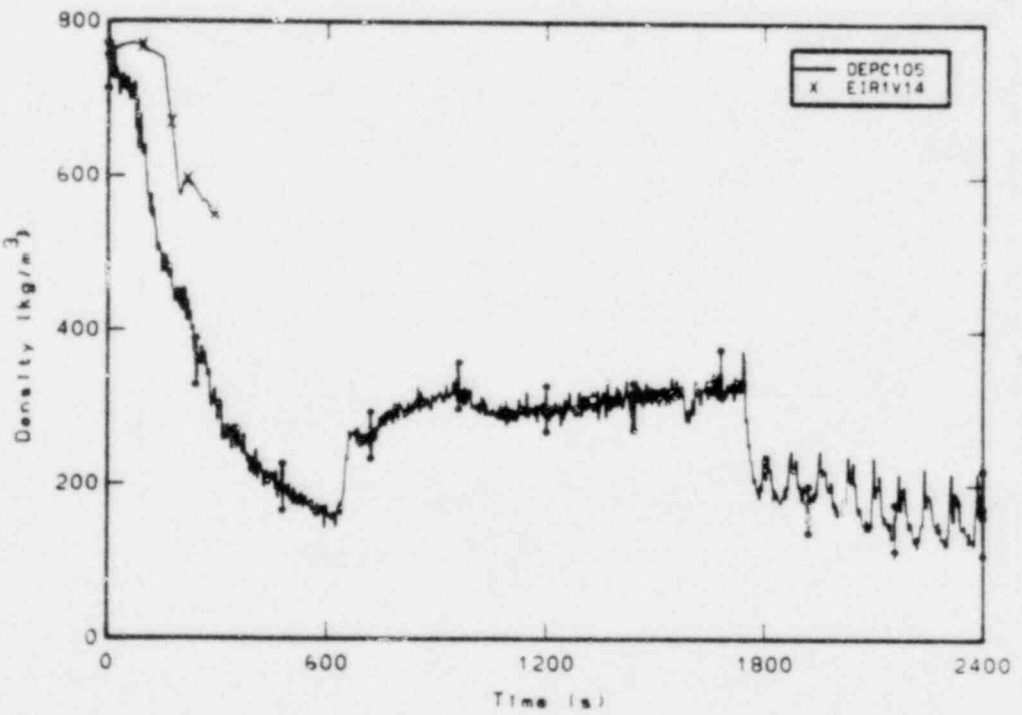

Figure D-6. Comparison of measured and EIR1 calculated average density in the intact loop cold leg.

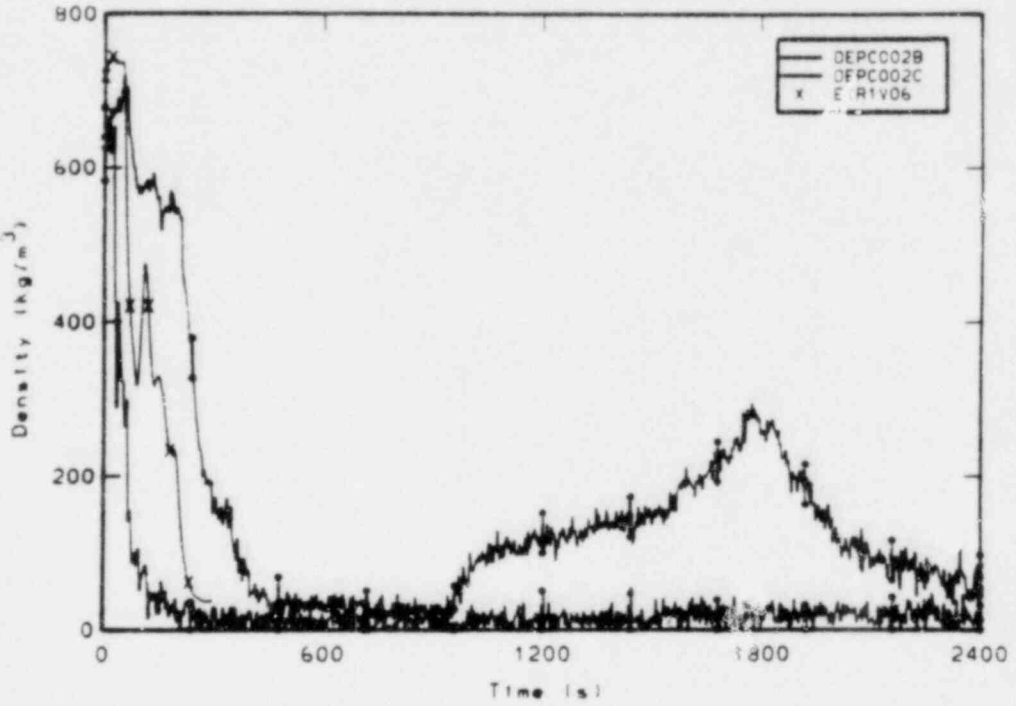

Figure D-7. Comparison of measured chordal densities and EIR1 calculated average density in the intact loop hot leg.

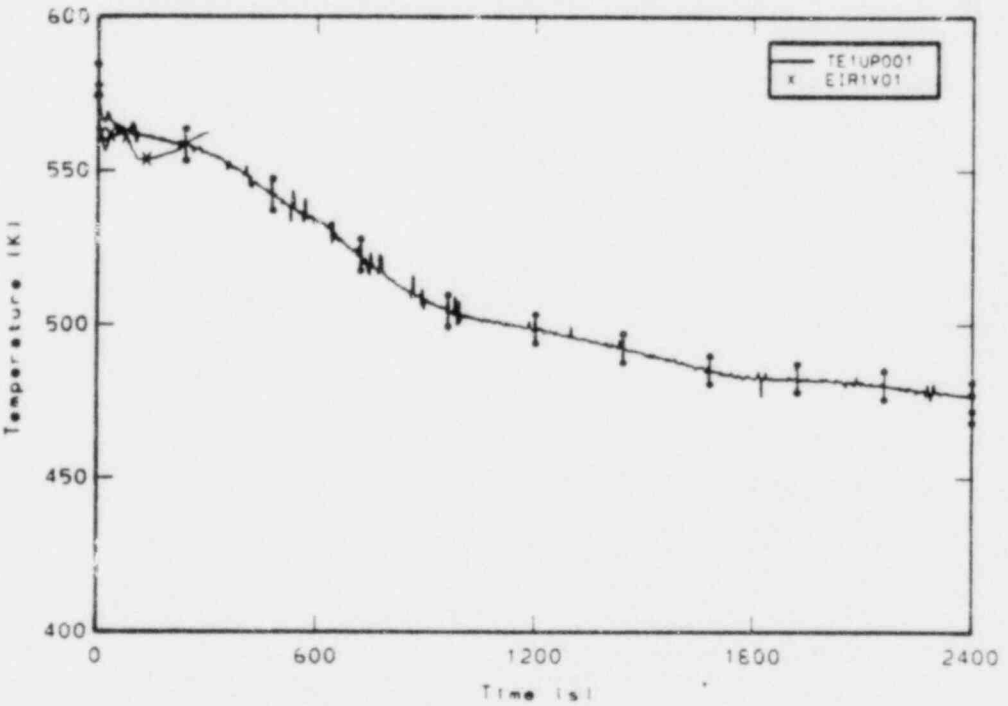

Figure D-8. Comparison of measured and EIR1 calculated upper plenum fluid temperature.

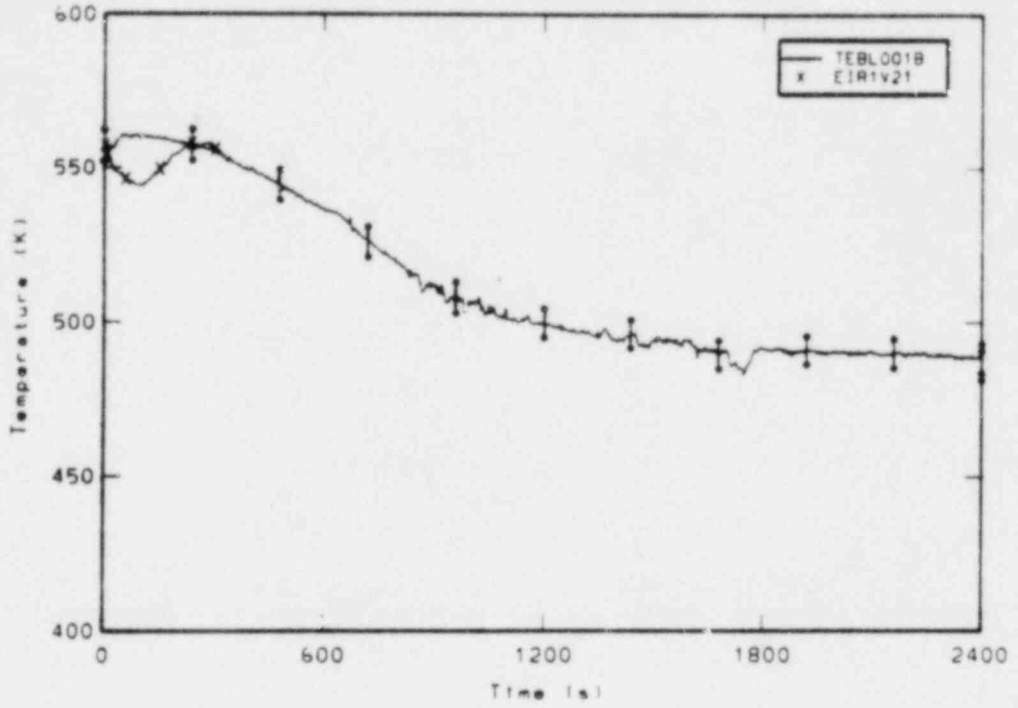

Figure D-9. Comparison of measured and EIA1 calculated broken loop cold leg fluid temperature.

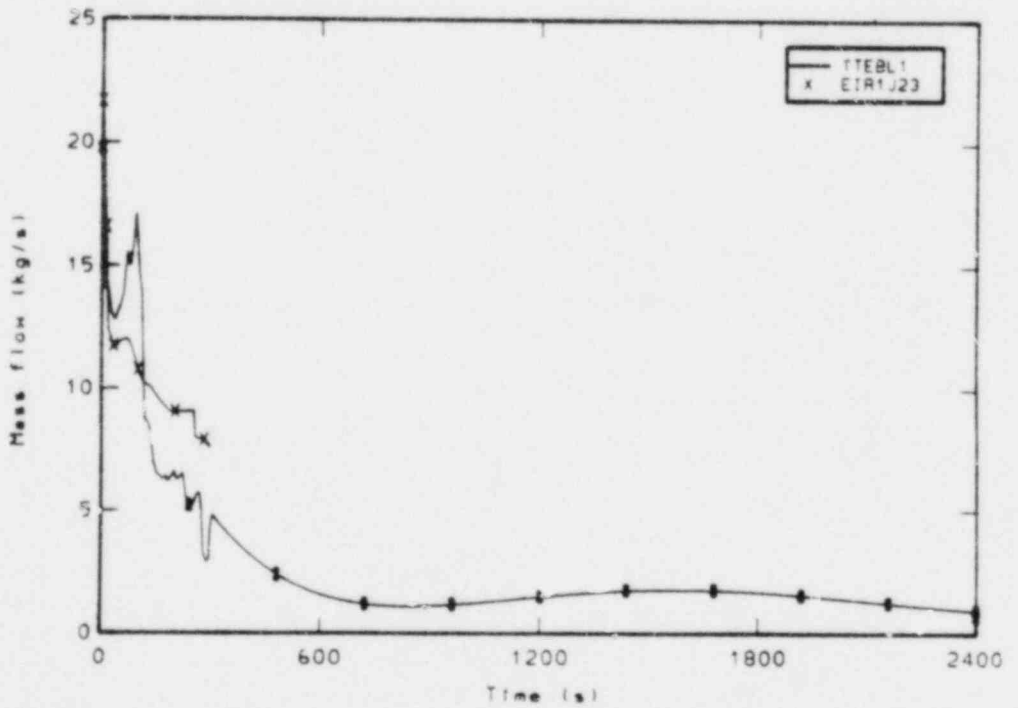

Figure D-10. Comparison of measured and EIA1 calculated mass flow rate at the break.

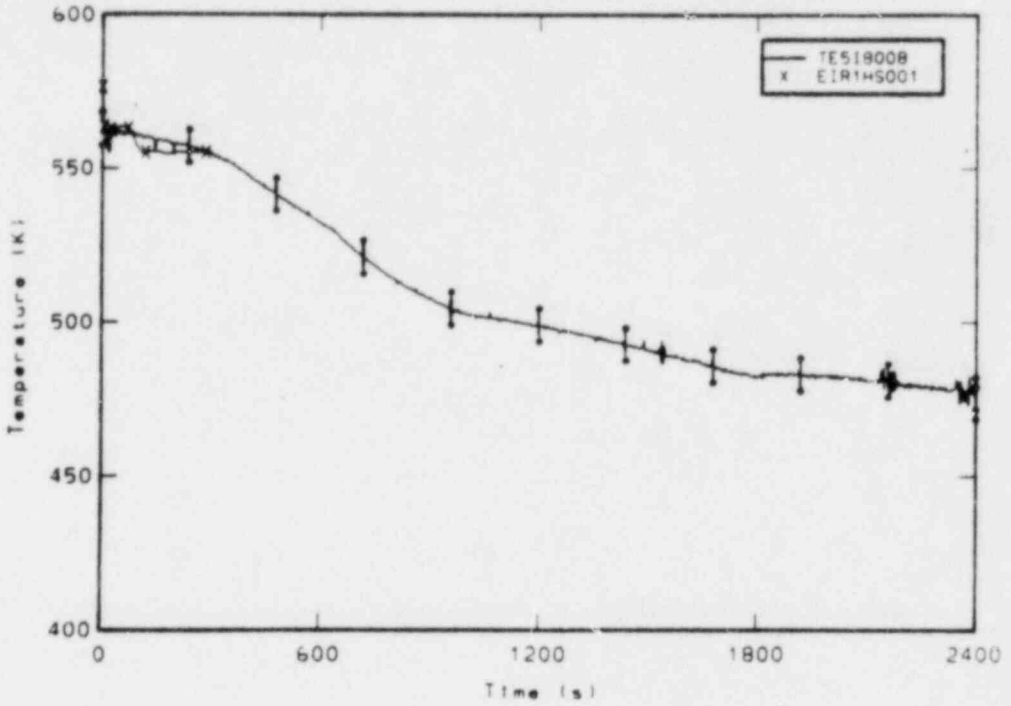

Figure D-11. Comparison of measured rod cladding temperature at the 0.20m elevation and EIR1 calculated rod cladding temperature.

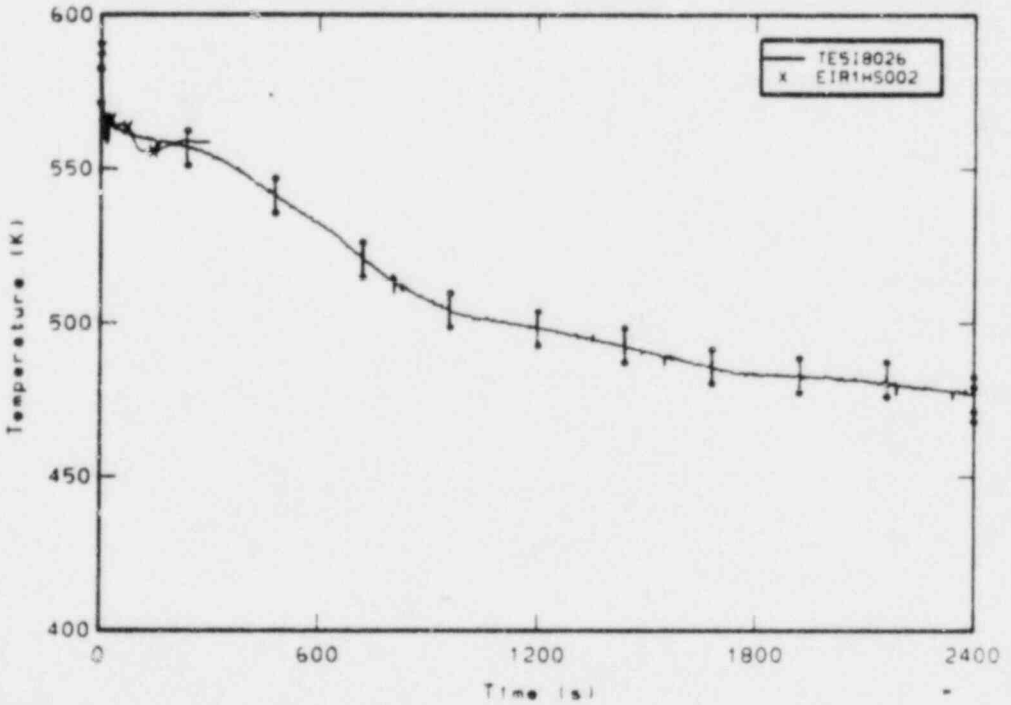

Figure D-12. Comparison of measured rod cladding temperature at the 0.66m elevation and EIR1 calculated rod cladding temperature.

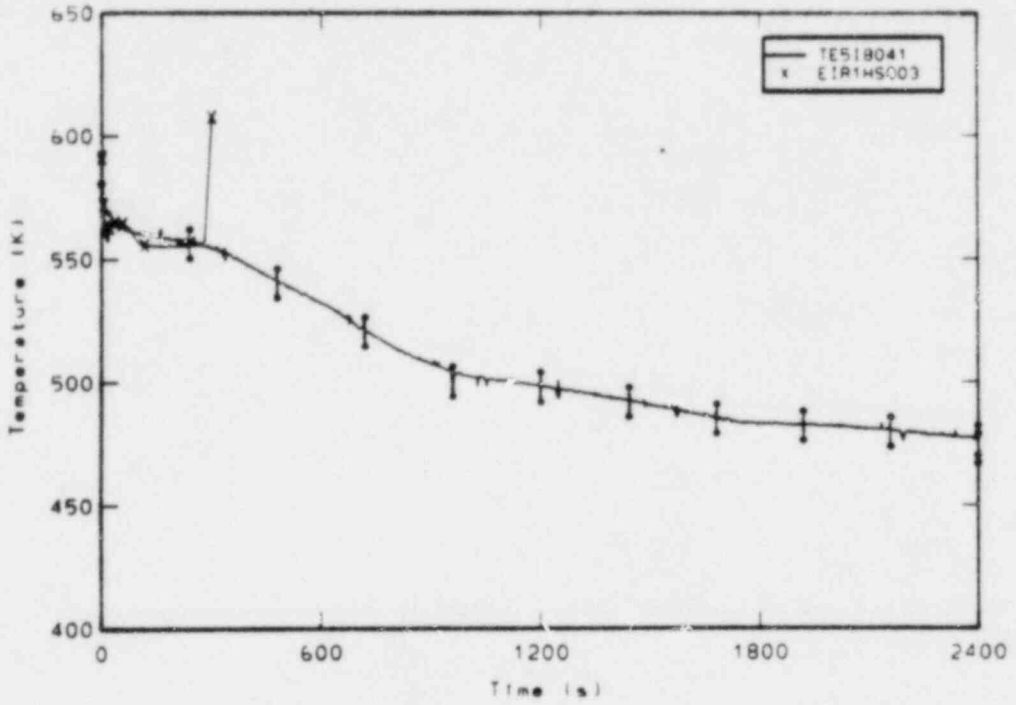

Figure D-13. Comparison of measured rod cladding temperature at the 1.04m elevation and EIA1 calculated rod cladding temperatures.

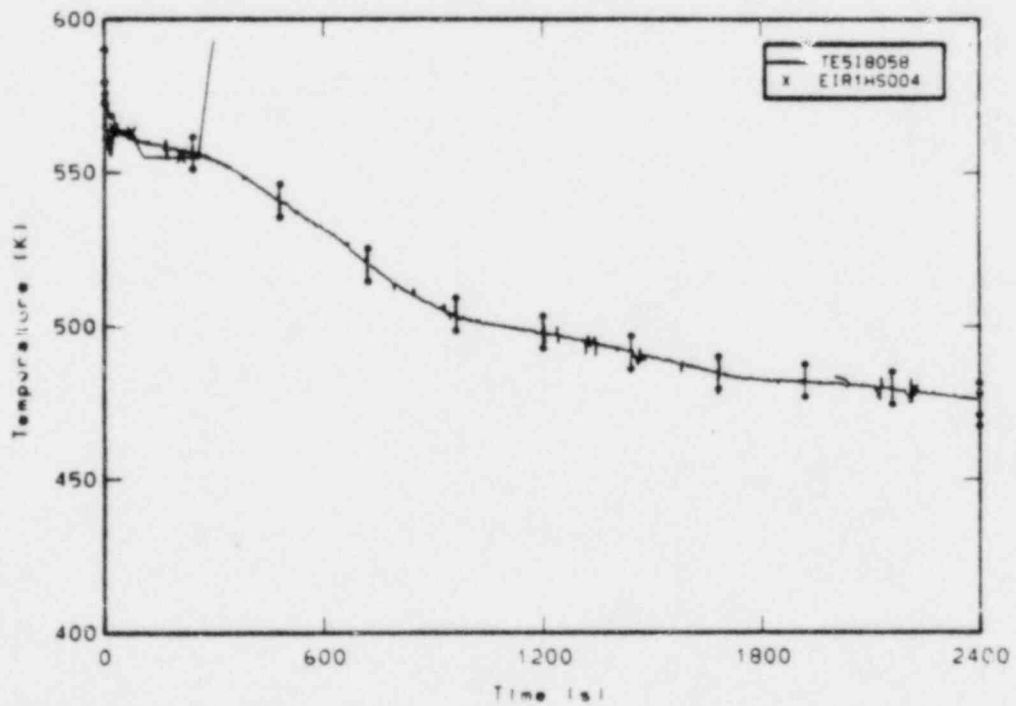

Figure D-14. Comparison of measured rod cladding temperature at the 1.47m elevation and EIA1 calculated rod cladding temperatures.

APPENDIX E

COMPARISONS OF EIDG. INSTITUT FÜR REAKTORFORSCHUNG MODEL 2 CALCULATED RESULTS WITH LOFT EXPERIMENT MEASUREMENTS

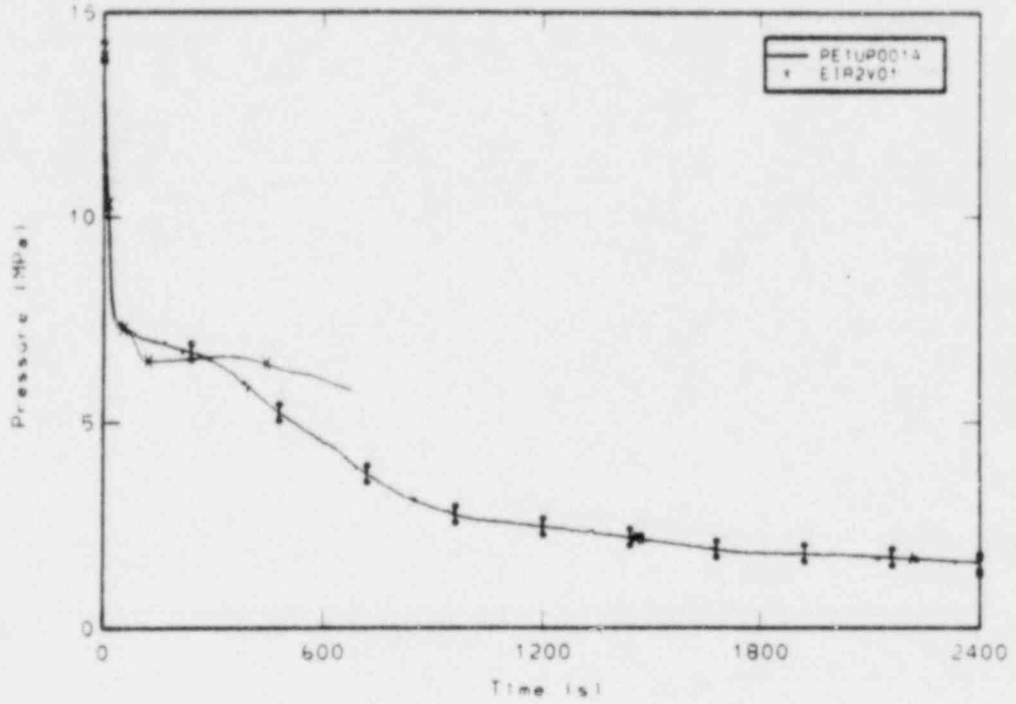

Figure E-1. Comparison of measured and E1R2 calculated upper plenum pressure.

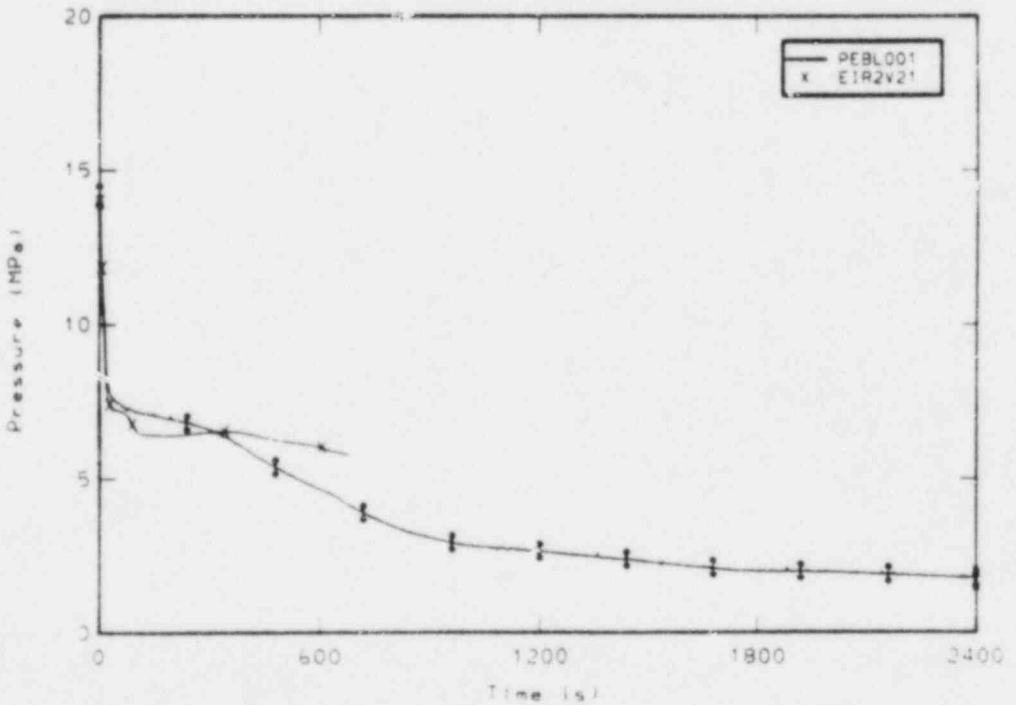

Figure E-2. Comparison of measured and E1R2 calculated broken loop cold leg pressure.

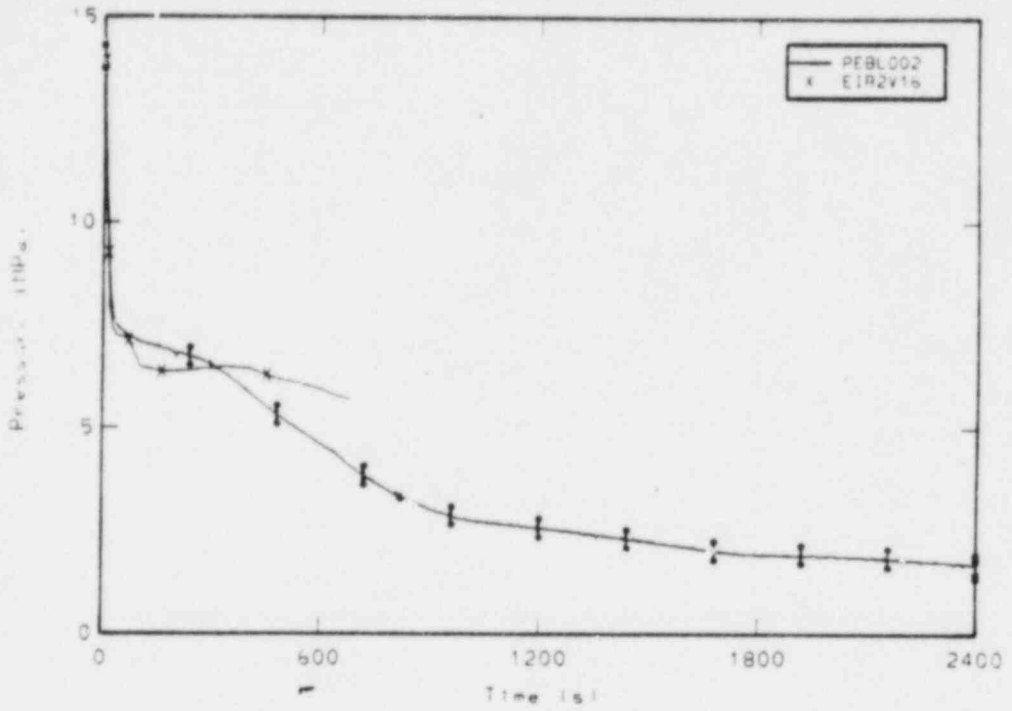

Figure E-3. Comparison of measured and EIR2 calculated broken loop hot leg pressure.

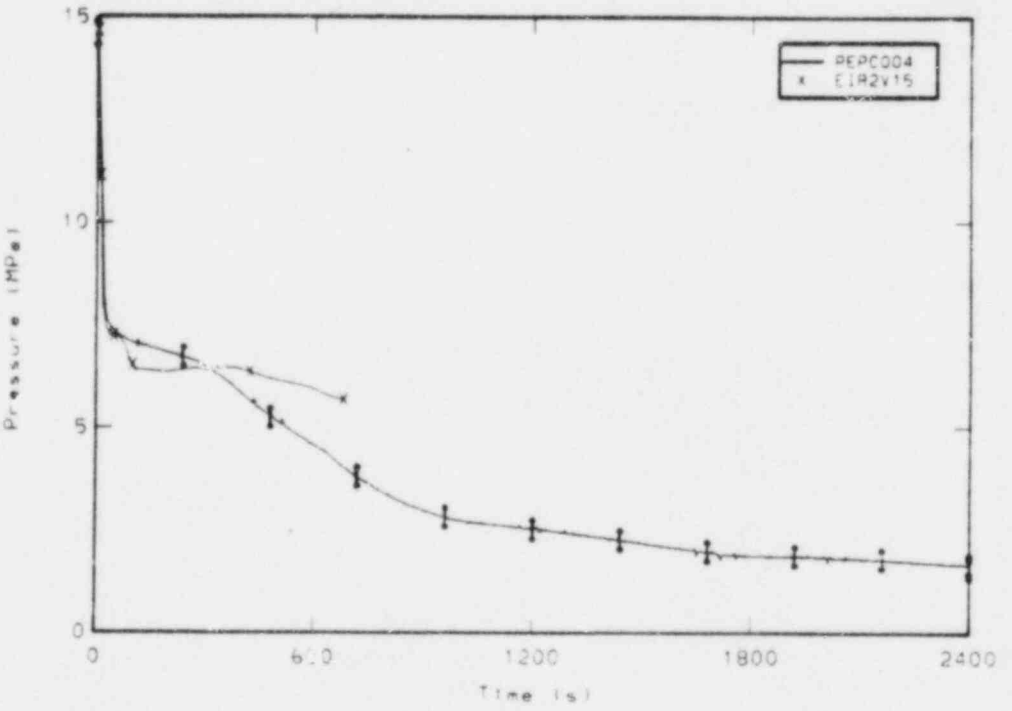

Figure E-4. Comparison of measured and EIR2 calculated pressurizer pressure.

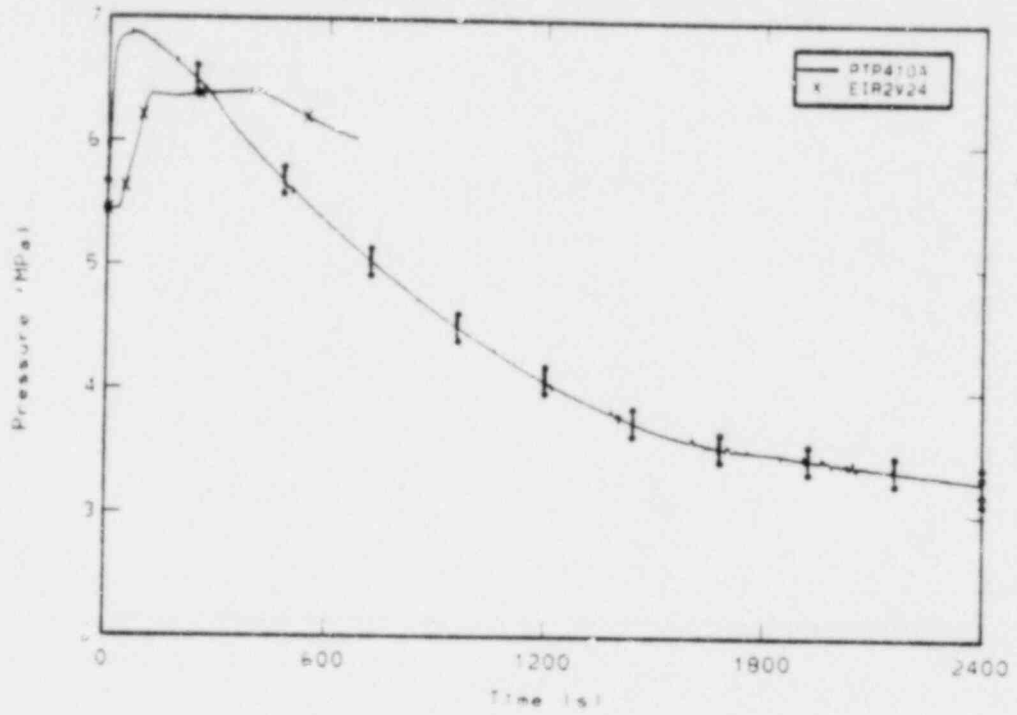

Figure E-5. Comparison of measured and EIR2 calculated steam generator secondary pressure.

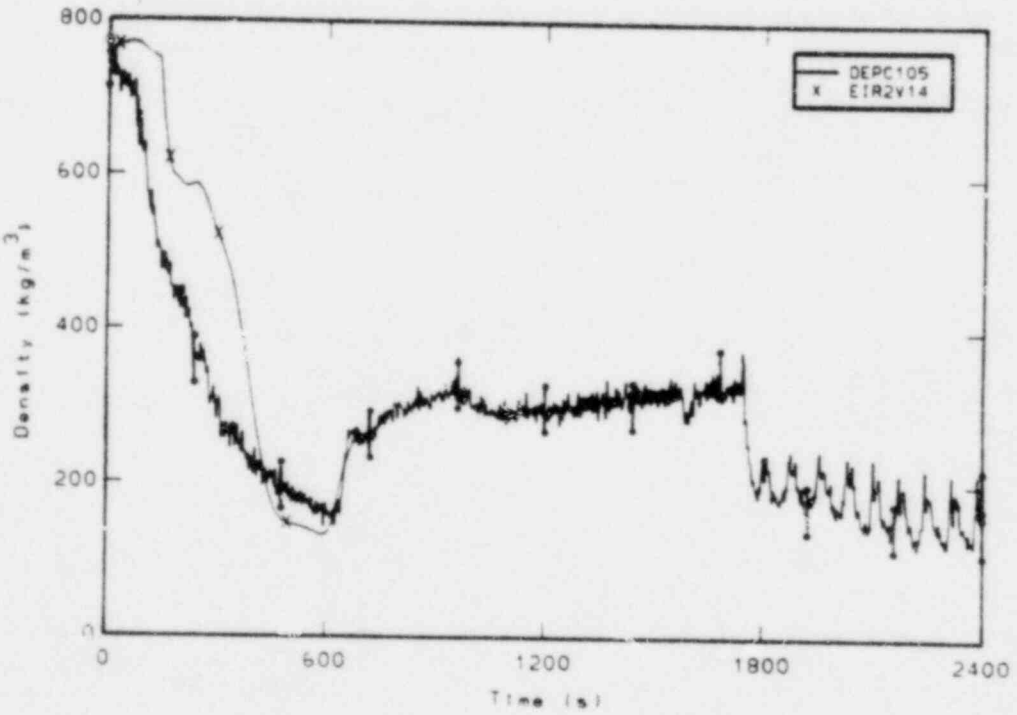

Figure E-6. Comparison of measured and EIR2 calculated average density in the intact loop cold leg.

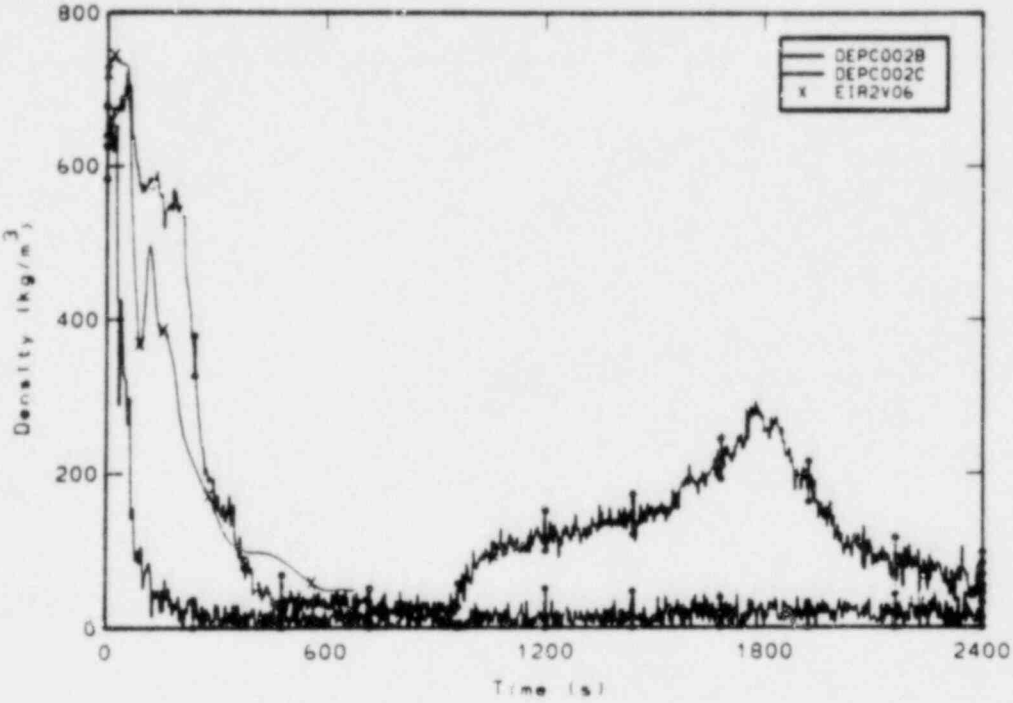

Figure E-7. Comparison of measured chordal densities and EIR2 calculated average density in the intact loop hot leg.

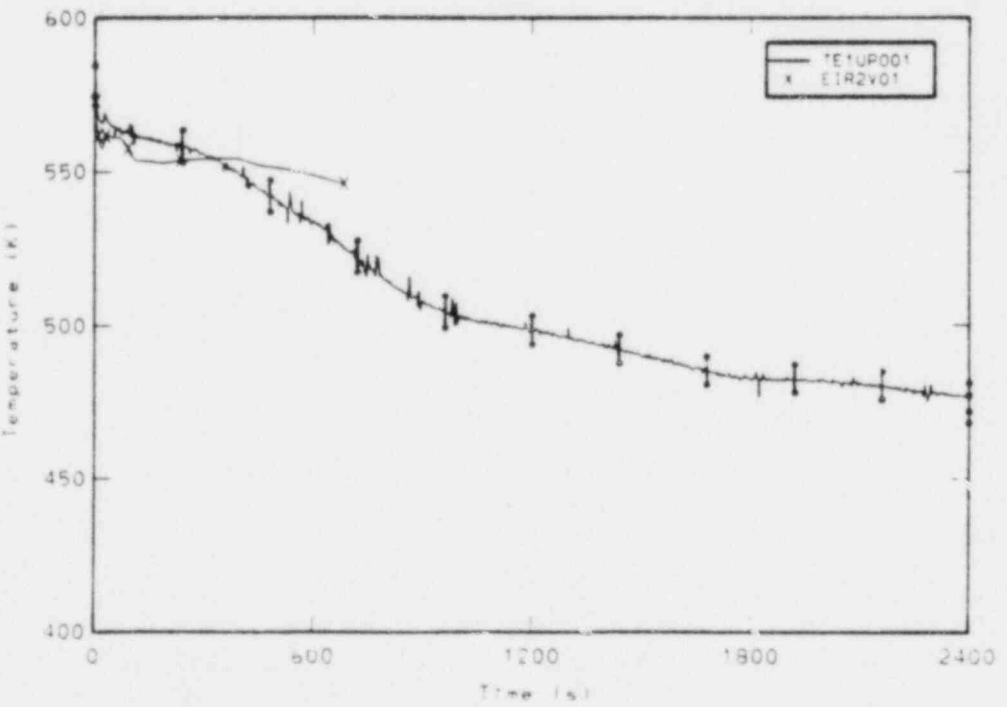

Figure E-8. Comparison of measured and EIR2 calculated upper plenum fluid temperature.

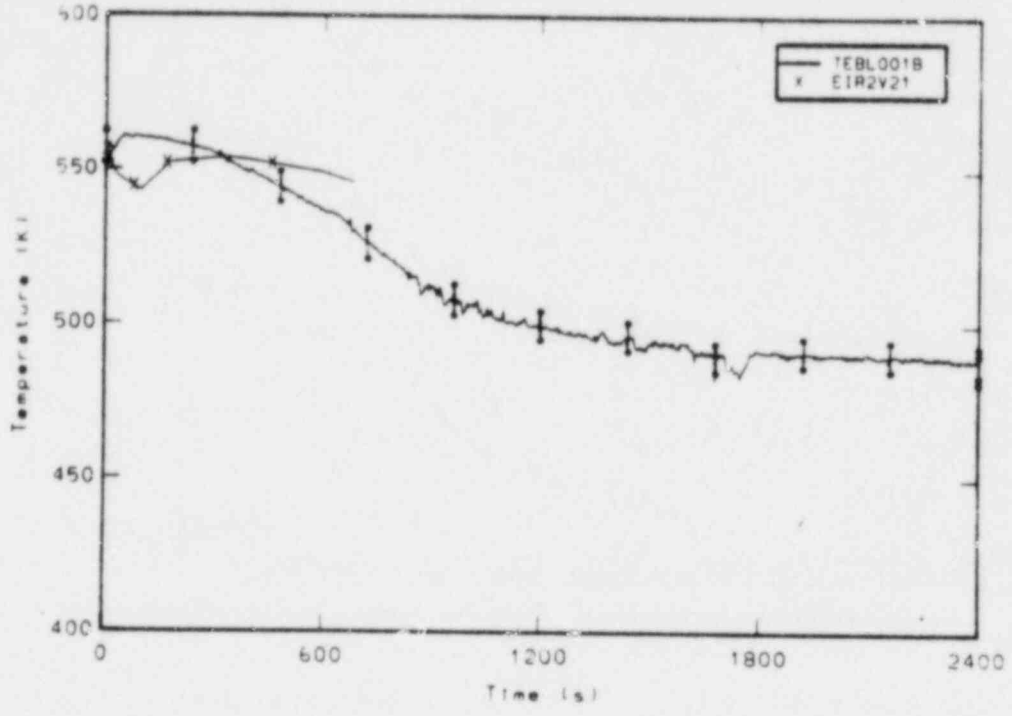

Figure E-9. Comparison of measured and EIR2 calculated broken loop cold leg fluid temperature.

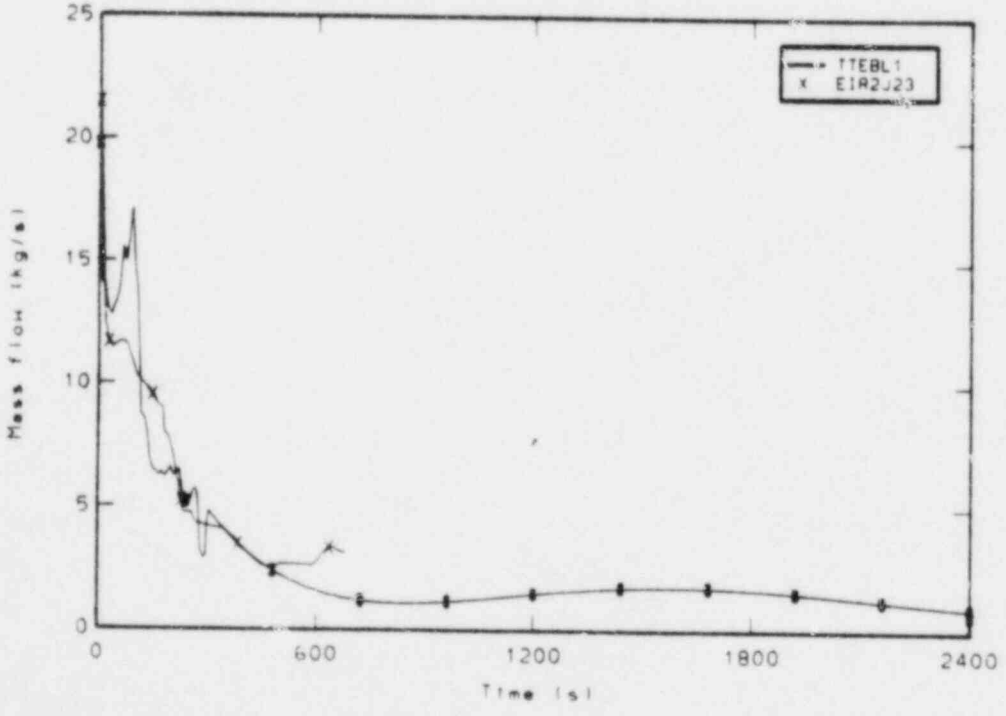

Figure E-10. Comparison of measured and EIR2 calculated mass flow rate at the break.

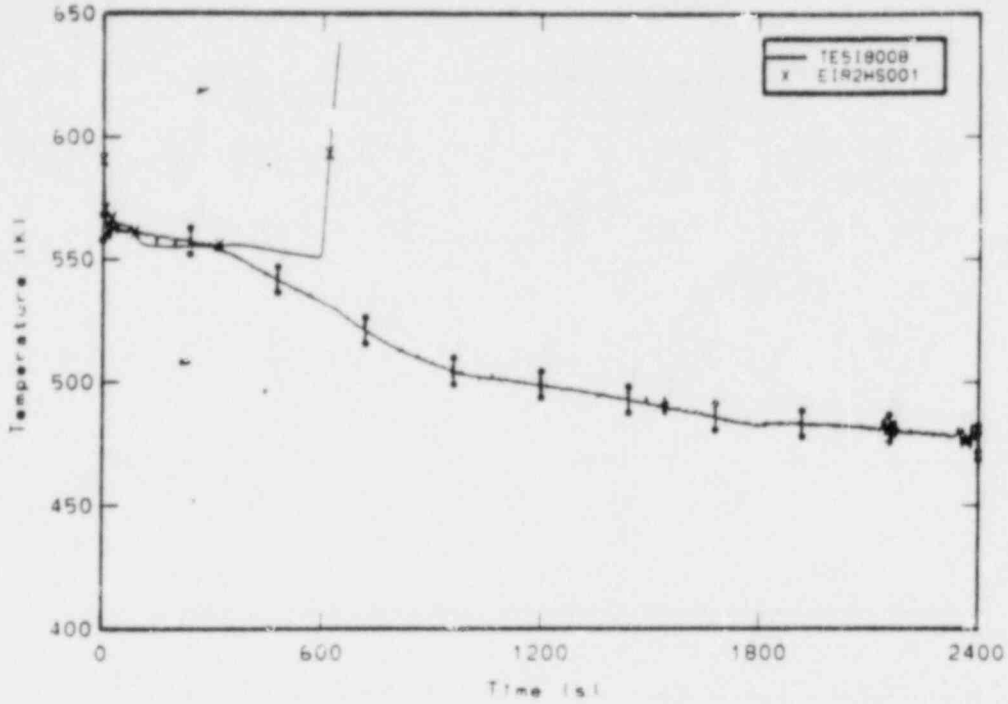

Figure E-11. Comparison of measured rod cladding temperature at the 0.20m elevation and EIR2 calculated rod cladding temperature.

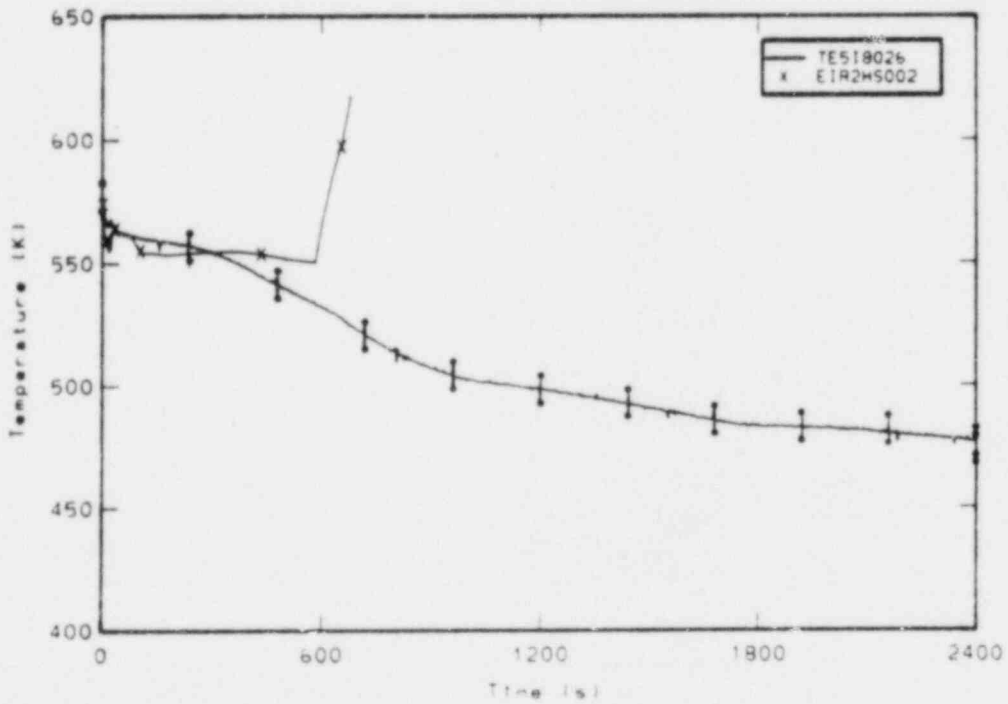

Figure E-12. Comparison of measured rod cladding temperature at the 0.66m elevation and EIR2 calculated rod cladding temperature.

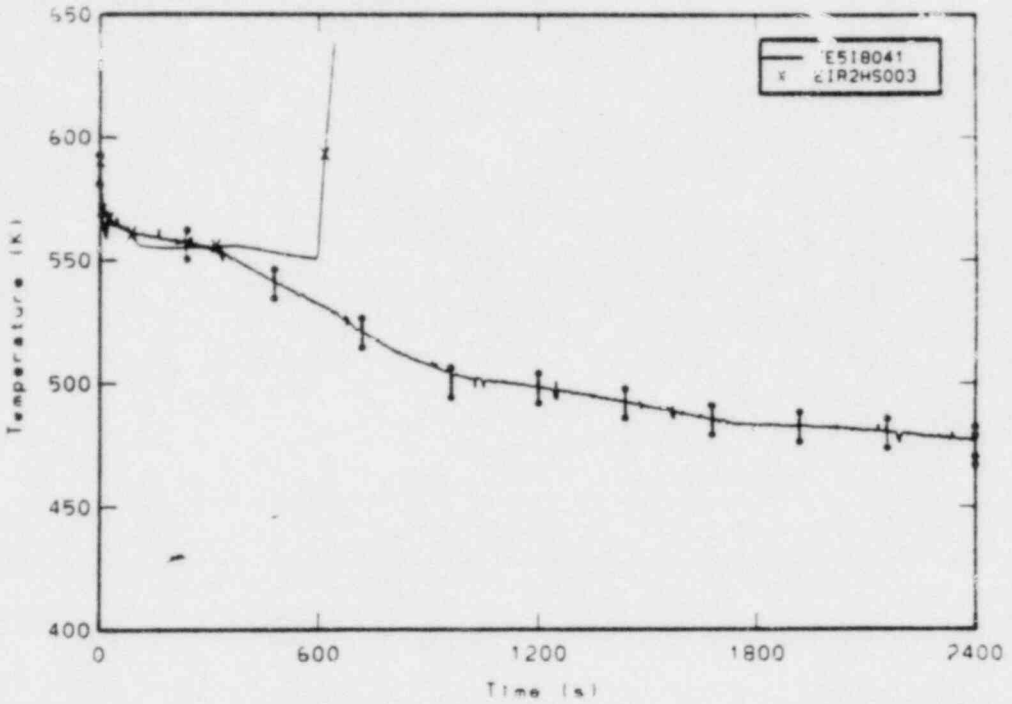

Figure E-13. Comparison of measured rod cladding temperature at the 1.04m elevation and EIR2 calculated rod cladding temperature.

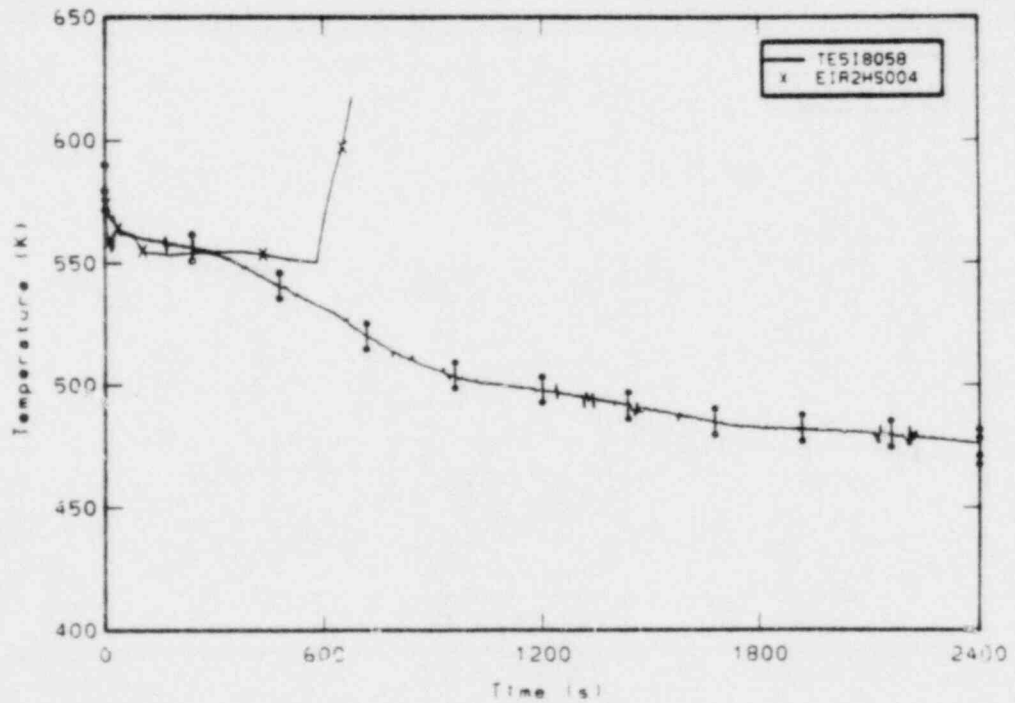

Figure E-14. Comparison of measured rod cladding temperature at the 1.47m elevation and EIR2 calculated rod cladding temperature.

APPENDIX F

COMPARISONS OF FRAMATOME CALCULATED RESULTS WITH LOFT EXPERIMENT MEASUREMENTS

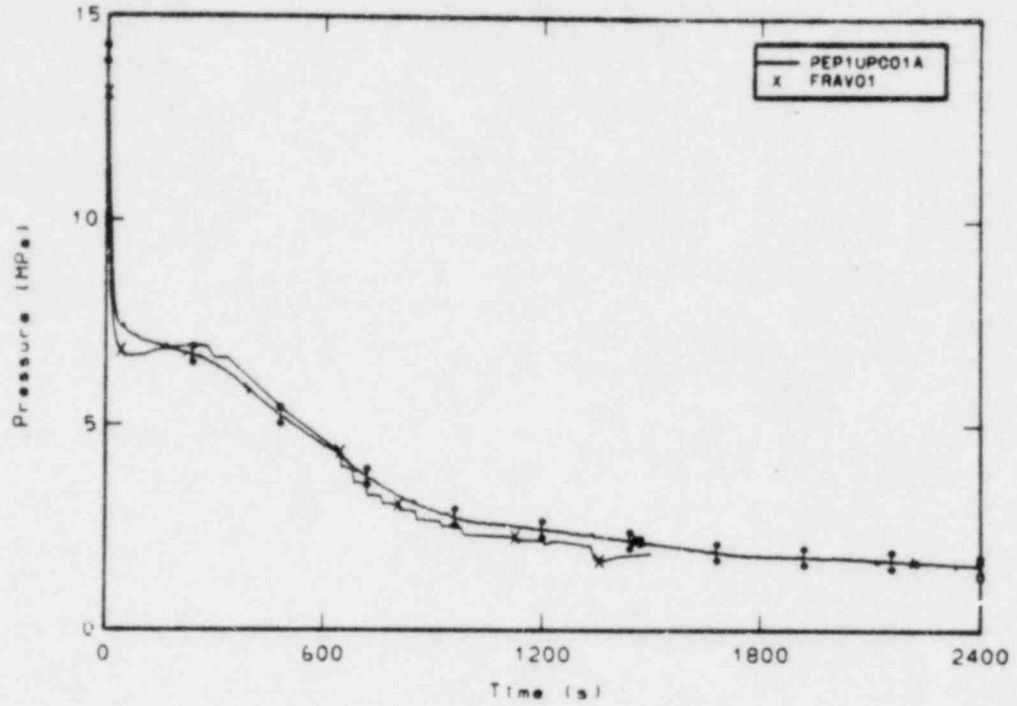

Figure F-1. Comparison of measured and FRA calculated upper plenum pressure.

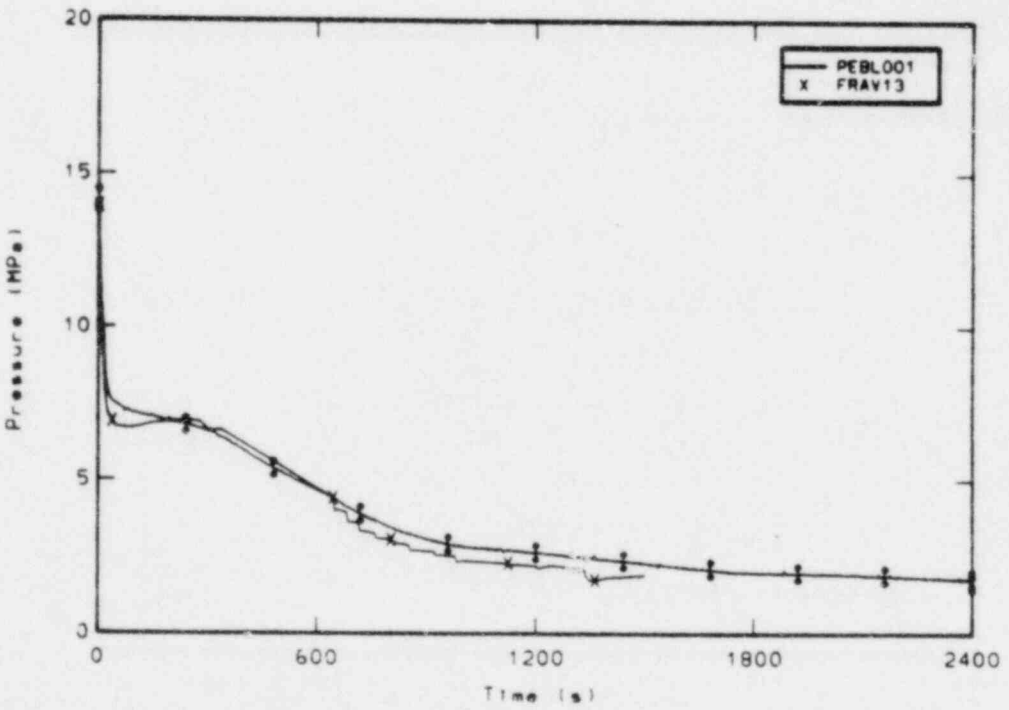

Figure F-2. Comparison of measured and FRA calculated broken loop cold leg pressure.

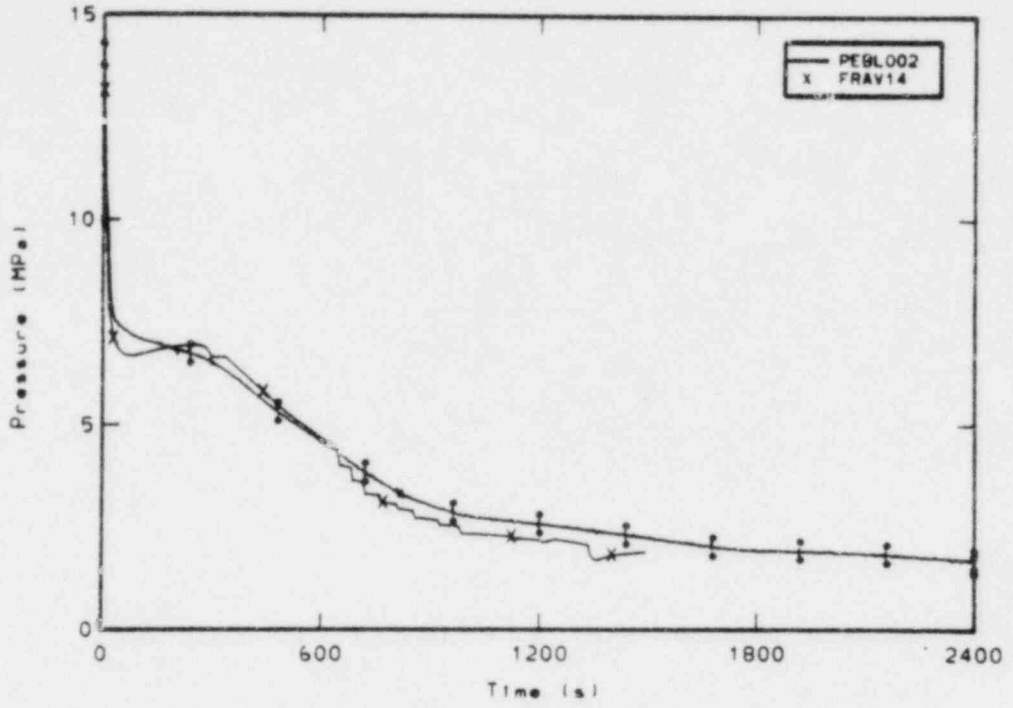

Figure F-3. Comparison of measured and FRA calculated broken loop hot leg pressure.

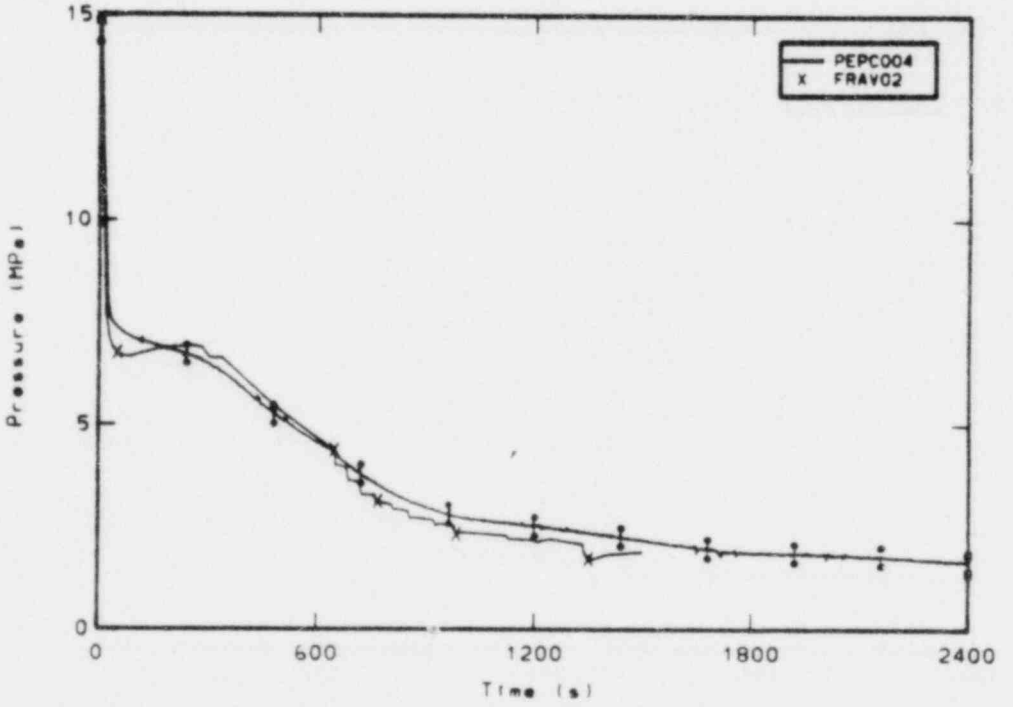

Figure F-4. Comparison of measured and FRA calculated pressurizer pressure.

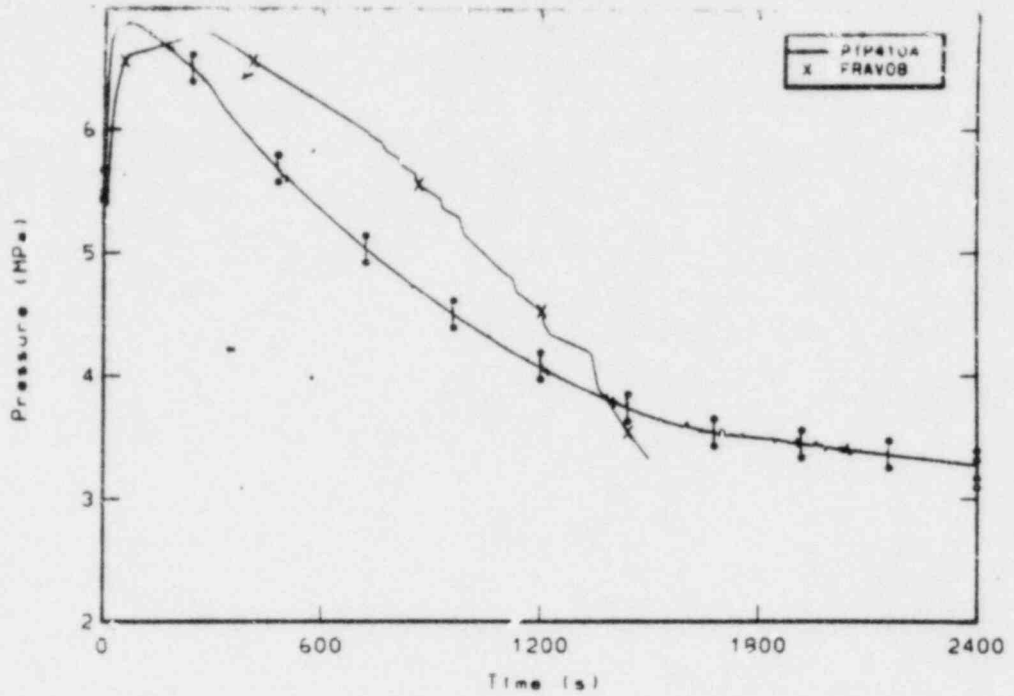

Figure F-5. Comparison of measured and FRA calculated steam generator secondary pressure.

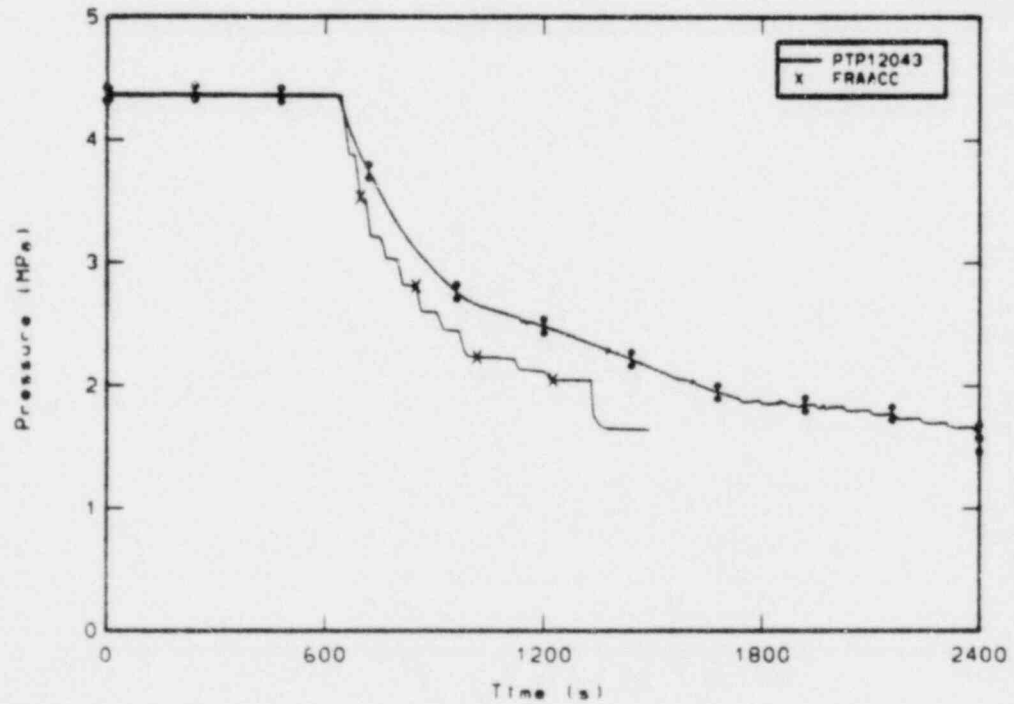

Figure F-6. Comparison of measured and FRA calculated accumulator pressure.

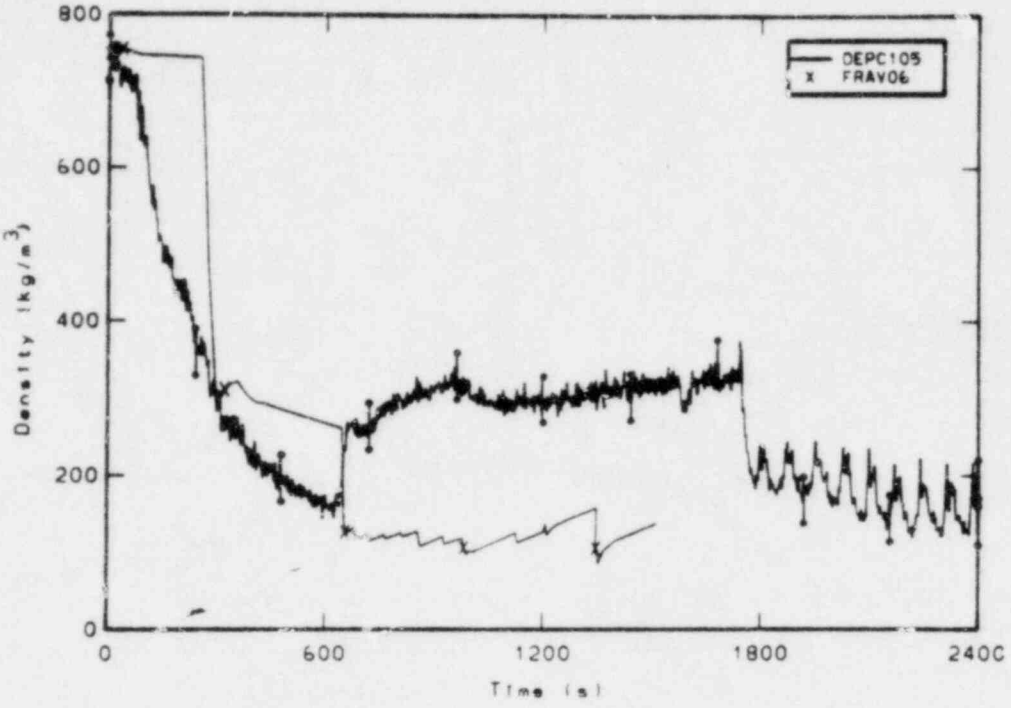

Figure F-7. Comparison of measured and FRA calculated average density in the intact loop cold leg.

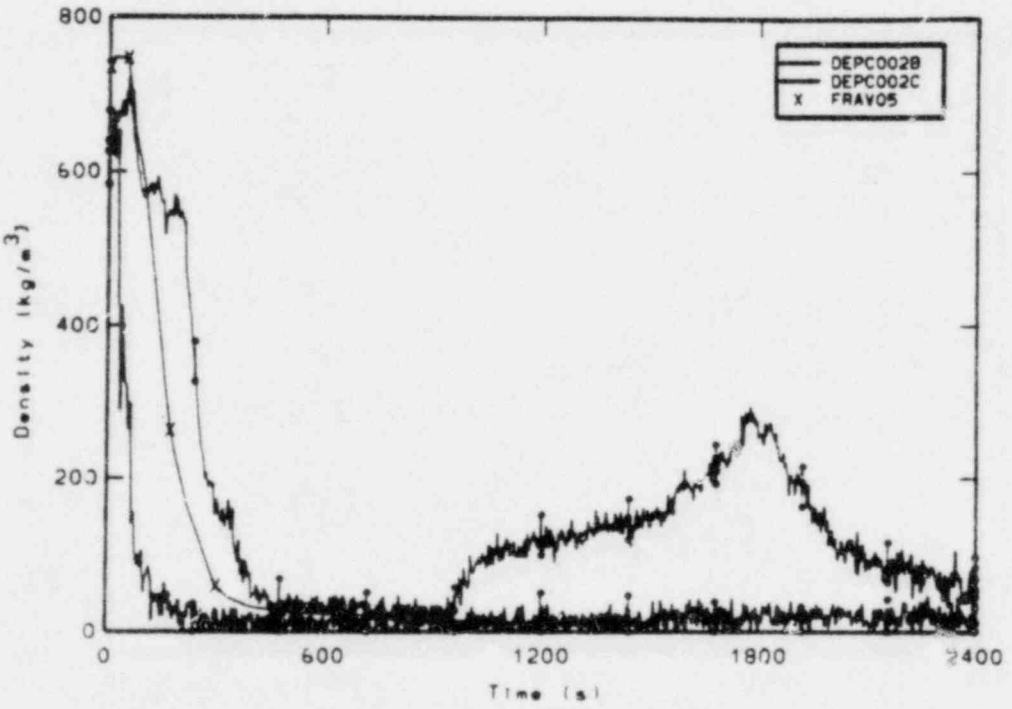

Figure F-8. Comparison of measured chordal densities and FRA calculated average density in the intact loop hot leg.

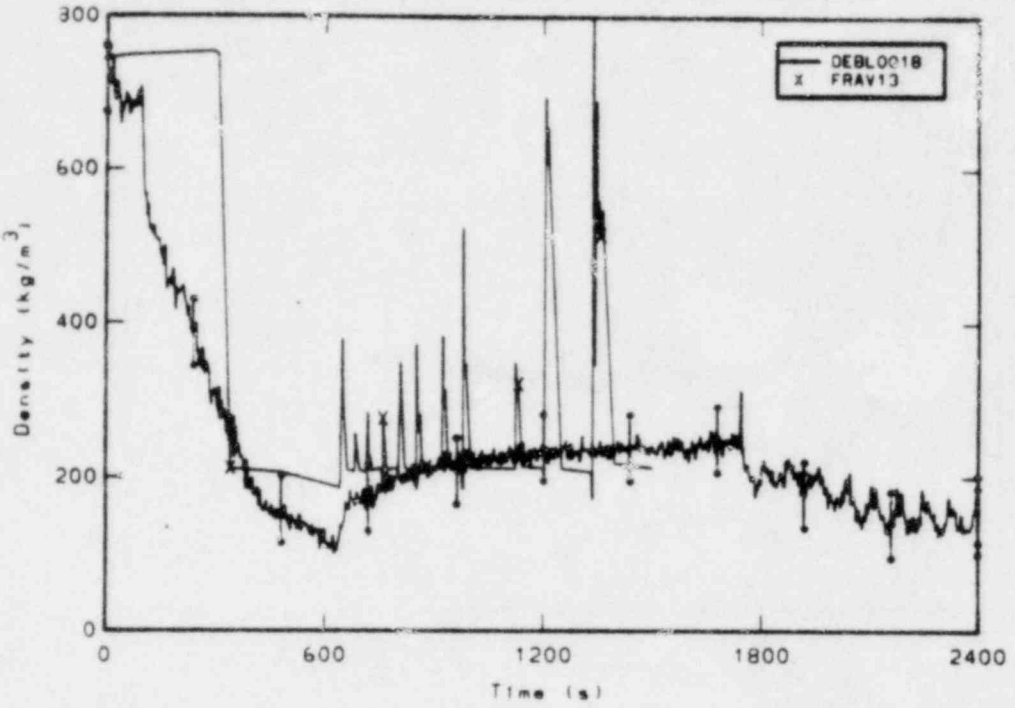

Figure F-9. Comparison of measured chordal density and FRA calculated average density in the broken loop cold leg.

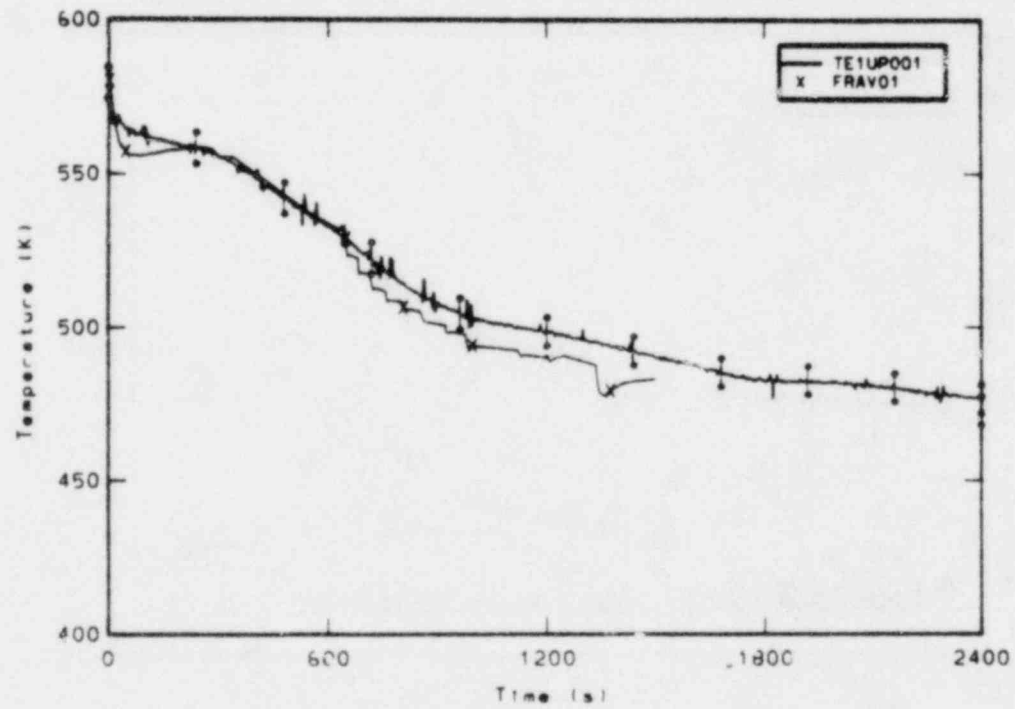

Figure F-10. Comparison of measured and FRA calculated upper plenum fluid temperature.

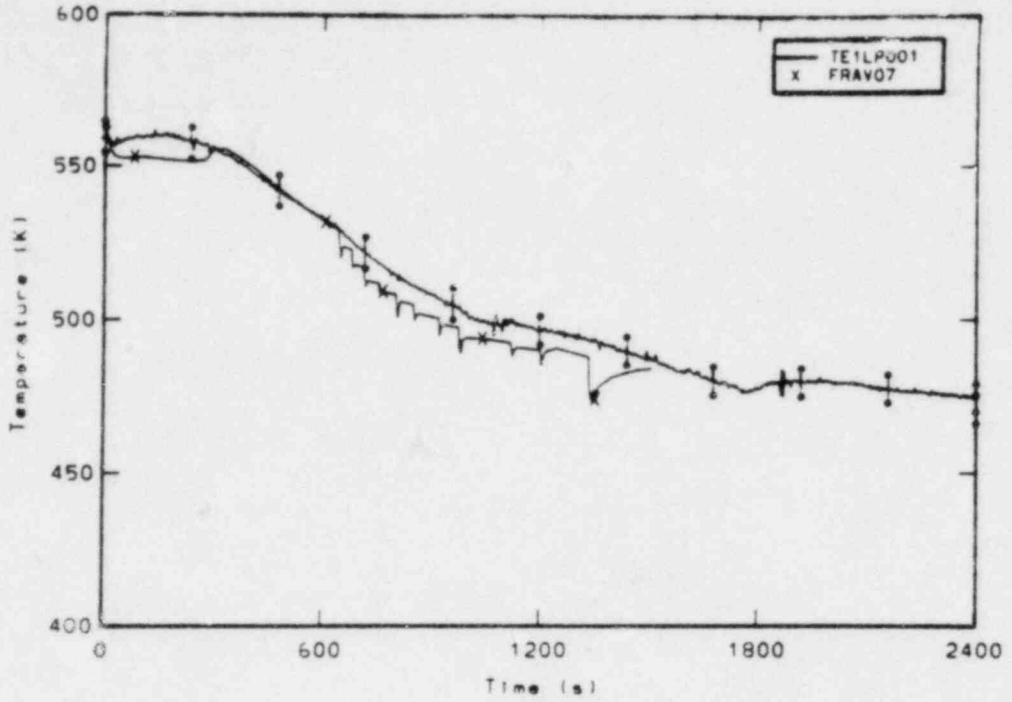

Figure F-11. Comparison of measured and FRA calculated lower plenum fluid temperature.

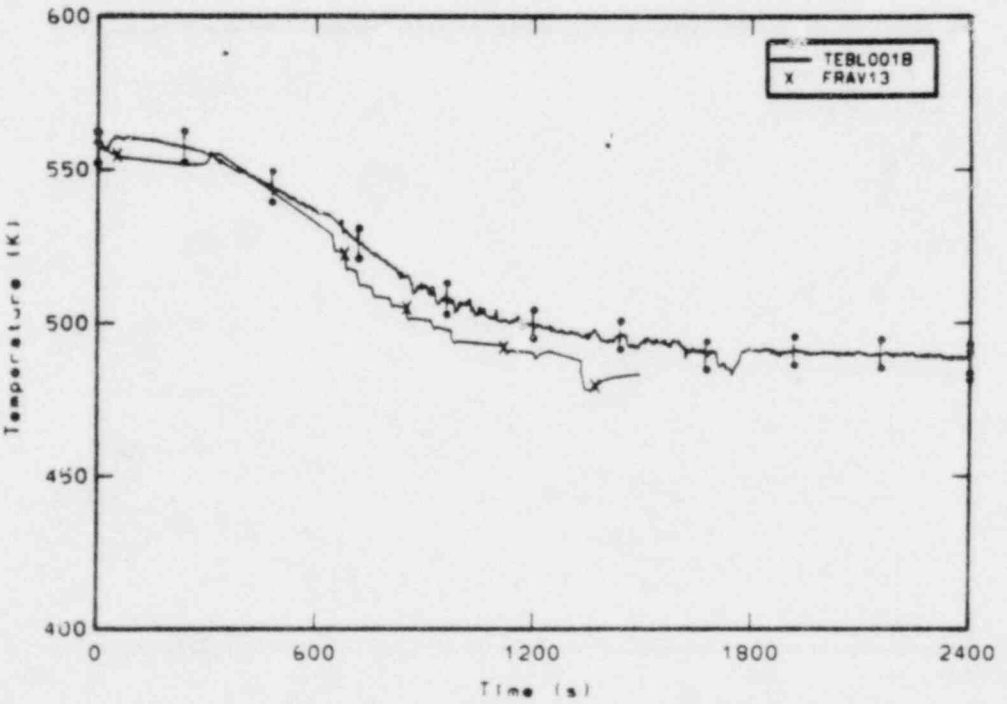

Figure F-12. Comparison of measured and FRA calculated broken loop cold leg fluid temperature.

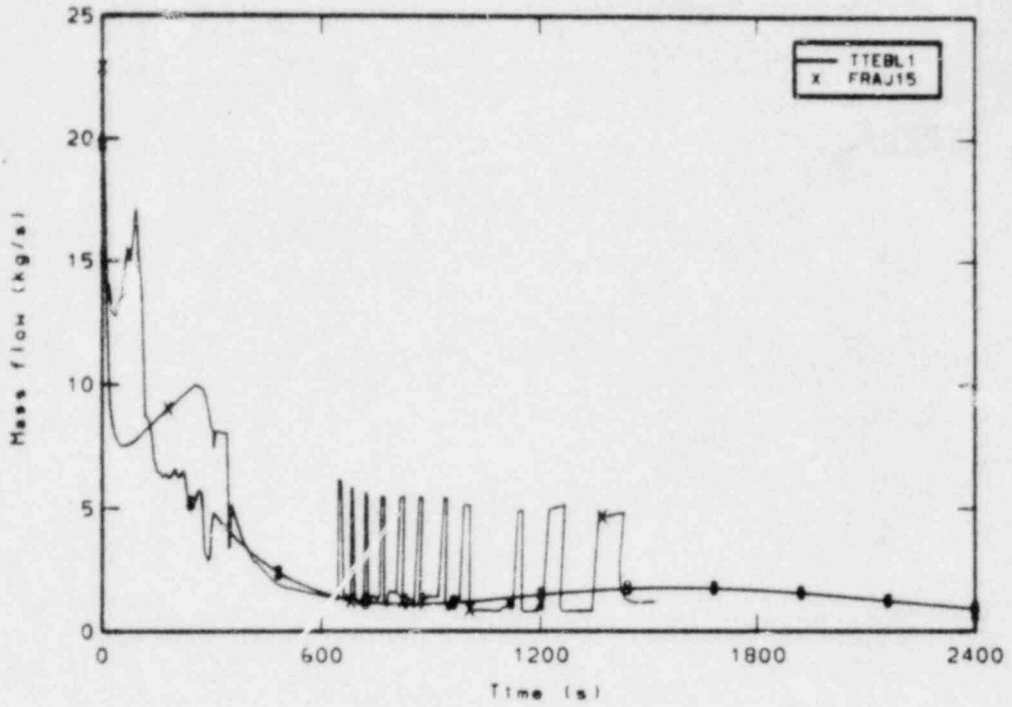

Figure F-13 Comparison of measured and FRA calculated mass flow rate at the break.

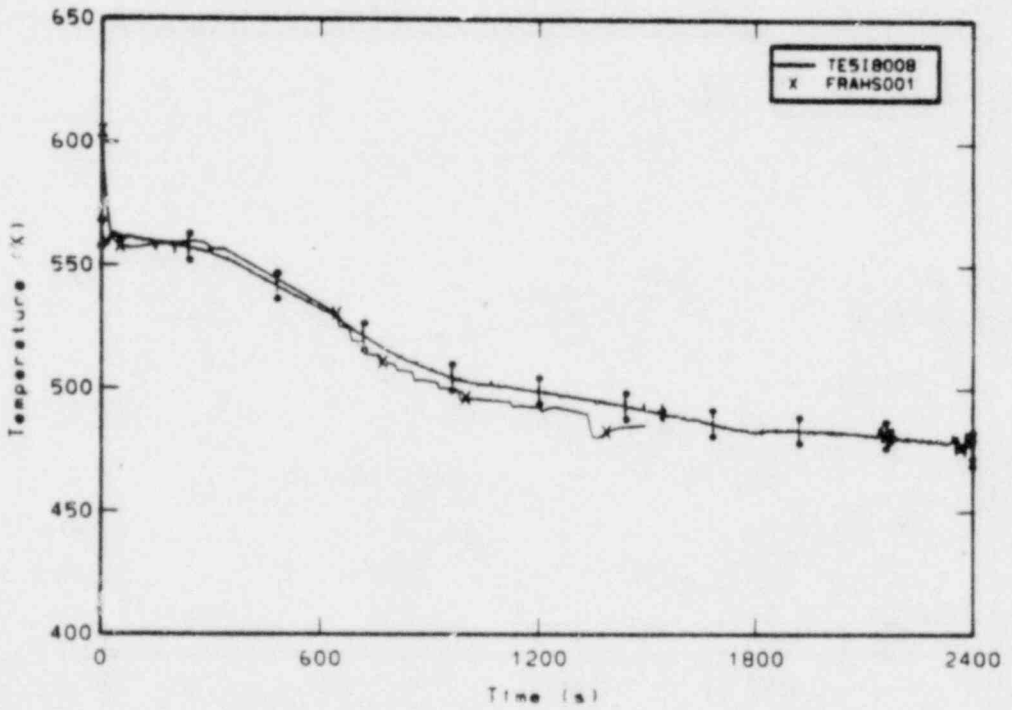

Figure F-14. Comparison of measured rod cladding temperature at the 0.20m elevation and FRA calculated rod cladding temperature.

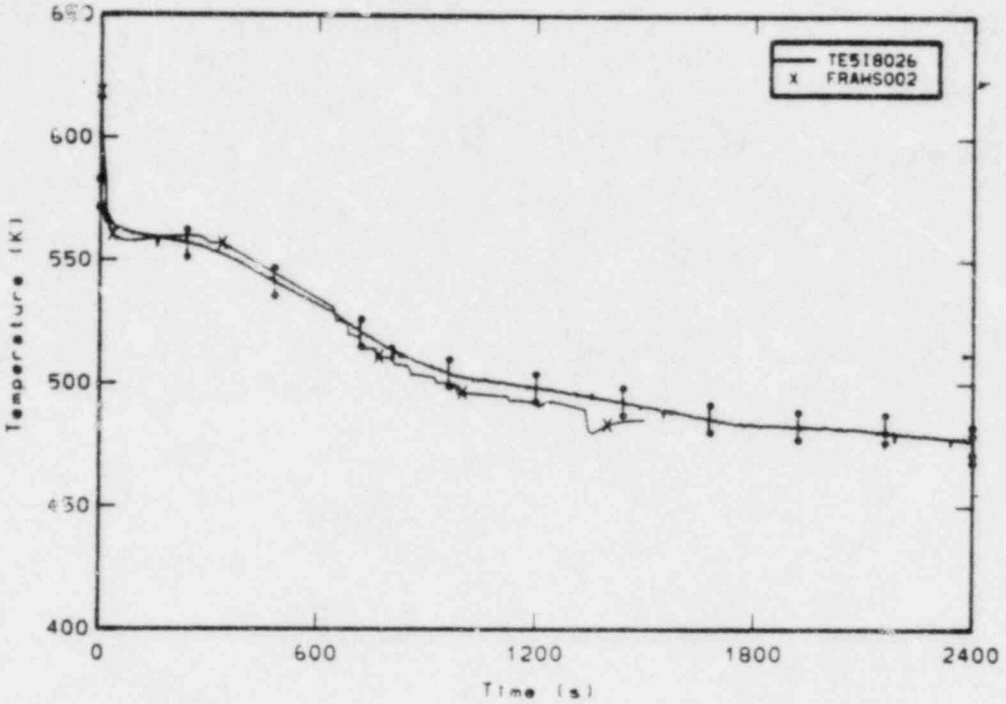

Figure F-15. Comparison of measured rod cladding temperature at the 0.66m elevation and FRA calculated rod cladding temperature.

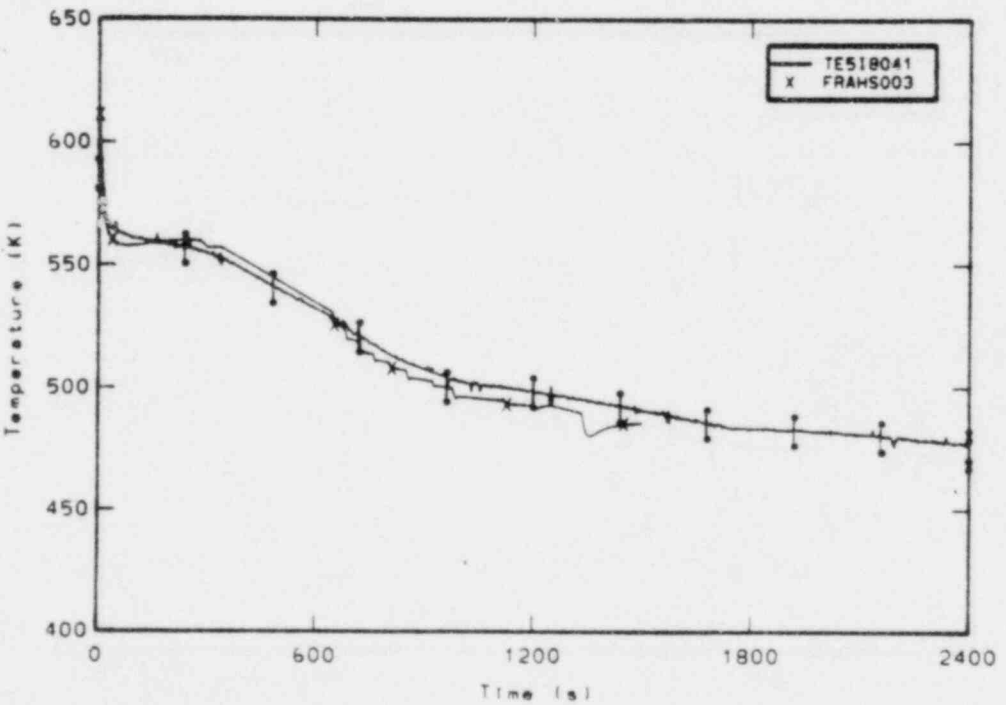

Figure F-16. Comparison of measured rod cladding temperature at the 1.04m elevation and FRA calculated rod cladding temperature.

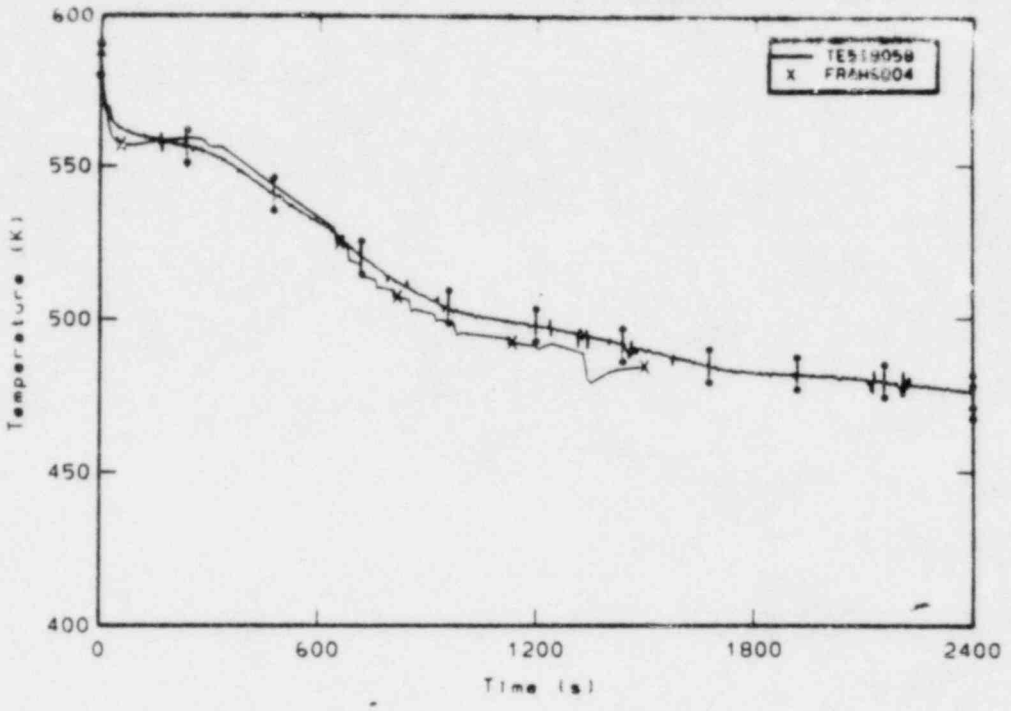

Figure F-17. Comparison of measured rod cladding temperature at the 1.47m elevation and FRA calculated rod cladding temperature.

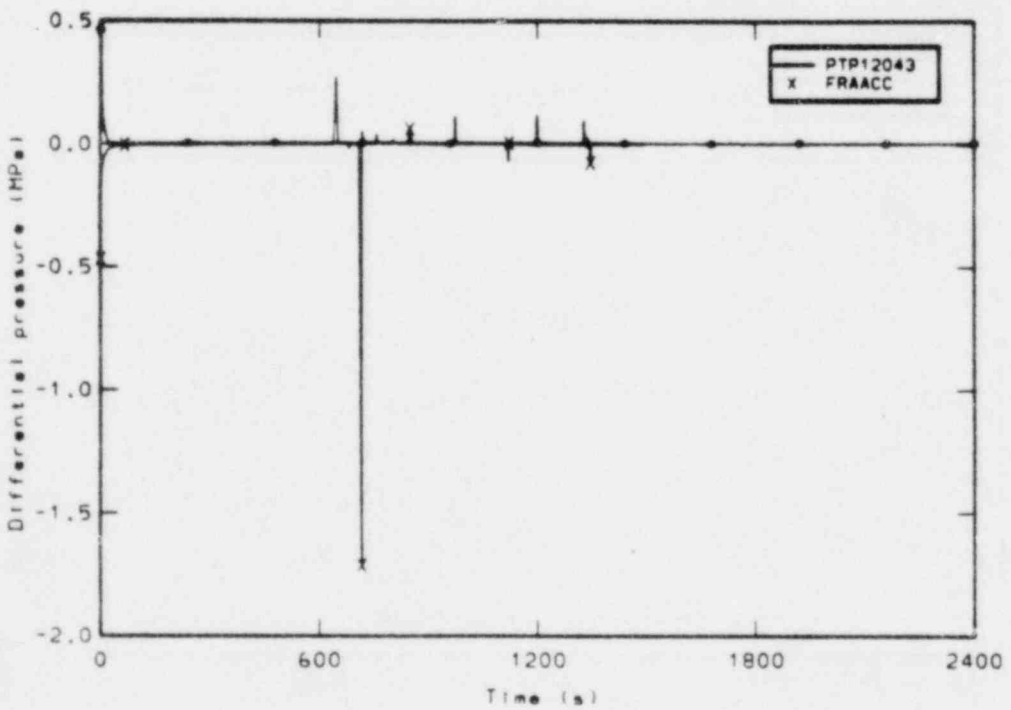

Figure F-18. Comparison of measured and FRA calculated differential pressure drop across the pumps.

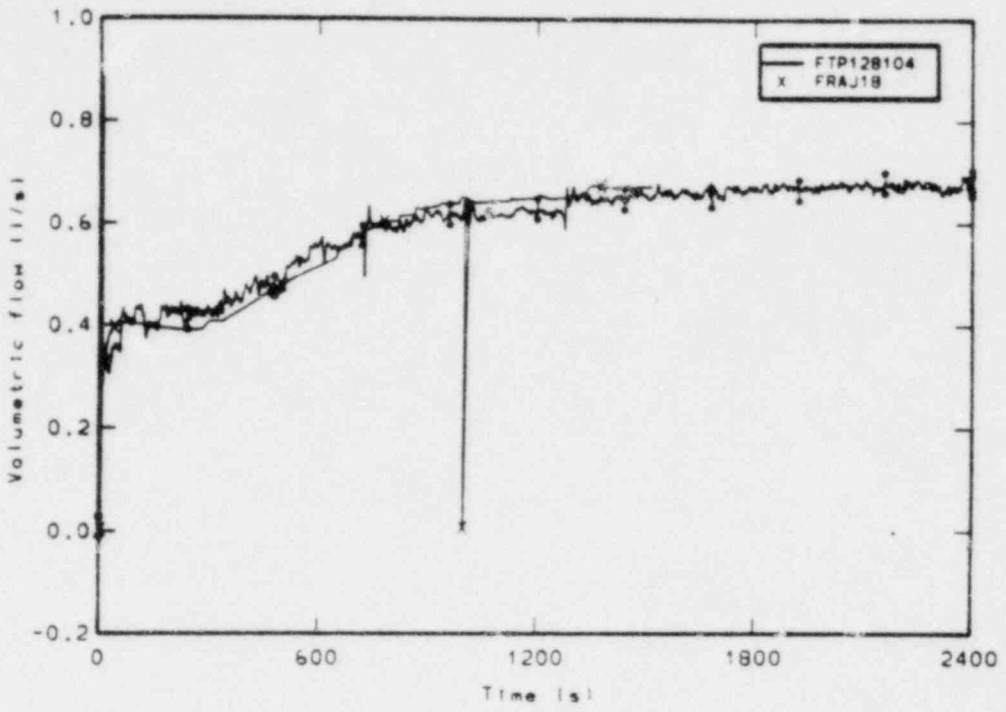

Figure F-19. Comparison of measured and FRA calculated high pressure injection system (HPIS) volumetric flow rate.

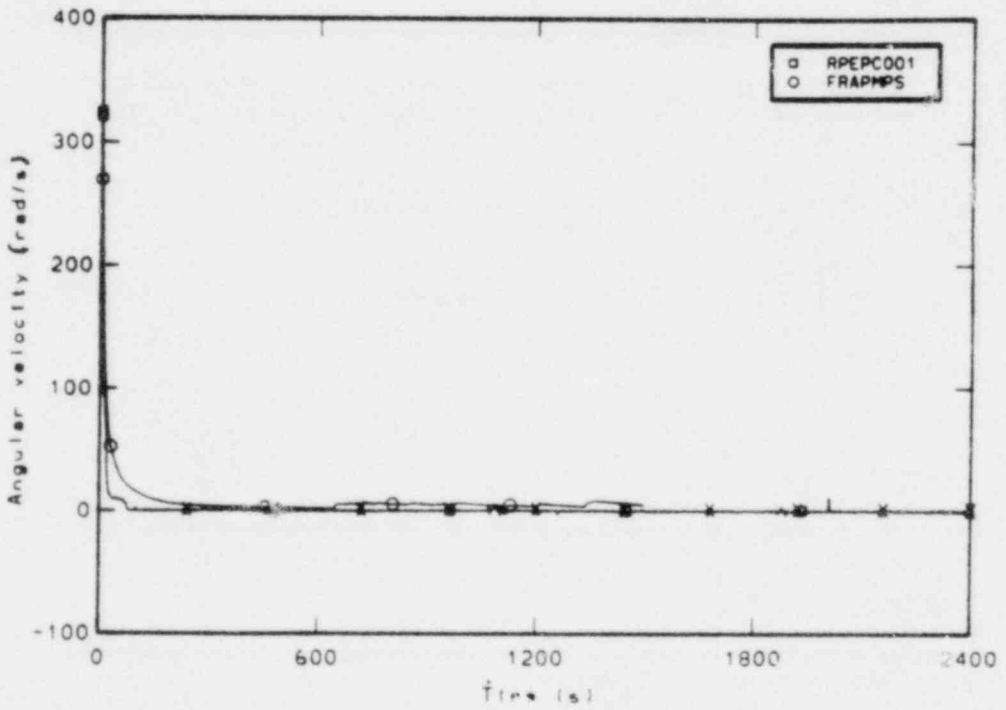

Figure F-20. Comparison of measured and FRA calculated pump speed.

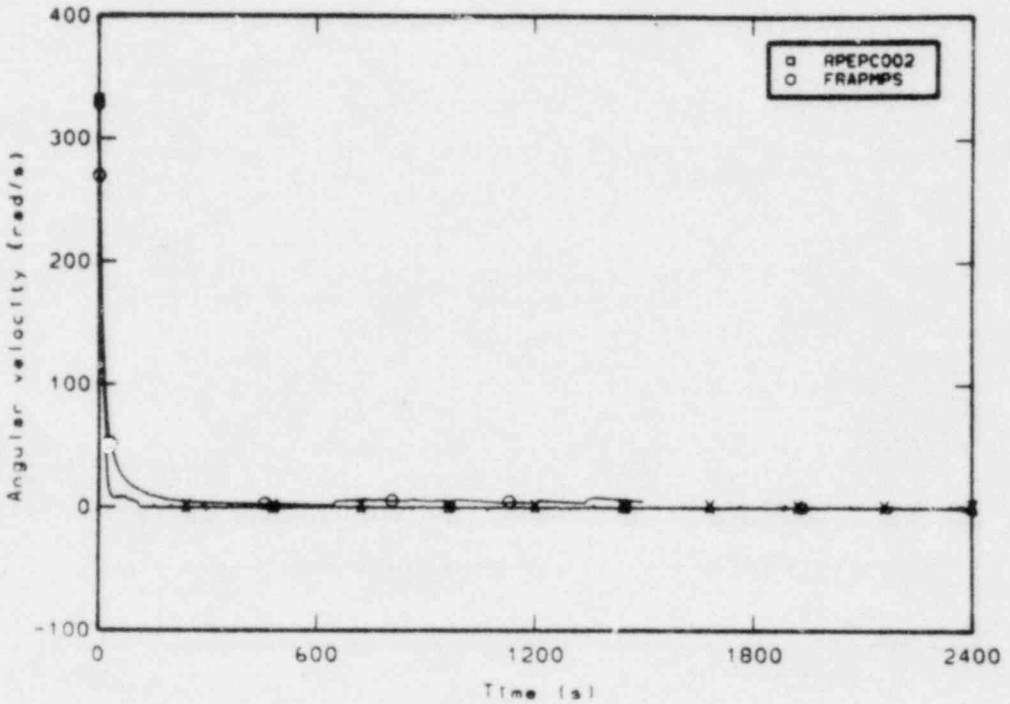

Figure F-21. Comparison of measured and FRA calculated pump speed.

APPENDIX G

COMPARISONS OF GESELLSCHAFT FÜR REAKTORSICHERHEIT CALCULATED RESULTS WITH LOFT EXPERIMENT MEASUREMENTS

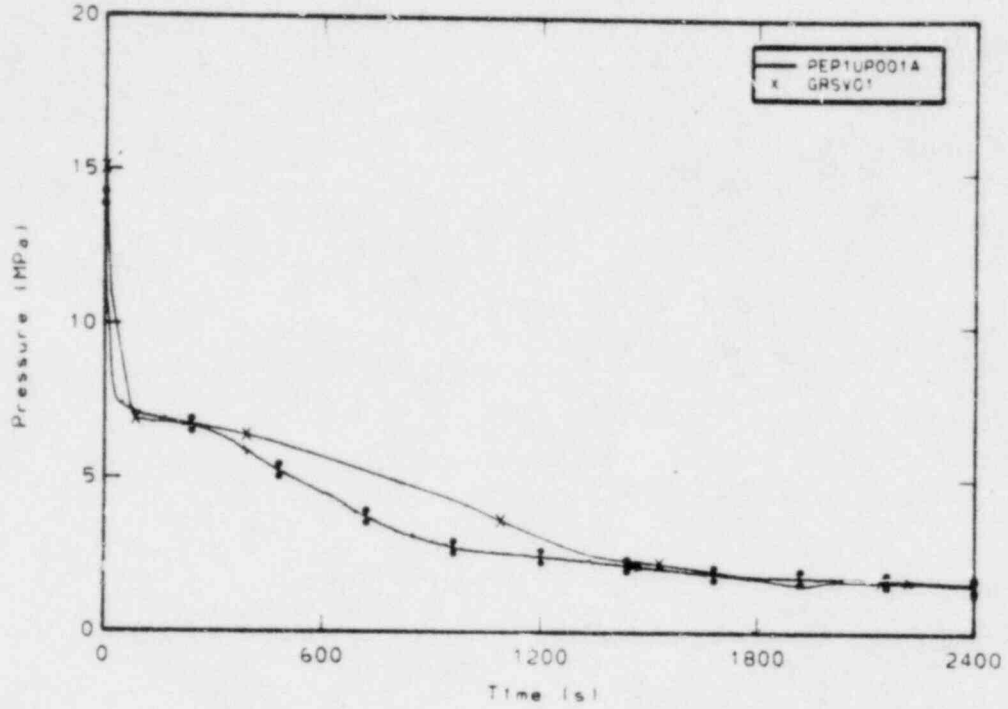

Figure G-1. Comparison of measured and GRS calculated upper plenum pressure.

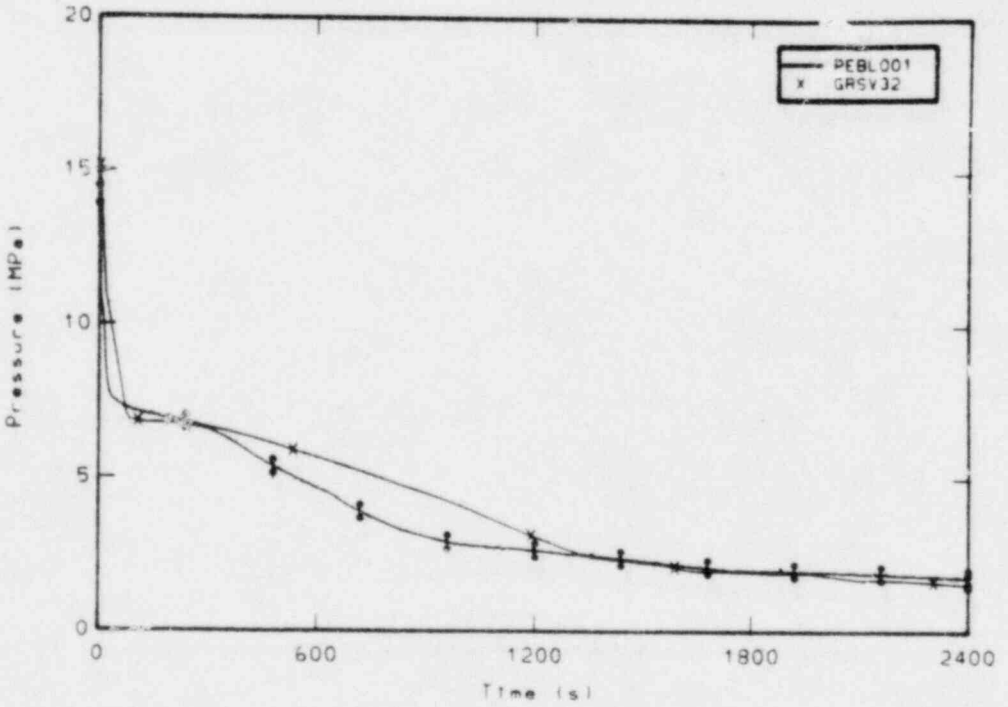

Figure G-2. Comparison of measured and GRS calculated broken loop cold leg pressure.

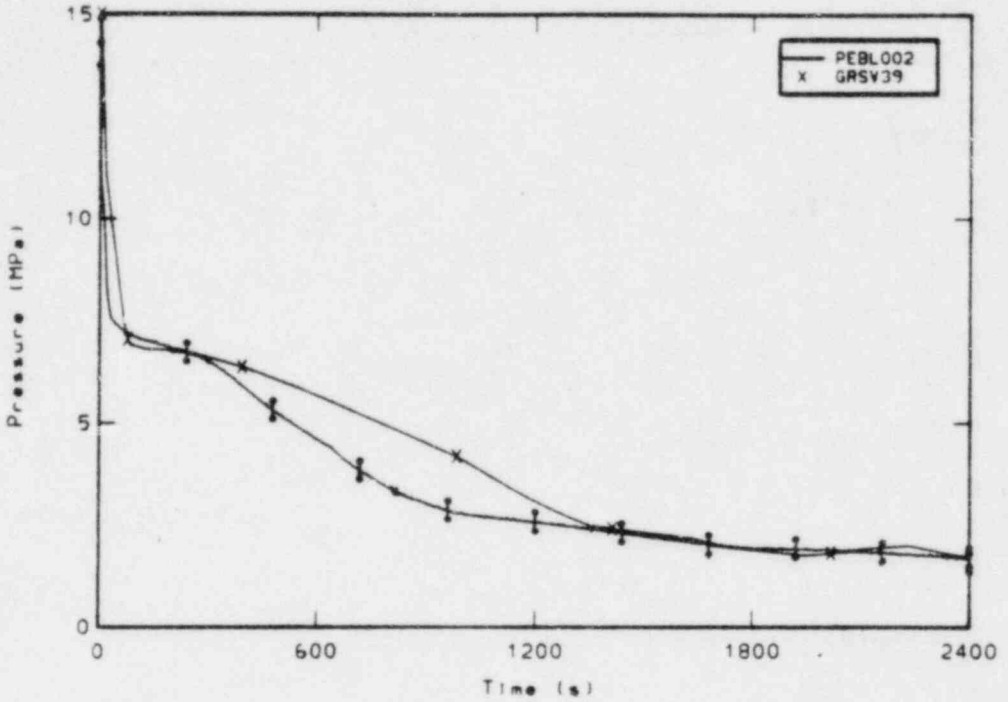

Figure G-3. Comparison of measured and GRS calculated broken loop hot leg pressure.

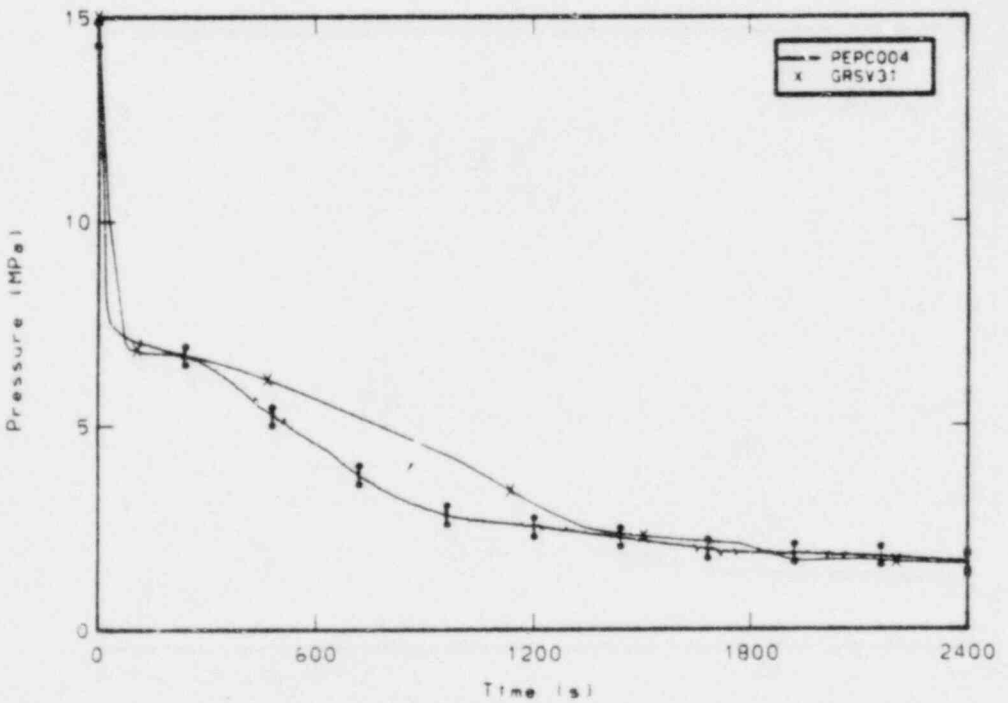

Figure G-4. Comparison of measured and GRS calculated pressurizer pressure.

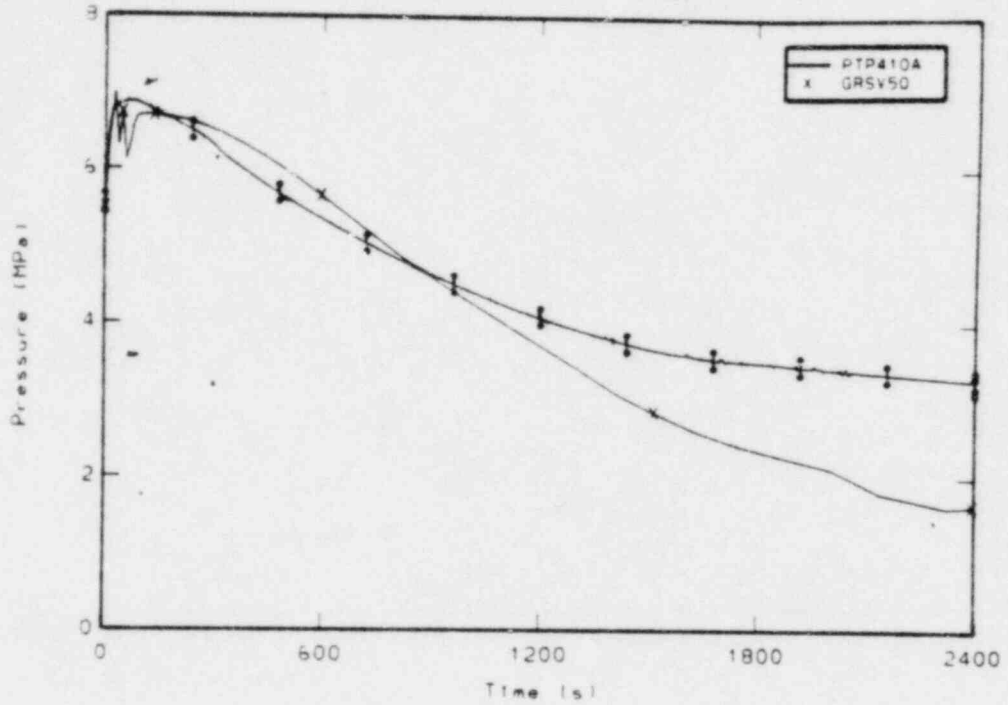

Figure G-5. Comparison of measured and GRS calculated steam generator secondary pressure.

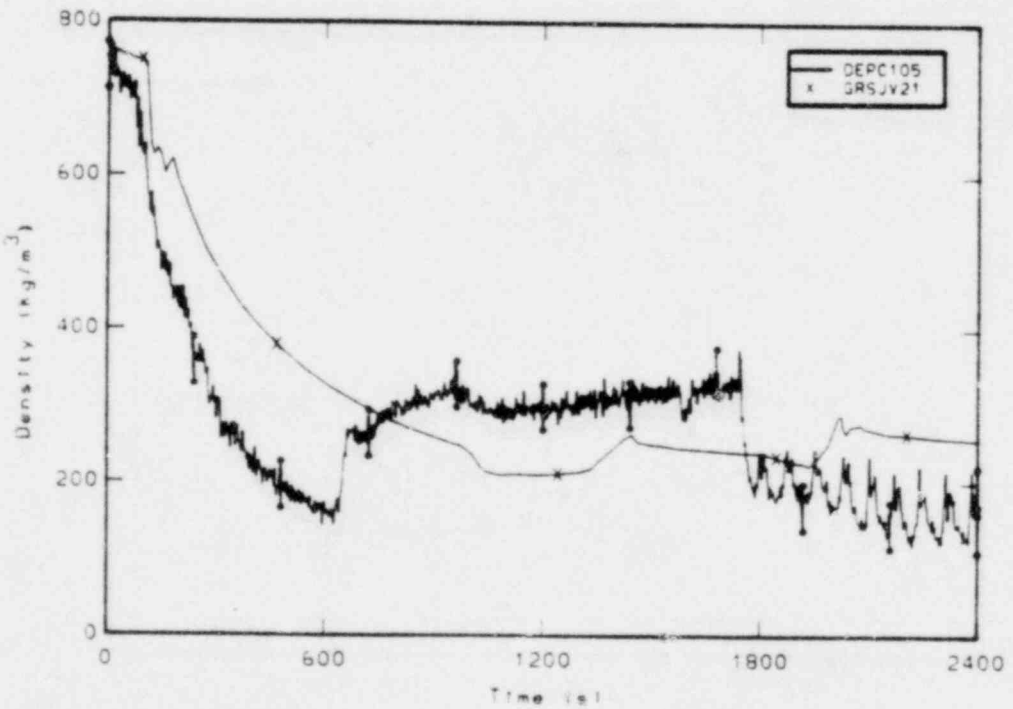

Figure G-6. Comparison of measured and GRS calculated average density in the intact loop cold leg.

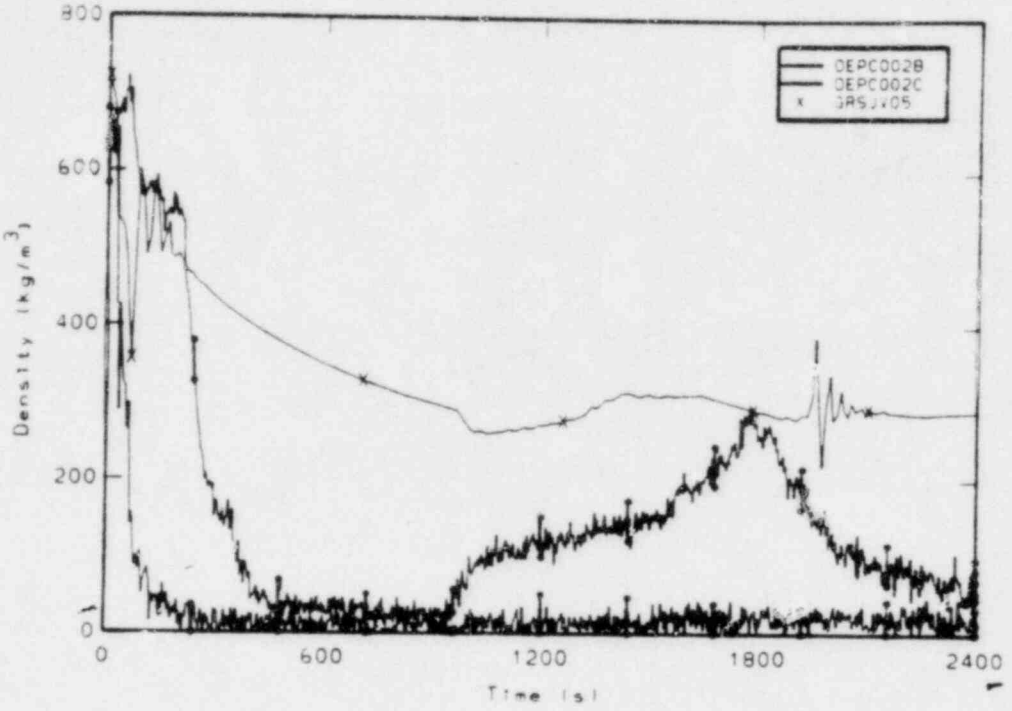

Figure G-7. Comparison of measured chordal densities and GRS calculated average density in the intact loop hot leg.

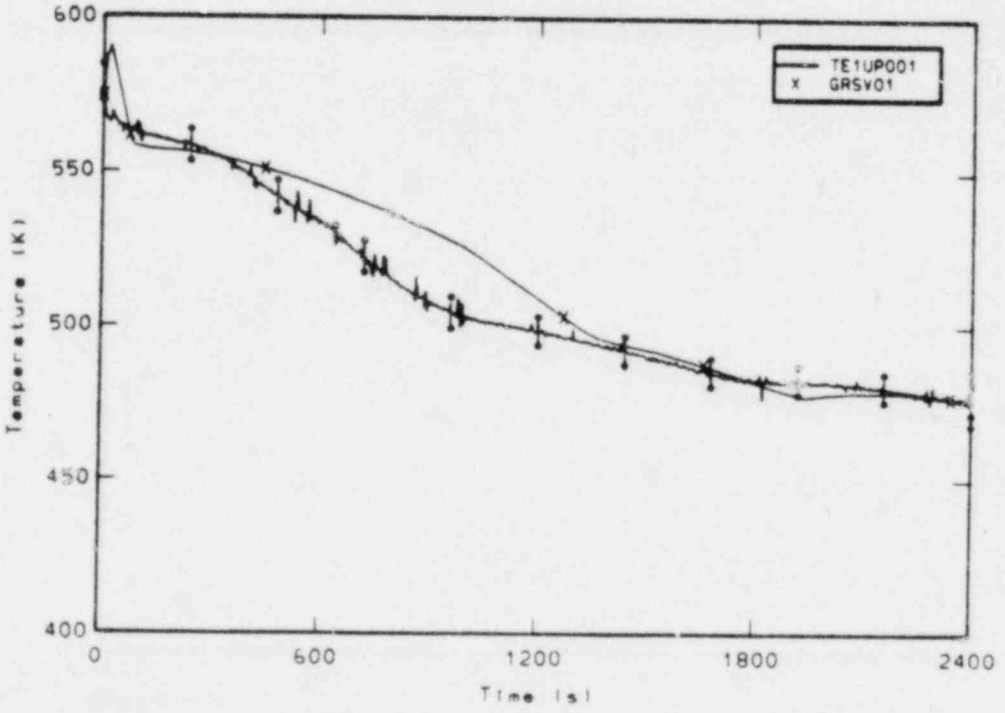

Figure G-8. Comparison of measured and GRS calculated upper plenum fluid temperature.

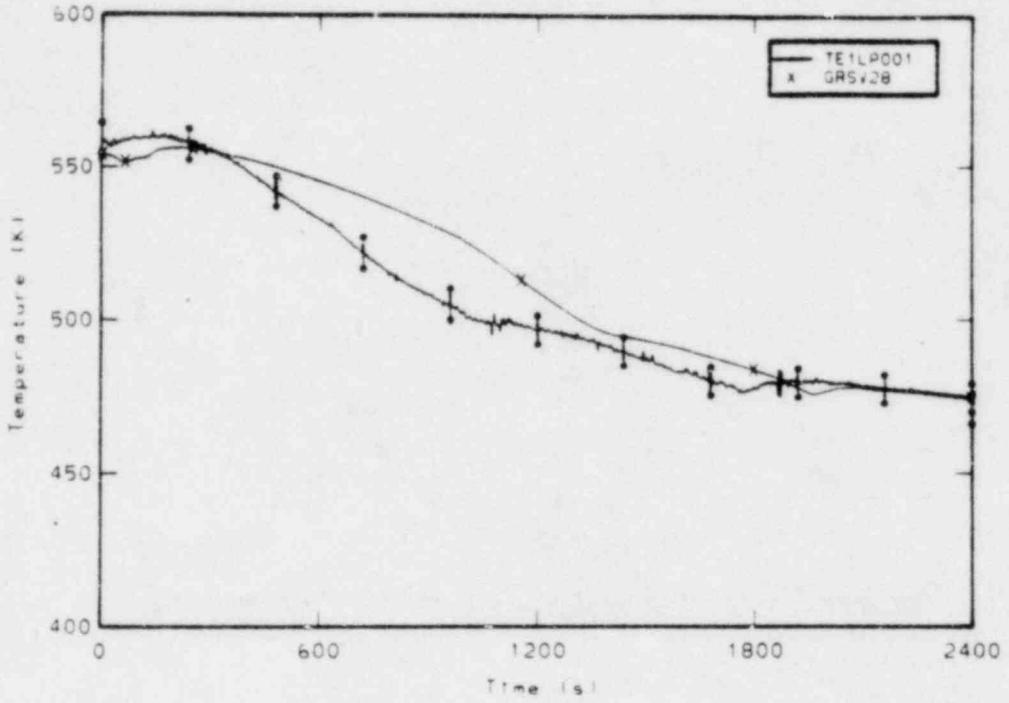

Figure G-9. Comparison of measured and GRS calculated lower plenum fluid temperature.

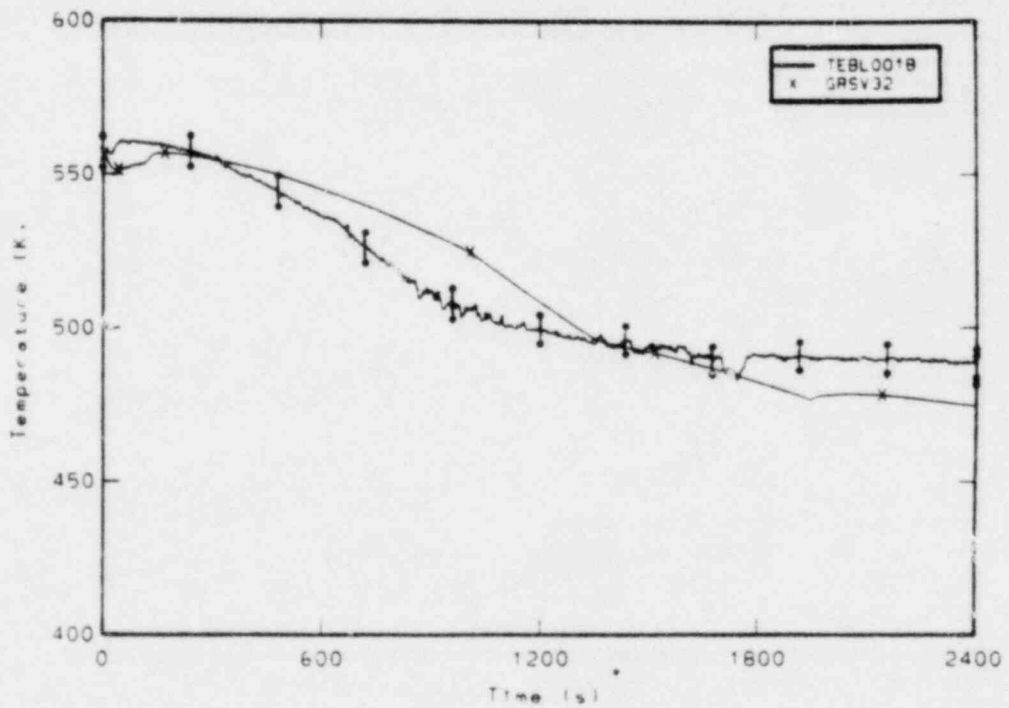

Figure G-10. Comparison of measured and GRS calculated broken loop cold leg fluid temperature.

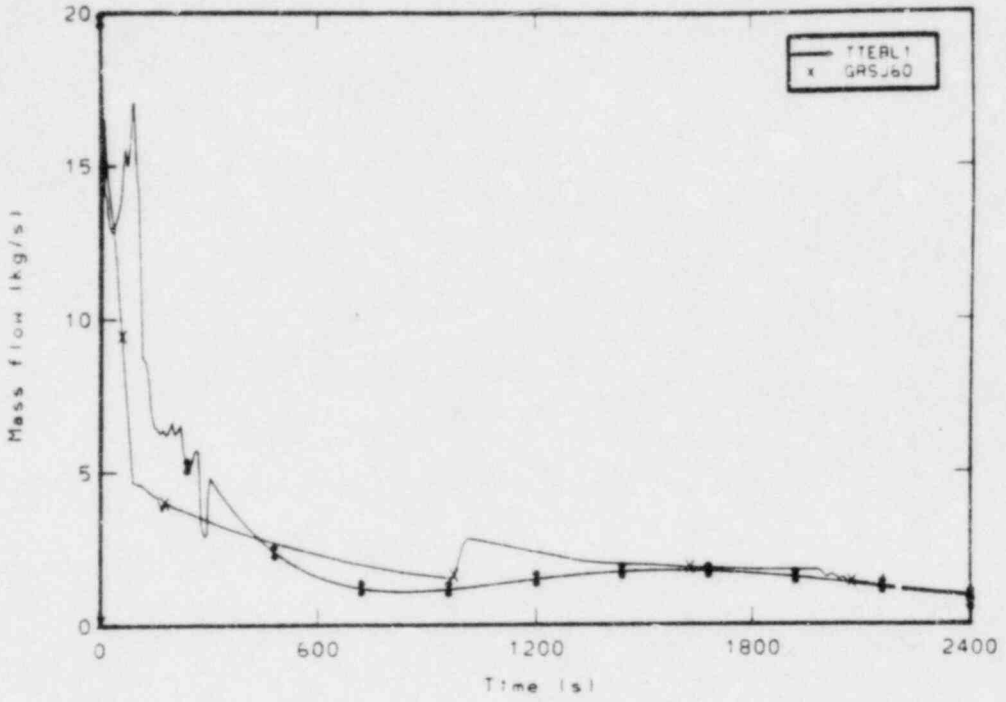

Figure G-11. Comparison of measured and GRS calculated mass flow rate at the break.

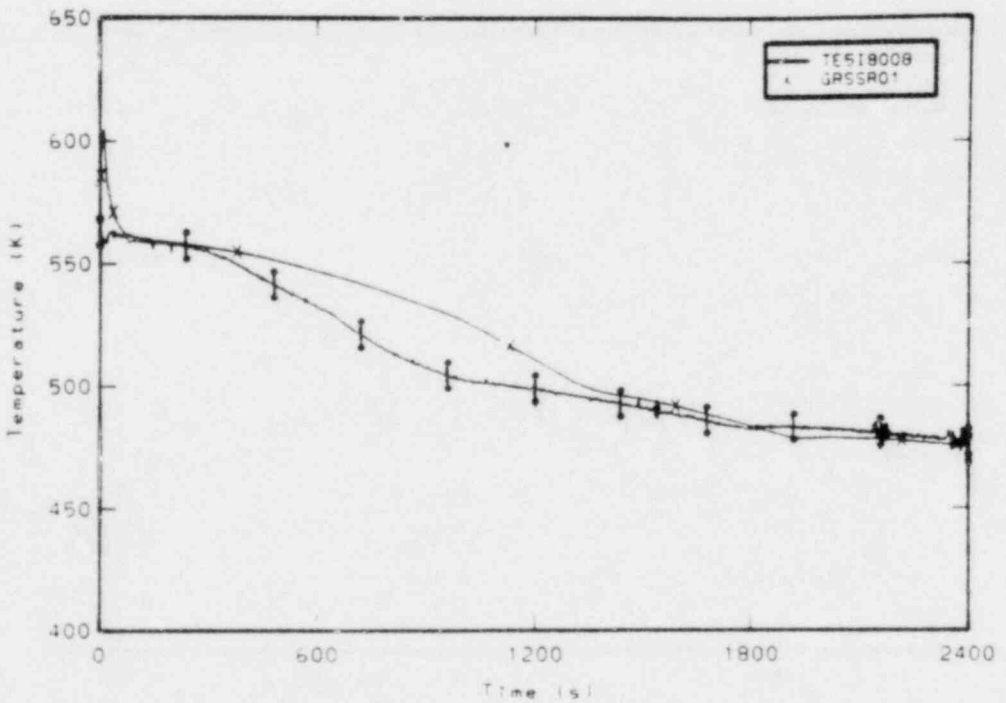

Figure G-12. Comparison of measured rod cladding temperature at the 0.20m elevation and GRS calculated rod cladding temperature.

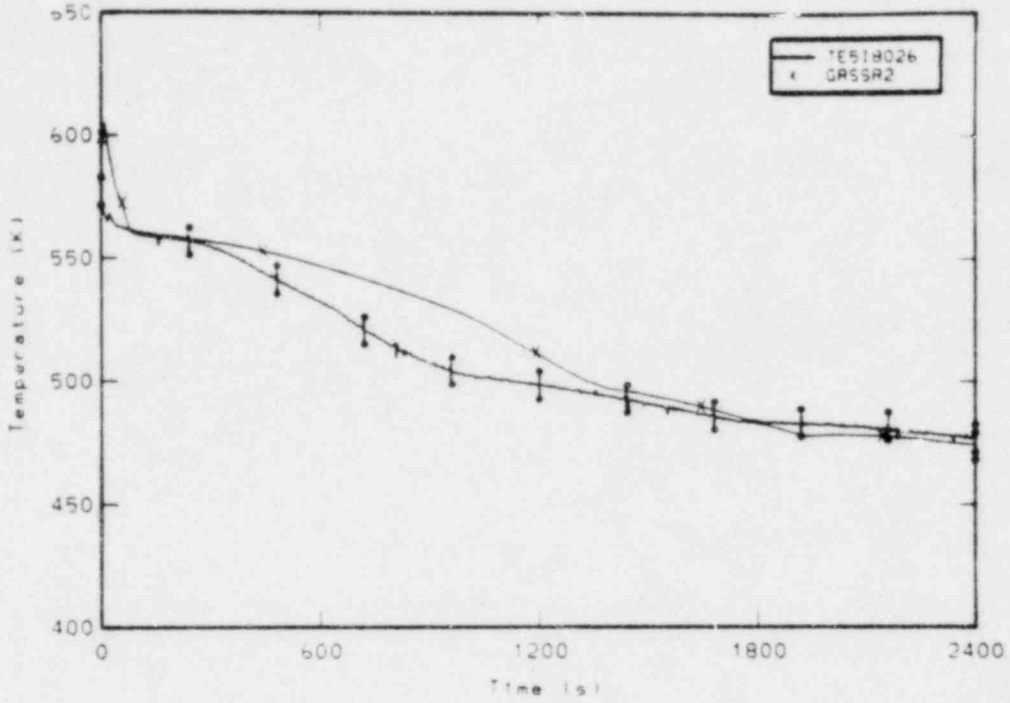

Figure G-13. Comparison of measured rod cladding temperature at the 0.66m elevation and GRS calculated rod cladding temperature.

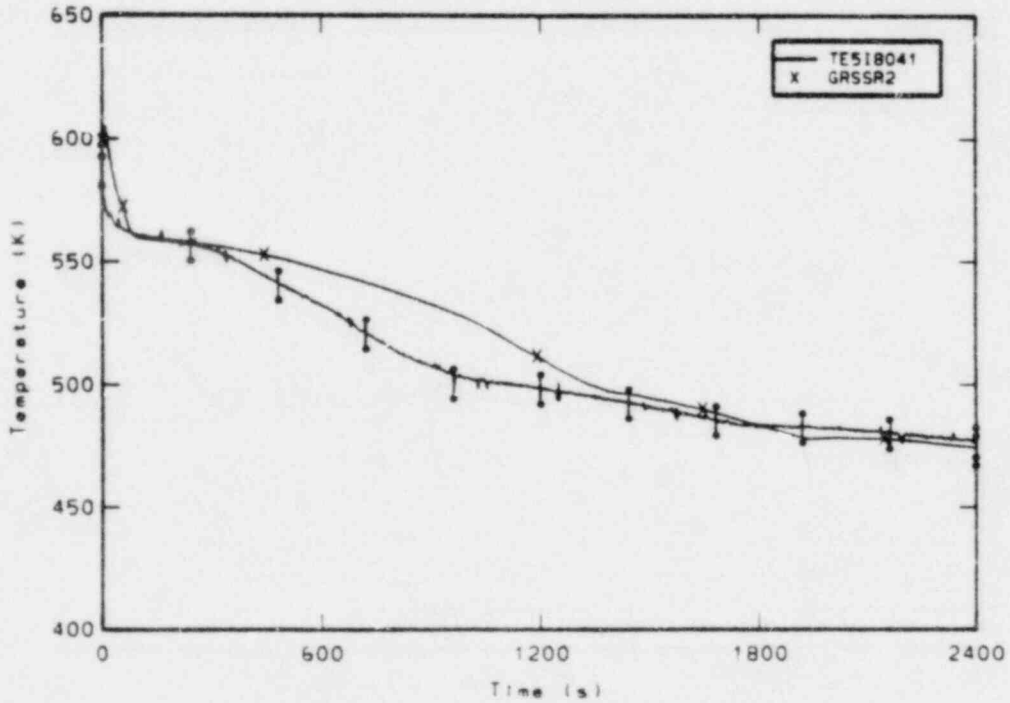

Figure G-14. Comparison of measured rod cladding temperature at the 1.04m elevation and GRS calculated rod cladding temperature.

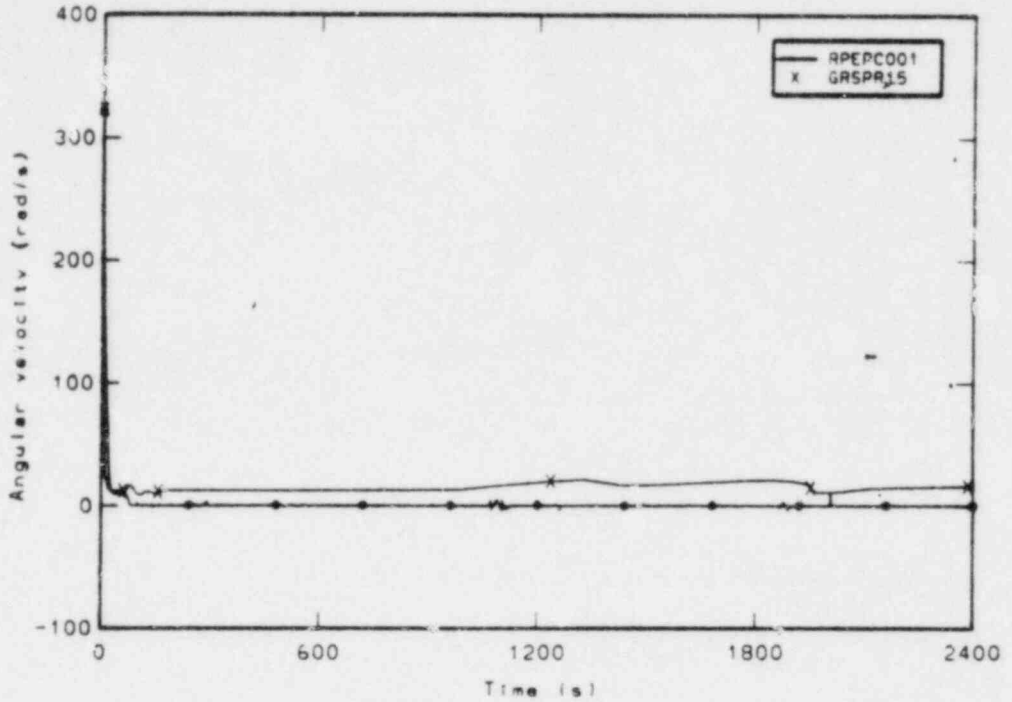

Figure G-15. Comparison of measured and GRS calculated pump speed.

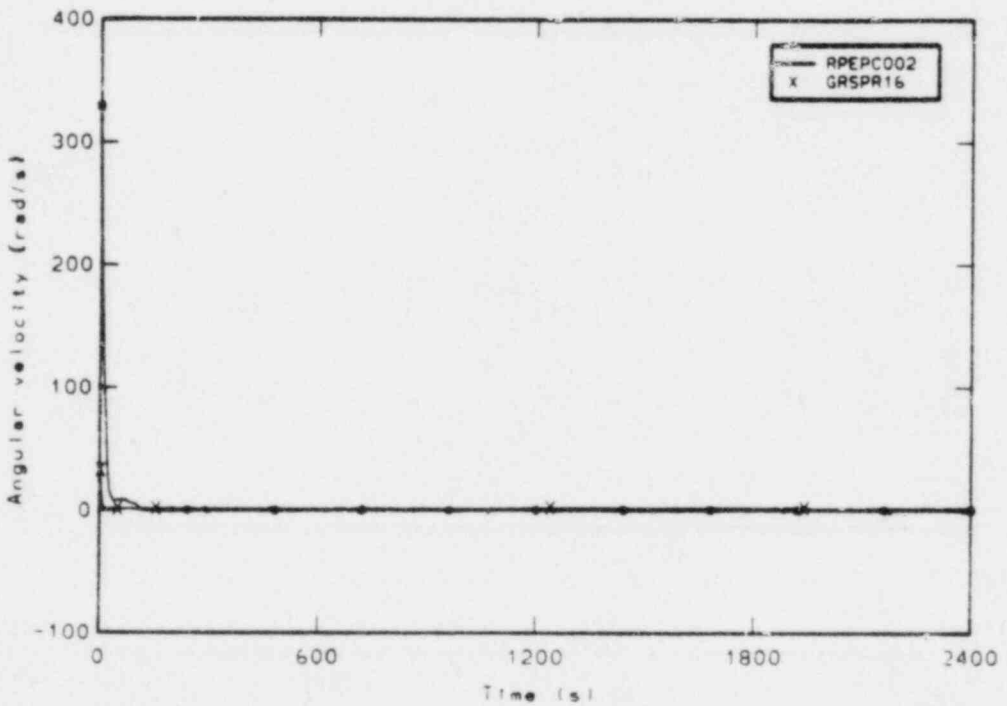

Figure G-16. Comparison of measured and GRS calculated pump speed.

APPENDIX H

COMPARISONS OF ISTITUTO DI IMPIANTI NUCLEARI CALCULATED RESULTS WITH LOFT EXPERIMENT MEASUREMENTS

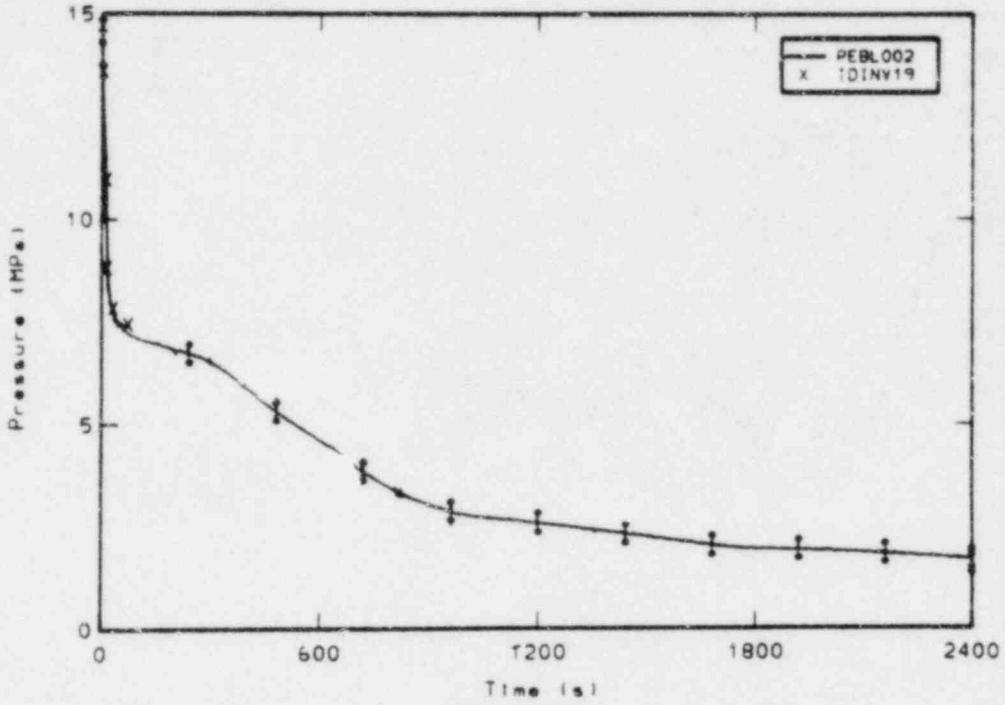

Figure H-1. Comparison of measured and IDIN calculated broken loop hot leg pressure.

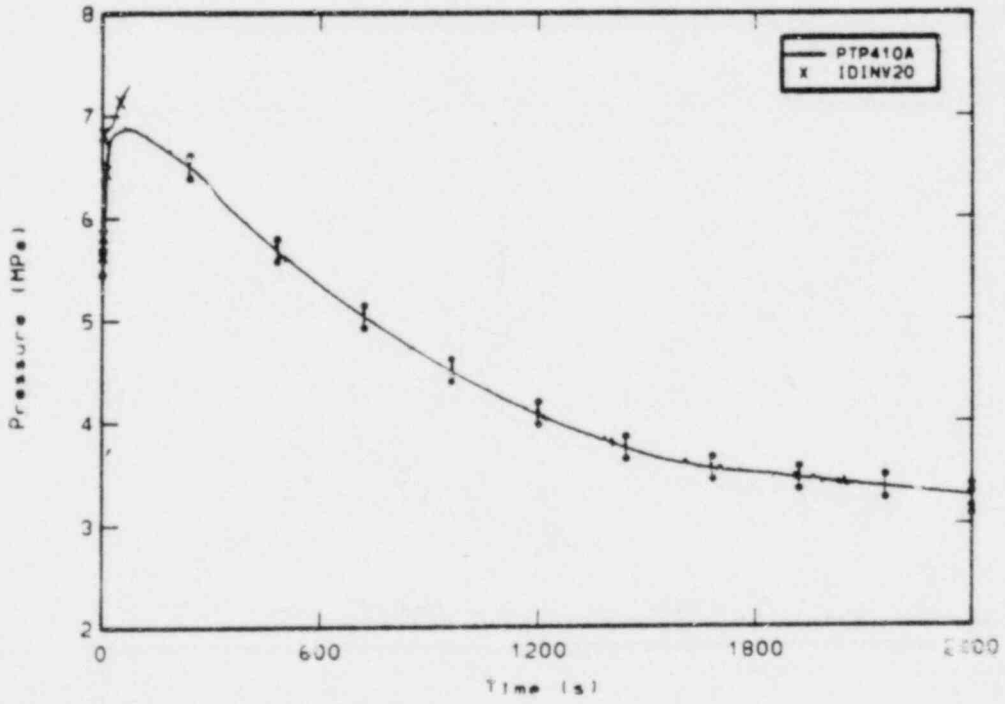

Figure H-2. Comparison of measured and IDIN calculated steam generator secondary pressure.

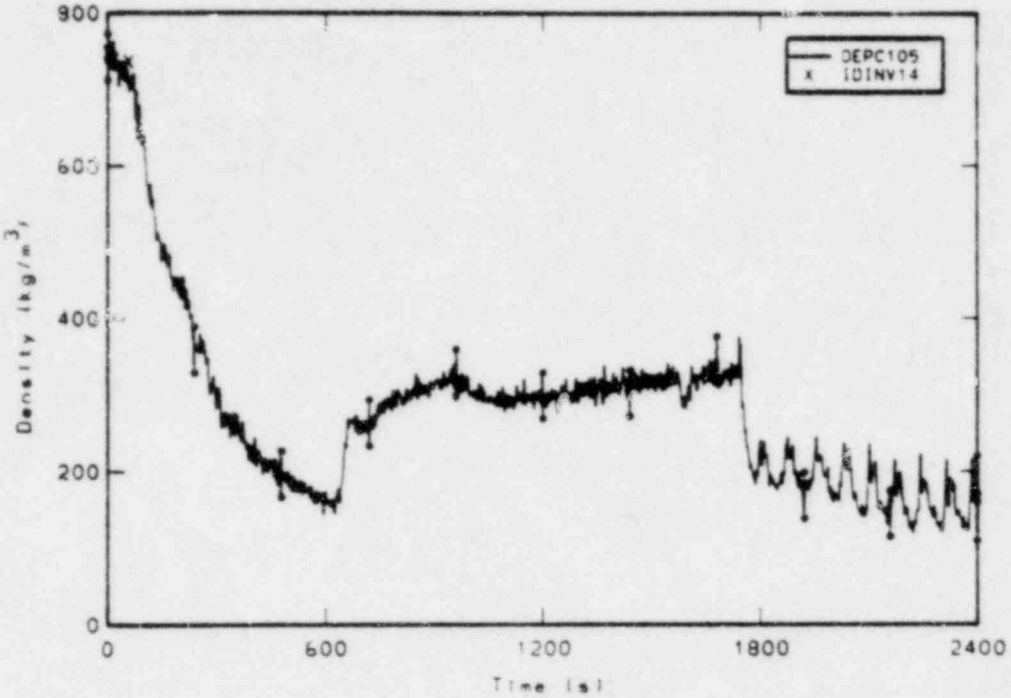

Figure H-3. Comparison of measured and IDIN calculated average density in the intact loop cold leg.

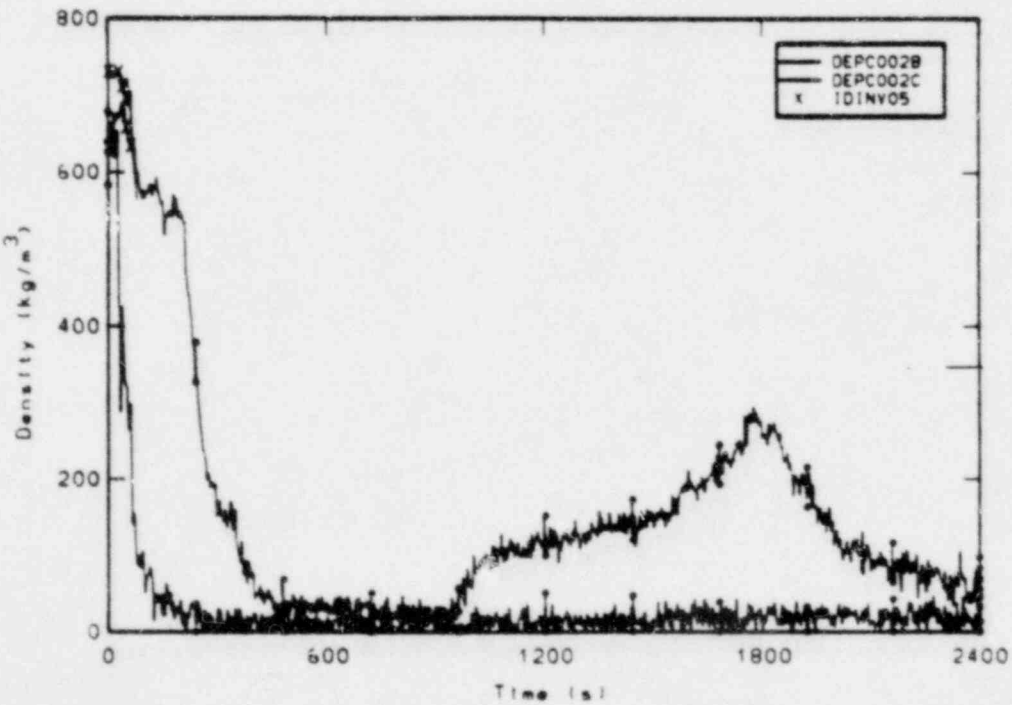

Figure H-4. Comparison of measured chordal densities and IDIN calculated average density in the intact loop hot leg.

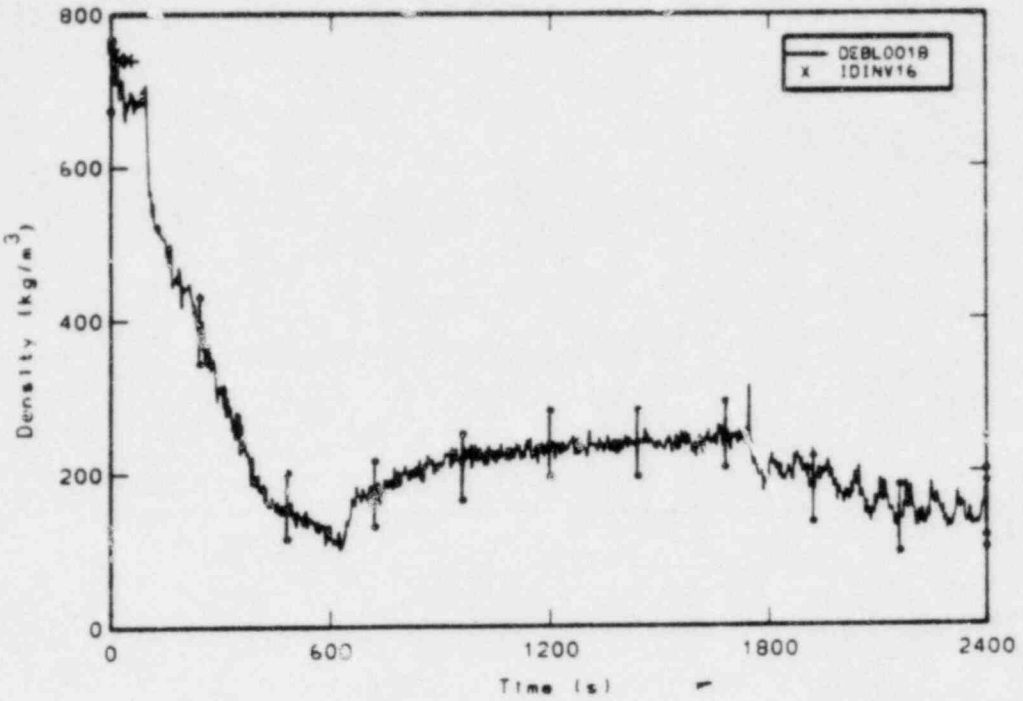

Figure H-5. Comparison of measured chordal density and IDIN calculated average density in the broken loop cold leg.

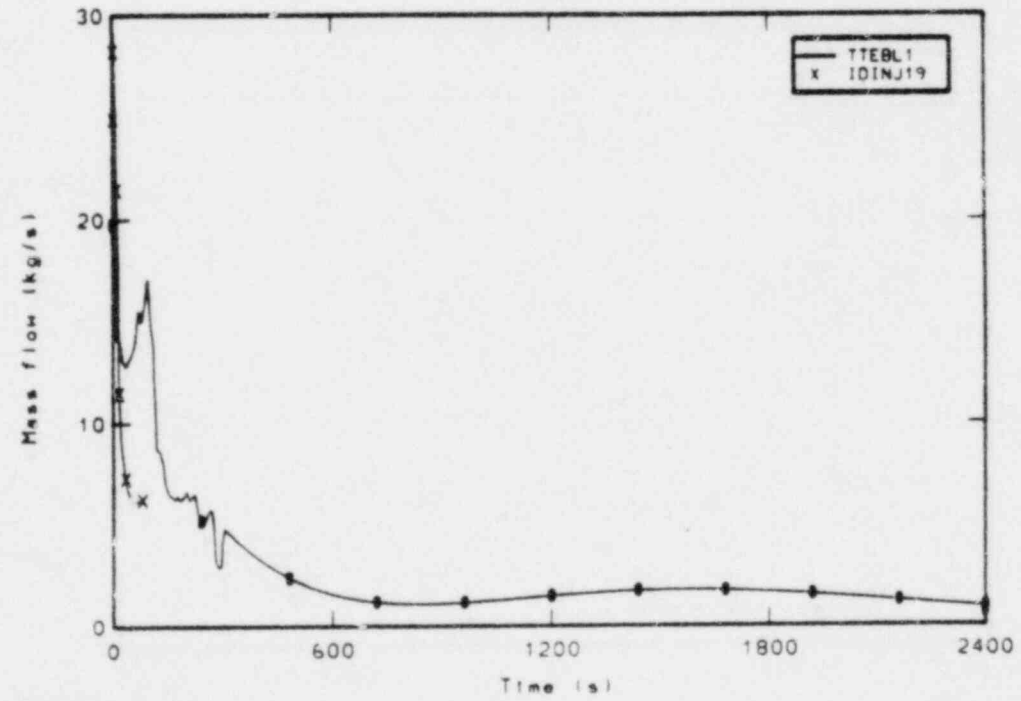

Figure H-6. Comparison of measured and IDIN calculated mass flow rate at the break.

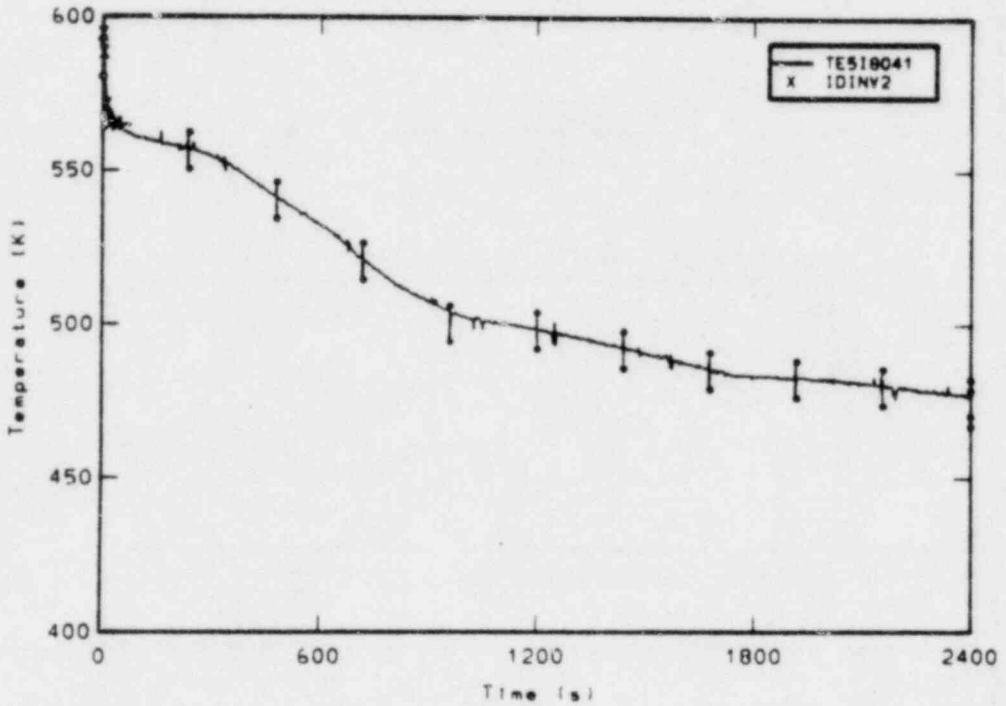

Figure H-7. Comparison of measured rod cladding temperatures at the 0.66m elevation and IDIN calculated rod cladding temperature.

APPENDIX I

COMPARISONS OF JAPAN ATOMIC ENERGY INSTITUTE CALCULATED RESULTS WTIH LOFT EXPERIMENT MEASUREMENTS

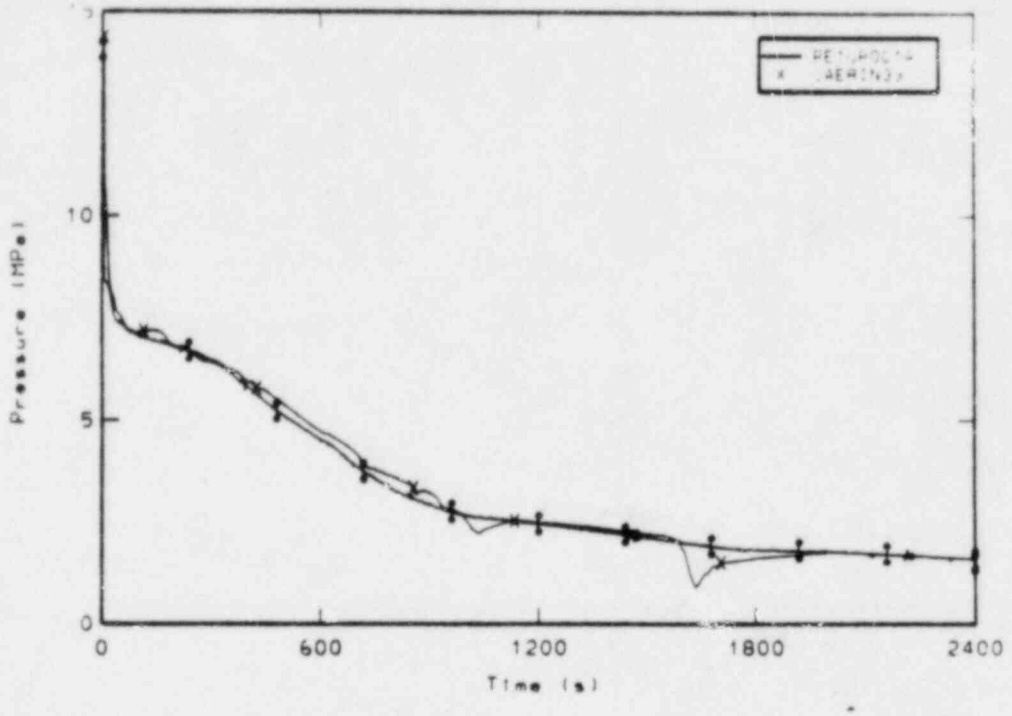

Figure I-1. Comparison of measured and JAERI calculated upper plenum pressure.

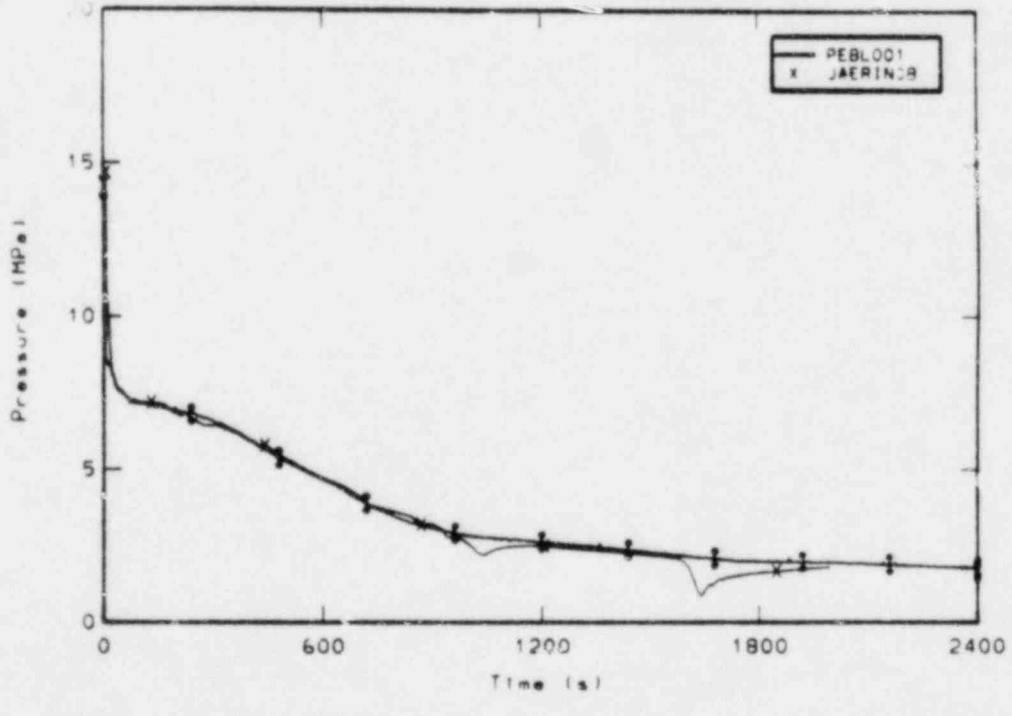

Figure I-2. Comparison of measured and JAERI calculated broken loop cold leg pressure.

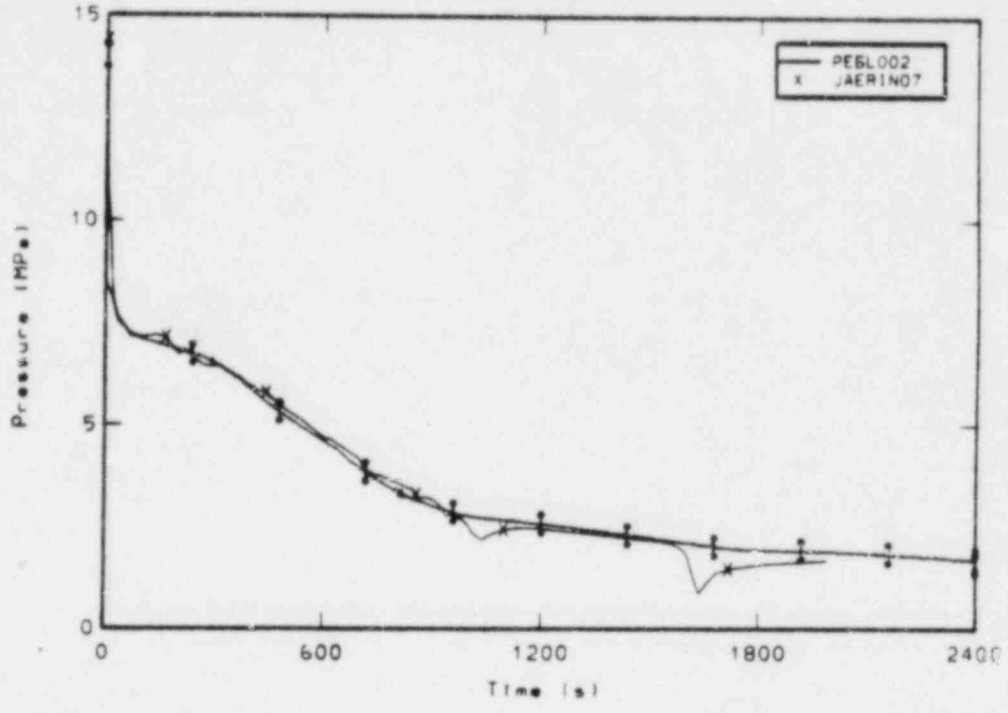

Figure I-3. Comparison of measured and JAERI calculated broken loop hot leg pressure.

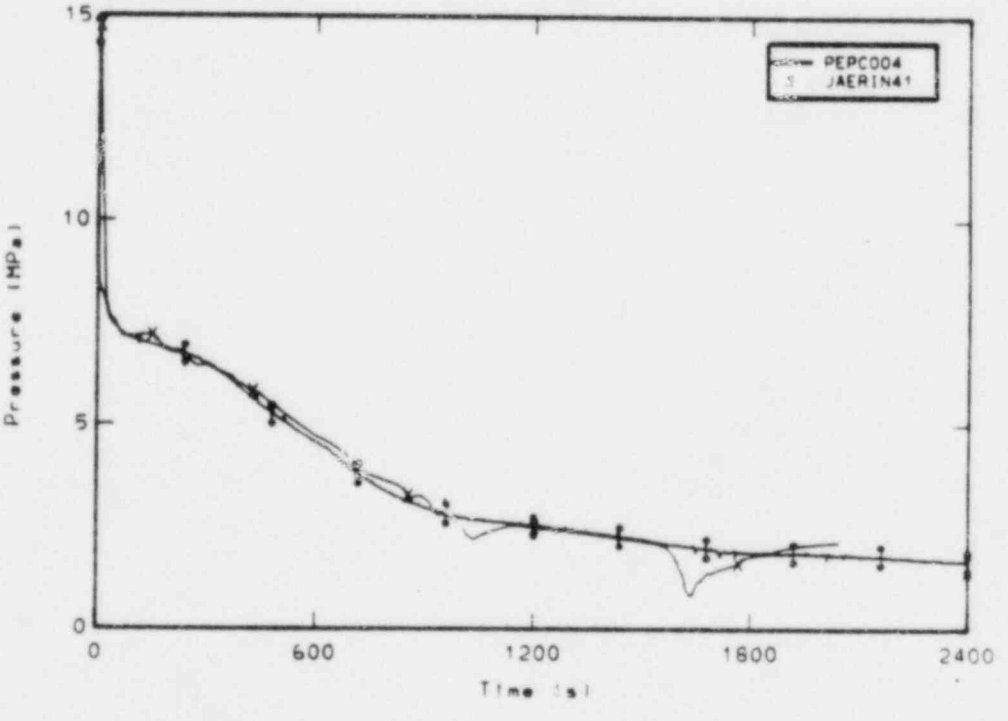

Figure I-4. Comparison of measured and JAERI calculated pressurizer pressure.

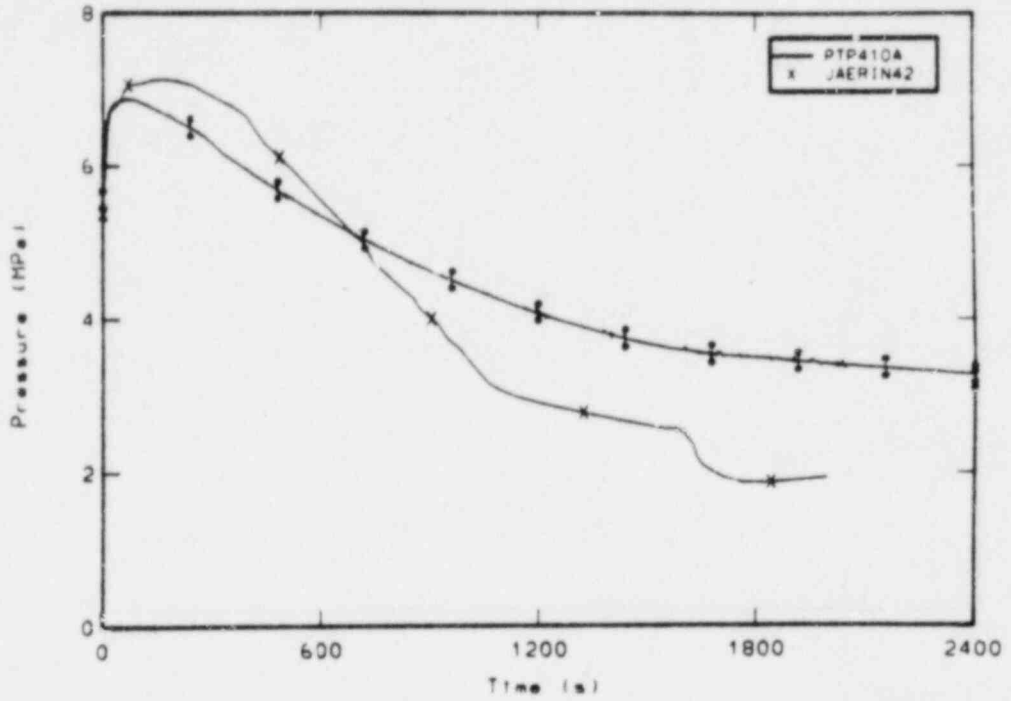

Figure I-5. Comparison of measured and JAERI calculated steam generator secondary pressure.

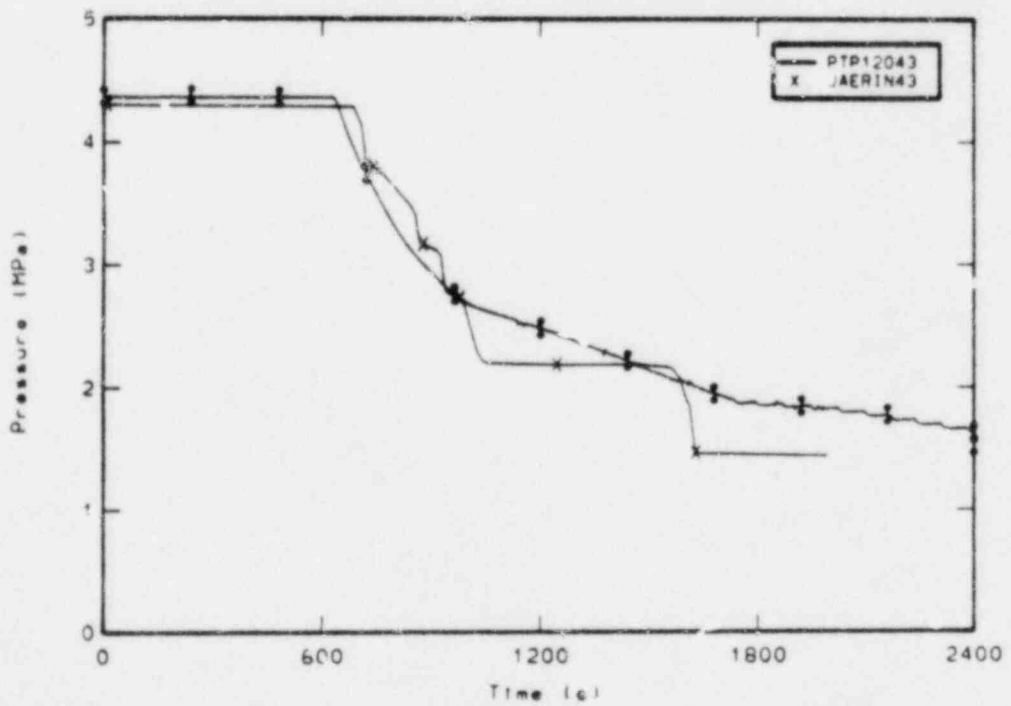

Figure I-6. Comparison of measured and JAERI accumulator pressure.

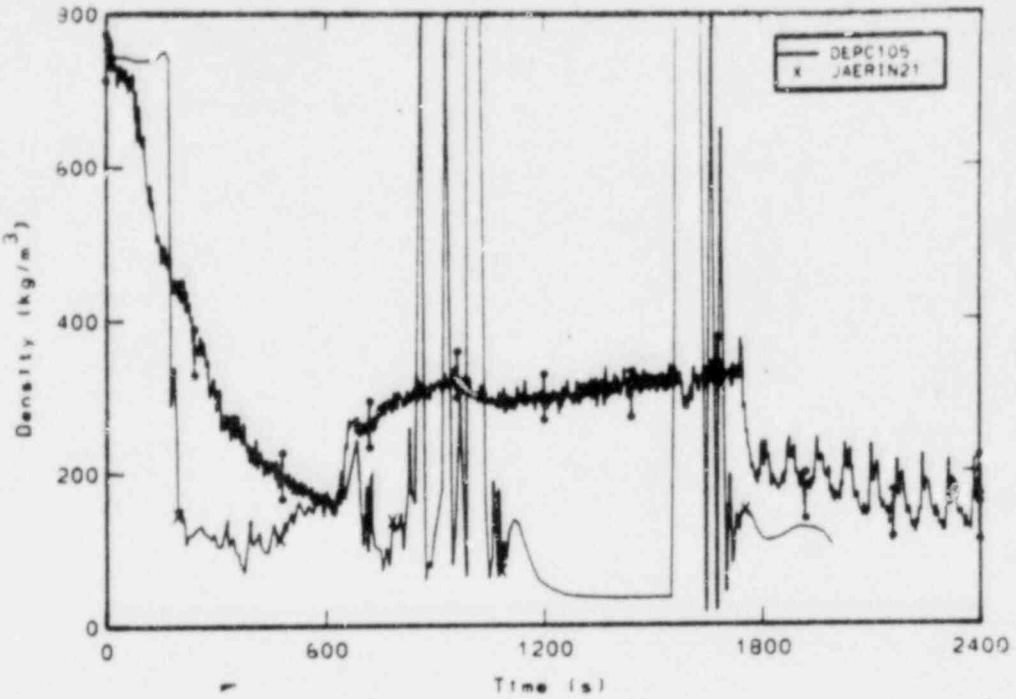

Figure I-7. Comparison of measured and JAERI average density in the intact loop cold leg.

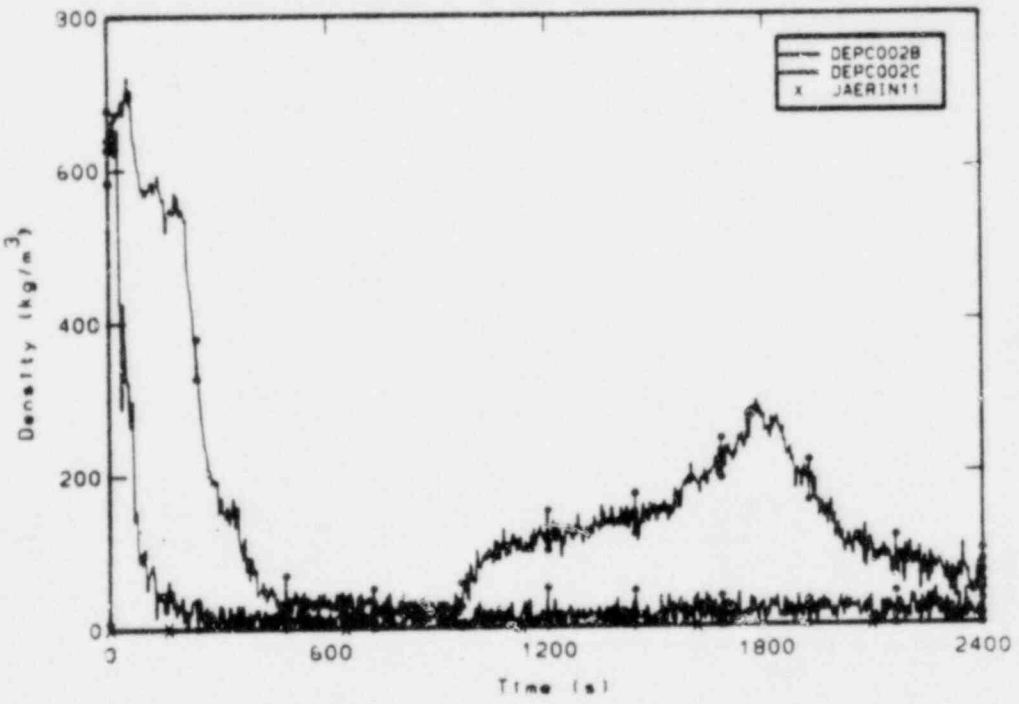

Figure I-8. Comparison of measured chordal densities and JAERI calculated average density in the intact loop hot leg.

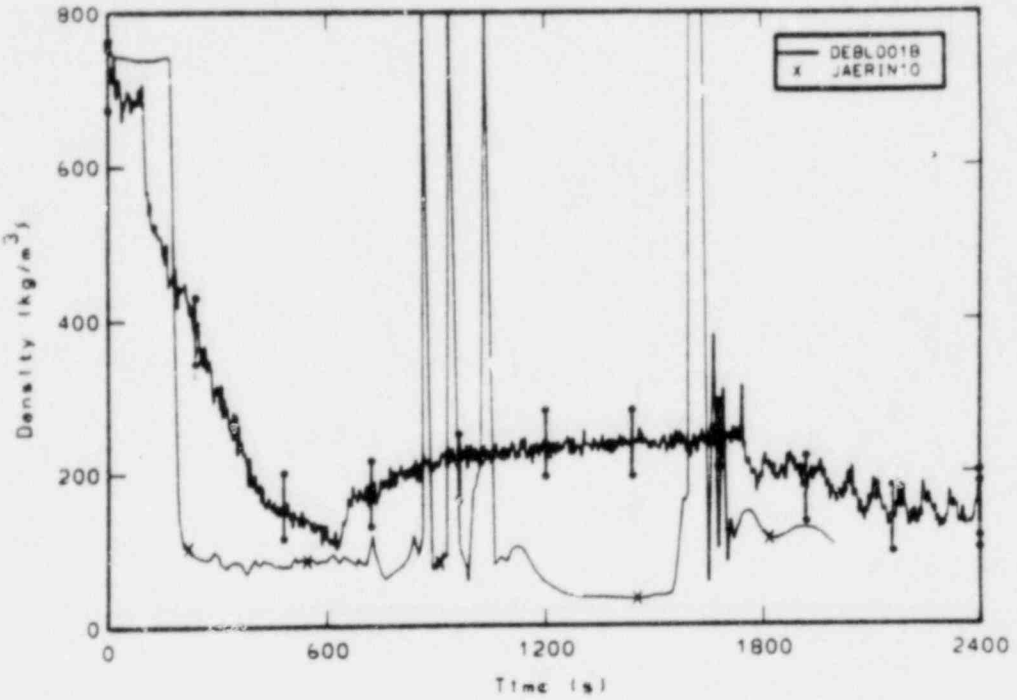

Figure I-9. Comparison of measured chordal density and JAERI calculated average density in the broken loop cold leg.

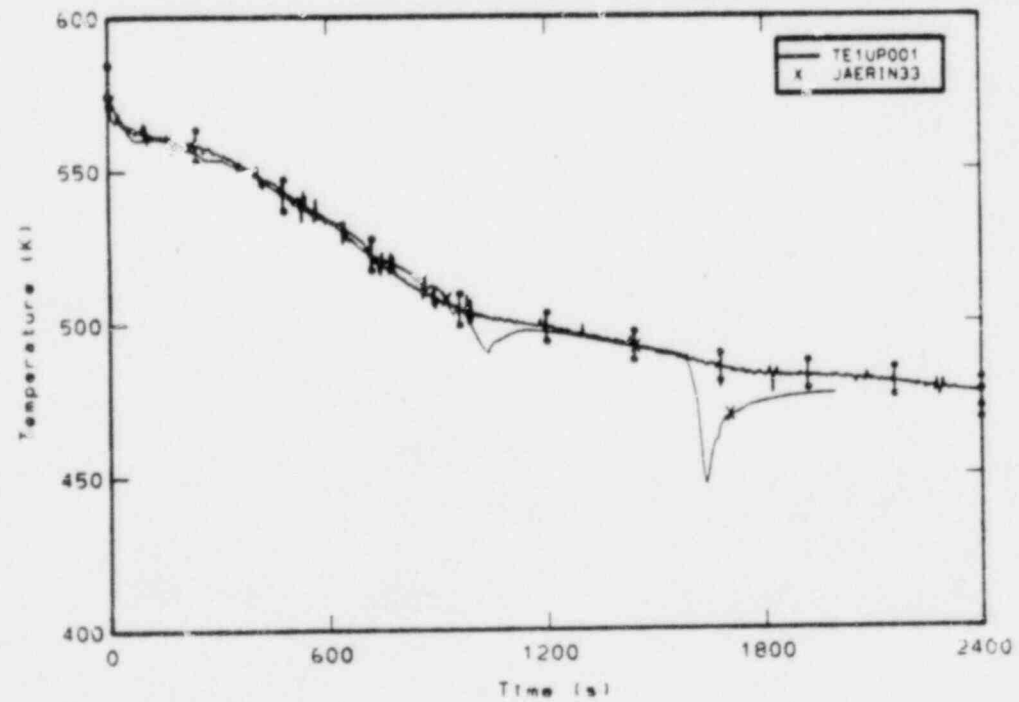

Figure I-10. Comparison of measured and JAERI calculated upper plenum fluid temperature.

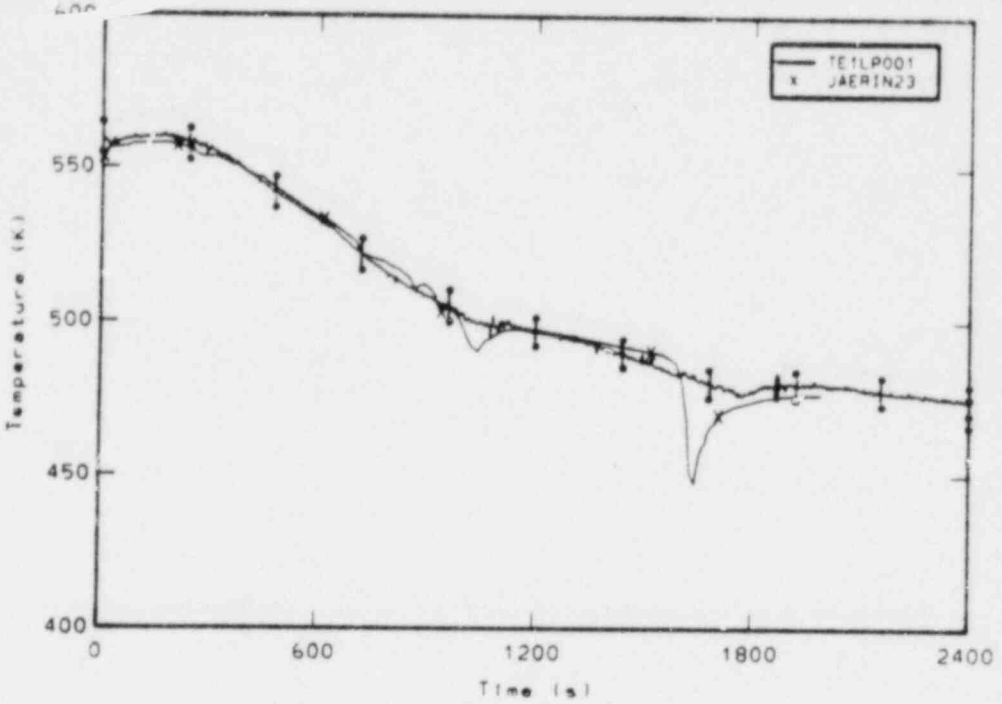

Figure I-11. Comparison of measured and JAERI calculated lower plenum fluid temperature.

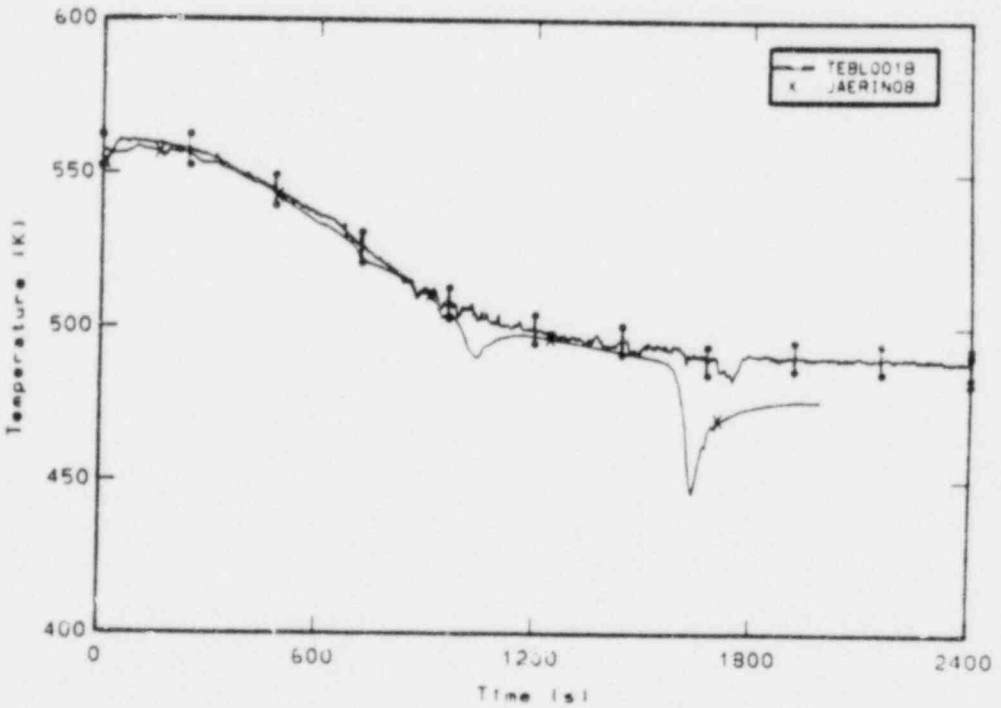

Figure I-12. Comparison of measured and JAERI calculated broken loop cold leg fluid temperature.

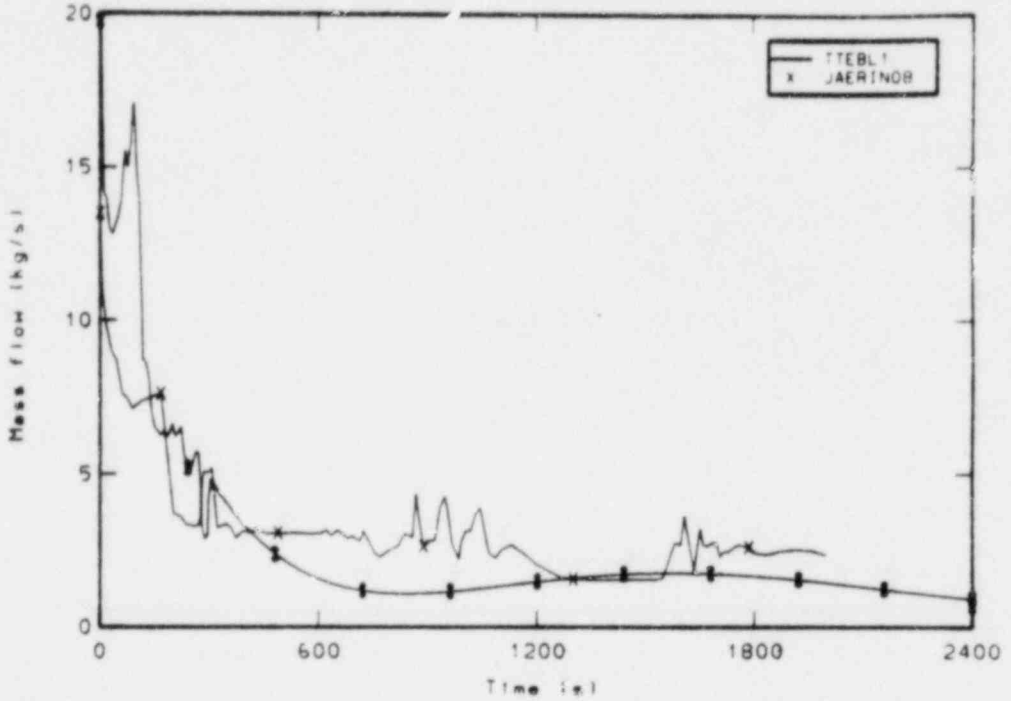

Figure I-13. Comparison of measured and JAERI calculated mass flow rate at the break.

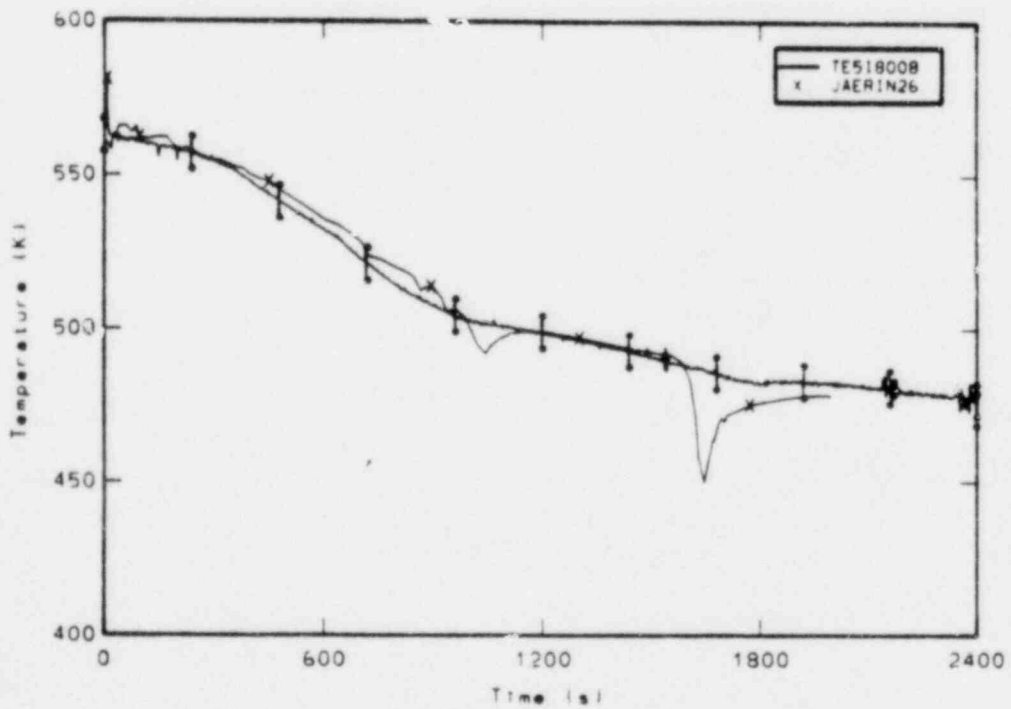

Figure I-14. Comparison of measured rod cladding temperature at the 0.20m elevation and JAERI calculated rod cladding temperature.

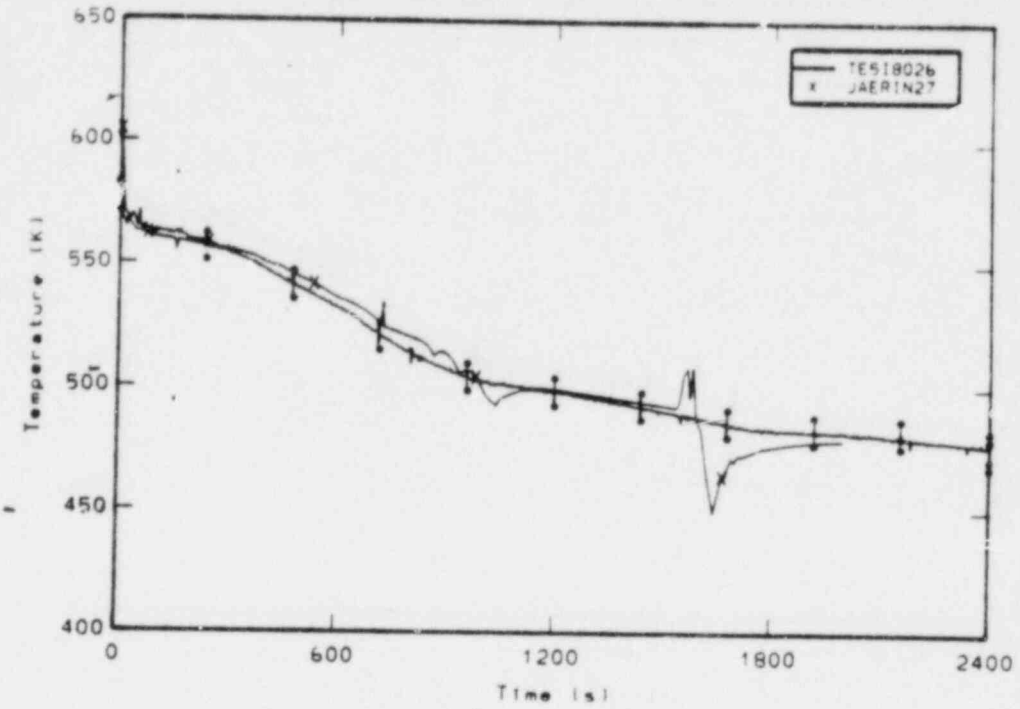

Figure I-15. Comparison of measured rod cladding temperature at the 0.65m elevation and JAERI calculated rod cladding temperature.

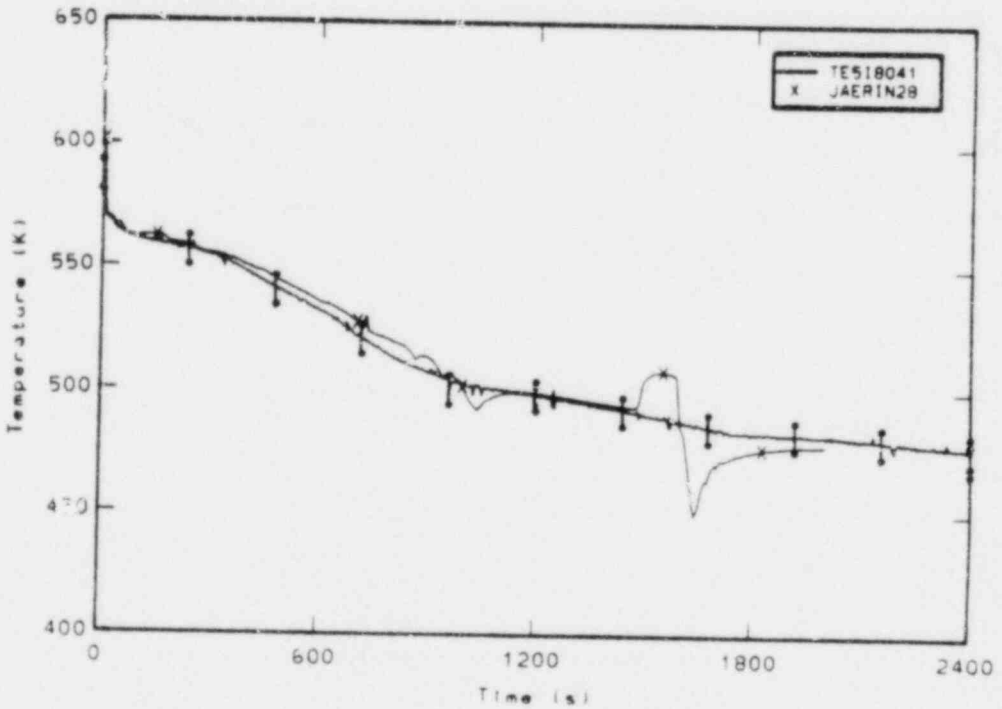

Figure I-16. Comparison of measured rod cladding temperature at the 1.04m elevation and JAERI calculated rod cladding temperature.

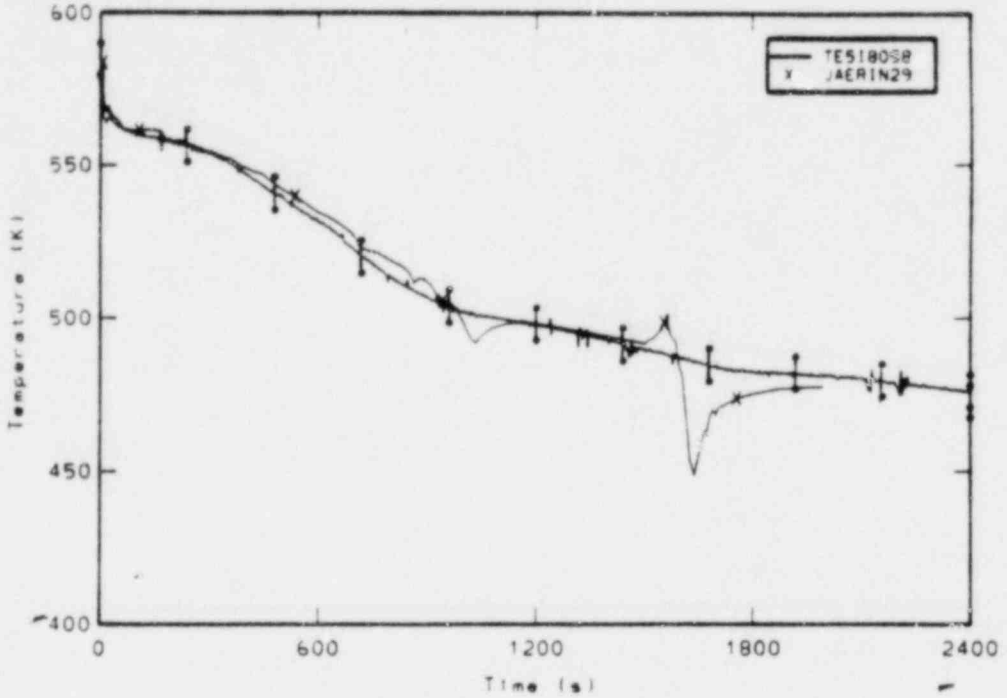

Figure I-17. Comparison of measured rod cladding temperature at the 1.47m elevation and JAERI calculated rod cladding temperature.

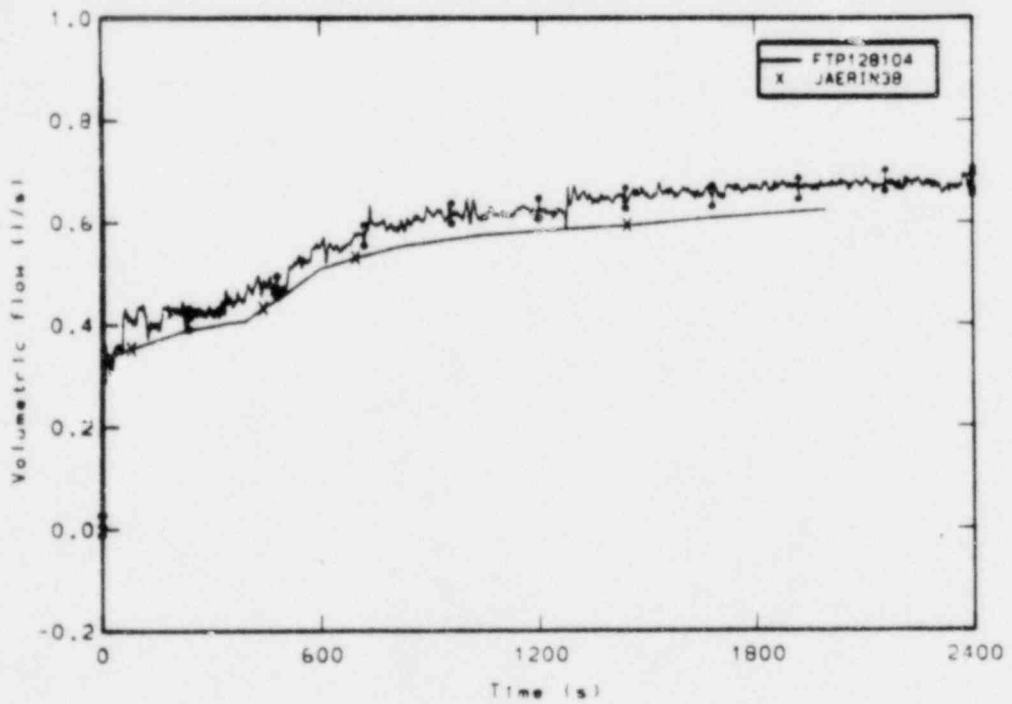

Figure I-18. Comparison of measured and JAERI calculated high pressure injection system (HPIS) volumetric flow rate.

APPENDIX J

COMPARISONS OF LOS ALAMOS SCIENTIFIC LABORATORY CALCULATED RESULTS WITH LOFT EXPERIMENT MEASUREMENTS

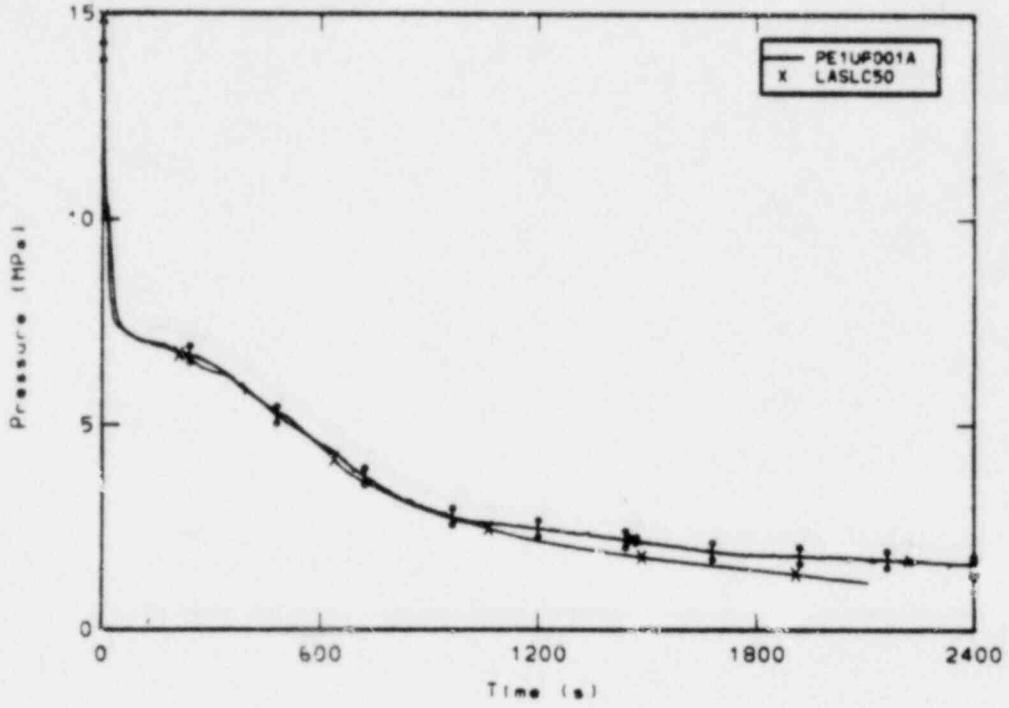

Figure J-1. Comparison of measured and LASL calculated upper plenum pressure.

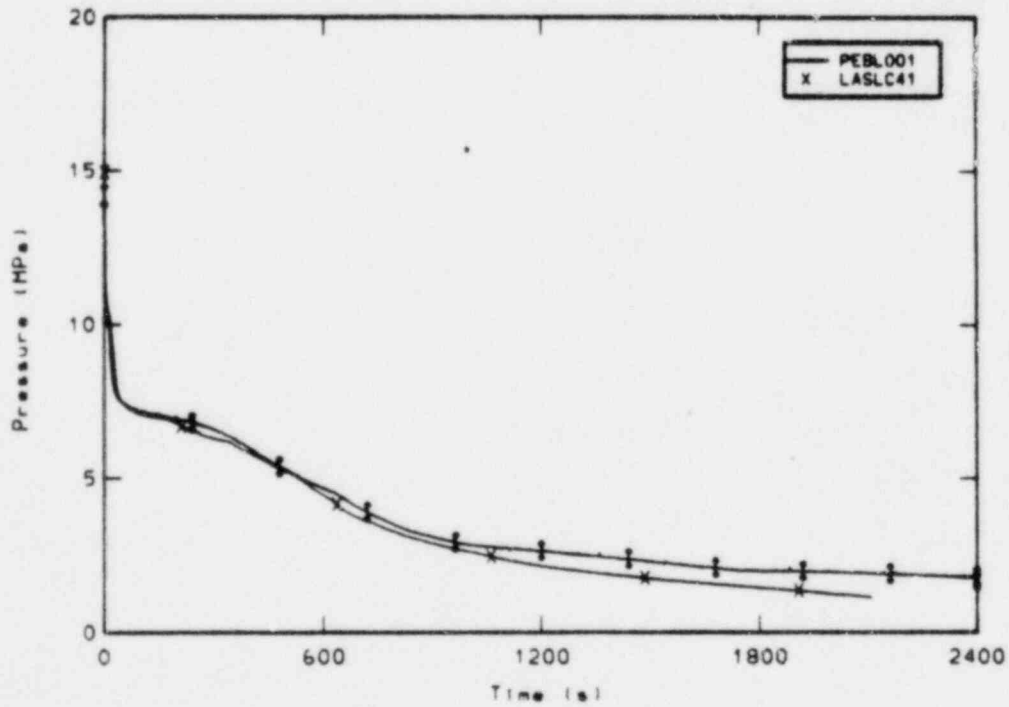

Figure J-2. Comparison of measured and LASL broken loop cold leg pressure.

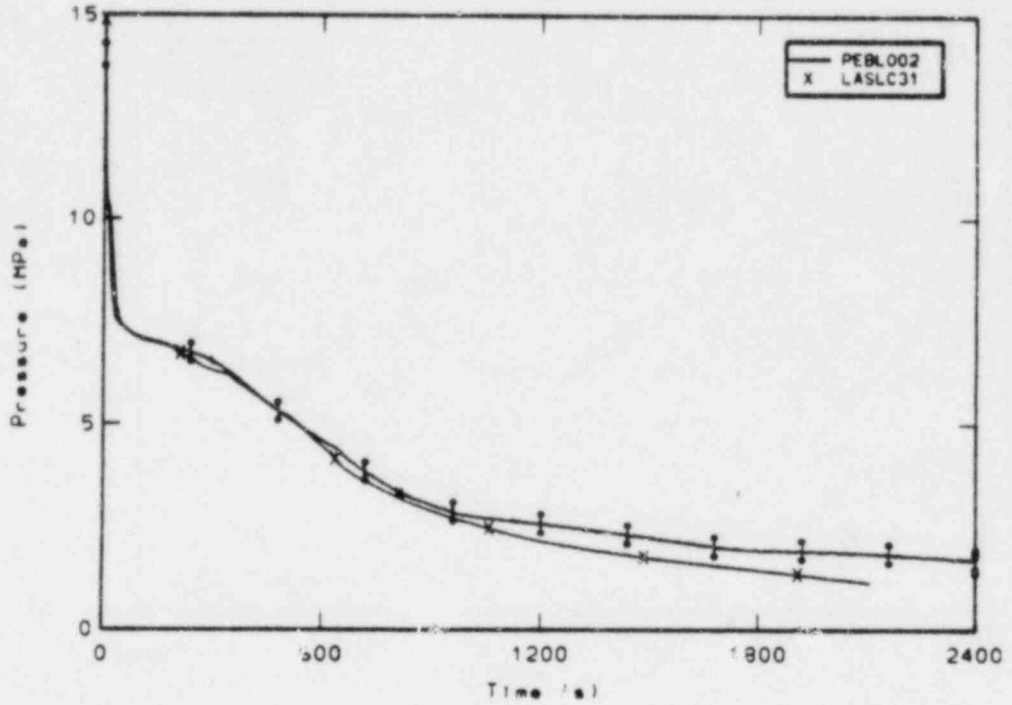

Figure J-3. Comparison of measured and LASL calculated broken loop hot leg pressure.

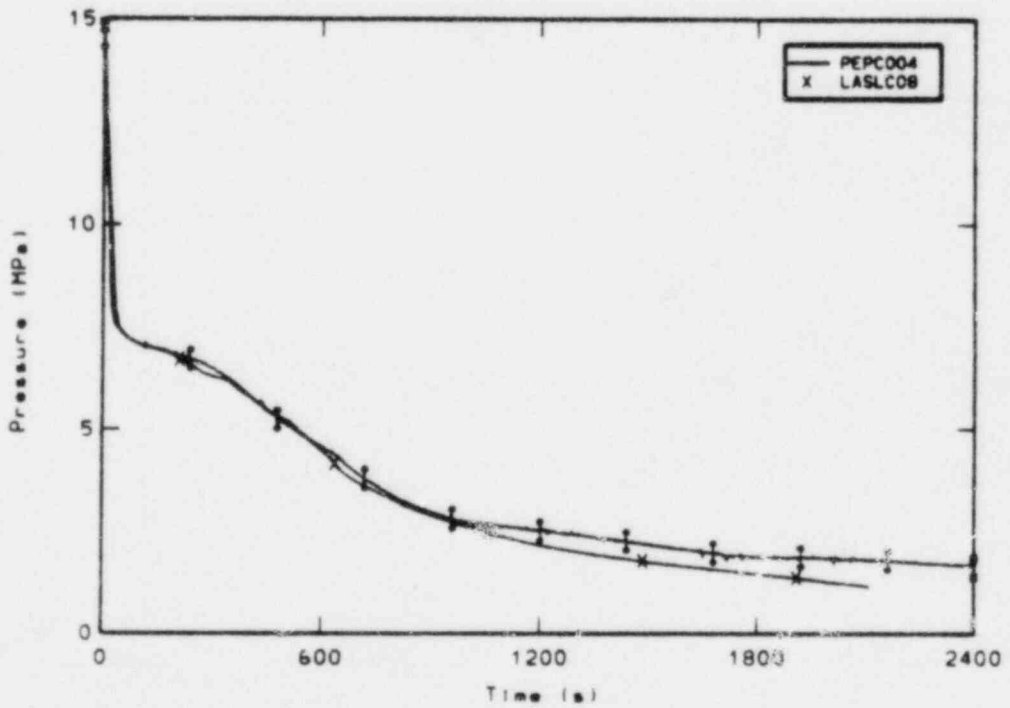

Figure J-4. Comparison of measured and LASL calculated pressurizer pressure.

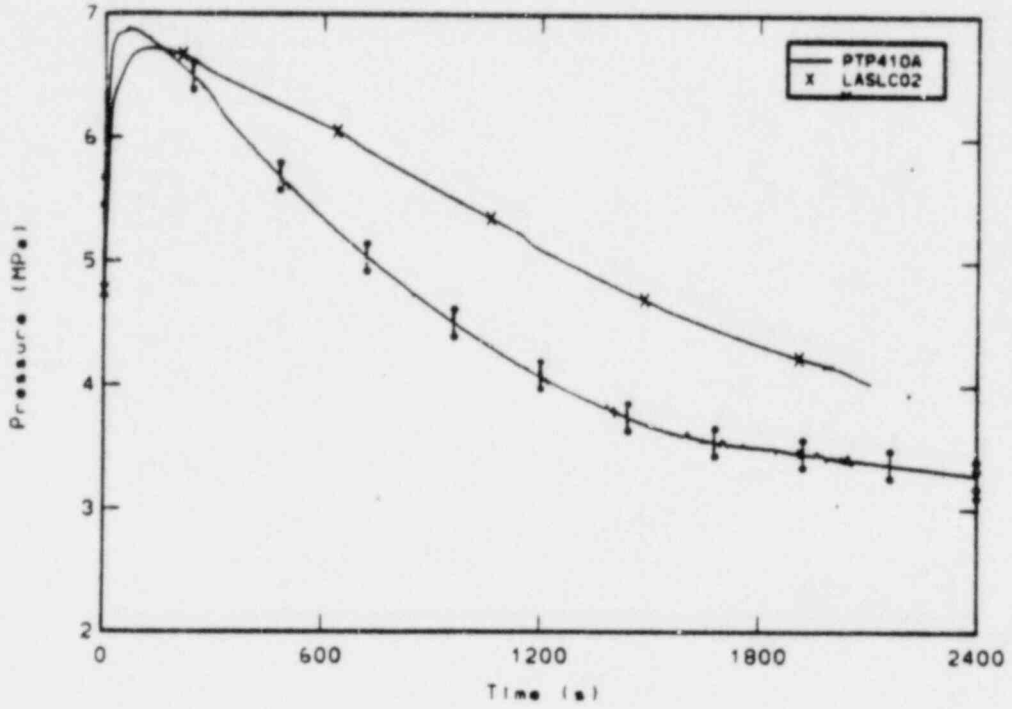

Figure J-5. Comparison of measured and LASL calculated steam generator secondary pressure.

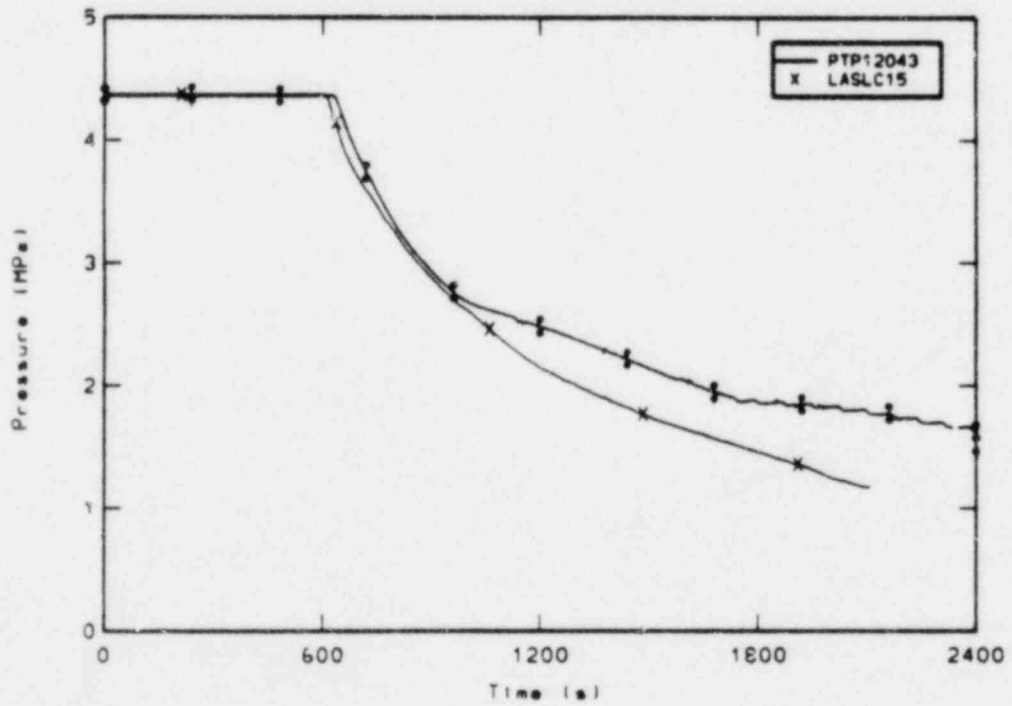

Figure J-6. Comparison of measured and LASL calculated accumulator pressure.

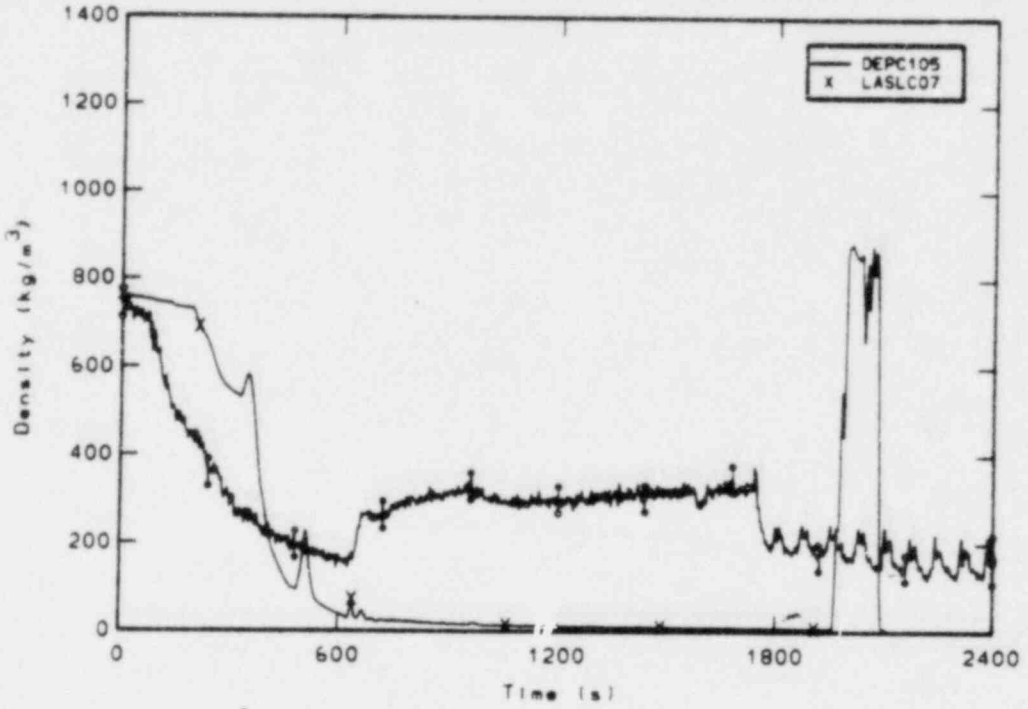

Figure J-7. Comparison of measured and LASL calculated average density in the intact loop cold leg.

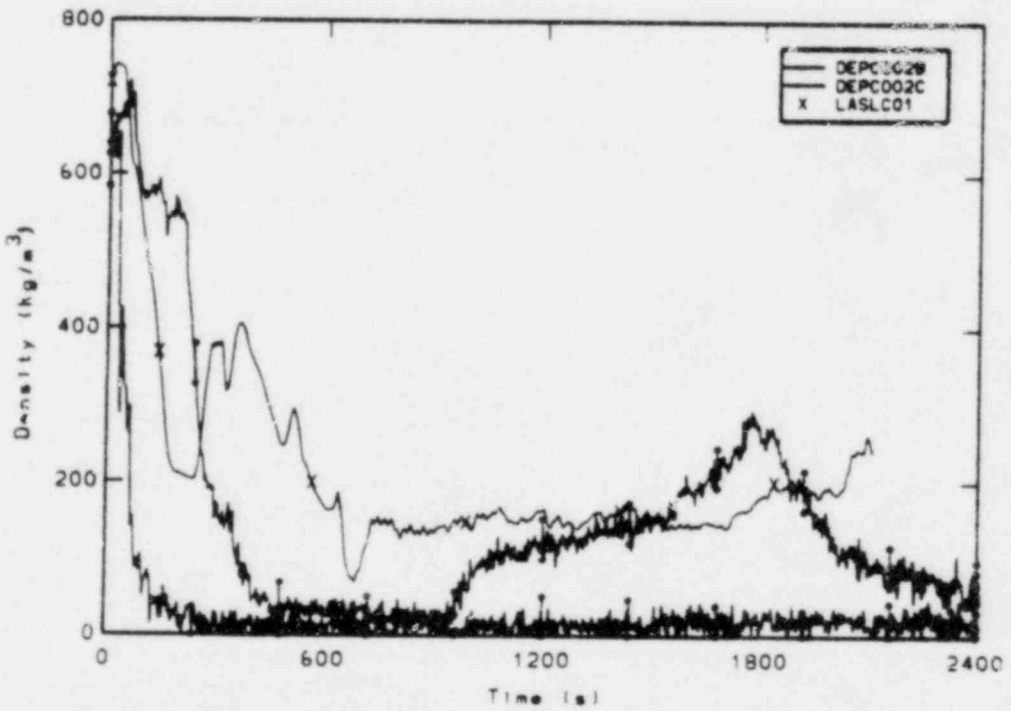

Figure J-8. Comparison of measured chordal densities and LASL calculated average density in the intact loop hot leg.

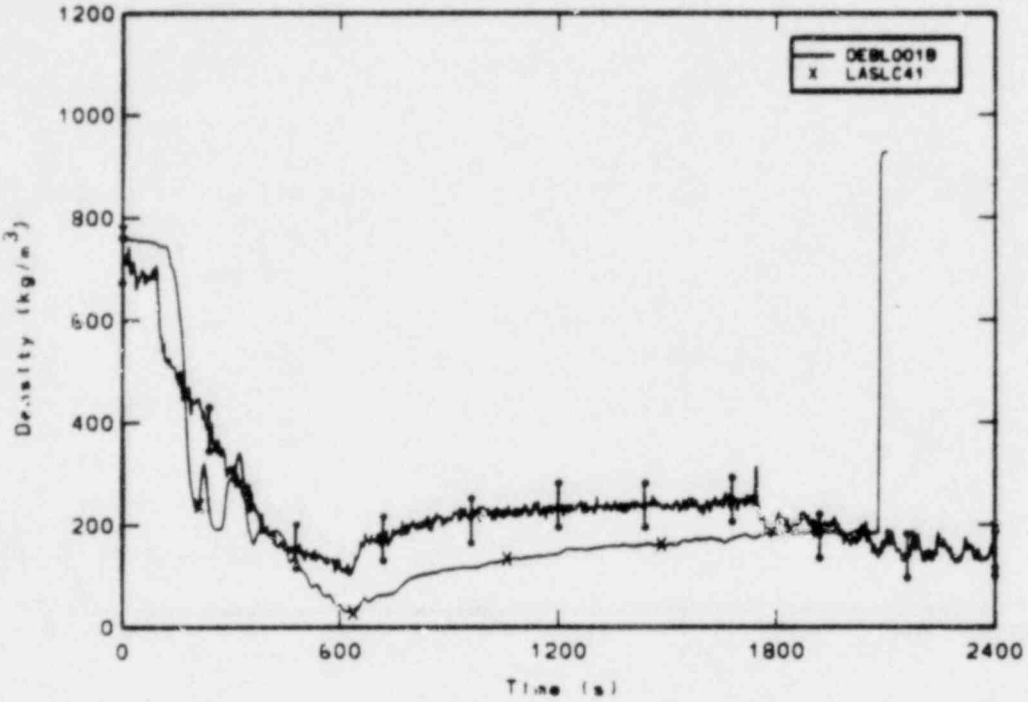

Figure J-9. Comparison of measured chordal density and LASL calculated average density in the broken loop cold leg.

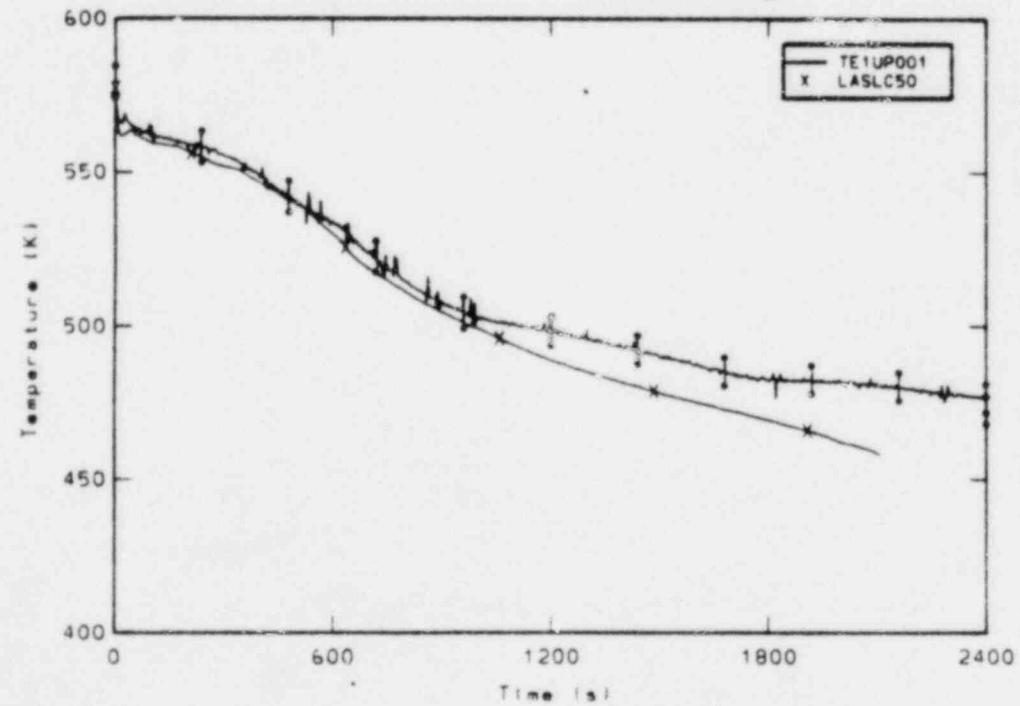

Figure J-10. Comparison of measured and LASL calculated upper plenum fluid temperature.

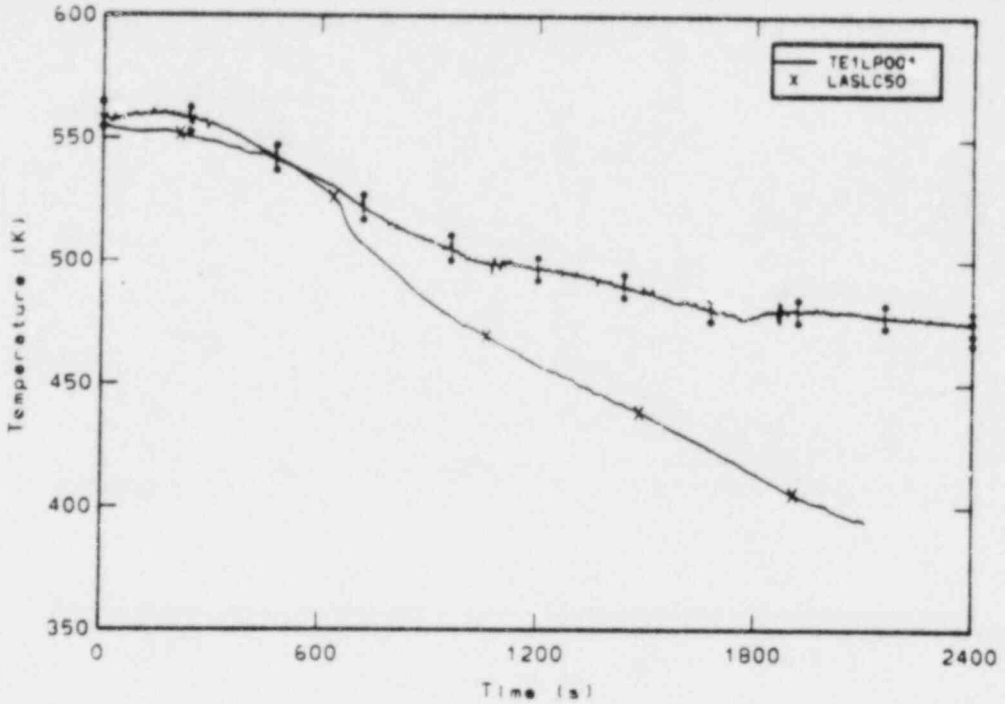

Figure J-11. Comparison of measured and LASL calculated lower plenum fluid temperature.

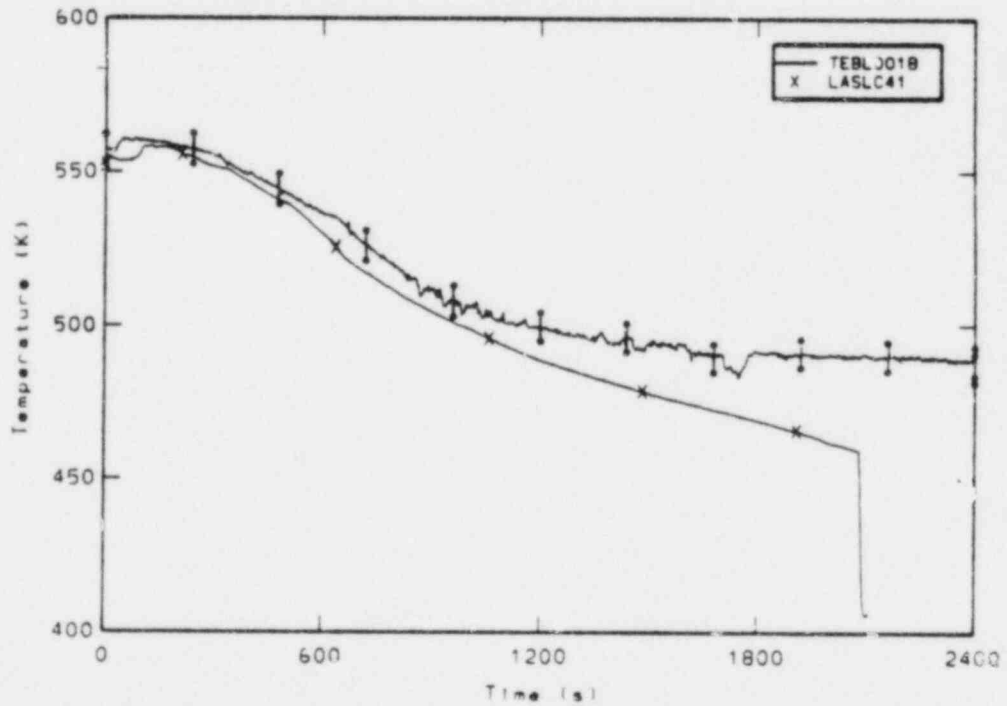

Figure J-12. Comparison of measured and LASL calculated broken loop cold leg fluid temperature.

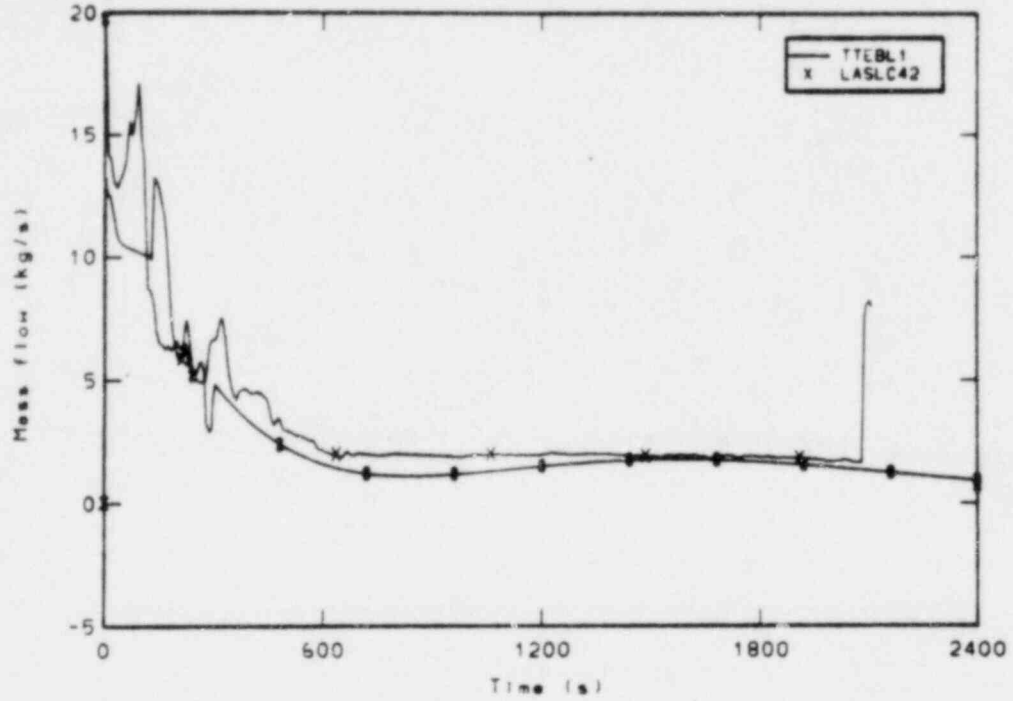

Figure J-13. Comparison of measured and LASL calculated mass flow rate at the break.

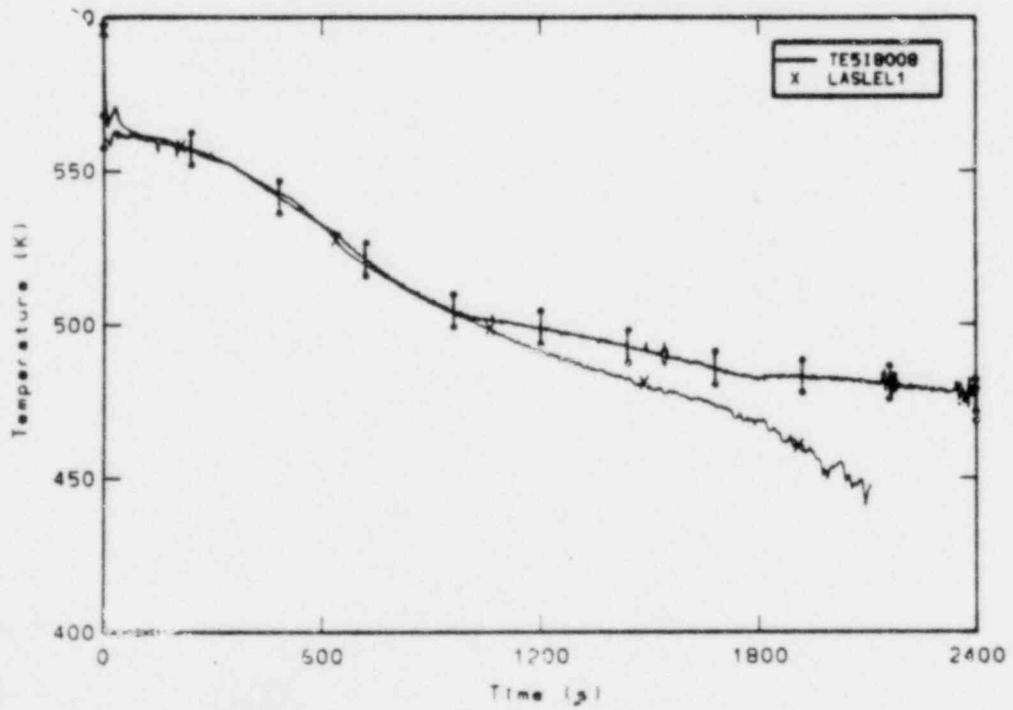

Figure J-14. Comparison of measured rod cladding temperature at the 0.20m elevation and LASL calculated rod cladding temperature.

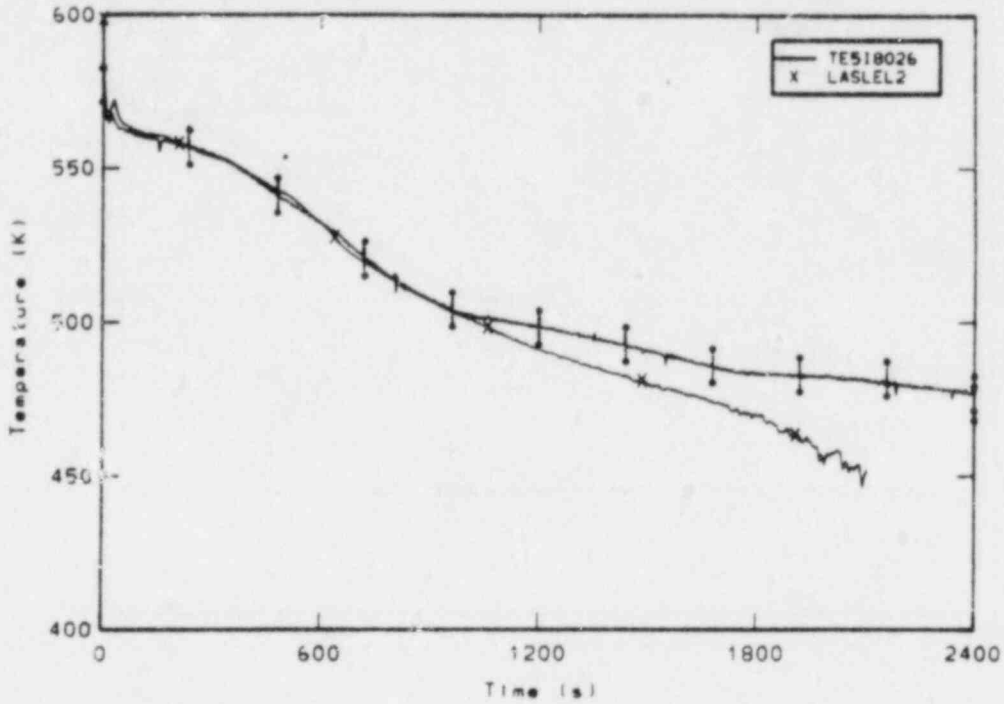

Figure J-15. Comparison of measured rod cladding temperatures at the 0.66m elevation and LASL calculated rod cladding temperature.

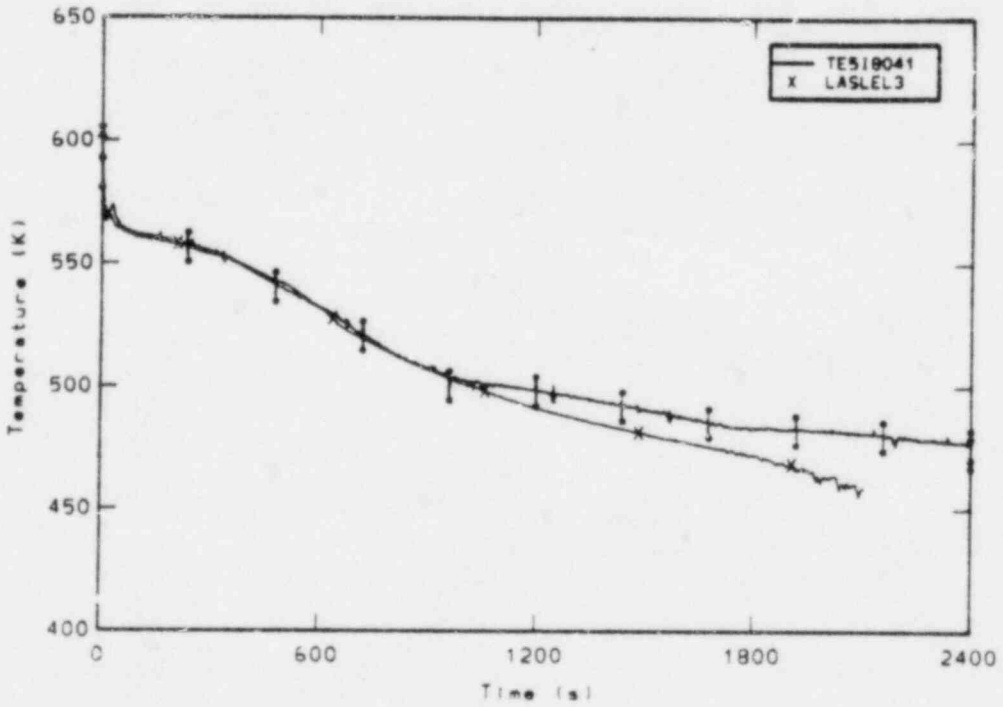

Figure J-16. Comparison of measured rod cladding temperatures at the 1.04m elevation and LASL calculated rod cladding temperature.

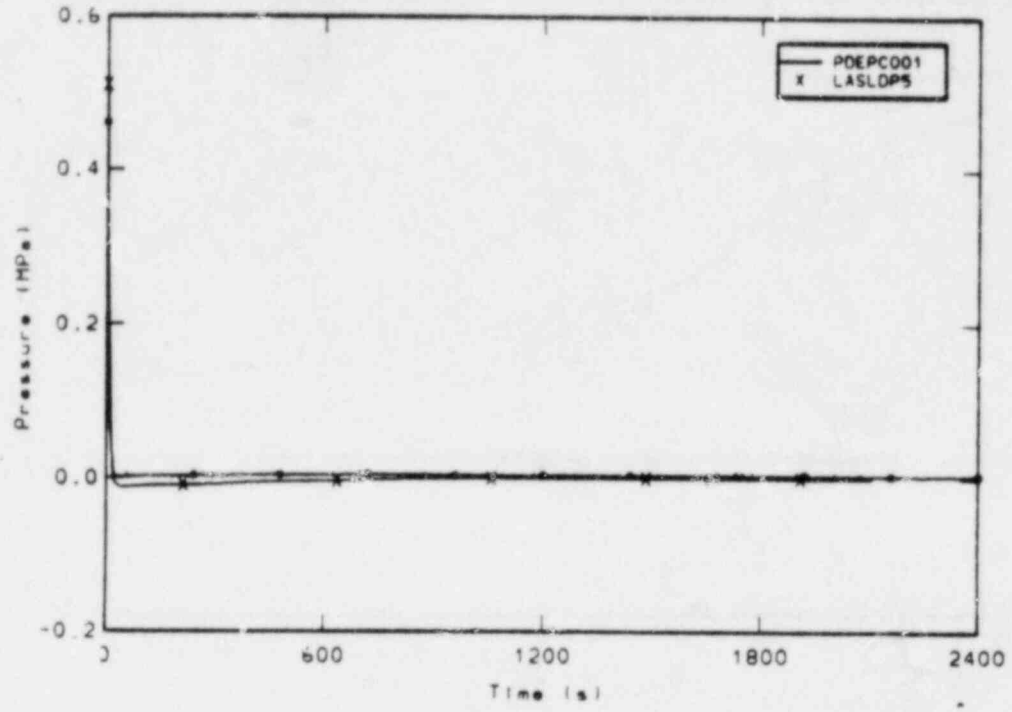

Figure J-17. Comparison of measured and LASL calculated differential pressure drop across the pumps.

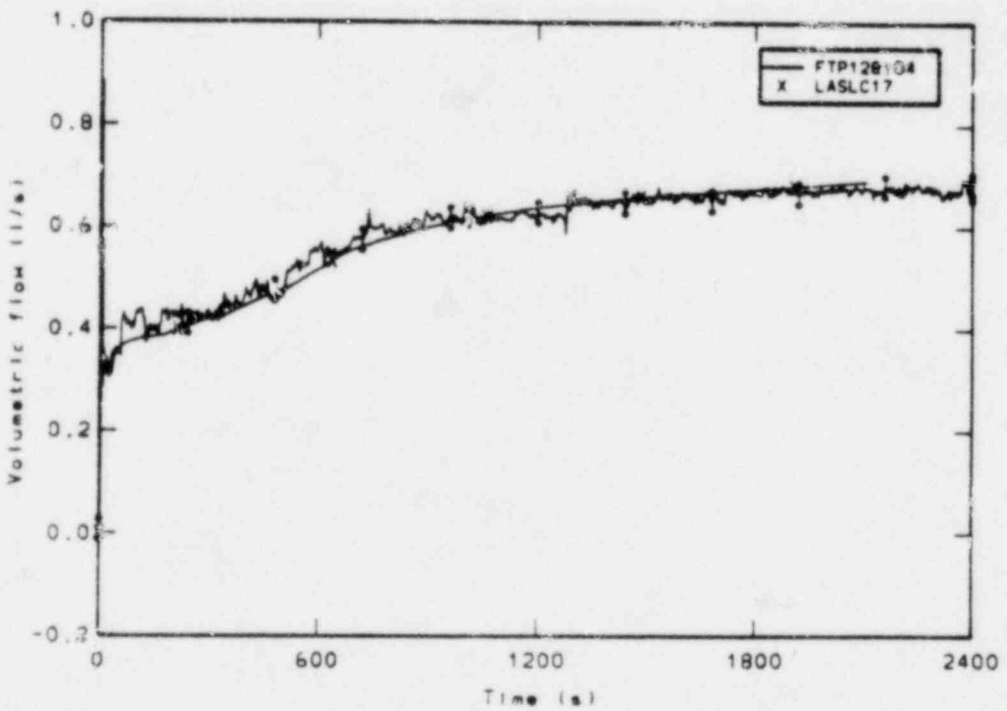

Figure J-18. Comparison of measured and LASL calculated high pressure injection system (HPIS) volumetric flow rate.

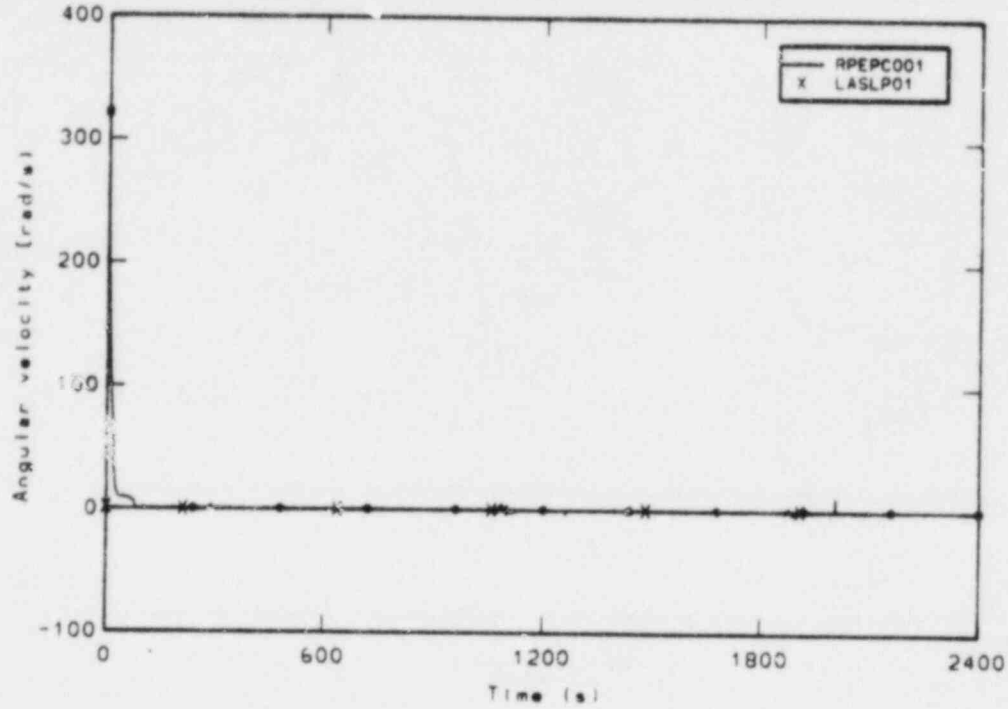

Figure J-19. Comparison of measured and LASL calculated pump speed.

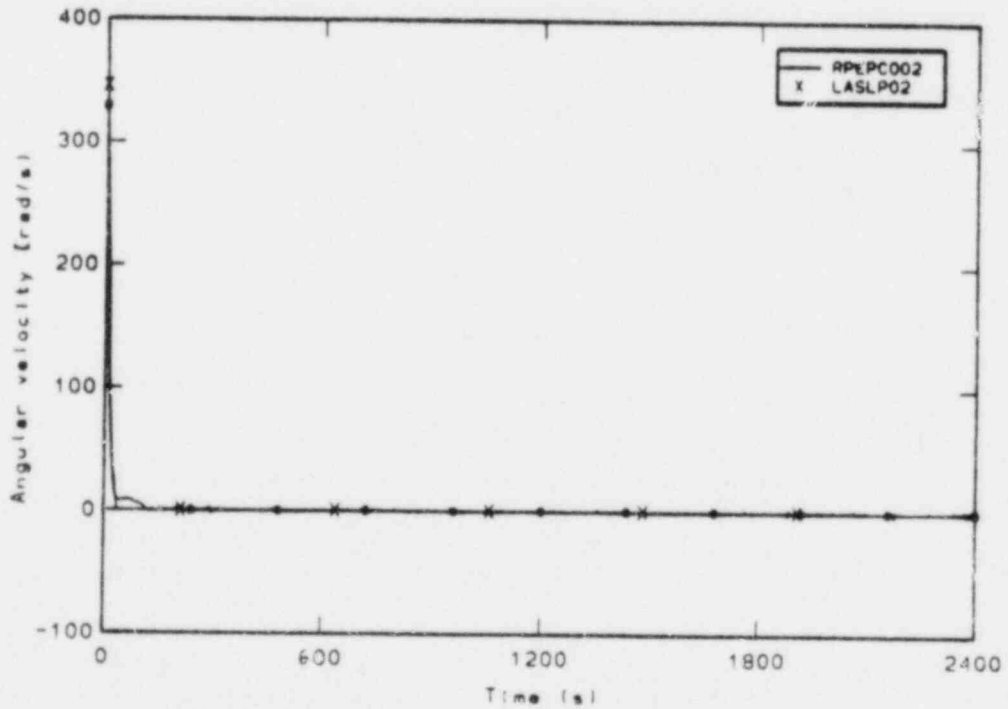

Figure J-20. Comparison of measured and LASL calculated pump speed.

APPENDIX K

COMPARSIONS OF NUCLEAR POWER COMPANY LIMITED MODEL NPCDA CALCULATED RESULTS WITH LOFT EXPERIMENT MEASUREMENTS

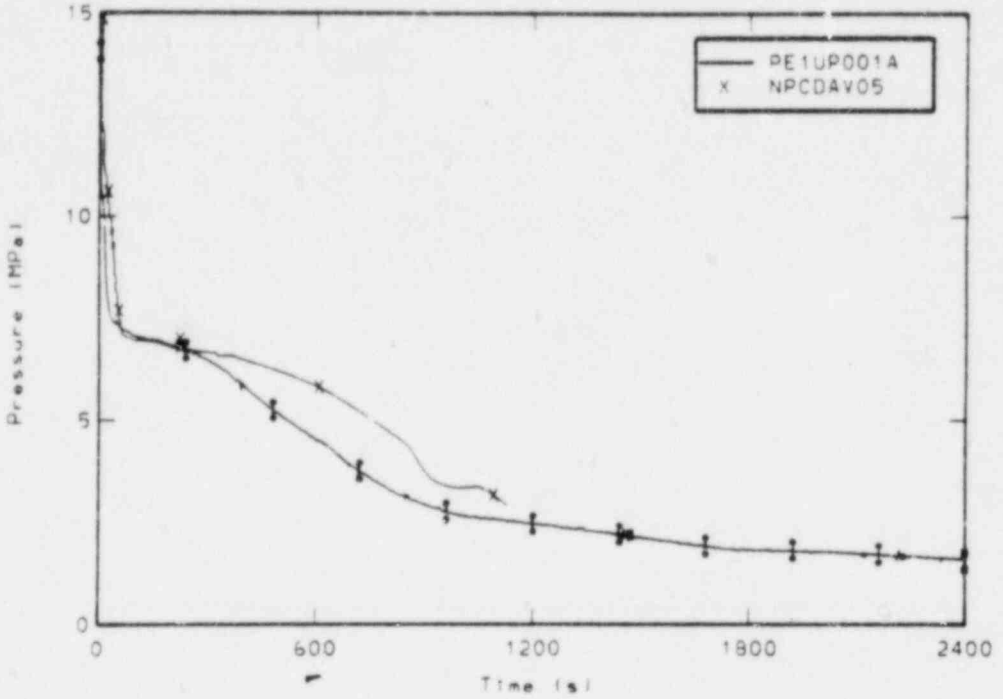

Figure K-1. Comparison of measured and NPCDA calculated upper plenum pressure.

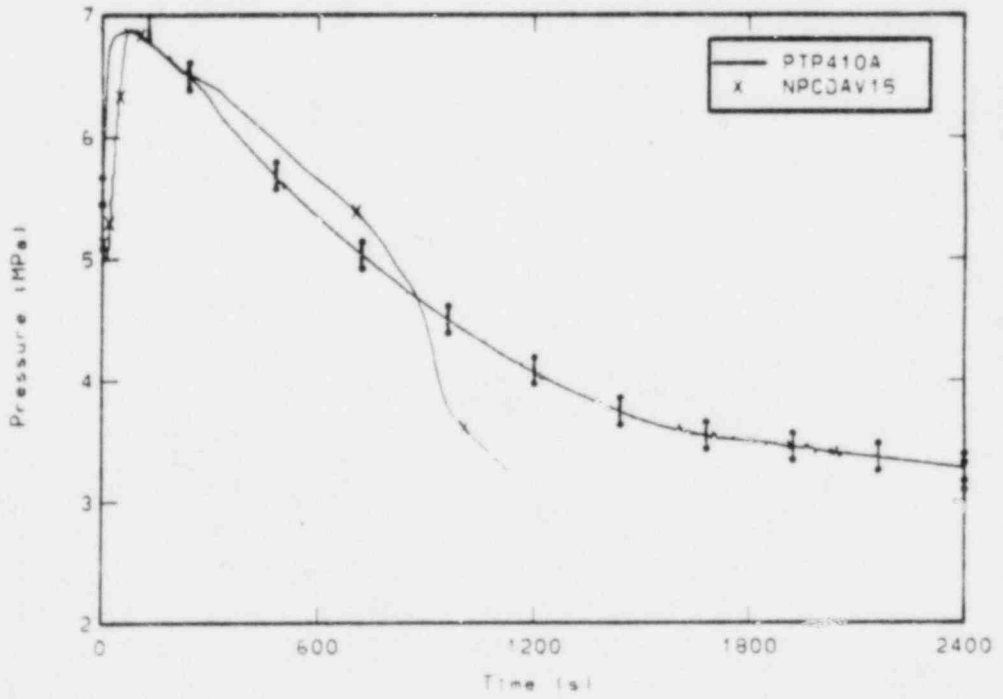

Figure K-2. Comparison of measured and NPCDA calculated steam generator secondary pressure.

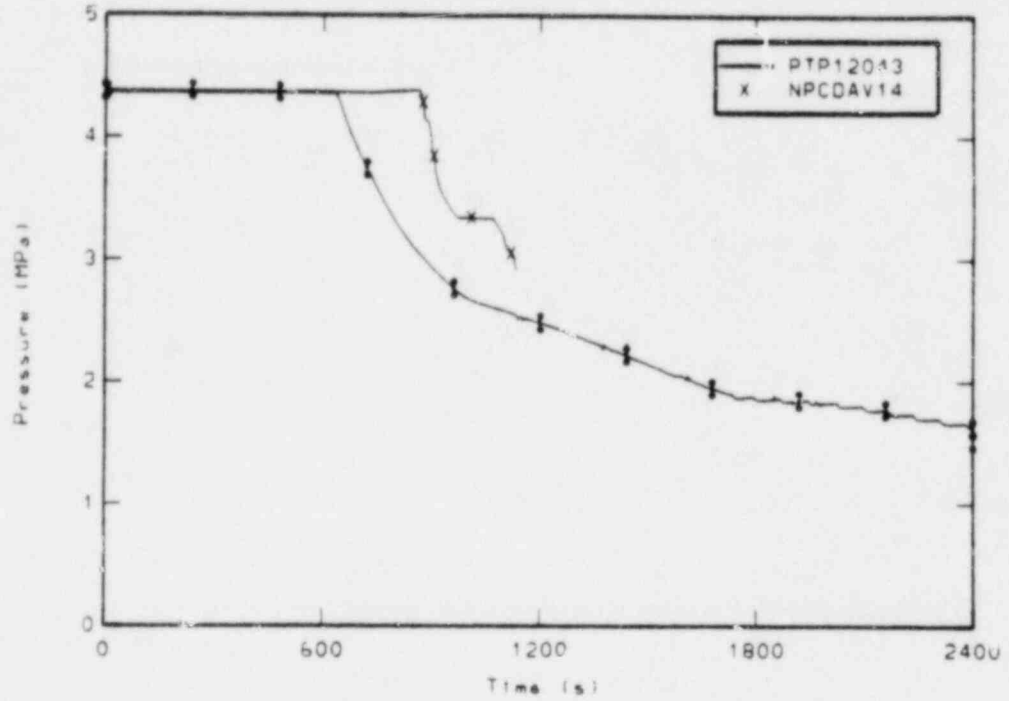

Figure X-3. Comparison of measured and NPCDA calculated accumulator pressure.

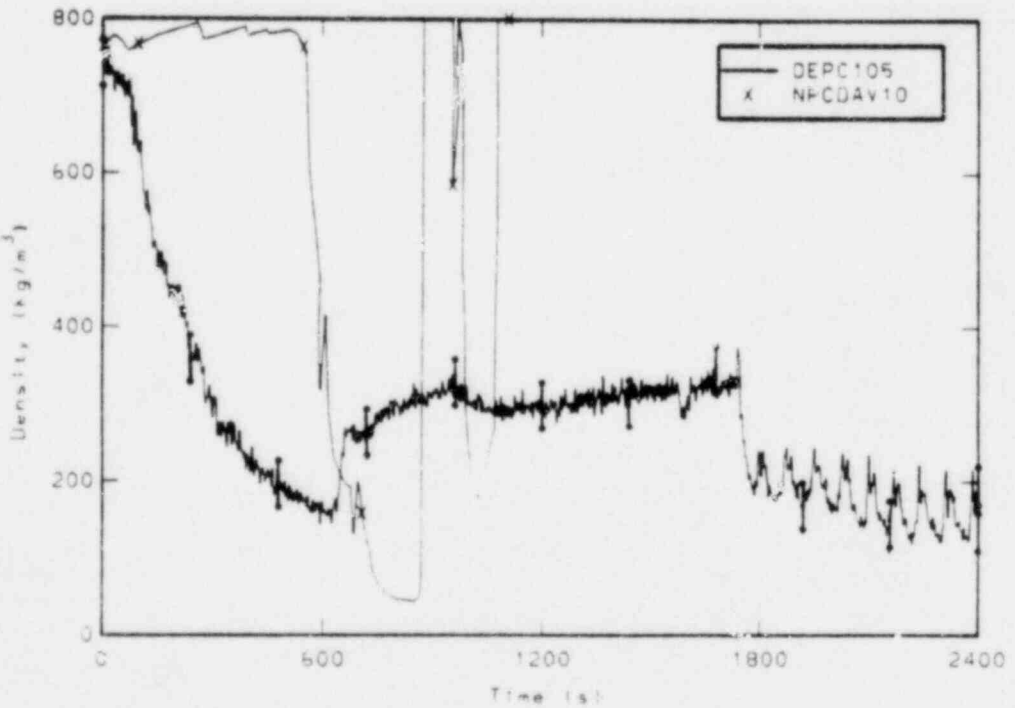

Figure X-4. Comparison of measured and NPCDA calculated average density in the intact loop cold leg.

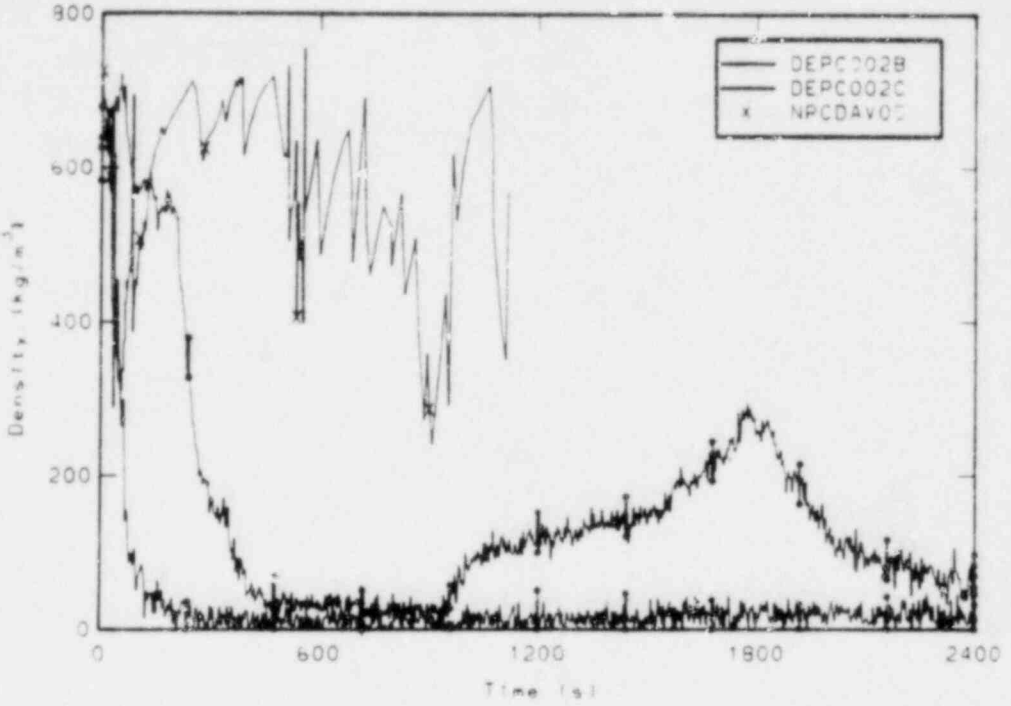

Figure 4-65. Comparison of measured chordal densities and NPCDA calculated average density in the intact loop hot leg.

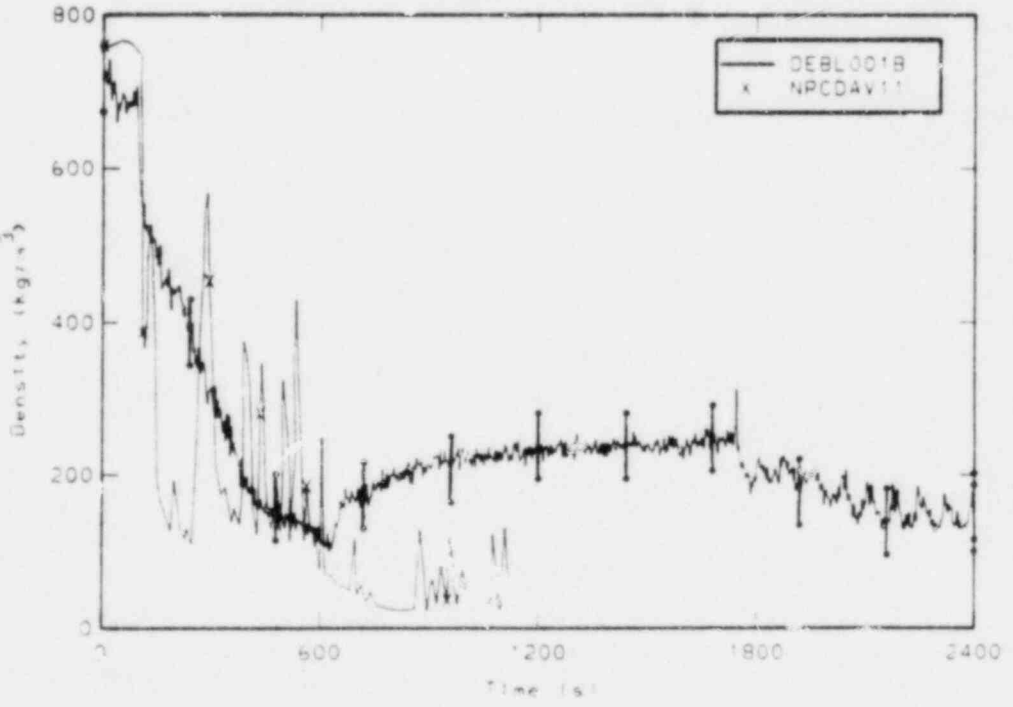

Figure 4-66. Comparison of measured chordal density and NPCDA calculated average density in the broken loop cold leg.

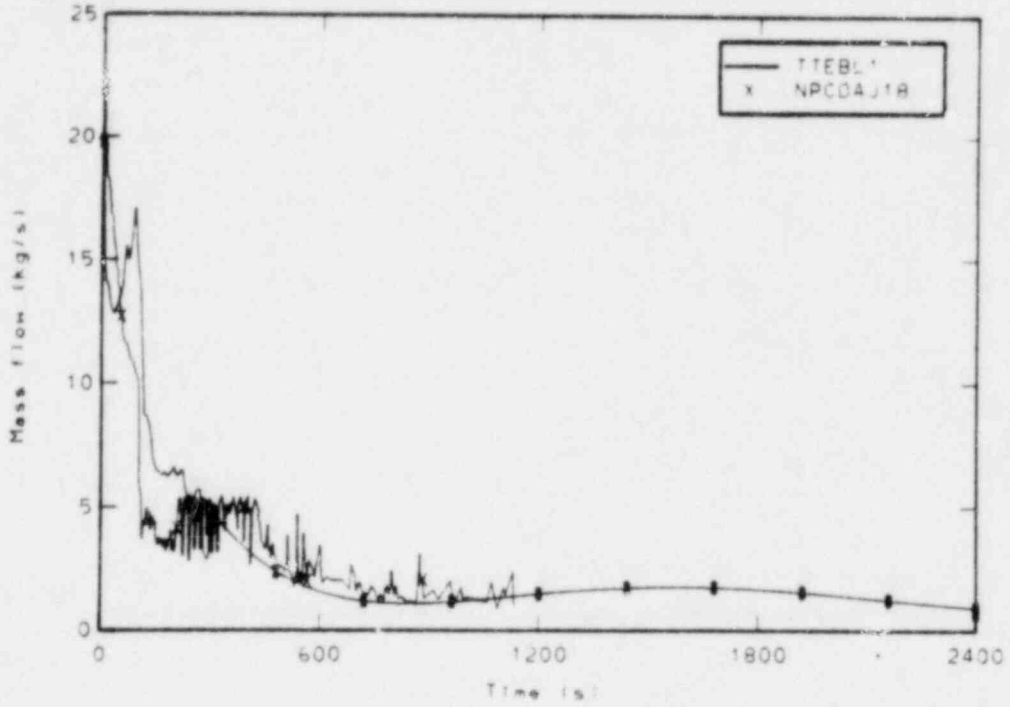

Figure A-7. Comparison of measured and NPCDA calculated mass flow rate at the break.

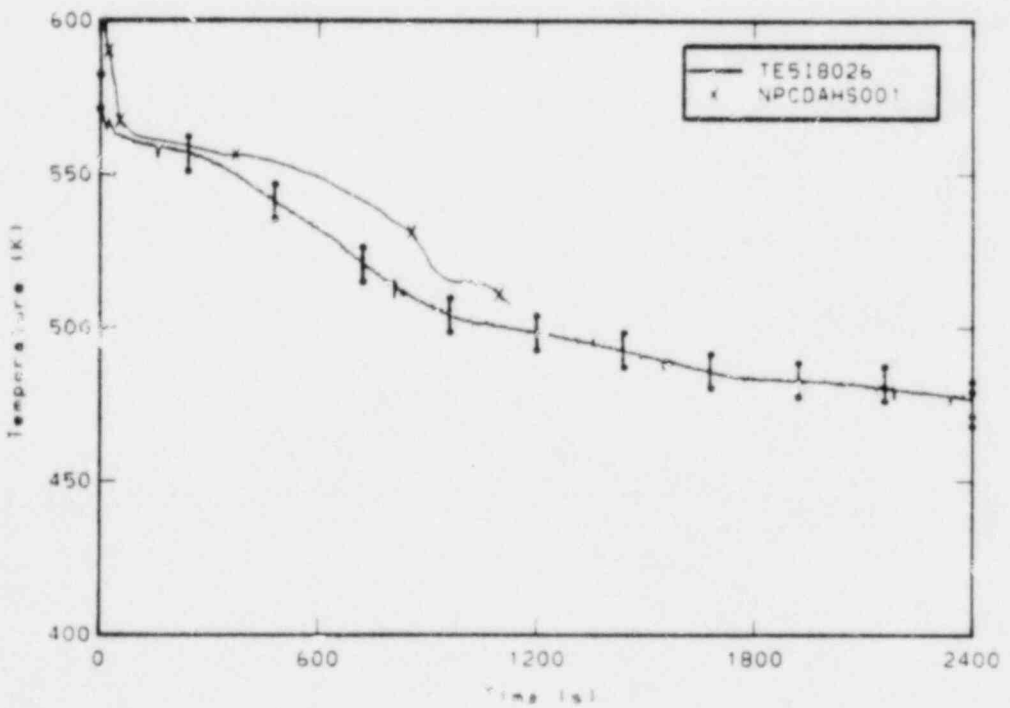

Figure A-8. Comparison of measured rod cladding temperatures at the 0.66m elevation and NPCDA calculated rod cladding temperature.

APPENDIX L

COMPARSIONS OF NUCLEAR POWER COMPANY LIMITED MODEL NPCBR CALCULATED RESULTS WITH LOFT EXPERIMENT MEASUREMENTS

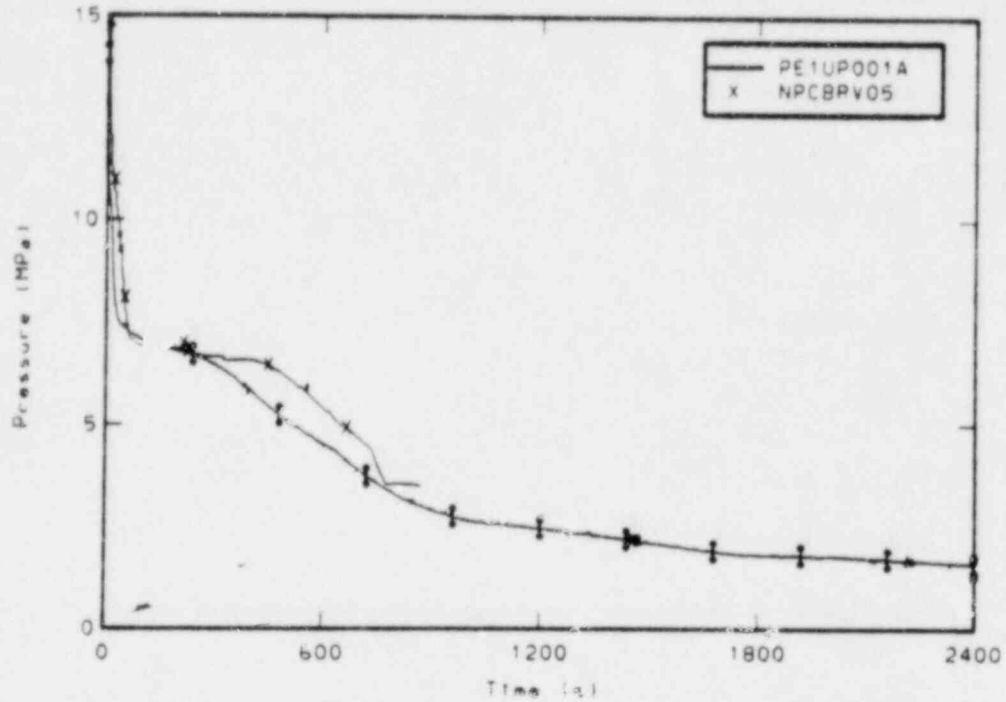

Figure L-1. Comparison of measured and NPCBR calculated upper plenum pressure.

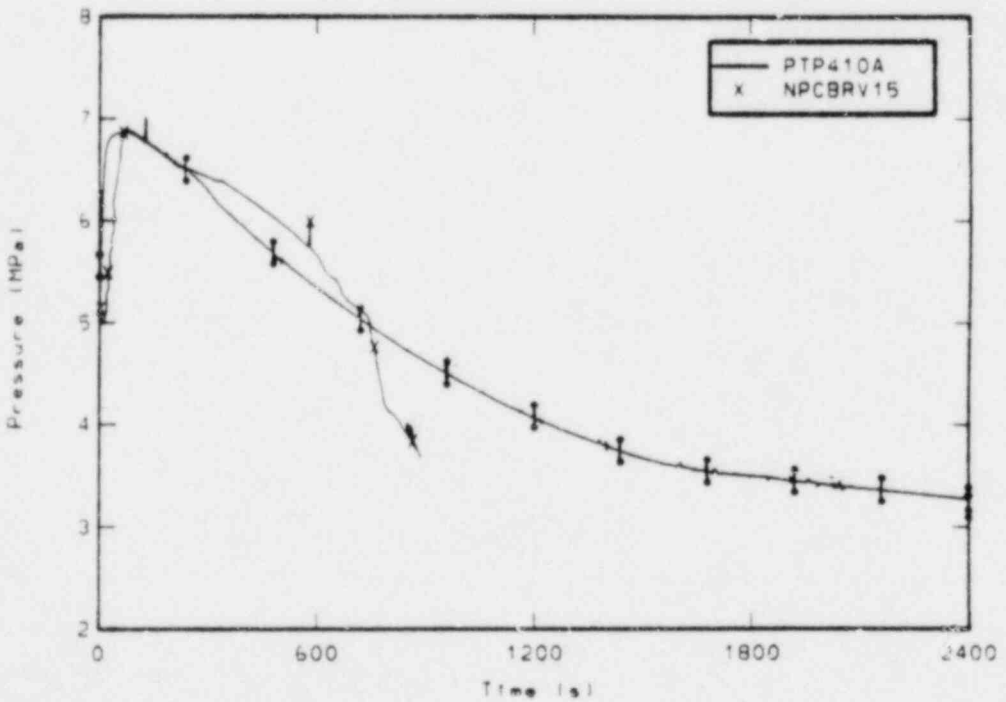

Figure L-2. Comparison of measured and NPCBR calculated steam generator secondary pressure.F3

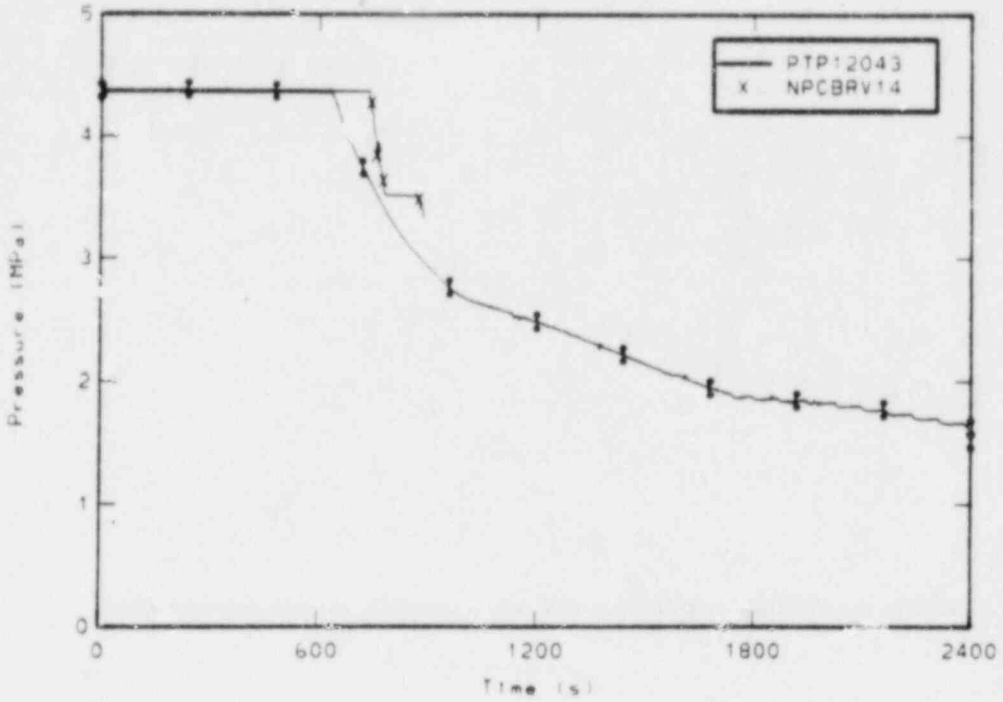

Figure L-3. Comparison of measured and NPCBR calculated accumulator pressure.

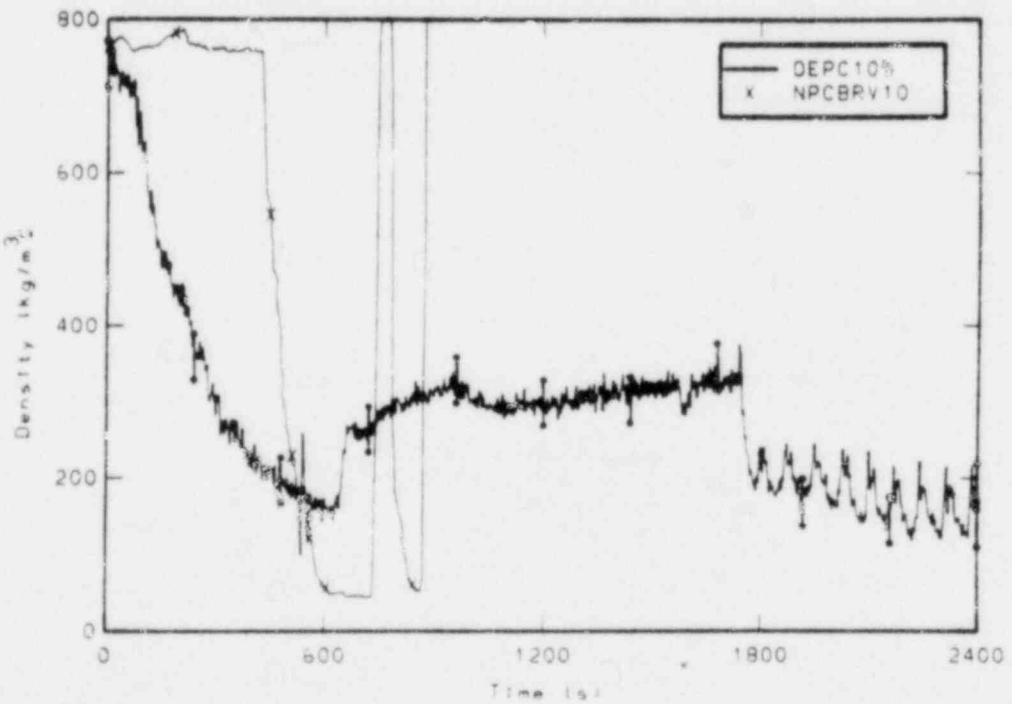

Figure L-4. Comparison of measured and NPCBR calculated average density in the intact loop cold leg.

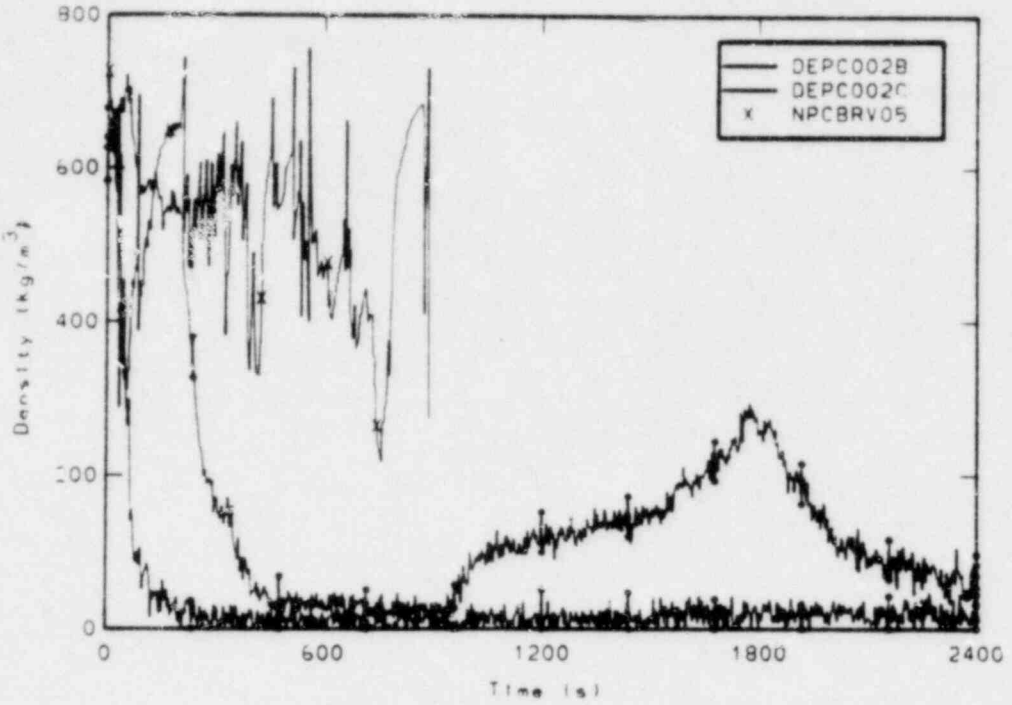

Figure L-5. Comparison of measured chordal densities and NPCBR calculated average density in the intact loop hot leg.

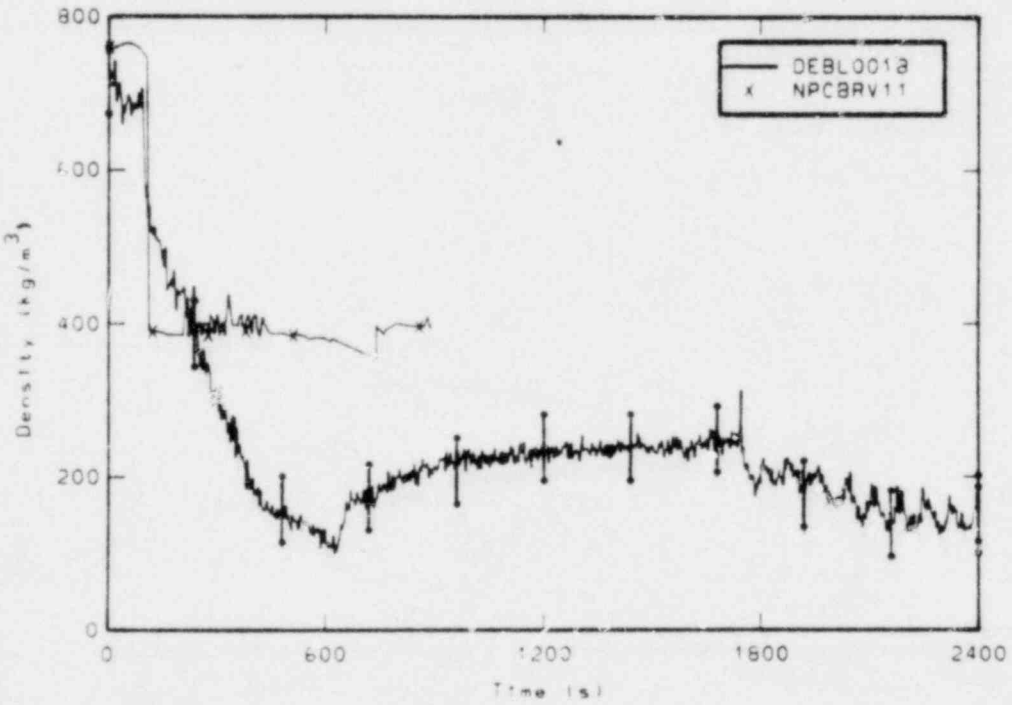

Figure L-6. Comparison of chordal density and NPCBR calculated average density in the broken loop cold leg.

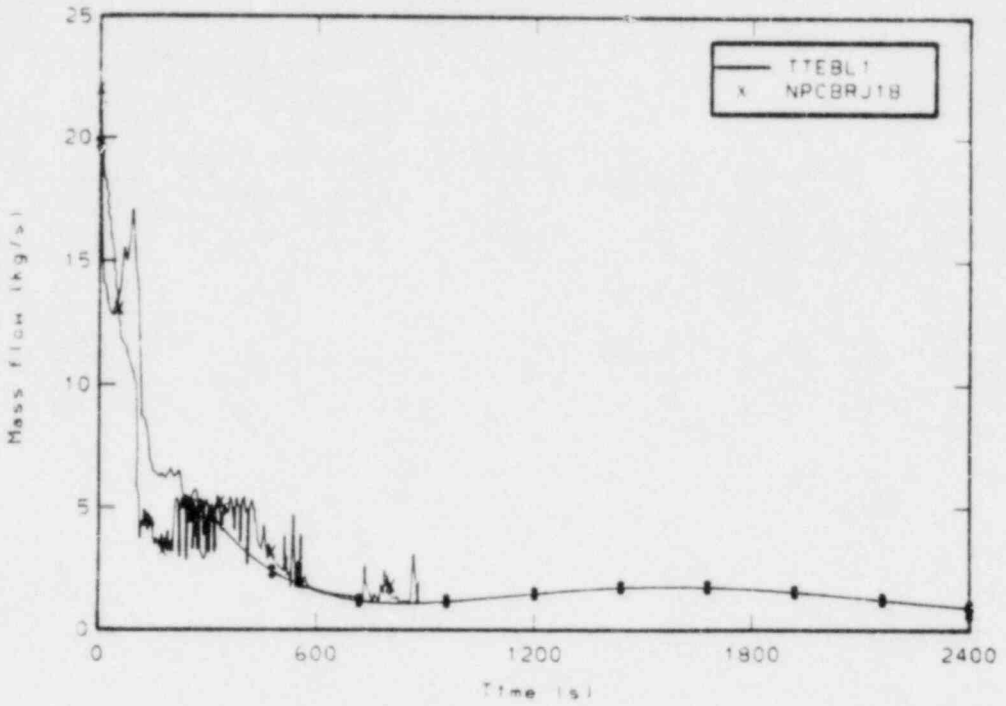

Figure L-7. Comparison of measured and NPCBR calculated mass flow rate at the break.

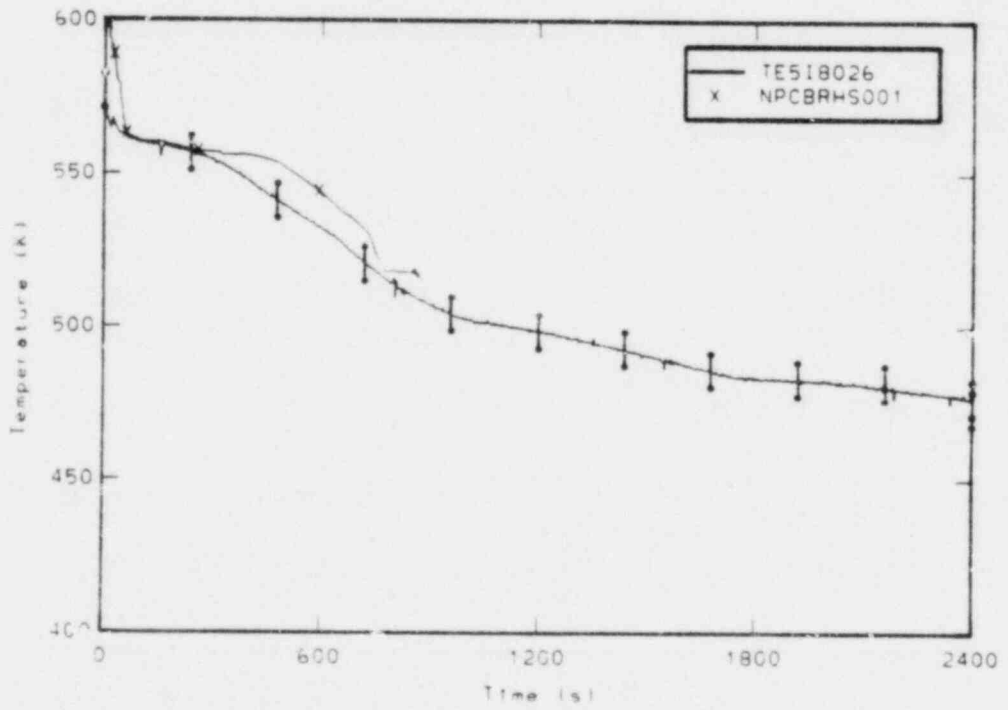

Figure L-8. Comparison of measured rod cladding temperature at the 0.66m elevation and NPCBR calculated rod cladding temperature.

APPENDIX M

COMPARISONS OF UNITED KINGDOM ATOMIC ENERGY AUTHORITY CALCULATED RESULTS WITH LOFT EXPERIMENT MEASUREMENTS

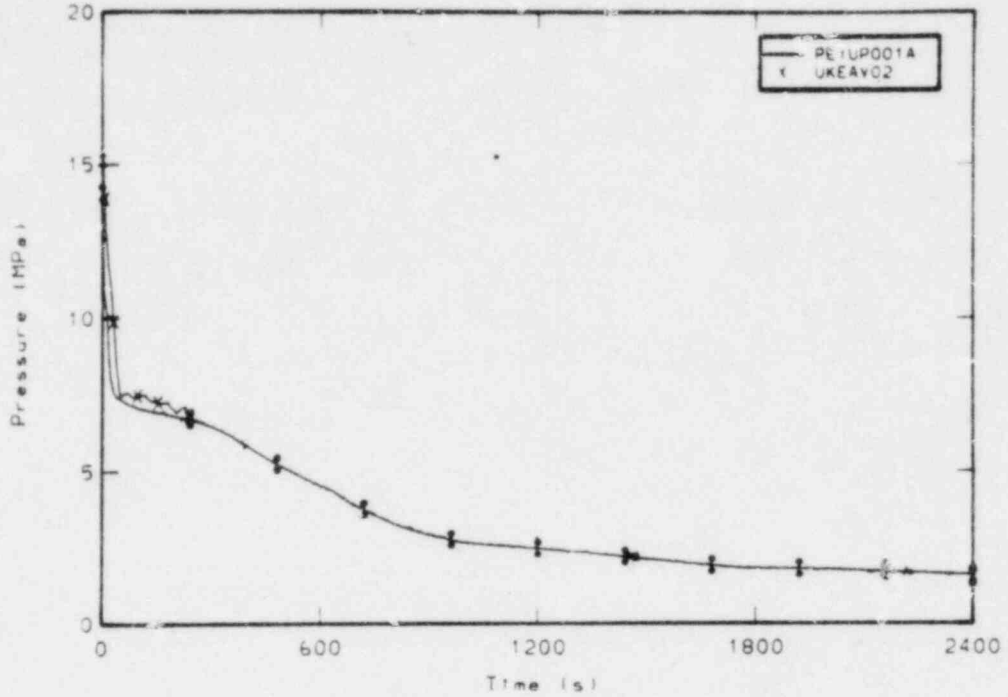

Figure M-1. Comparison of measured and UKEA calculated upper plenum pressure.

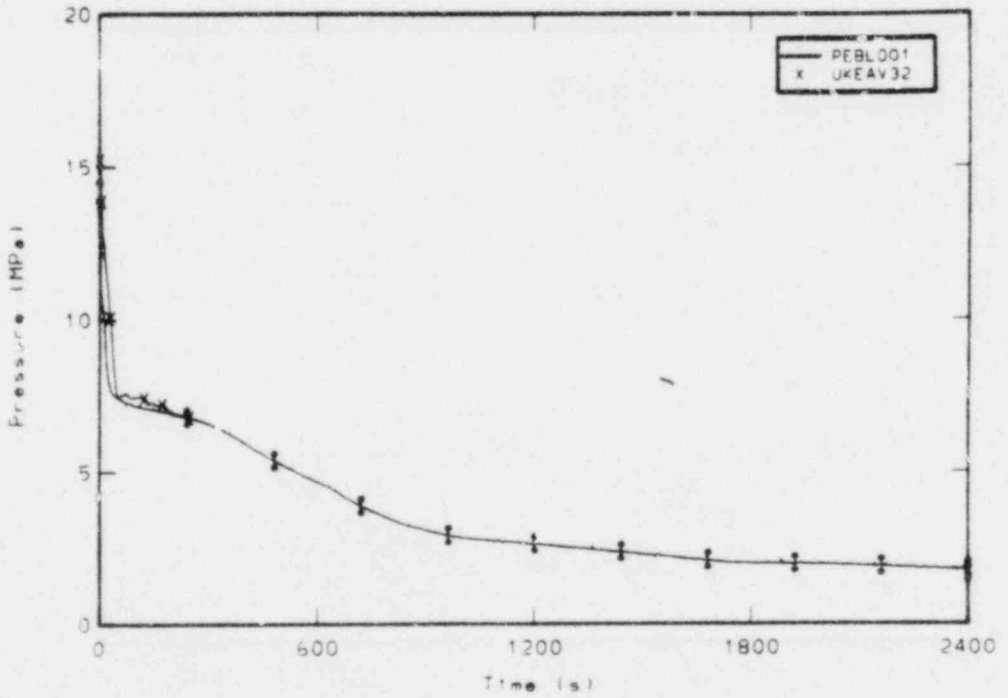

Figure M-2. Comparison of measured and UKEA calculated broken loop cold leg pressure.

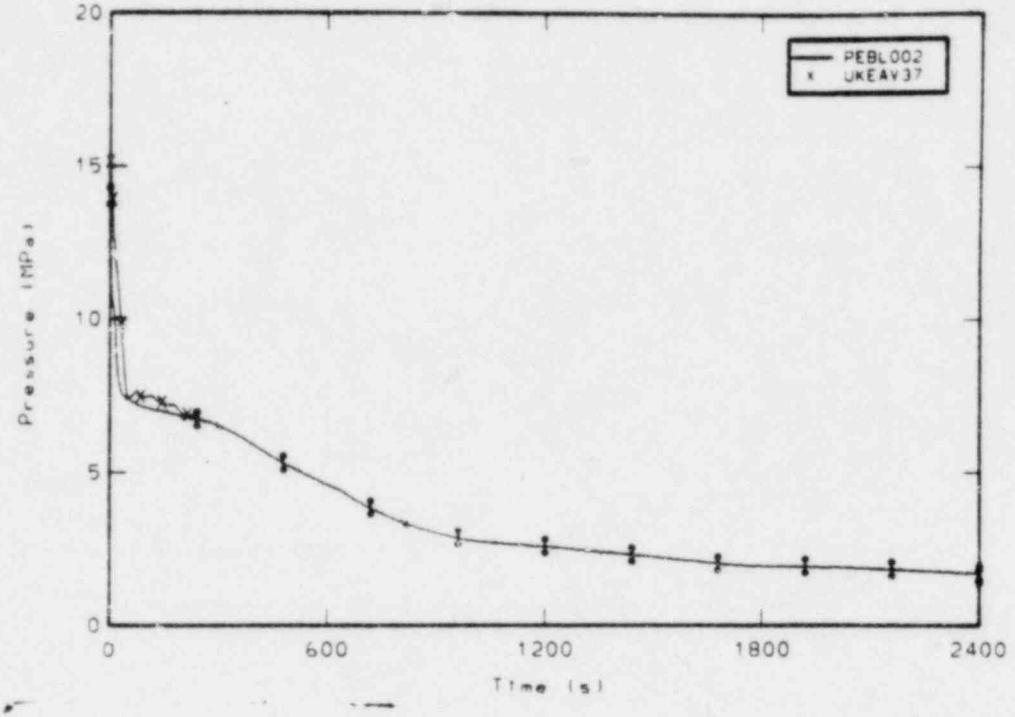

Figure M-3. Comparison of measured and UKEA calculated broken loop hot leg pressure.

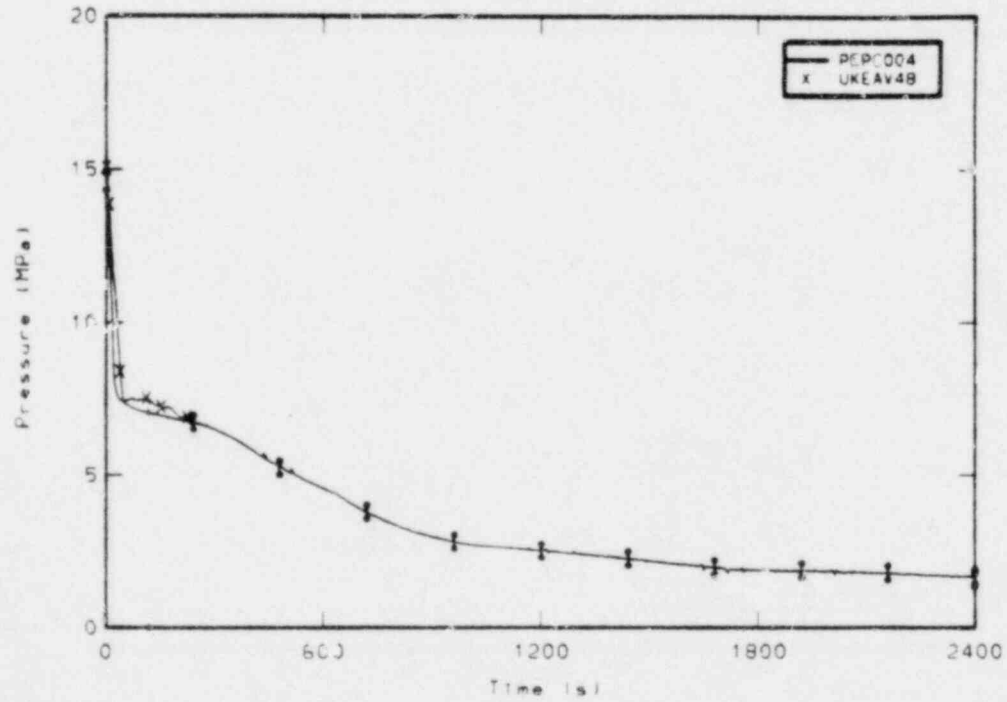

Figure M-4. Comparison of measured and UKEA calculated pressurizer pressure.

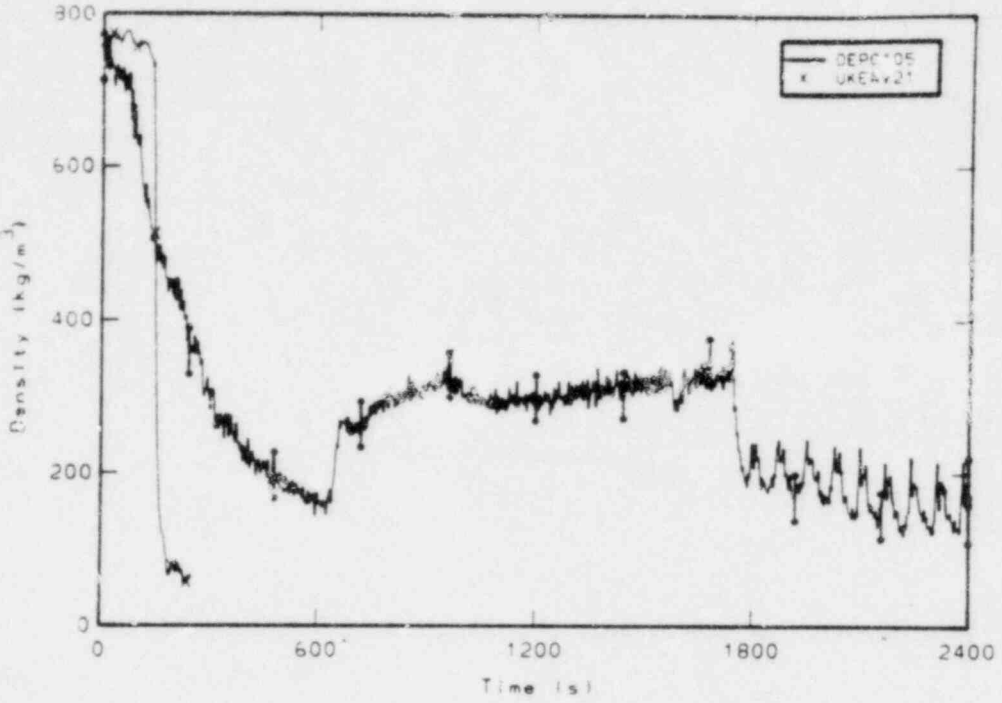

Figure M-5. Comparison of measured and UKEA calculated average density in the intact loop cold leg.

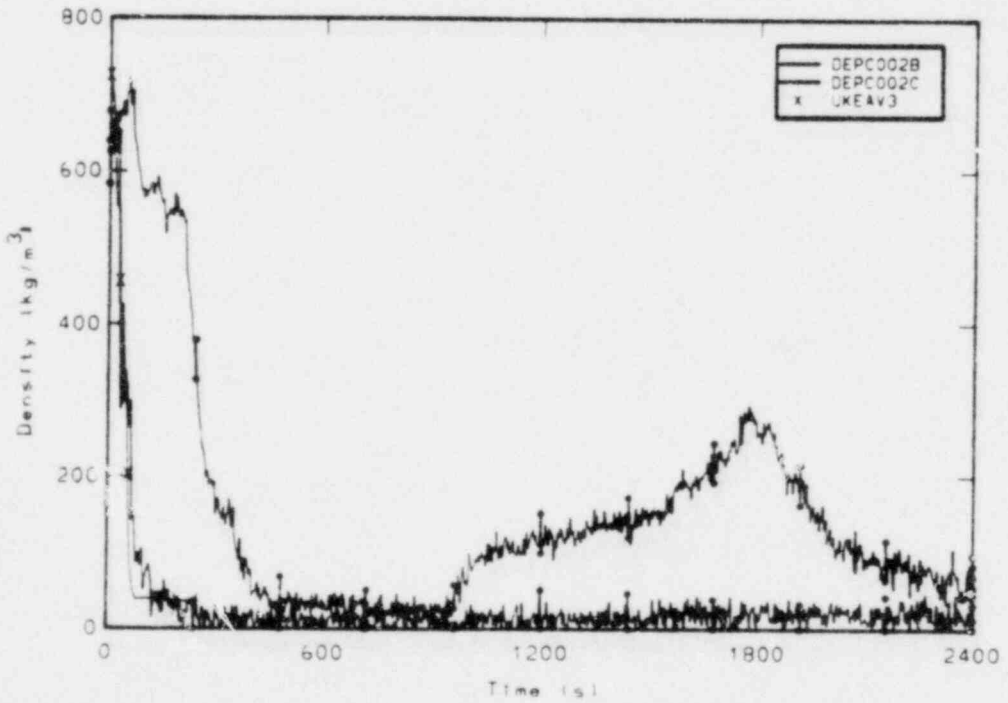

Figure M-6. Comparison of measured chordal densities and UKEA calculated average density in the intact loop hot leg.

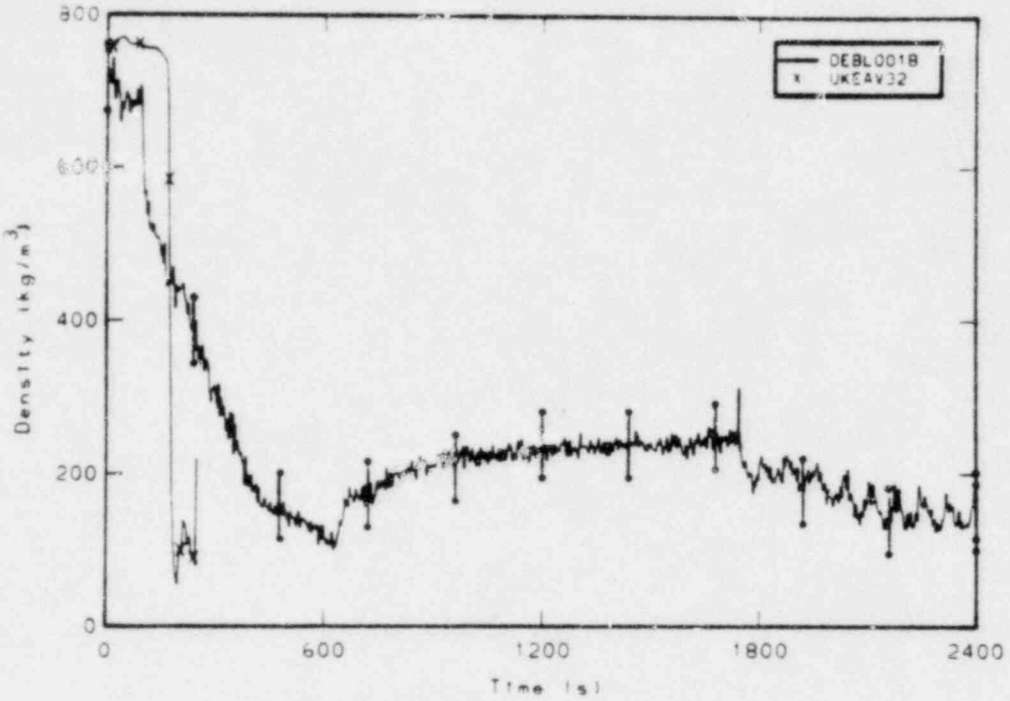

Figure M-7. Comparison of measured churdal density and UKEA calculated average density in the broken loop cold leg.

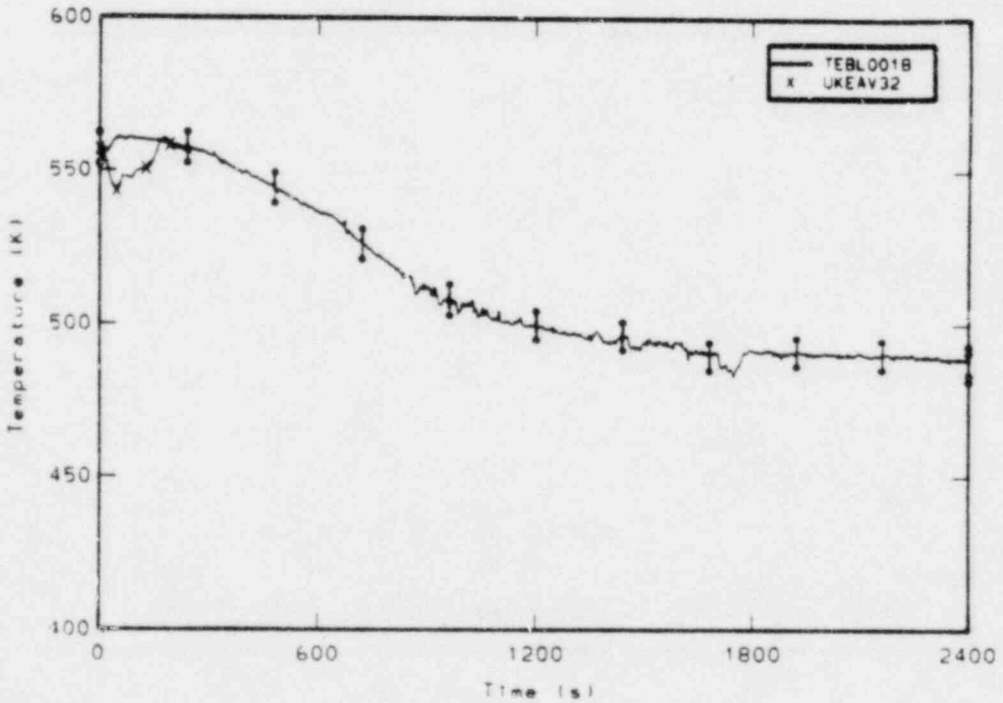

Figure M-8. Comparison of measured and UKEA calculated broken loop cold leg fluid temperature.

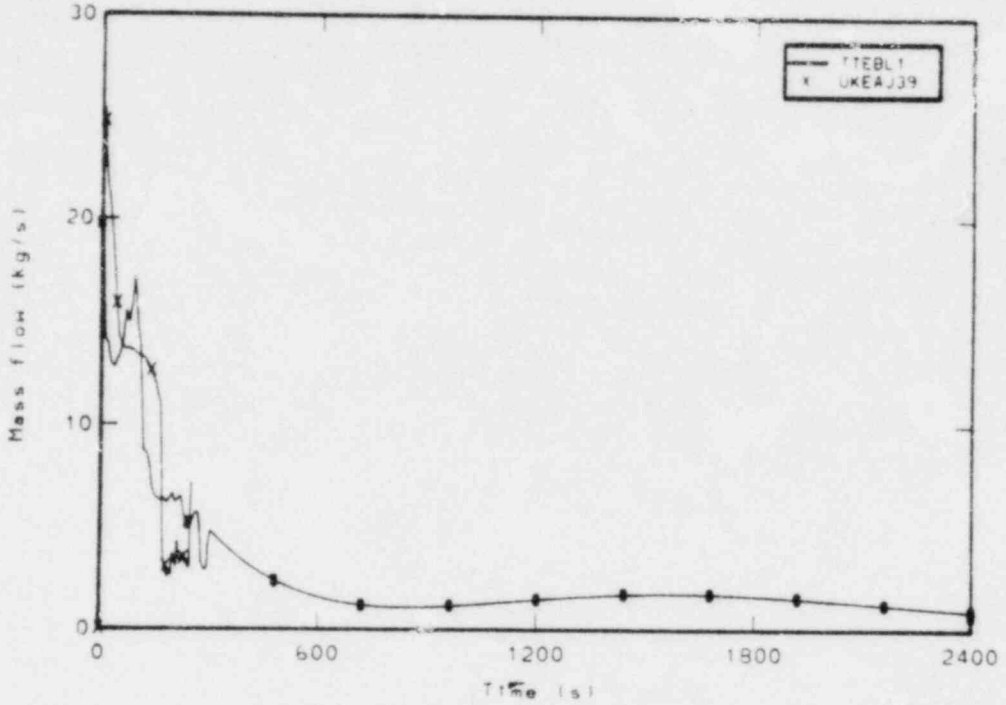

Figure M-9. Comparison of measured and UKEA calculated mass flow rate at the break.

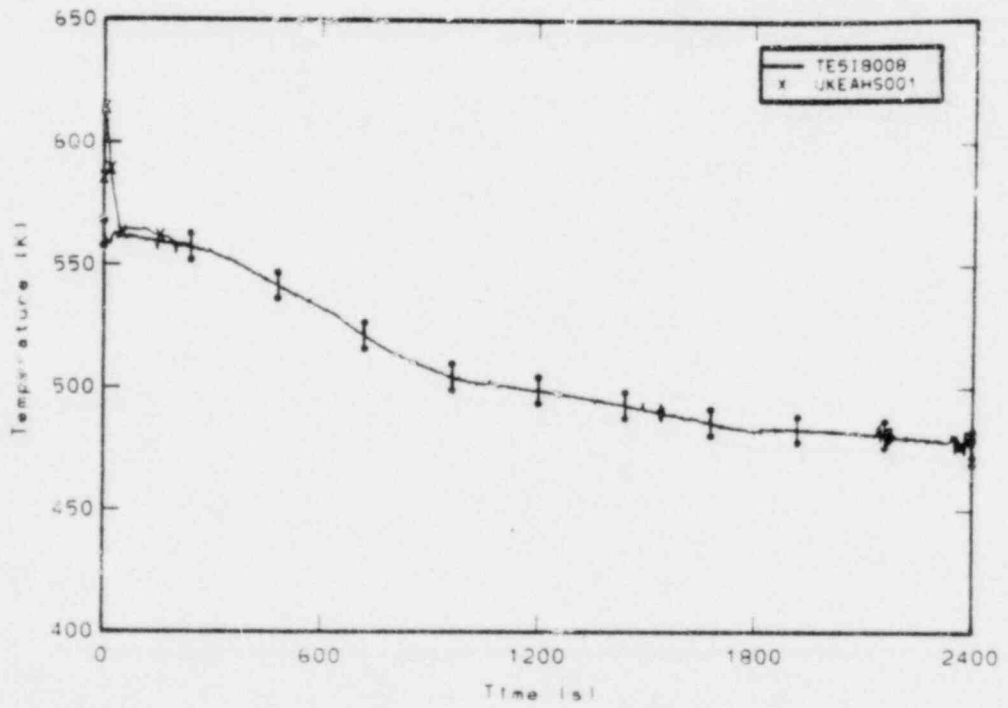

Figure M-10. Comparison of measured rod cladding temperature at the 0.20m elevation and UKEA calculated rod cladding temperature.

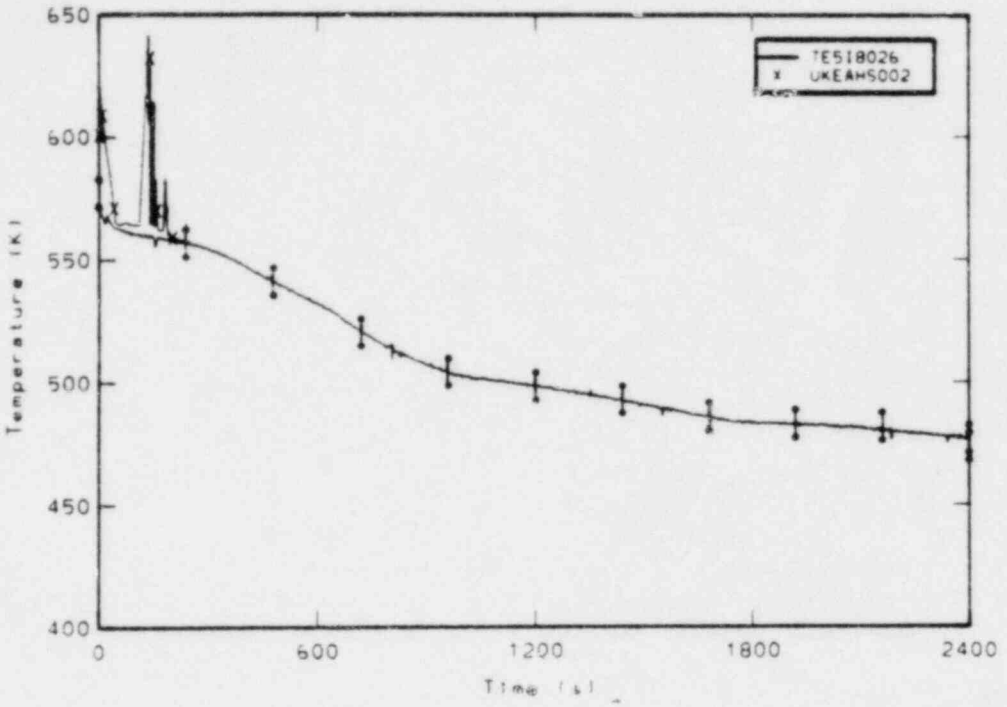

Figure M-11. Comparison of measured rod cladding temperature at the 0.66m elevation and UKEA calculated rod cladding temperature.

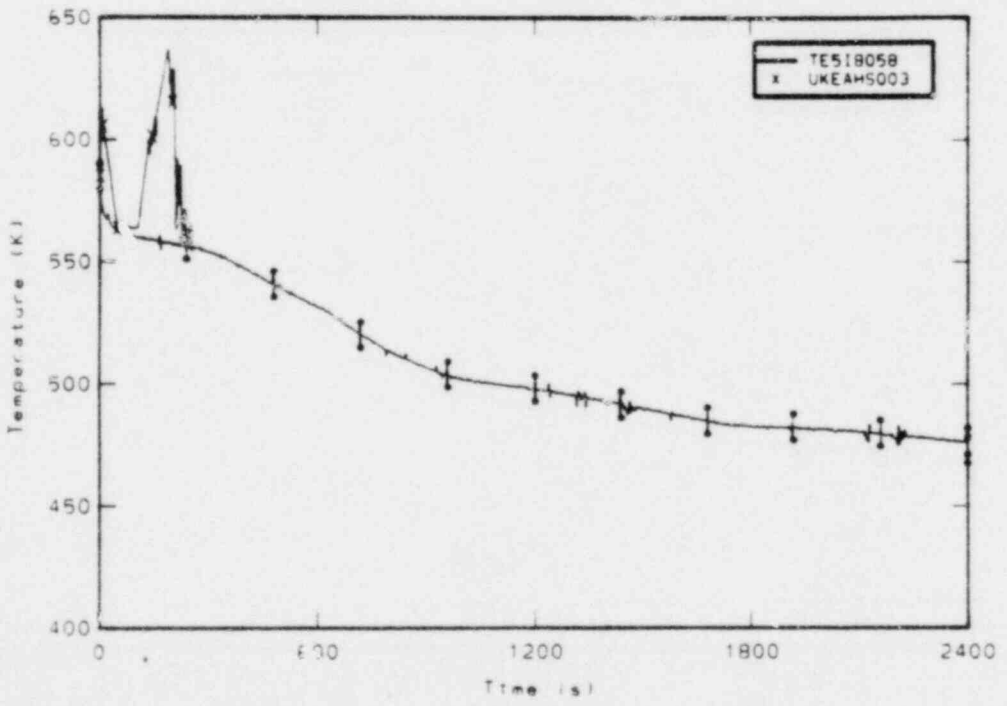

Figure M-12. Comparison of measured rod cladding temperature at the 1.47m elevation and UKEA calculated rod cladding temperature.

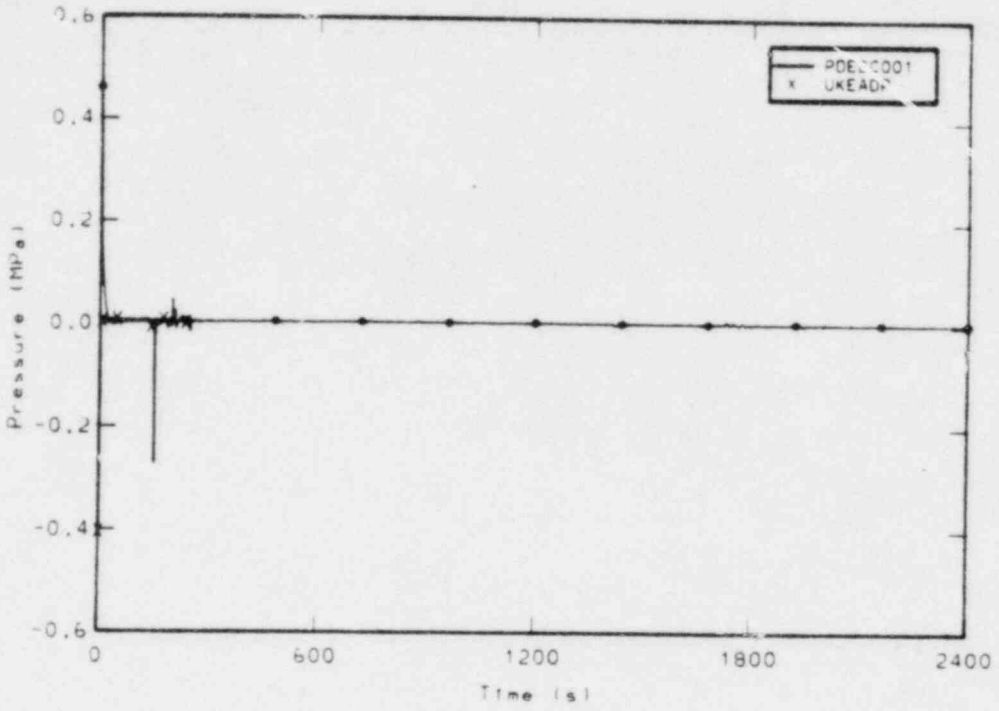

Figure M-13. Comparison of measured and UKEA calculated differential pressure drop across the pumps.

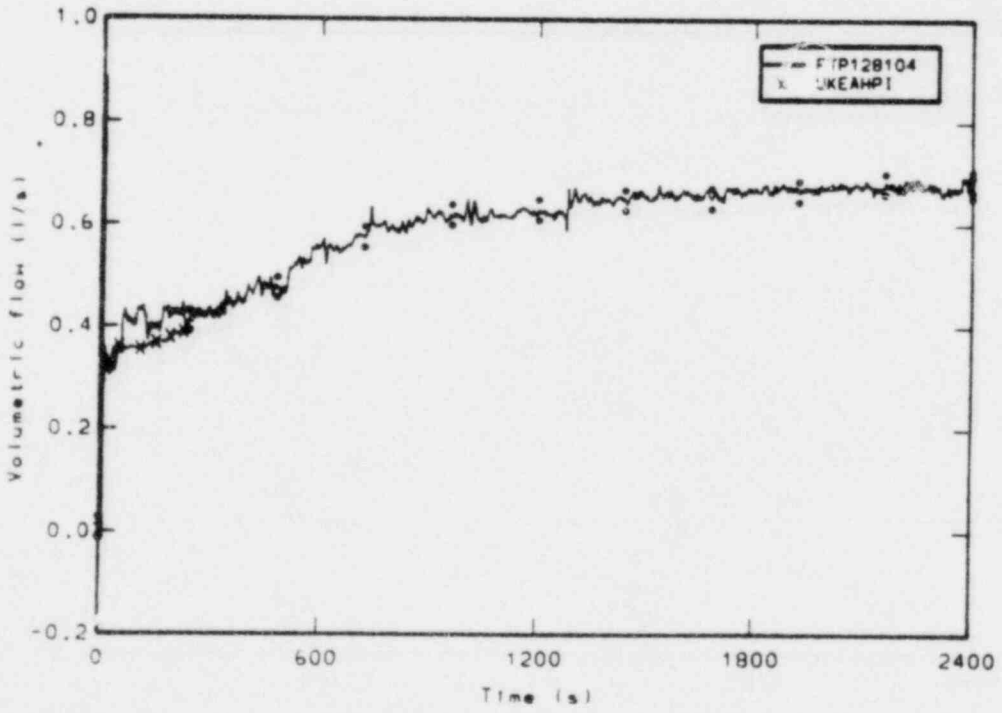

Figure M-14. Comparison of measured and UKEA calculated high pressue injection system (HPIS) volumetric flow rate.

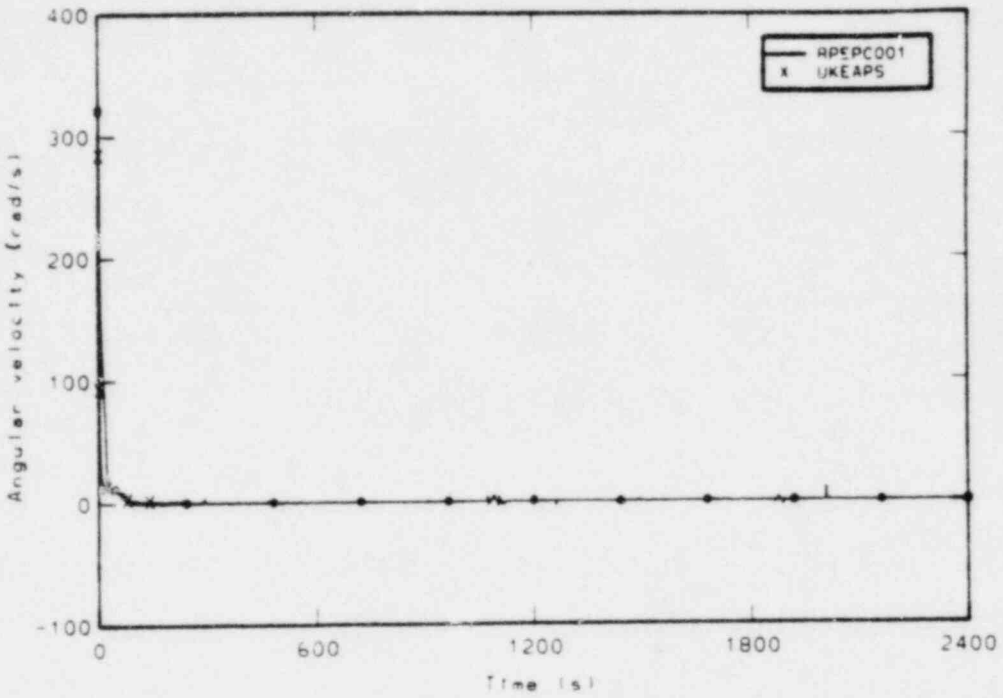

Figure M-15. Comparison of measured and UKEA calculated pump speed.

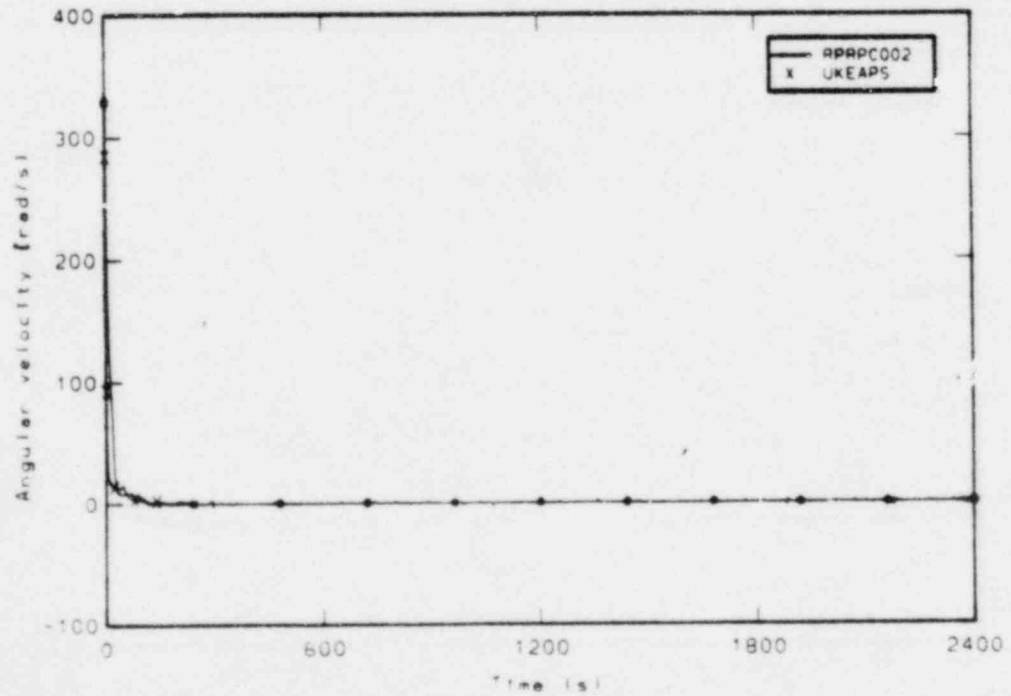

Figure M-16. Comparison of measured and UKEA calculated pump speed.

APPENDIX N

COMPARISONS OF UNITED KINGDOM ATOMIC ENERGY ESTABLISHMENT CALCULATED RESULTS WITH LOFT EXPERIMENT MEASUREMENTS

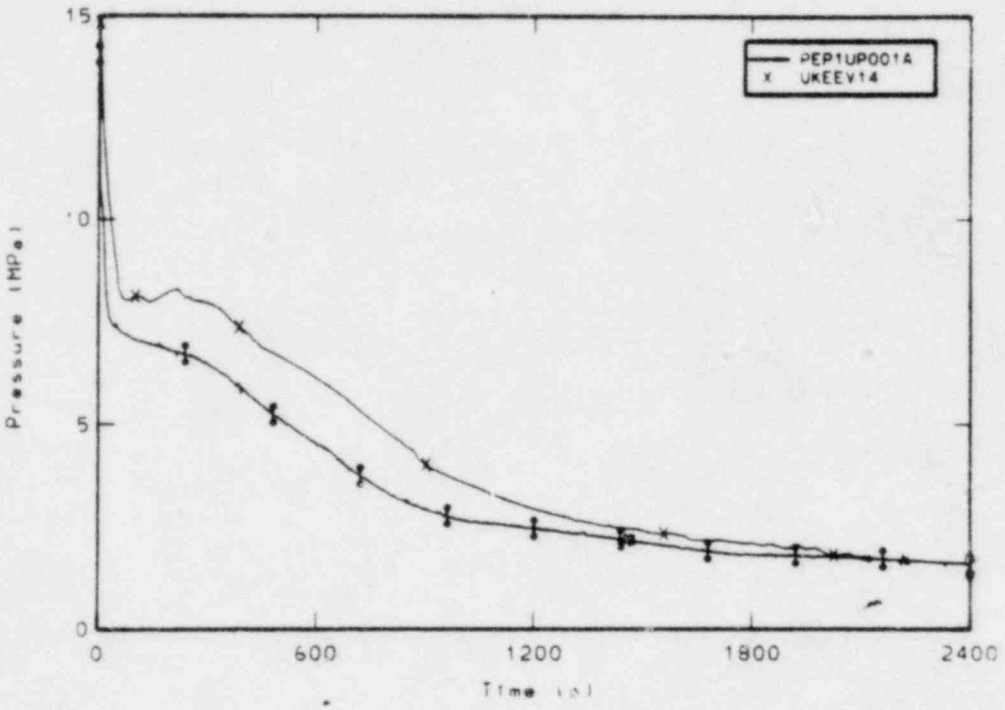

Figure N-1. Comparison of measured and UKEE calculated upper plenum pressure.

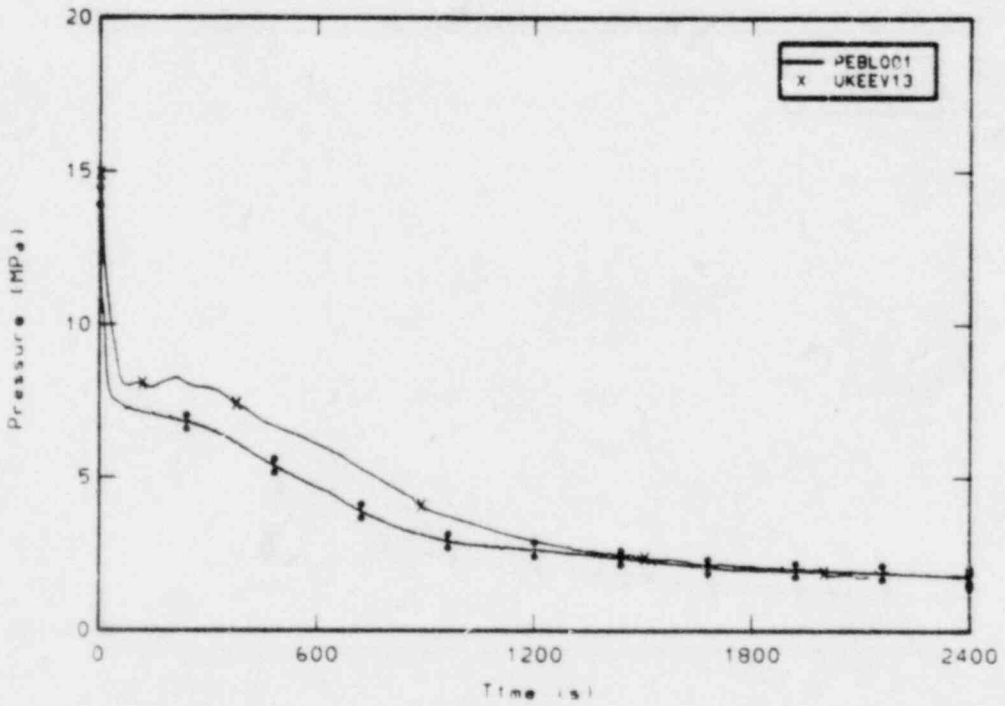

Figure N-2. Comparison of measured and UKEE calculated broken loop cold leg pressure.

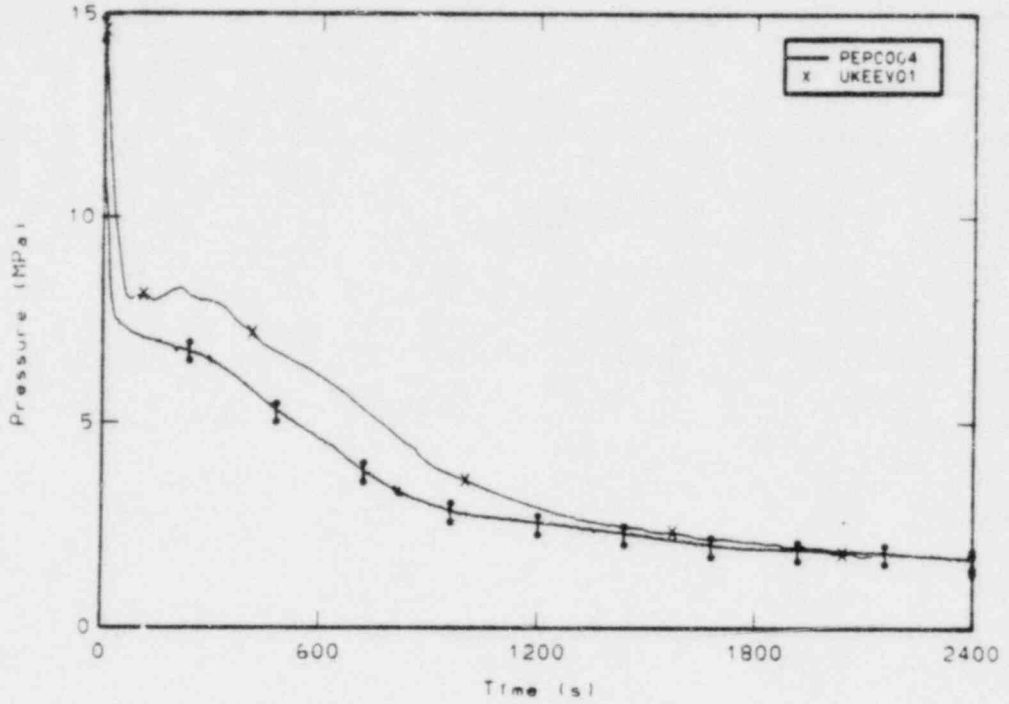

Figure N-3. Comparison of measured and UKEE calculated pressurizer pressure.

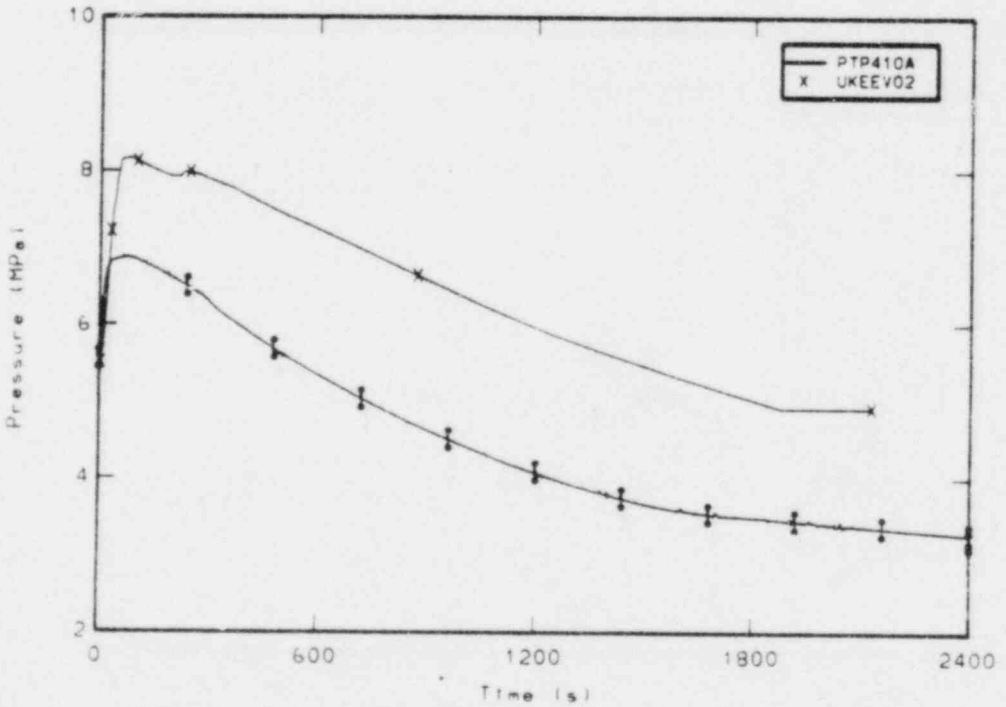

Figure N-4. Comparison of measured and UKEE calculated steam generator secondary pressure.

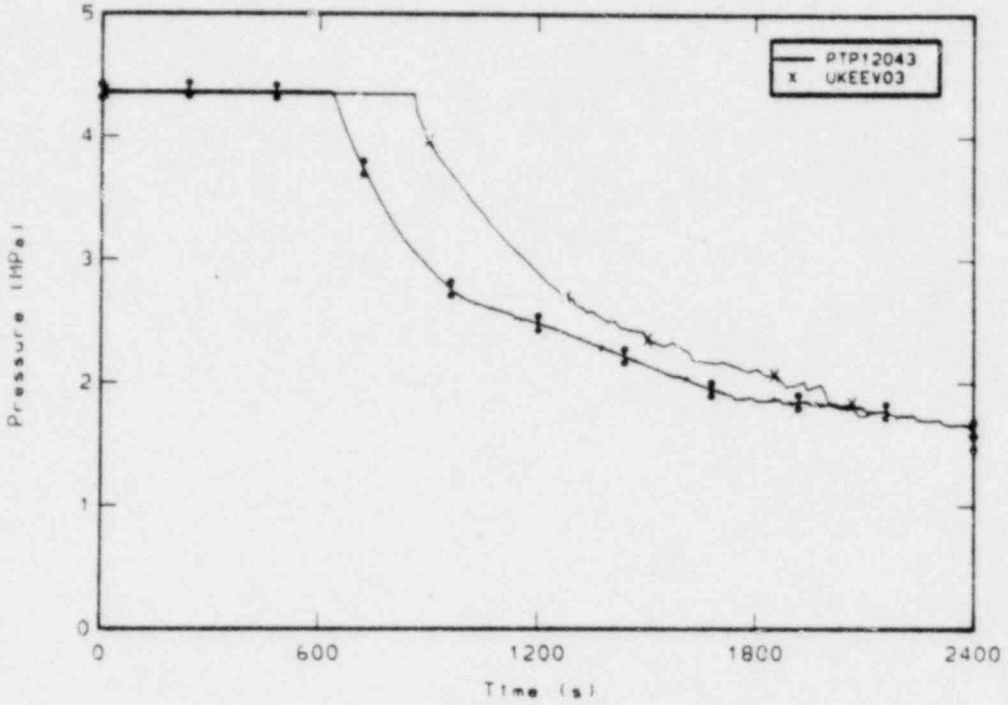

Figure N-5. Comparison of measured and UKEE calculated accumulator pressure.

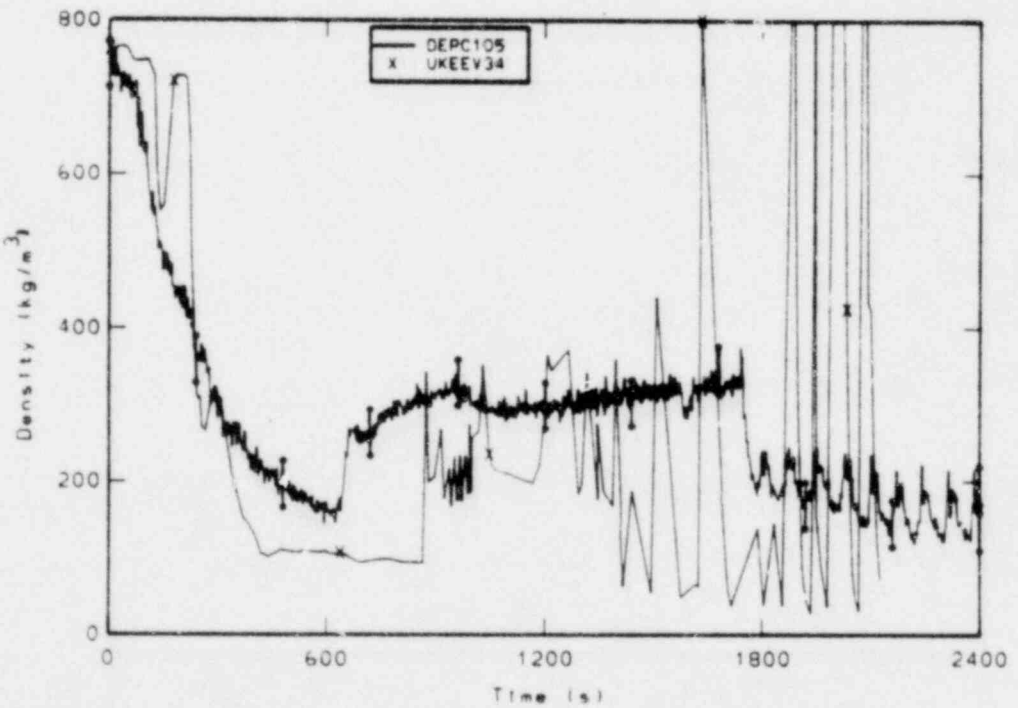

Figure N-6. Comparison of measured and UKEE calculated differential pressure drop across the pumps.

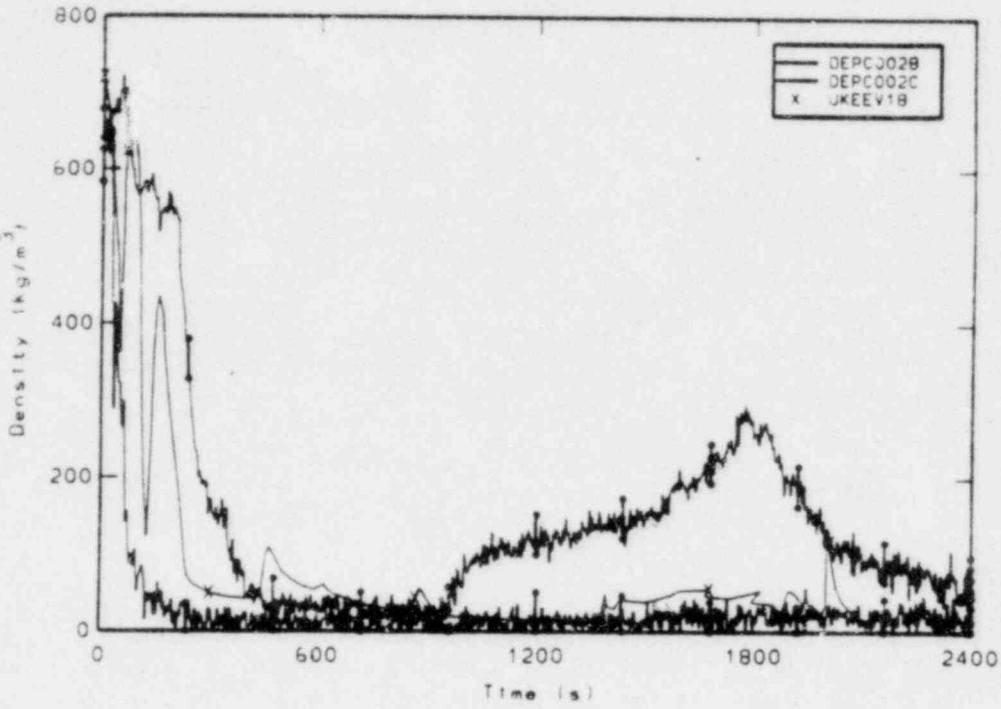

Figure N-7. Comparison of measured chordal densities and UKEE calculated average density in the intact loop hot leg.

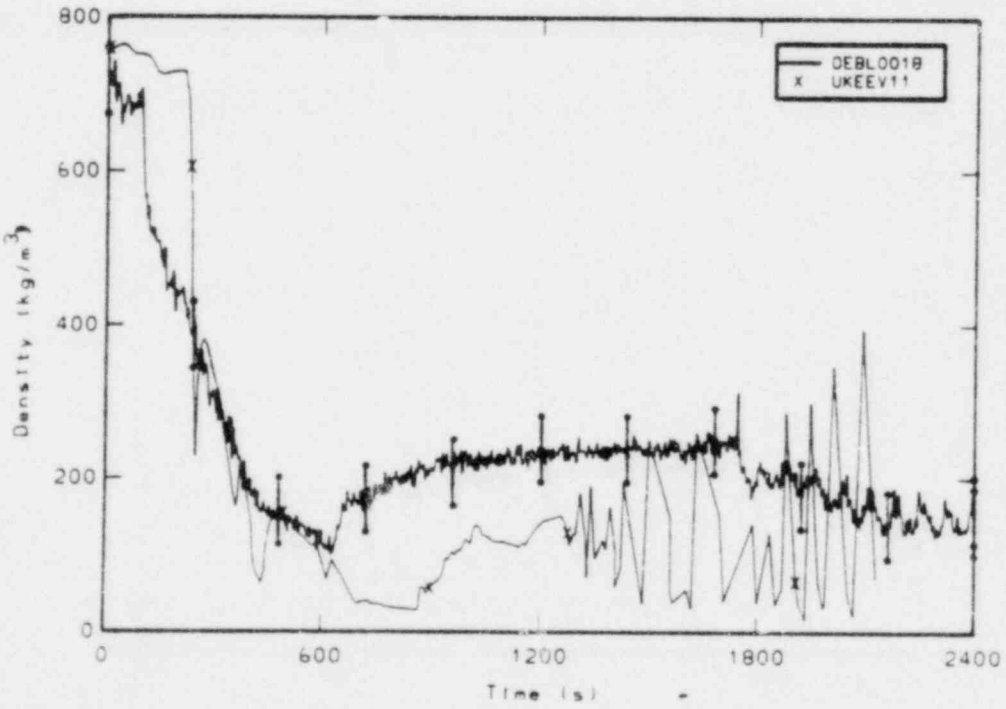

Figure N-8. Comparison of measured chordal density and UKEE calculated average density in the broken loop cold leg.

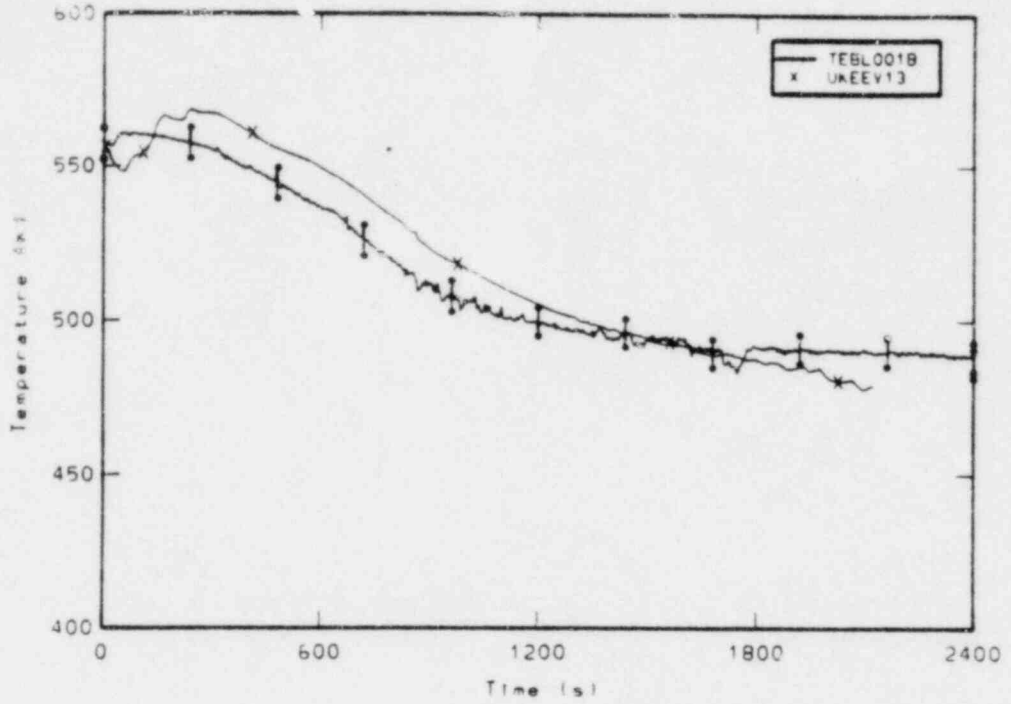

Figure N-9. Comparison of measured and UKEE calculated broken loop cold leg fluid temperature.

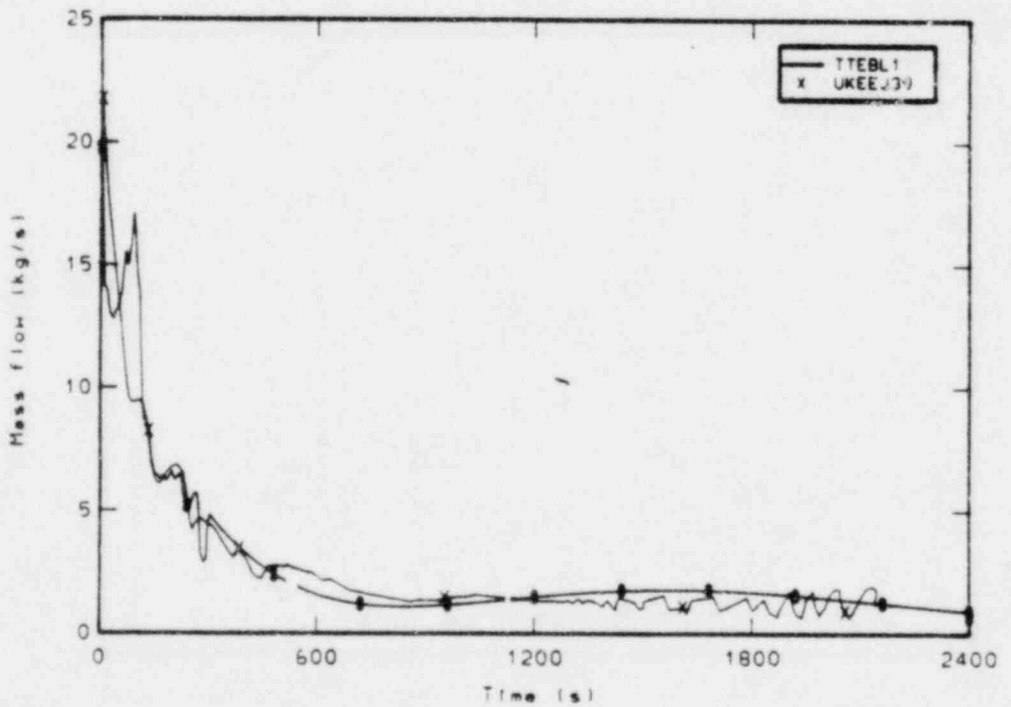

Figure N-10. Comparison of measured and UKEE calculated mass flow rate at the break.

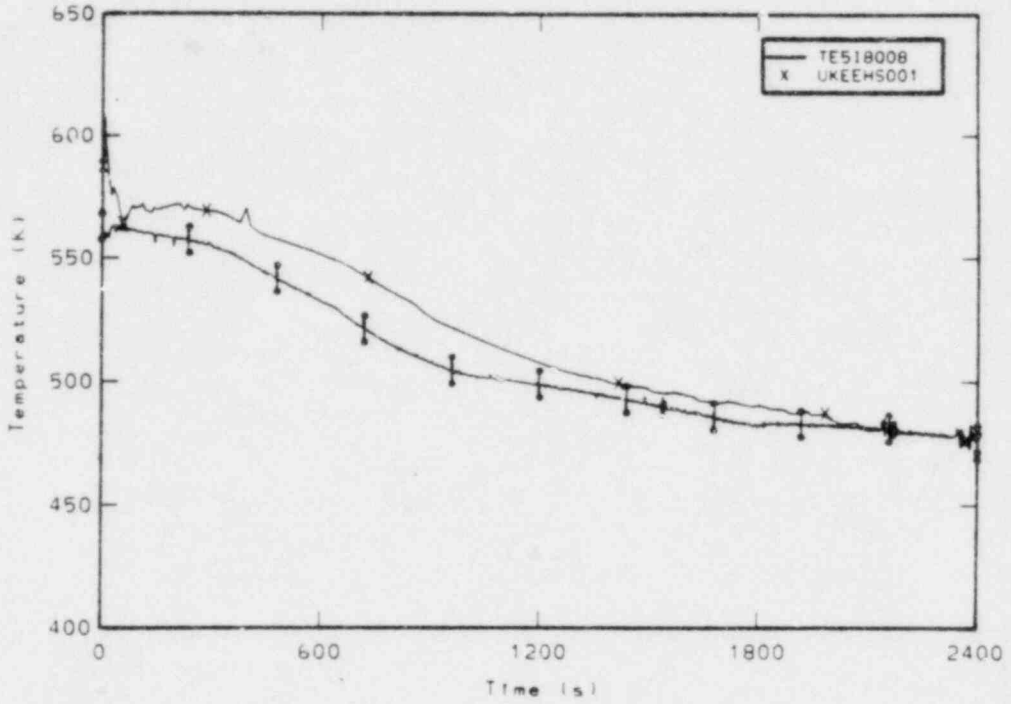

Figure N-11. Comparison of measured rod cladding temperature at the 0.20m elevation and UKEE calculated rod cladding temperature.

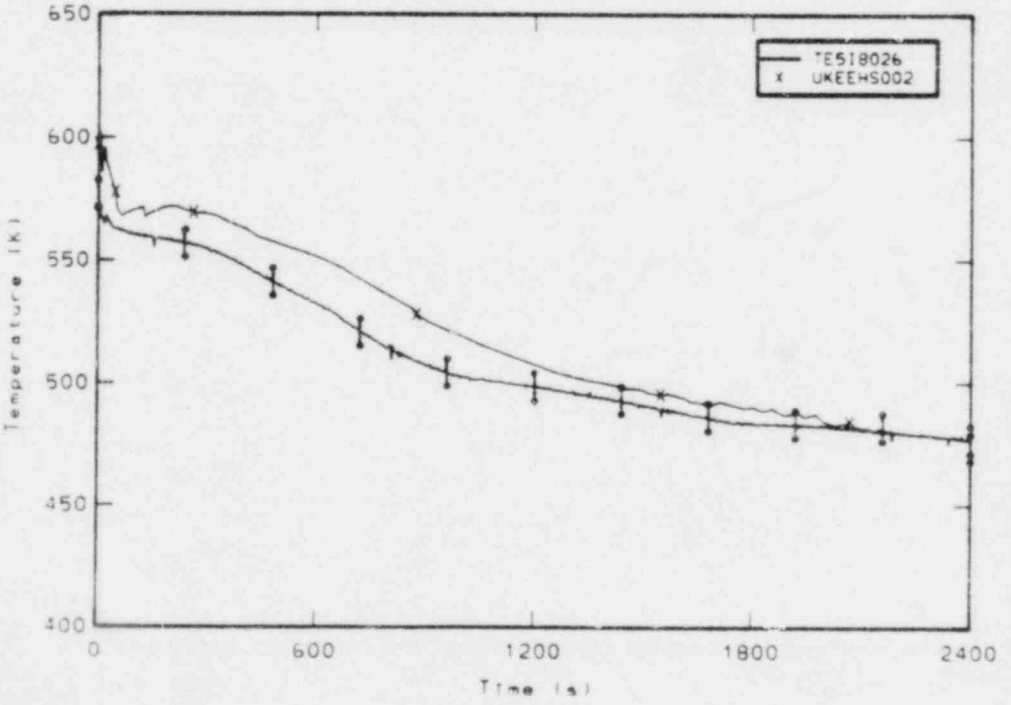

Figure N-12. Comparison of measured rod cladding temperature at the 0.66m elevation and UKEE calculated rod cladding temperature.

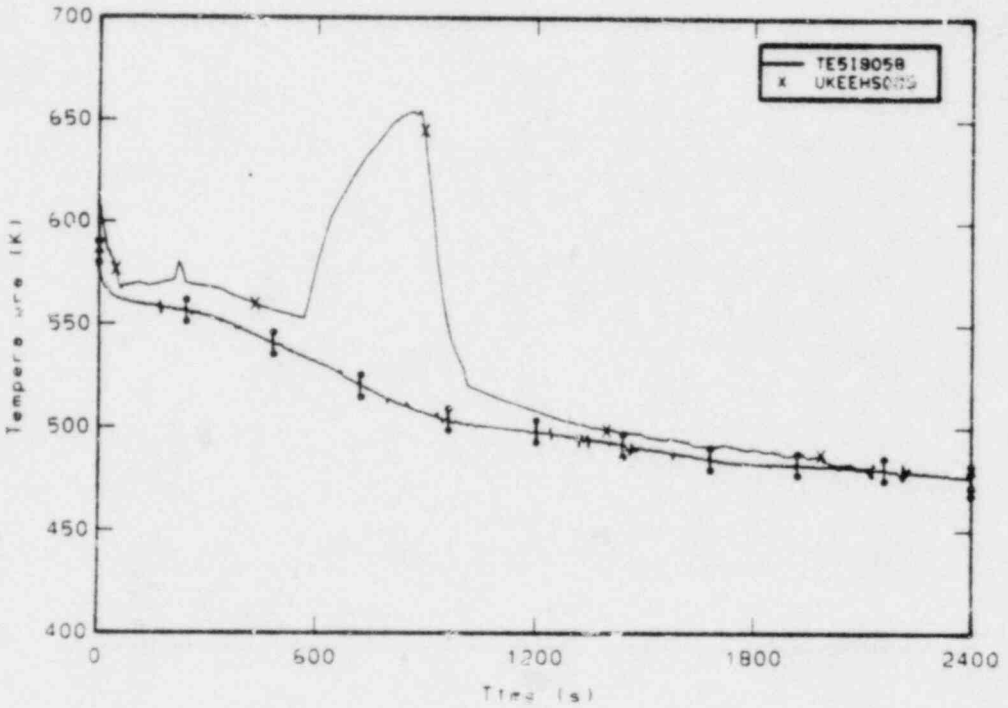

Figure N-13. Comparison of measured rod cladding temperature at the 1.47m elevation and UKEE calculated rod cladding temperature.